

PUBLICATION NO. 38

# NORDIC CONCRETE RESEARCH



THE NORDIC CONCRETE FEDERATION  
2/2008

**PUBLICATION NO. 38 2/2008**

# **NORDIC CONCRETE RESEARCH**

**EDITED BY  
THE NORDIC CONCRETE FEDERATION  
CONCRETE ASSOCIATION OF: DENMARK  
FINLAND  
ICELAND  
NORWAY  
SWEDEN**

**PUBLISHER: NORSK BETONGFORENING  
POSTBOKS 2312, SOLLI  
0201 OSLO**

**AALBORG, DECEMBER 2008**



## CONTENTS

1.	Linn Grepstad & Jan Arve Øverli <b>Hybrid concrete structures - Experimental and numerical investigation of beams with lightweight concrete and fibre-reinforcement</b> .....	11
2.	Anette Jansson, Kent Gylltoft & Ingemar Löfgren <b>Design methods for fibre-reinforced concrete: A state-of-the-art review</b> .....	31
3.	Mats Emborg & Peter Simonsson <b>Industrial concrete construction for a better economy and working environment - possibilities and obstacles with self compacting concrete</b> .....	47
4.	Jonas Carlswärd <b>Test methods and a theoretical model to assess shrinkage cracking of steel fibre reinforced concrete overlays</b> .....	61
5.	Anders Ansell & Richard Malm <b>Modelling of Thermally Induced Cracking of a Concrete Buttress Dam</b> .....	79
6.	Mario Plos et. al. <b>Structural assessment of concrete bridges</b> .....	97
7.	Peter Billberg & Mikael Westerholm <b>Robustness of Fresh VMA-modified SCC to Varying Aggregate Moisture</b> .....	113
8.	Arto Puurula et. al. <b>Full-Scale Test to Failure of a Strengthened Reinforced Concrete Bridge. Calibration of Assessment Models for Load-bearing Capacities of Existing Bridges</b> .....	131
9.	Thomas Blanksvärd & Björn Täljsten <b>Strengthening of concrete structures with cement based bonded composites</b> .....	143
10.	Rasmus Rempling, Karin Lundgren & Kent Gylltoft <b>Modelling of Concrete in Tension - Energy Dissipation in Cyclic Loops</b> .....	165
11.	Magnus Åhs & Anders Sjöberg <b>Moisture distribution in screeded concrete slabs</b> .....	179





## **Preface**

*Nordic Concrete Research* is since 1982 the leading scientific journal concerning concrete research in the five Nordic countries, e.g., Denmark, Finland, Iceland, Norway, and Sweden. The content of *Nordic Concrete Research* reflects the major trends in the concrete research.

*Nordic Concrete Research* is published by the Nordic Concrete Federation that beside the publication activity also organizes the Nordic Concrete Research Symposia that have constituted a continuous series since 1953 in Stockholm. The Symposium circulates between the five countries and takes place every third year. The next will be held in Finland during the summer of 2011.

The homepage of the Nordic Concrete Federation, [www.nordicconcrete.org](http://www.nordicconcrete.org) have now been established. During the coming months, the missing items will be added.

In 2009, the layout of the *Nordic Concrete Research* journal will be changed. Further information regarding this will be published on the homepage.

In the series of proceedings from Nordic Miniseminars, the following have been published during the last year:

- Proceeding No. 6: "Ice Abrasion on Concrete Structures"  
- Helsingfors October 2007
- Proceeding No. 7: "Fibre Reinforced Concrete"  
- Trondheim November 2007
- and in January 2009, proceedings from the latest miniseminar will be published:
- Proceeding No. 8: "Nordic Exposure Sites - Input to revision of EN 206-1"  
- Hirtshals November 2008.

Aalborg, December 2008

**Dirch H. Bager**

Editor, *Nordic Concrete Research*





## Research Committee

Mr. Klaus Söderlund, Chairman for the Research Committee

Dr. Dirch H. Bager, Editor of Nordic Concrete Research

### Denmark

Dr. Dirch H. Bager  
Aalborg Portland A/S  
Product Technology  
Rørdalsvej 44  
P.O. Box 165  
DK - 9100 Aalborg  
Tel: +45 9933 7712  
Mobile: +45 2429 1028  
Fax: +45 98 16 47 41  
E-mail: dirch.bager@aalborgportland.com

Mr. Claus Pade  
Concrete Centre,  
Danish Technological Institute  
Gregersensvej  
DK - 2630 Taastrup  
Tel: + 45 7220 2183  
Mobile: +45  
Fax: + 45 7220 2373  
E-mail: claus.pade@teknologisk.dk

### Finland

Mr. Klaus Söderlund  
Concrete Association of Finland  
Unionkatu 14 PL 11  
FIN - 00130 Helsinki  
Tel: +358 9 6962 3620  
Mobile: +358 40 900 3576  
Fax: +358 965 1145  
E-mail: klaus.soderlund@fise.fi

Lic.Sc.Tech. Klaus Juvas  
Consolis Technology Oy Ab  
Box 72  
FIN - 21291 Rusko  
Tel: +358 205 77 5386  
Mobile: +358 40 5160 316  
Fax: +358 205 77 5377  
E-mail: klaus.juvas@consolis.com

### Iceland

Dr. Þorgeir Johannes Wigum  
Mannvit  
Grensásvegur 1  
IS - 108 Reykjavík  
Tel: +354 422 3030  
Mobile: +354 896-0756  
Fax: +354 422 3001  
E-mail: wigum@vgkhonnun.is

Dr. Jón E. Wallevik  
Innovation Center Iceland  
IS - 112 Keldnaholti  
Tel: +354 522 9362  
Mobile: +354  
Fax: +354 522 9111  
E-mail: jon.w@nmi.is

### Norway

Dr. Terje F. Rønning  
Norcem, FoU Department  
P.O.Box 38  
N - 3991 Brevik  
Tel.: +47 3557 2347  
Mobile: +47 9157 6046  
Fax: +47 3557 0400  
E-mail: Terje.ronning@norcem.no

Mr. Hans Stemland  
SINTEF  
Concrete  
N - 7465 Trondheim  
Tel: +47 7359 4527  
Fax: +47 7359 7136  
E-mail: Hans.stemland@sintef.no

### Sweden

Tekn.Dr. Docent Mikael Hallgren  
Tyréns AB Byggprojektering  
Peter Myndes Backe 16  
SE - 118 86 Stockholm  
Tel: +46 8566 411 33  
Mobile: +46 70 661 05 33  
Fax: +46 8566 410 50  
E-mail: Mikael.Hallgren@tyrens.se

Tekn. Dr. Peter Utgenannt  
SP Sveriges Tekniska Forskningsinstitut  
Bygg och Mekanik  
P.O. Box 857  
SE - 501 15 Borås  
Tel: +46 105 165 107  
Mobile:  
Fax: +46 33 13 45 16  
E-mail: peter.utgenannt@sp.se

### Publishing

Mr. Knut R. Berg  
Norsk Betongforening  
Postboks 2312 Solli  
N - 0201 Oslo  
Tel: +47 22 94 75 00  
Mobile: +47 9325 9554  
Fax: +47 2294 7501  
E-mail: knut.berg@tekna.no

Wednesday, 17 December 2008



## Hybrid concrete structures – Experimental and numerical investigation of beams with lightweight concrete and fibre-reinforcement



Linn Grepstad  
MSc, PhD-student at NTNU, Norway  
Department of Structural Engineering  
Rich. Birkelandsvei 1A, 7491 Trondheim  
E-mail: linn.grepstad@ntnu.no



Jan Arve Øverli  
Associate Professor  
Department of Civil Engineering  
Sør-Trøndelag University College  
7004 Trondheim, Norway  
E-mail: jan.overli@hist.no

### ABSTRACT

Hybrid concrete beams of different size, consisting of a top layer of lightweight concrete and a 50mm bottom layer of fibre-reinforced concrete, were exposed to a four-point bending test [1]. The beams were analysed numerically using the finite element code DIANA [2]. Tests showed that the response for the small beams was dominated by one cracked zone and moment failures, while a distributed crack pattern was observed for the large beams where the ultimate capacity were governed by moment and shear failures. The numerical analyses were capable of simulating the global response of the beams.

**Key words:** Fibre-reinforced concrete, lightweight concrete, four-point bending test, finite element analysis

### 1. INTRODUCTION

The continuous demand for improvement of structures is often rooted in economic considerations, better working conditions and environmental issues. Hence, it is important to develop new types of structures which optimize and utilize the properties of materials. The beams presented here are a result of a need for innovation, and consist of a top layer of lightweight concrete and a 50mm bottom layer of fibre-reinforced concrete [1]. The purpose of this study is to investigate the flexural behaviour of such hybrid concrete beams, based on i) two series of four-point bending tests on small and large beams, ii) finite element (FEM) analyses of the small beams for obtaining material parameters and stress-strain ( $\sigma$ - $\epsilon$ ) relationships and iii) FEM analyses of large beams using the obtained material parameters from the investigation of the small beams. The aim of this study is also to investigate the influence different material parameters have on the accuracy of the simulations compared to results from the four-point bending test. The financial support for this study is provided by the Concrete Innovation Centre, COIN [3].

## 1.1 General

Two types of beams are investigated and contain either 3% synthetic macro fibres (SNFR) or 2% Dramix steel fibres (SFR) in the bottom layer. The top layer consists of lightweight concrete (LWAC). The investigation of these hybrid concrete beams is an attempt on utilizing factors that have a favourable effect on the mechanical properties of fibre-reinforced concrete structures. Firstly, the beam has a low self-weight due to the lightweight concrete layer. Also, the casting method has proved to be favourable in order to align the fibres in the direction of stress.

To investigate the structural behaviour of the hybrid beams they were exposed to a four-point bending test where deflections and strains were measured. The experimental program covers six small beams and four larger beams, where half of them contain steel fibre reinforcement and the rest are reinforced with synthetic fibres in the bottom layer. This experimental program is considered as a first step on investigating the behaviour of such hybrid concrete beams, and tests for obtaining the real material properties were limited. Hence, the following investigation on the behaviour of these hybrid concrete beams is based on some assumptions related to the material properties available.

Based on the experiments, numerical analyses are executed using the finite element code DIANA [2]. Test-results from the small beams and pull-out tests are used to obtain  $\sigma$ - $\varepsilon$  relationships which are input to the analyses of the beams. As a smeared crack concept is employed, the results depend among other things on fracture energy and element size. The numerical analyses of both small and large beams also study the influence of different material properties. This is presented by comparing results with different values of E-modulus, tensile strength and fracture energy.

## 1.2 Small beams

The small beams in Figure 1 were made from a concrete plate (600x600x150mm), and then cut into beams with dimensions 600x150x150mm. The bottom layer of fibre-reinforced concrete is 50mm thick and the thickness of the lightweight concrete layer is then 100mm.

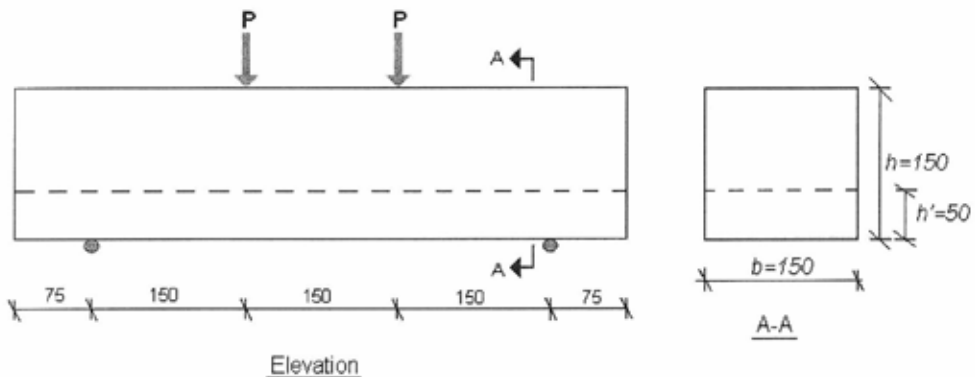


Figure 1 – Geometry and loading of the small beam (measures in mm).

### 1.3 Large beams

The large beams in Figure 2 are of dimensions 3000x150x250mm and have 2ø8 reinforcement bars between the concrete layers. The thickness of the bottom layer is still 50mm, but the lightweight concrete layer has a thickness of 200mm.

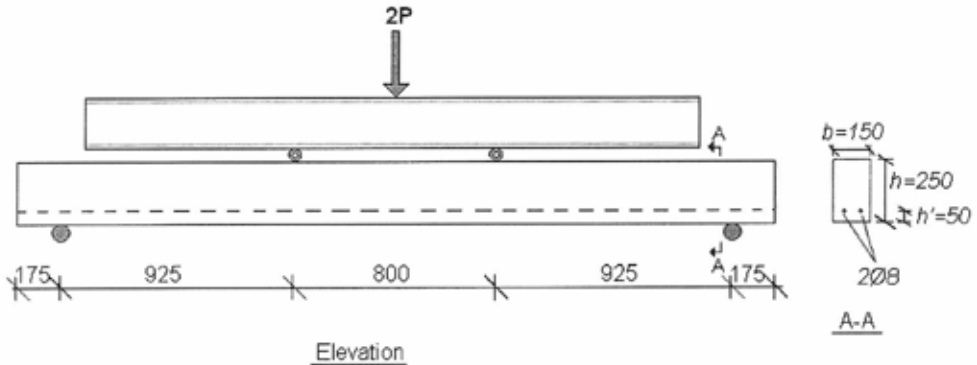


Figure 2 – Geometry and loading of the large beam (measures in mm).

## 2. CONCRETE AND CASTING

### 2.1 Mixtures

Table 1 gives an overview of the mix design for the three different types of concrete. Both the synthetic fibre-reinforced concrete (SNFRC) and the steel fibre-reinforced concrete (SFRC) mixes are self-compacting concrete, where the maximum aggregate size is 8mm [1]. The properties of the two fibre qualities are presented in section 3 below.

Table 1 – Mix design for concrete

Material	LWAC [kg/m <sup>3</sup> ]	Material	SFRC [kg/m <sup>3</sup> ]	SNFRC [kg/m <sup>3</sup> ]
Cement Norcem Anlegg	396.1	Cement Norcem Standard FA	441.7	442.4
EN 197-1-CEM I 52,5 N		EN 197-1-CEM II/A-V 42,5 R		
Elkem Microsilica	39.6	Elkem Microsilica 940U	26.5	26.5
Water	174.3	Water	197.9	198.2
Absorbed water	95.1	Absorbed water	12.6	12.4
Liapor 6.5	398.5	(Årdal) 0-8mm	1575.3	1547.5
Liapor L 0/2	296.1	Glenium SKY 550	5.3	5.3
Glenium SKY 550	4.0	SFR	156.0 (2%)	-
MICROAIR 100	0.6	SNFR	-	27.3 (3%)

Remarks to Table 1:

\* Elkem Microsilica - condensed silica fume

\* Liapor- lightweight (expanded clay) aggregate

\* Glenium SKY 550 - polycarboxylate based superplasticizer (water reducer)

\* MICROAIR - air-entraining admixture



## 2.2 Concrete properties

In order to determine the concrete properties given in Table 2, specimens from each type of concrete were tested:

- six cylinders of SFRC and three cylinders of LWAC
- three cylinders of SNFRC and three cylinders of LWAC

*Table 2 – Concrete properties (average values)*

Specimen	Type	Density [kg/m <sup>3</sup> ]	Cylinder strength [MPa]	Achieved strength class NS3473 [4]	Aimed strength class NS3473 [4]
1. SFRC	Cylinder	2450	61.86	B55 (C55/67)	B45 (C45/55)
1. LWAC	Cylinder	1478	38.19	LB35 (LC35/38)	LB30 (LC30/33)
2. SNFRC	Cylinder	2290	53.99	B45 (C45/55)	B45 (C45/55)
2. LWAC	Cylinder	1450	37.90	LB35 (LC35/38)	LB30 (LC30/33)

The strength values given in Table 2 are relevant for tests carried out 33 days after casting [1].

## 2.3 Casting of the beams

The different concrete layers of the beams were cast wet-on-wet. The casting of the bottom layer was done horizontally by pouring fibre-reinforced self-compacting concrete in the longitudinal direction of the beams.

When calculating some material properties of fibre-reinforced concrete, a factor indicating the amount of fibres which is effective normal to the crack plane is used. For plane oriented fibres this factor is 0.5 [5]. Due to the casting method, a capacity factor of  $\eta_0=0.43$  is assumed for the fibre-reinforcement in the hybrid concrete beams [1].

## 3. FIBRE-REINFORCEMENT

### 3.1 Synthetic macrofibres

Compared to steel fibres, synthetic fibres have a low self-weight and do less damage to the equipment and physical surroundings when mixing and casting. The synthetic fibres have a lower E-modulus and tensile strength than steel fibres, and for maximum load the fibre's deformation is larger. Material properties of the fibre used in the hybrid concrete beams, BarChip Shogun, are given in Table 3. The fibres are straight and have a rough surface [1].

### 3.2 Dramix steel fibres

This fibre is a frequently used steel fibre in Norway and is produced in many variants. In these tests, Dramix RC-65/60-BN is used, which is a fibre of bright steel with end hooks. Table 3 gives an overview of different material properties for the Dramix fibre [1].

Table 3 – Fibre-reinforcement properties

Type of fibre	Dramix RC-65/60-BN (SFR)	BarChip Shogun (SNFR)
Type of material	Steel	Polyolefin
Length [mm]	60	48
Diameter / cross-section [mm]	D = 0.9	A = 0.8 x 1.1
L/d	65	44
Density [kg/m <sup>3</sup> ]	7700	910
E-modulus [MPa]	200 000	6000
Tensile strength [MPa]	950	480-550

### 3.3 Pull-out tests

Pull-out tests were performed on the same type of fibre-reinforced concrete as in the hybrid concrete beams. The pull-out tests were executed in the laboratory at NTNU, according to the Norwegian draft guidelines for design and execution of steel fibre-reinforced concrete [5]. The main results from these pull-out tests were:

1. Synthetic fibres experience larger deformations at maximum load than steel fibres.
2. The end hooks of steel fibres constitute the main contribution of the pull-out capacity.
3. Bond and the fibres load capacity improve with increased concrete strength.

Figure 3 shows typical stress-displacement ( $\sigma$ -w) curves from pull-out tests of Dramix fibre (SFR) and BarChip Shogun fibre (SNFR).

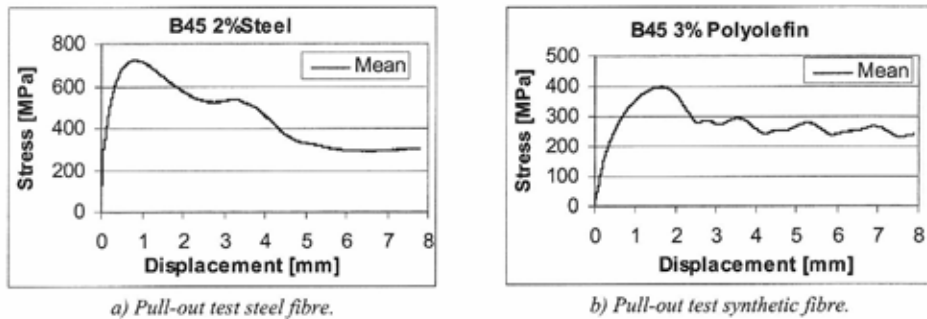


Figure 3 – Results from pull-out tests, mean values [6].

## 4. TEST-RESULTS

### 4.1 General

Three small beams of each type were tested and the tests were terminated at a deflection of about 4mm. The load-deflection diagrams show good correspondence with each other. The response was dominated by one cracked zone developing at midspan, followed by a moment failure for the beams. The small beams were tested 20 days after casting.

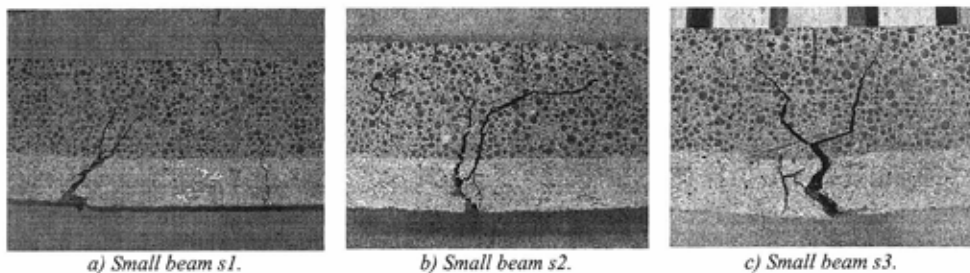
Two large beams of each type were exposed to the four-point bending test. The results from these tests also give relatively good correspondence with each other up to a certain point, but the results show a variation on deflection at final failure. Distributed crack patterns were observed and the ultimate capacities were governed by moment and shear failures.

### 4.2 Results from small beams, s1, s2 and s3

The small beams with steel fibre-reinforcement in the bottom layer experienced moment failure and the outline of the results is given in Table 4. The crack patterns are shown in Figure 4.

*Table 4 – Results of small beams with steel fibre-reinforcement (SFR) [1]*

Load / Deflection	Small beam s1	Small beam s2	Small beam s3
Load at crack initiation [kN]	47.5	Not registered	Not registered
Load at main crack [kN]	52.6	52.7	59.4
Maximum load [kN]	54.1	52.7	59.4
Deflection at maximum load [mm]	0.60	0.39	0.43



*Figure 4 – Crack pattern of small beams with steel fibre-reinforcement (SFR) [1].*

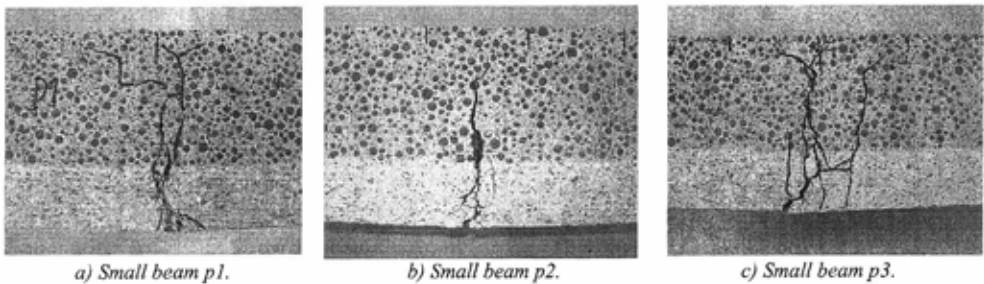
The first beam initially developed four cracks, but two of them (located near the bearing) closed during the test. The cracks in Figure 4 a) did not close during the test, and were located at a distance approximately 150mm from the bearing [1].

### 4.3 Results from small beams, p1, p2 and p3

The small beams reinforced with synthetic fibres all experienced moment failure and an outline of the results is given in Table 5. The crack patterns of these beams are shown in Figure 5.

*Table 5 – Results of small beams with synthetic fibre-reinforced concrete (SNFR) [1]*

Load / Deflection	Small beam p1	Small beam p2	Small beam p3
Load at crack initiation [kN]	35.0	27	33.0
Load at main crack [kN]	35.0	27.5	33.0
Maximum load [kN]	39.4	31.2	38.3
Deflection at maximum load [mm]	1.03	0.97	1.50



*Figure 5 – Crack pattern of small beams with synthetic fibre-reinforcement (SNFR) [1].*

The third beam, p3, developed initially three cracks, where the third crack was located near the bearing and closed after reaching maximum load. Of the two cracks at midpoint, depicted in Figure 5 c), especially the left one developed during the test [1].

From the results on the small beams, one can observe that the maximum load is reached at a larger deflection for the synthetic fibre-reinforced beams than for the steel fibre-reinforced beams. The SFRC beams also reach a higher maximum load than the SNFRC beams. The crack development, on the other hand, indicates a similar pattern for both types of beams.

### 4.4 Results from large beams, S1 and S2

Table 6 gives an overview of the main results from the analyses, and Figure 6 shows the crack patterns of the large steel fibre-reinforced concrete beams.

*Table 6 – Results from the four-point bending test of large beams with steel fibre-reinforcement (SFR) [1]*

	Large beam S1	Large beam S2
Shear area [mm]	600*	925
Area of constant moment [mm]	1450	800
Load at crack initiation [kN]	23	18
Moment at crack initiation [kNm]	6.9	8.3
Maximum load [kN]	48.2	34.6
Deflection at maximum load [mm]	13.1	13.7
Maximum moment [kNm]	14.5	16.2
Type of failure	Shear	Bending

\*Because of the fact that this first test resulted in shear failure, the loading was moved.



*a) Crack pattern large beam S1.*



*b) Crack pattern large beam S2.*

*Figure 6 – Crack pattern of large beams with steel fibre-reinforcement (SFR) [1].*

Due to the shear failure of beam S1, the investigation focuses on the second beam, S2. This beam experienced moment failure and initially there were only vertical cracks at midspan. At a later stage in the test, a diagonal crack started to open. At the same time one of the vertical cracks at midpoint developed, causing the moment failure of the beam [1].

#### **4.5 Results from large beams, P1 and P2**

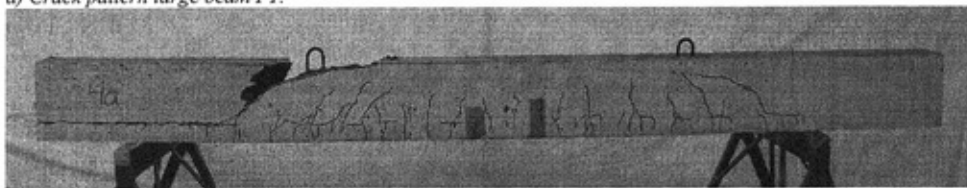
Table 7 gives an overview of the main results from the analyses, and Figure 7 shows the crack pattern of the large synthetic fibre-reinforced concrete beams.

*Table 7 – Results from the four-point bending test of large beams with synthetic fibre-reinforcement (SNFR) [1]*

	Large beam P1	Large beam P2
Shear area [mm]	925	925
Area of constant moment [mm]	800	800
Load at crack initiation [kN]	8.0	10.0
Moment at crack initiation [kNm]	7.4	9.3
Maximum load [kN]	31.5	27.2
Deflection at maximum load [mm]	40.5	18.6
Maximum moment [kNm]	14.7	12.7
Type of failure	Shear	Shear



*a) Crack pattern large beam P1.*



*b) Crack pattern large beam P2.*

*Figure 7 – Crack pattern of large beams with synthetic fibre-reinforcement (SNFR) [1].*

For the first beam P1, some vertical cracks between the loadings opened early. During the test, these cracks experienced a change of direction when they reached the LWAC layer, and oriented towards the loadings. Failure was caused due to one of these diagonal cracks at a large deflection.

Both vertical and horizontal cracks, located under the loading, opened at an early stage in the test of beam P2. The development of diagonal cracks resulted in a shear failure [1].

## 5. FINITE ELEMENT ANALYSES

The analyses were carried out using the finite element code DIANA [2].

### 5.1 Finite element model

The aim with the analyses is to investigate the behaviour of the hybrid beams subjected to four-point bending. Due to symmetry, the finite element model represents only half of the beams. Eight-noded quadrilateral isoparametric plane stress elements are used in the analyses. The elements are based on quadratic interpolation and Gauss integration. The models for both the small and large beams employ quadratic elements of 25 mm. Hence, the small model consists of 72 elements and the large model of 600 elements. The analyses assume perfect bonding between the two layers of concrete. However, this is not verified by testing, but will be considered in another project.

### 5.2 Material models

In tension the analyses are based on a smeared crack approach. The small beams employ a rotating crack model based on total strains. In this model there is coaxiality between principal stresses and principal strains. It is a constitutive model developed along the lines of the modified compression field theory [7]. The large beams use a plasticity formulation based on the Rankine principal stress yield criterion with work hardening, to describe the tensile behaviour [8].

The responses of the beams are dominated by cracking. Thus, compressive behaviour is described with linear elasticity in the numerical analyses.

The steel reinforcement in the large beams is represented by a linear perfect-plastic material model. The material properties are 200 000 MPa for Young's modulus of elasticity and 550 MPa for the yield stress.

### 5.3 Material properties and constitutive models

In order to study the influence of different material parameters, two main approaches are used in the numerical analyses:

1. Obtaining material parameters from the measured cylinder strength, and the corresponding achieved strength class according to NS3473 [4]
2. Obtaining material parameters from the aimed strength class according to NS3473 [4]

The cylinder strength is tested after 33 days and material parameters from strength classes are based on 28 days old concrete. Due to a tight time schedule the small beams were tested already after 20 days. The large beams were tested after 28 days. Therefore, the material properties are adjusted to the age of 20 days and 28 days for the small and large beams respectively [9].

### Fibre-reinforced concrete layer

In the numerical analyses of the small beams, an inverse method is employed to find  $\sigma$ - $\varepsilon$  relationships for the fibre-reinforced concrete layer in tension. Based on the shapes of the  $\sigma$ - $w$  curves from the pull-out tests [6] and curve-fitting during the analyses, descending  $\sigma$ - $\varepsilon$  relationships are obtained and used in the analyses. The approach of obtaining a stress-strain relationship for the two types of fibre-reinforced concrete layer is as follows:

1. Employ the tensile strength and initial E-modulus of the fibre-reinforced concrete layer to find the point of first crack.
2. The peak-point is determined from the test at a load of 0.5mm deflection for the SFRC and 1.0mm deflection for the SNFRC, under the assumption of a maximum compression strain of  $\varepsilon_c = 0.001$  and a linear strain distribution over the cross-section, see Figure 8.
3. Curve fitting of the descending part of the  $\sigma$ - $\varepsilon$  relationship from preliminary analyses of the beams.

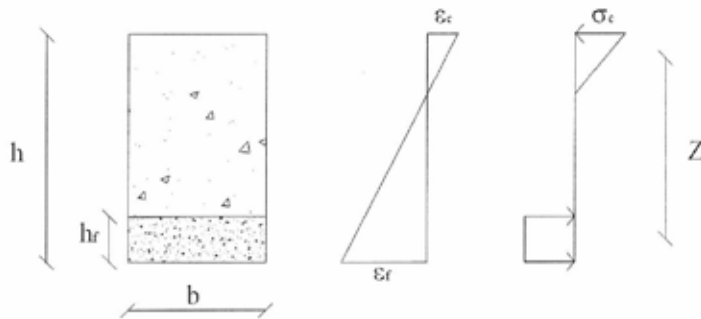


Figure 8 – Assumed stress and strain distribution over the cross-section [1].

This approach results in  $\sigma$ - $\varepsilon$  relationships for the fibre-reinforced concrete layer which exhibit a descending branch after reaching the peak point. This was also expected due to the relatively large amount of fibres added to the concrete and the results from the four-point bending test also reflect this behaviour. Figure 9 illustrates typical  $\sigma$ - $\varepsilon$  relationships obtained for the small beams.

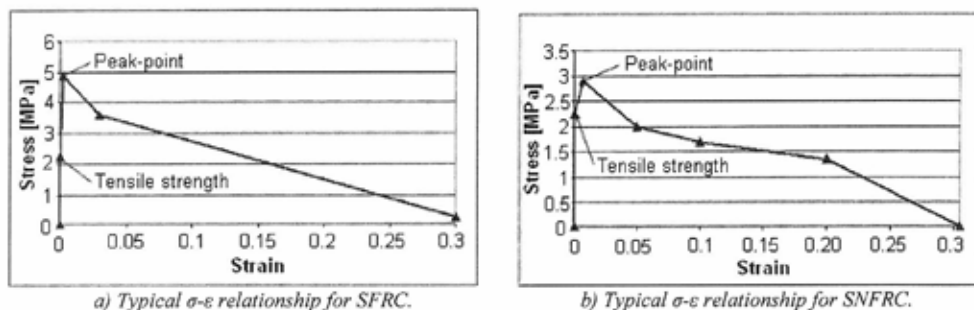


Figure 9 – Typical  $\sigma$ - $\varepsilon$  relationships for the fibre-reinforced concrete layers.

The analyses of the large beams employ the obtained  $\sigma$ - $\varepsilon$  relationships for the small beams.



### *Lightweight concrete layer*

After cracking the analyses employ a linear tension softening behaviour of the LWAC layer. In a smeared crack approach, the fracture energy and a crack band width must be introduced. The fracture energies used in the analyses of the large beams are  $G_F = 23.4 \text{ Nm/m}^2$  for the synthetic fibre-reinforced concrete beams and  $G_F = 86.3 \text{ Nm/m}^2$  for the steel fibre-reinforced concrete beams. The difference in values is based on the material behaviour of the fibre-reinforced layer. Compared to the synthetic fibres, the pull-out tests show that the steel fibre reaches a higher maximum load at a smaller displacement. It is therefore assumed a larger instant influence from the steel fibre-reinforced concrete layer on the lower parts of the lightweight concrete layer.

Estimating the crack band width in this type of analyses is difficult. The small beams have a cracked zone at mid point in the test. The numerical analyses show a distributed crack pattern in the longitudinal direction of the beam. Therefore, the crack band width is taken as 225mm for the small beams. In the experiments the large beams showed a crack spacing of approximately 70mm and 100mm for the synthetic and steel fibre beams respectively. Hence, the corresponding crack spacing is taken as the crack band width in these analyses.

The fibre-reinforced layer, and not the lightweight concrete layer, dominates the global responses of the beams. Thus, the influence of the fracture energy and crack band width in the analyses should be minor. However, the numerical solution is strongly dependent on these two factors. To get converged equilibrium solutions in global softening type of analyses, the ultimate tensile strains cannot be too low. The effect of varying the fracture energy will be investigated in the numerical analyses.

## **5.4 Small beam analyses**

In order to investigate the influence of different material parameters, different analyses were performed. The analyses are mainly based on two basic values of the E-modulus and tensile strengths according to concrete strength classes in NS3473 [4]. Further, the influence of the fracture energy was investigated for one of the analyses. The following analyses were performed with material properties according to Table 8.

### *Steel fibre-reinforced beam*

- s-1a: E-modulus according to the achieved cylinder strength and tensile strengths according to the corresponding strength classes LB35/B55, see Figure 10.
- s-1b: E-modulus according to the achieved cylinder strength and tensile strengths according to the corresponding strength classes LB35/B55. However, the tensile strength and peak-point of the stress-strain relationship for the fibre-reinforced concrete layer is adjusted by curve fitting, see Figure 10.
- s-2a: E-modulus and tensile strength according to the aimed strength class (LB30/B45).

### *Synthetic fibre-reinforced beam*

- p-1a: E-modulus according to the achieved cylinder strength and tensile strengths according to the corresponding strength classes LB35/B45.
- p-2a: E-modulus and tensile strength according to the aimed strength class (LB30/B45).
- p-2b: E-modulus according to the aimed strength class (LB30/B45) and double the value of the fracture energy  $G_F$ .

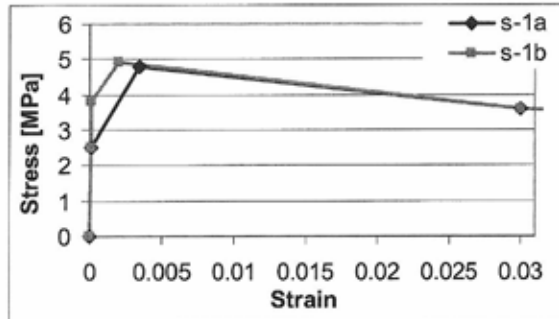


Figure 10 – A comparison of the first part of the  $\sigma$ - $\epsilon$  relationships for the SFRC layer used in the analyses s-1a and s-1b.

Table 8 – Material properties of small beams used in the analyses

Analysis	E-modulus	E-modulus	$f_m$	$f_m$	$G_F$
	LWAC	FRC	LWAC	FRC	LWAC
	[MPa]	[MPa]	[MPa]	[MPa]	[Nm/m <sup>2</sup> ]
s-1a	14300	31210	1.39	2.49	86.3
s-1b	14300	31210	1.39	3.80	86.3
s-2a	11730	28570	1.25	2.25	77.3
p-1a	14300	29925	1.39	2.25	23.4
p-2a	11730	28570	1.25	2.25	21.1
p-2b	11730	28570	1.25	2.25	42.2

As the investigation focuses on the tensile behaviour of the hybrid concrete beams, the behaviour of the concrete in compression is assumed to be linear elastic.

## 5.5 Large beam analyses

In these analyses the material properties from the measured cylinder strength were used only. The investigation focuses on the influence of the stress-strain relationships and the fracture energy. The following analyses were performed with material properties according to Table 9.

### Steel fibre-reinforced beam

S-1: E-modulus according to the achieved cylinder strength and tensile strengths according to the corresponding strength classes LB35/B55. The tensile strength and peak-point of the stress-strain relationship for the fibre-reinforced concrete layer is adjusted due to small beam analysis s1-b.

### Synthetic fibre-reinforced beam

P-1: E-modulus according to the achieved cylinder strength and tensile strengths according to the corresponding strength classes LB35/B45.

Table 9 – Material properties in the analyses of the large beams

Analysis	E-modulus LWAC [MPa]	E-modulus FRC [MPa]	$f_m$ LWAC [MPa]	Yield value FRC [MPa]	$G_F$ LWAC [Nm/m <sup>2</sup> ]
S-1	14500	31430	1.42	3.86	86.3
P-1	14500	30253	1.42	2.3	23.4

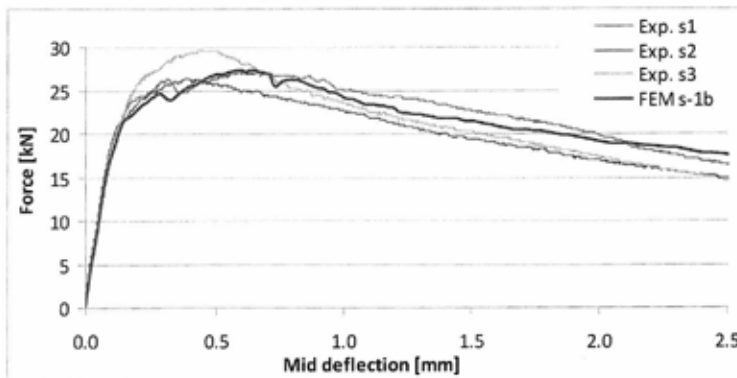
## 6. RESULTS

Results from the four-point bending test and the FEM-analyses are compared and presented in the following.

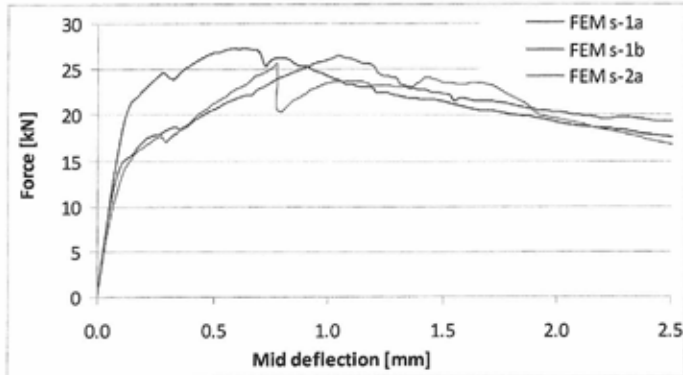
### 6.1 Small beams

#### Steel fibre-reinforced concrete beams

Load-deflection relationships from the four-point bending tests and the FEM-analyses are compared in Figure 11. The results from the experiments show good correlation with each other, and the the analysis of the beam with adjusted material properties on the steel fibre-reinforced concrete layer also corresponds well with the experiments.



a) Load-deflection relationships from four-point bending test compared with FEM s-1b.



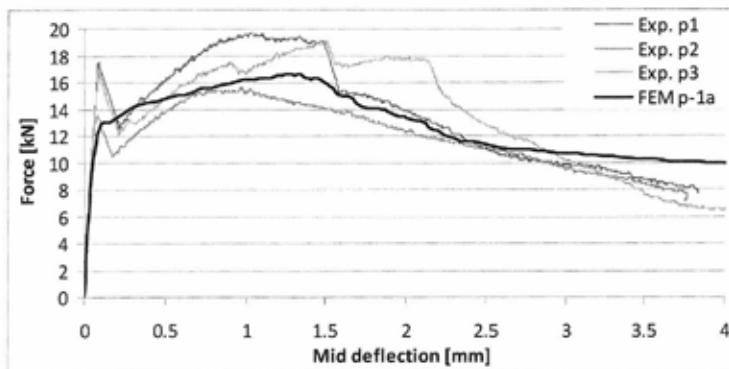
b) Comparison of load-deflection relationships from the FEM analyses.

Figure 11 – Comparison of load-deflection relationships from four-point bending test and the FEM-analyses of the small steel fibre-reinforced beams.

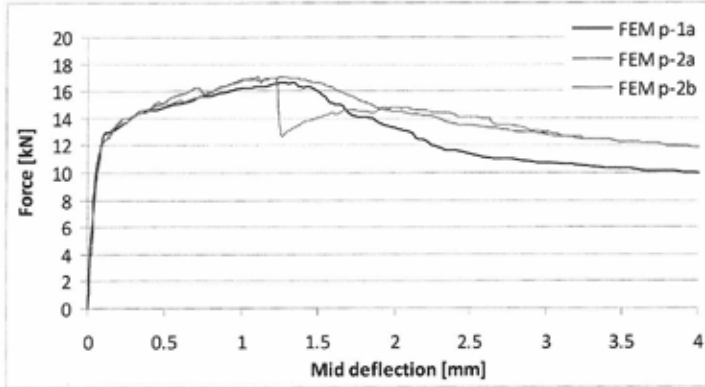
When employing the calculated peakpoint of the stress-strain relationship for the steel fibre-reinforced layer, the analysis (FEM s-1a) shows a larger displacement at maximum load compared to the the four-point bending test. The tensile strength of the steel fibre-reinforced concrete is also underestimated (FEM s-1a). After adjusting the peakpoint and increasing the tensile strength of the SFRC layer, the load-displacement curve from the analyses corresponds well with the results from the four-point bending tests (FEM s-1b). These analyses are based on material properties obtained from the measured cylinder strength. The final analysis (FEM s-2a) is based on material properties from the aimed strength class. In general this analysis does not differ a lot from the first (FEM s-1a). However, the load-displacement curve tends to deviate more from the experimental load-displacement curve, and no further analyses were performed with these material properties.

#### Synthetic fibre-reinforced concrete beams

Load-deflection relationships from the four-point bending tests and the FEM-analyses are compared in Figure 12. The results from the experiments show good correlation, Figure 12 a). The analysis “FEM p-1a” provides the best results compared with the experiments.



a) Load-deflection relationships from four-point bending test compared with FEM p-1a.



b) Comparison of load-deflection relationships from the FEM analyses.

Figure 12 – Comparison of load-deflection relationships from four-point bending test and the FEM-analyses of the small synthetic fibre-reinforced beams.

According to the load-deflection relationships in Figure 12, different E-modulus does not influence the result in the ascending part of the diagram. The analysis with material properties according to the aimed strength class (FEM p-2a), gains an unloading when reaching maximum load, indicating the fracture energy is too low. However, when doubling the value of  $G_F$  the load-deflection curves corresponds well (FEM p-2b). Based on these results, the analyses of the large beams with synthetic fibre-reinforcement employs the material properties obtained from the measured cylinder strength.

## 6.2 Large beams

### Steel fibre-reinforced concrete beams

Figure 13 shows a comparison of the load-deflection curves from the four-point bending test and the FEM-analysis.

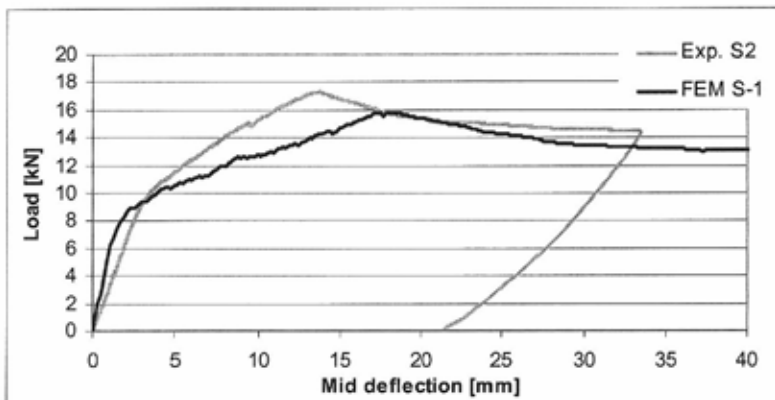
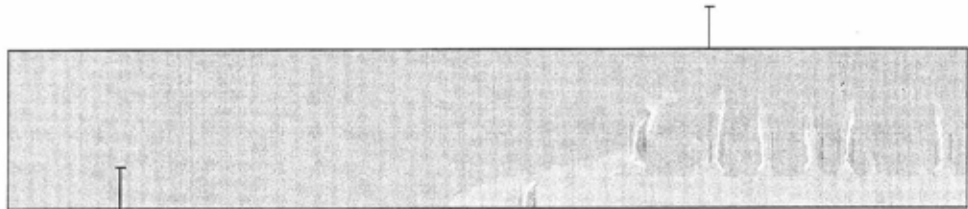
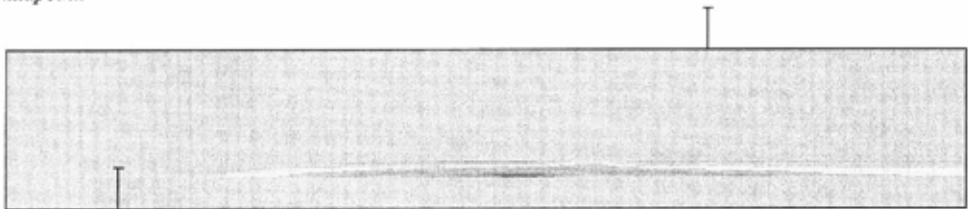


Figure 13 – Comparison of load-deflection relationships from four-point bending test and the FEM-analyses of the large steel fibre-reinforced beam S2.

According to the load-deflection relationships in Figure 13, the FEM-analysis is too stiff before cracking and too soft after cracking. Maximum load level is reached at a larger displacement than the experiment. However, the shape of the diagram from the analysis is satisfying. To enhance the agreement, a more detailed investigation of material properties and shape of the stress strain relationships must be performed. This is not done in this study.



a) Concentration of principal tensile strains, illustrating the vertical crack pattern at a deflection of 9,5mm at midpoint.



b) Concentration of principal tensile strains, illustrating the horizontal crack pattern at a deflection of 9,5mm at midpoint.

Figure 14 – Principal tensile strain distribution from the FEM-analyses of the large steel fibre-reinforced beam.

Figure 14 a) and b) show the principal tensile strain distribution obtained from the FEM-analyses. These results indicate good correlation between the observed crack pattern from the four-point bending test and the FEM-analysis. The experiments showed crack spacing of approximately 100mm, and the numerical analyses give crack spacing of 75-125mm. A large strain concentration is observed between the different concrete layers, indicating horizontal cracks in this area. A further investigation of this requires use of interface elements between the layers.

Between the concrete layers in the large beams, there are two Ø8 ordinary reinforcement bars. In the analysis the steel bars do not reach the yield-stress of 550 MPa. At maximum load level where the mid deflection is approximately 20mm, the steel stress is 400 MPa. This indicates that the ordinary bar-reinforcement does not contribute significantly to the capacity of the beams.

#### *Synthetic fibre-reinforced concrete beams*

The load-deflection relationships from the four-point bending tests and the FEM-analysis are compared in Figure 15. In the experiments the two beams have similar response until failure of beam P1. Deflection at failure is significantly larger for beam P2. Despite the attempt to achieve moment-failure, both beams experienced shear-failure.

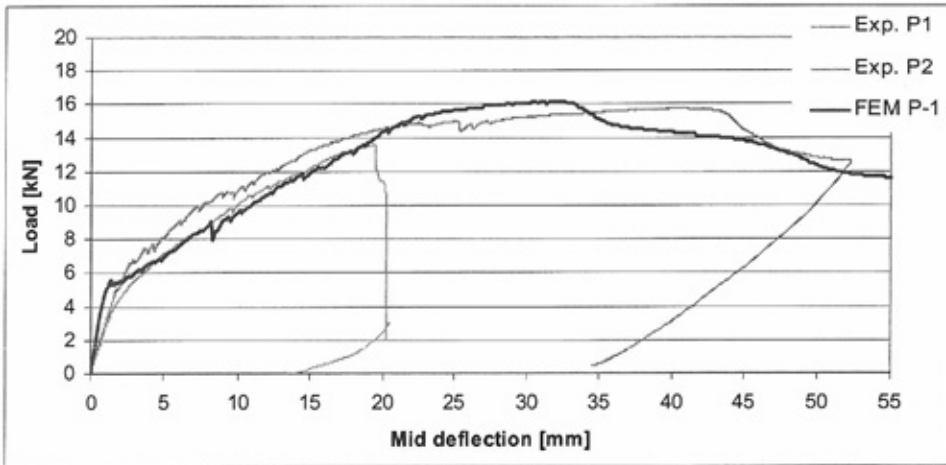
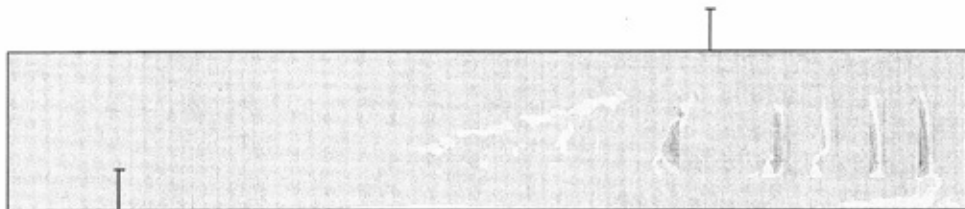


Figure 15 – Comparison of load-deflection relationships from four-point bending test and the FEM-analyses of the large synthetic fibre-reinforced beams.

Figure 15 shows that there is good correlation between the results from the FEM-analyses and the load-deflection relationship of “Exp. P1”. The shape of these curves is similar.

In the analysis the two Ø8 reinforcement bars reach the yield strength of 550 MPa at a deflection of 23 mm.



a) Concentration of principal tensile strains, illustrating the vertical crack pattern at a deflection of 30mm at midpoint.



b) Concentration of principal tensile strains, illustrating the horizontal and diagonal crack pattern at a deflection of 30mm at midpoint.

Figure 16 – Principal tensile strain distribution from the FEM-analyses of the large synthetic fibre-reinforced beam.

Figure 16 a) and b) show the principal tensile strain distribution obtained from the FEM-analysis. These results also indicate good correlation between the observed crack pattern from the four-point bending test and the FEM-analysis. The experiments showed crack spacing of approximately 70mm, and the numerical analyses give crack spacing of approximately 75mm. The concentration of strains illustrates the horizontal cracks between the concrete layers, but as for the SFRC beam no further investigation with interface elements between the different concrete layers was performed.

## 7. CONCLUSIONS AND SUGGESTIONS FOR FURTHER WORK

The following conclusions are based on results from four-point bending tests and numerical analyses of both steel fibre-reinforced concrete beams and synthetic fibre-reinforced concrete beams.

Firstly, the results show that the different types of concrete used in the hybrid beams work relatively good together and that the casting method (wet-on-wet) is favourable. Secondly, the following numerical analyses of the hybrid beams, using a smeared crack approach, give satisfactory results in recreating the behaviour of the beams:

- The strain distribution which illustrates the crack patterns shows good agreement with the real crack patterns observed in the four-point bending tests.
- The inverse method of obtaining the post-cracking behaviour of the FRC layer provides good correspondence between results from the four-point bending tests and the numerical analyses.

The numerical analyses also show that the global behaviour of the beams ( $P-\delta$ ) is governed mainly by the  $\sigma-\epsilon$  relationships for the FRC layer.

Based on experiences from these investigations, some suggestions on further work can be made:

- Prepare and perform an extended experimental program on similar hybrid concrete beams. The experimental program should provide detailed information about the beam, hence, more instrumentation and additional tests are needed.
- Numerical analyses using interface elements in order to investigate the zone between the different concrete layers.
- Numerical analyses using a discrete crack approach.

Due to different shrinkage properties for the concrete layers, an investigation of the long-term behaviour of such hybrid beams should also be performed as further work.

## 8. ACKNOWLEDGEMENT

The research presented in this paper is financed by **COIN – The Concrete Innovation Centre** – which is a centre for research based innovation with funding from the Norwegian Research Council and industrial partners. The program period is from 2007 to 2014. The vision of **COIN** is creation of more attractive concrete buildings and structures. Attractiveness implies aesthetics, functionality, sustainability, energy efficiency, indoor climate, industrialized construction,



improved work environment, and cost efficiency during the whole service life. The host for COIN is SINTEF in Trondheim with NTNU as the leading academic partner. The corporate partners are leading multinational companies in the cement and building industry [3].

## REFERENCES

1. Thomassen L. and Thue T. "Hybrid concrete structures". Master thesis at Department of Structural Engineering, NTNU, Trondheim, Norway. June 2007 (in Norwegian).
2. Diana – Finite Element Analysis. Release 9. 2005. TNO Diana bv. The Netherlands.
3. COIN -Concrete Innovation Centre- a centre for research based innovation with funding from the Norwegian Research Council and industrial partners. [www.sintef.no/coin](http://www.sintef.no/coin)
4. NS3473 Norges Standardiseringsråd (2003): "Concrete structures – Design and detailing rules", Norwegian Standard Institution.
5. Thorenfeldt E., Fjeld S. et.al. (2006): "Stålfiberarmering i betong. Veiledning for prosjektering, utførelse og kontroll" (in Norwegian). Draft.
6. Sandbakk S., Døssland Å.L. and Kanstad T. "Pull-out testing of different fibre types," Proceedings of the Nordic Miniseminar: Fibre-reinforced concrete structures, NTNU, Trondheim, Norway. November 2007.
7. Vecchio, F. J., Collins, M. P., "The modified compression field theory for reinforced concrete elements subjected to shear". *ACI Journal* 83, 22 (1986), 219-231.
8. Feenstra, P. H., "Computational aspects of biaxial stress in plain and reinforced concrete". PhD thesis, Delft University of Technology, The Netherlands, 1993.
9. Kanstad, T., Hammer, T.A., Bjøntegaard, Ø. and Sellevold, E.J. "Mechanical properties of young concrete: Part 2: Determination of model parameters and test program proposals" *Materials and structures*. Vol. 36, May 2003, pp 226-230.

## Design methods for fibre-reinforced concrete: a state-of-the-art review



Anette Jansson, PhD student  
 Kent Gylltoft, Professor  
 CHALMERS University of Technology  
 Dept. of Civil and Environmental Engineering,  
 Div. of Structural Engineering  
 412 96 Göteborg, Sweden  
 E-mail: [anette.jansson@chalmers.se](mailto:anette.jansson@chalmers.se)

Ingemar Löfgren, Thomas Concrete Group AB,  
 Göteborg, Sweden



### ABSTRACT

The increasing interest in the use of fibre reinforcement has created a need for established design and analysis methods. Fibre reinforcement is mainly used in applications such as industrial floors and sprayed concrete, although other application areas exist. Apart from increased load-carrying capacity, one of the main benefits of adding fibres to concrete is the potential reduction in crack width, which depends on the amount of fibres added and positively affects the durability of the finished structure. By comparing ten design methods proposed by technical committees, this paper provides a basis for further research aimed at developing a common design basis. Evaluation is based on the way the fibre capacity is considered. In addition, a “good” design method should also consider all (or most) design situations. It was found that, for design, the Italian proposal provides comprehensiveness. However, some amendments are needed, e.g. a suggestion is that the proposed formula for calculating crack width/crack spacing should be modified to include the residual tensile strength.

**Key words:** Fibre-reinforced concrete, design methods, state-of-the-art review

### INTRODUCTION

Fibre-reinforced concrete (FRC) is a cement-based composite material reinforced with discrete, usually randomly distributed, fibres. Fibres of various shapes and sizes produced from steel, synthetics, glass, and natural materials can be used. However, for most structural purposes, steel fibres are the most used of all fibre materials, whereas synthetic fibres (e.g. polypropylene and nylon) are mainly used to control the early cracking (plastic-shrinkage cracks) in slabs [1]. Fibre reinforcement mainly enhances the post-cracking properties of concrete and leads to a more ductile material behavior. The increased ductility is due to the ability of the fibres to transfer tensile stresses across a cracked section, potentially leading to a reduction in crack widths. The extent of the crack-width reduction depends on the amount of fibres added as well as their

physical properties (e.g. surface roughness and chemical stability) and mechanical properties (e.g. tensile strength).

Typical applications where steel fibres may be used as sole reinforcement include slabs on grade and tunnel linings. In other applications the steel fibres are used as a complement to the conventional reinforcement, where, in some cases, the amount of conventional reinforcement can be reduced. Extensive research has been carried out by technical committees in several countries, such as RILEM TC 162-TDF [2], [3] and CNR-DT 204/2006 [4], which has resulted in recommendations/guidelines for design of steel-fibre-reinforced concrete (SFRC). Although the use of SFRC in structural applications is already a common practice within the construction field, generally accepted design methods have not yet been established. Due to this, many engineers are hesitant to use SFRC. If the technique with fibre-reinforced concrete is to be further developed and accepted by practicing engineers, the concrete community should agree about the design methods to use, refine them, and introduce them in codes.

This paper is a summary of the report "Analysis and design methods of fibre reinforced concrete: a state-of-the-art report", [5], where by means of comparing and evaluating several proposals for design as well as analysis methods, the objective was to create a basis for further research aiming at finding/developing a generally accepted design method. Criteria for evaluating the methods were the way the material characteristics are determined together with how different load situations are treated (e.g. comprehensiveness), with emphasis on the way the fibre capacity is considered.

## 1 BACKGROUND

Combining concrete with dispersed "fibres" consisting of grains of steel left-overs is an idea patented already in 1874 by the American A. Berard, thus creating a new more ductile material. Today steel and synthetic fibres are used for both non-structural and structural purposes. Although it has been found that adding fibres to concrete mainly enhances the post-cracking properties in terms of a more ductile behaviour and reduced crack widths (e.g. Stang & Aarre [6] and Löfgren [1]), it still remains to show that these enhanced mechanical properties can be predicted with reasonable accuracy and that they can be incorporated into design methods.

Many attempts have been made to develop methods/models which can predict the behaviour (especially in bending) of fibre-reinforced concrete members, e.g. Zhang & Stang [7], Lok & Xiao [8] and Casanova & Rossi [9]. Two main approaches may be identified: (1) obtaining material properties by testing, or (2) estimating material properties on a theoretical basis (e.g. [8]). The obtained material properties may be used in e.g. FEM analyses (often based on fracture mechanics), e.g. [7], or analytical models e.g. based on the non-linear hinge concept as in [9]. One theory based on the theoretical approach is that if the pull-out behaviour of one fibre can be described, then by considering different factors, the behaviour of a specimen with randomly distributed fibres can be described. These factors can be e.g. the shape and size of the concrete specimen, the orientation and amount of fibres added, and the geometrical and mechanical properties of the fibres, e.g. length and cross-sectional shape. To estimate how effective the fibres are in a certain FRC mixture, a so-called fibre-efficiency factor can be estimated. One proposed method to consider this factor for differently shaped and sized specimens can be found in Voo and Foster [10] and also in the Norwegian guidelines [11]. In general the fibre-efficiency factor depends on the number of fibres that bridge a crack (calculated or estimated) and the fibre orientation (i.e. the fibre alignment with reference to the crack surface). Additionally, it

considers the thickness and height of the specimen in relation to the fibre geometry and amount of fibres added. In a small flat body (1-D) this factor is 1.0, compared to an infinitely large body (3-D), where it theoretically may be estimated as 0.5.

To derive the material properties used in the currently available design methods, several test methods can be used, although the bending test is the most frequently recommended (e.g. [2]). Since this test method yields results in the form of flexural capacities (bending load–CMOD or bending load–deflection) (CMOD = crack-mouth-opening displacement), and the calculation methods usually require direct tensile capacities, a translation method is needed. A question which arises is how to perform this translation in the best possible way. All of the reviewed design methods propose similar methods for how the flexural strength can be translated into direct tensile strength. The differences between the methods can be found in the coefficient used to translate flexural stress into tensile stress and in the way measured crack opening is translated into strain. In one respect the Italian method takes a step forward compared to the other methods, by the introduction of a so-called characteristic length  $l_{cs}$ , which depends on the calculated average crack spacing, or either the height of the tensile zone if conventional reinforcement is present or without rebars  $l_{cs}$  = the cross-section height [4] .

## 2 METHODOLOGY

A systematic line-up of the contents makes it possible to compare the different methods step by step. It should be kept in mind, though, that not all of the investigated documents are first-hand material. Comparisons are made between the assumptions made for each method in total as well as between the different design situations each method considers.

With crack-width reduction being one of the main benefits from fibre reinforcement, and since the size of those benefits (that can be utilized in design) is governed by the assumptions on which the stress-strain diagram is based, these are especially examined and compared with the ones for the stress-crack-width based method. Furthermore, since the final fibre capacities are determined by the characteristic values of the residual strengths, also the procedures of how to determine these values are given extra attention.

## 3 RESULTS AND COMMENTS

For details on the notations used in section 4 the reader is referred to each specific reference.

### 3.1 Classification of the design methods

In the attempts to provide material properties for design of FRC members, different approaches have been proposed by the technical committees reviewed in this paper. Although some differences are noticeable, the proposals can be classified into two basic approaches, namely:

- The  $\sigma$ - $\varepsilon$  method, where testing yields a load–deflection or load–CMOD relationship, where either the load at predefined deflections/CMODs, or the area beneath the curve up to a predefined deflection, is the basis for residual or equivalent flexural strengths. The chosen deflections or CMODs are translated into strains and the residual (or equivalent) flexural strengths are translated into direct tensile strengths.

- The  $\sigma$ - $w$  method, where testing yields a load–crack width relationship which is mainly used directly in formulations for fracture mechanics.

When comparing the two basic approaches ( $\sigma$ - $\varepsilon$  and  $\sigma$ - $w$ ) it is obvious, from the viewpoint of simplicity for practical design, that the stress-strain-relationship method is faster and less complicated. On the other hand, one can question the accuracy of the values representing the stress-strain diagram (discussed in section 5).

### 3.2 Applicability

All of the investigated proposals are valid for FRC with strain-softening behaviour and are mainly intended for design using steel fibres, although the Italian proposal is valid also for FRC exhibiting strain hardening, and may be applied to other types of fibres besides steel. Strain (or deflection) softening refers to a material which exhibits a decreasing stress level after the cracking, whereas a strain (or deflection) hardening material increases its load-bearing capacity after cracking, and additionally more but smaller cracks are produced; see Figure 1. Strain softening/hardening refers to a direct tensile response while deflection softening/hardening refers to a flexural response.

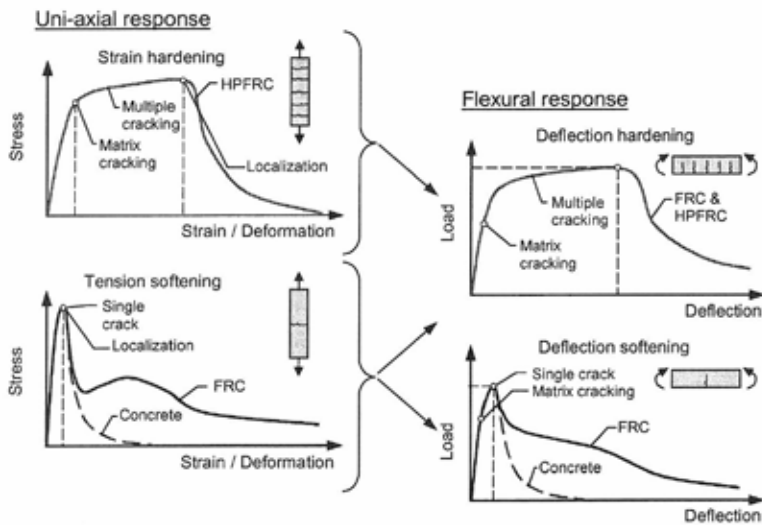


Figure 1 - Characterization of the tensile and flexural behaviour. From Löfgren [1].

### 3.3 Material properties

Typically the compressive strength of a fibre-reinforced concrete material is assumed comparable to that of regular (plain) concrete, while the flexural tensile strength is usually determined directly from bending tests or empirically from the compressive strength. The residual flexural strength, on the other hand, may only be determined from test results, which for the  $\sigma$ - $\varepsilon$  methods are based on bending of beam or plate specimens. For design, in a majority of the reviewed proposals, a stress-strain relationship similar to the one shown in Figure 2 is used. The relationship is based on direct tensile stress, and thus the flexural test results are translated into direct tensile strengths according to expressions given in the proposed methods; see Figure

3 for an example of how the direct tensile stress may be obtained. The strain values in a stress-strain relationship must be determined from measured crack openings or deflections, where for instance the crack opening is divided by a so-called characteristic length to obtain the strain. How to choose the characteristic length is not completely straightforward when it comes to fibre-reinforced concrete. In the Italian proposal [4] there are some suggestions, but it should be kept in mind that this choice greatly affects the calculated load capacity; see Jansson [12]. For the  $\sigma$ - $w$  approach by RILEM, a uniaxial tension test may be used to directly obtain the  $\sigma$ - $w$  relationship after cracking.

In order to determine the nominal residual strength, the load is often measured at two predetermined deflections or CMODs, e.g. as in Figure 4. The first of these values is then used to determine the residual strength for the serviceability limit state (SLS) and the second is used for the ultimate limit state (ULS), e.g. [2], [4] and DAfStb [13], [14]. A common formula to determine the residual flexural tensile strength from the load measured in a three-point bending test is shown in Eq.1. Another approach is to determine an equivalent residual strength. The procedure is basically the same, only here the area beneath the load-deformation curve (i.e. energy dissipation) is used to calculate either one average value which is valid for all design stages (e.g. DBV Merkblatt for industrial floors [15]), or else one value for the SLS and one for the ULS. Examples of the latter can be found in DBV Merkblatt for tunnel applications; see [15].

$$f_{R,J} = \frac{3F_{R,J}L}{2bh_{sp}^2} \quad (1)$$

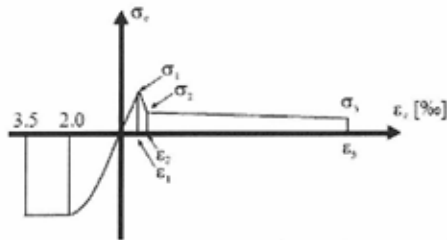


Figure 2 - Stress-strain relationship according to RILEM TC 162-TDF. [2]

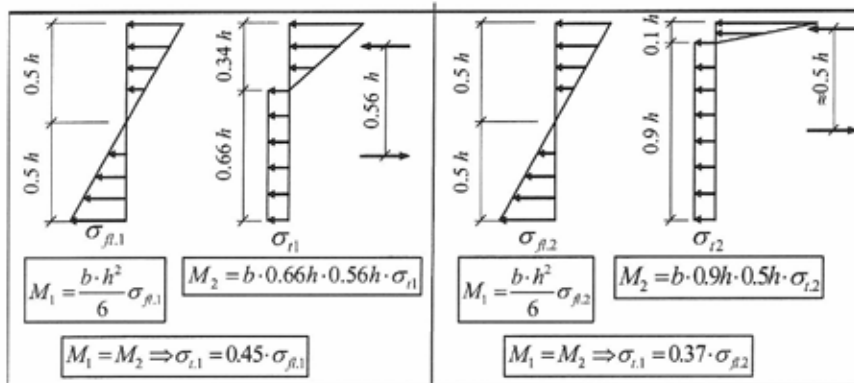


Figure 3 - Assumed stress distributions – the top figures for small crack widths (i.e. SLS) and the lower figures for large crack widths (i.e. ULS). [2] (modified).

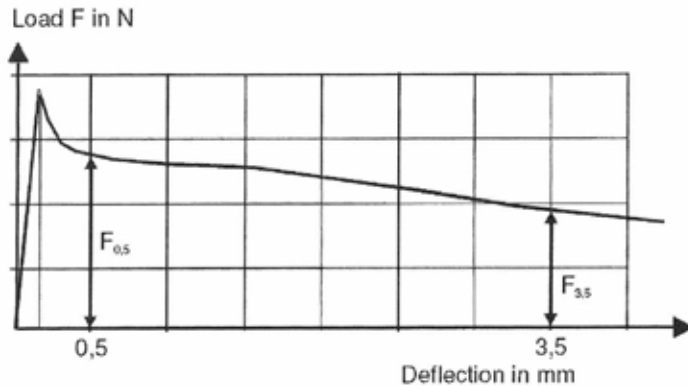


Figure 4 - Example of a load–deflection diagram from bending test. [13]

### 3.4 Test methods

The most recommended method to determine the residual strength is the bending test, which can be performed in various ways, e.g. as three- or four-point loading, using either notched or unnotched test specimen. Testing is performed on prisms with width and height ranging from 75 to 150 mm, and a length from 550 to 750 mm. Technically speaking a bending test is relatively simple to perform. The difficulties arise when the obtained flexural strength needs to be translated into direct tensile stress and, similarly, when translating the measured crack opening displacement or deflection into a strain value. Since a majority of the reviewed design methods are based on a relationship between direct tensile stress and strain, this translation procedure needs to be performed frequently. Other test methods may be used according to some proposals, e.g. the plate test which is recommended by SIA 162/6 [15], and the uniaxial tension test, which is one of the two options in the Italian proposal [4].

Besides the difficulty with the bending test mentioned above, a second drawback is the large scatter in the test results. This is partly due to the nature of fibres, i.e. randomly distributed fibres do not allow the same control of the exact location of the reinforcement (contrary to conventional reinforcement); but it also owes to the small size of the test specimens in comparison with the size of the structural members they represent. In contrast, the plate test, where the test specimen is larger (i.e. with a larger crack area), will yield less scatter in the results; see Lambrechts [16].

### 3.5 Safety concept

Due to the large scatter in the test results for fibre-reinforced concrete beam specimens tested in bending, a characteristic value derived from the commonly used statistical approach may result in rather low strength values. Testing of FRC members has shown that small test specimens generally yield more scatter than larger specimens; see e.g. Lambrechts [16] and Kooiman [17]. For a specimen that exhibits large scatter in the test results, a greater number of tested specimens is required in order to obtain a characteristic value comparable to that obtained from a method that exhibits less scatter. Since the test specimens in most cases are significantly smaller than the structural member they represent, a characteristic value based solely on the 5% fractile seems to

describe the residual strength inadequately. On the other hand, in real structures, problems may arise due to inhomogeneous fibre distribution, which depends on the casting technique and the concrete composition.

The negative effect of the large scatter obtained from a small test specimen seems to have been considered in some of the methods, e.g. in DBV Merkblatt for industrial floors, where the characteristic equivalent flexural tensile strength is instead taken as the 20% fractile.

However, the most advanced improvement in the estimation of a characteristic value can be found in the Italian recommendation. The characteristic tensile values are obtained through a statistical approach referring to the 5% fractile, although with some improvements. In addition to the standard deviation and the number of test specimens, also the size of the test specimen and the size and type of the structure to be designed are considered by introducing a factor,  $\alpha$ , which depends on the total area (or volume) where cracking is expected. The characteristic value is then obtained by subtracting the adjusted standard deviation,  $s$ , from the mean value as:  $f_{Ftk} = f_{Fm} - \alpha \cdot k \cdot s$ , with  $k$  referring to the 5% fractile, but where  $\alpha$  leads to a more refined determination of the characteristic value.

In other recommendations the statistical approach is not used when determining characteristic post-cracking strength, but instead 70% of the mean value is used. This may be expressed as  $f'_{Rtk} = 0.70 \cdot f_{Rim}$  as in DAFStb [13] and similarly in the recommendation by Bekaert [18]. According to SIA 162/6 [15], the characteristic value for the tensile strength is taken as the mean value of at least three specimens if based on plate testing; if based on beam bending, the standard statistical approach is used here as well.

Since FRC is often used in statically indeterminate structures, the method of using the 5% fractile, without any consideration of what type of structure is to be analyzed, seems less suited. To utilize the extra capacity provided by the fibres in the best possible way, a test method which yields a smaller scatter than those currently existing is needed, or alternatively a new way of interpreting the results. Possibly the structure could be looked upon as a system where the load resistance is not governed by the "weakest link", but depends on the ability of the structure to redistribute forces. This means that e.g. the capability of an indeterminate structure to redistribute loads, i.e. the gradual formation of plastic hinges, as well as the probability of the capacity being governed by the weakest area, are considered in the design.

### 3.6 Calculation of crack width / crack spacing

Addition of fibres to a concrete matrix affects the crack width positively and in addition, e.g. for large amounts of fibres, crack distribution with only fibre reinforcement may be achieved. The formulae for calculation of crack width, found in ENV 1992-1-1 [19] (Eq.2) and EN 1992-1-1 [20] (Eq.3), are intended for conventional concrete, i.e. concrete without fibre reinforcement.

$$w_k = \beta s_{rm} \varepsilon_{sm} \quad (2)$$

$$w_k = s_{r,max} \cdot (\varepsilon_{sm} - \varepsilon_{cm}) \quad (3)$$

$$\text{where } (\varepsilon_{sm} - \varepsilon_{cm}) = \frac{\sigma_s - k_1 \frac{f_{ct,eff}}{\rho_{p,eff}} (1 + \alpha_e \rho_{p,eff})}{E_s} \geq 0.6 \frac{\sigma_s}{E_s} \quad (4)$$



In order to account for the positive effects of the fibres, attempts have been made to adapt the formula in [19] for calculation of crack width to be applicable also for fibre-reinforced concrete; see RILEM [2] and Italy [4]. Both [2] and [4] propose a change in the formula for computing the crack spacing,  $s_{rm}$ . The modification made by [2] considers the fibre-aspect ratio ( $l_f / d_f$ ), where the original formula in [19] for crack spacing is multiplied by a factor ( $50 d_f / l_f$ ) with 1.0 as upper limit; see Eq.5. The modification according to [4] is similar, but here also a lower limit for the multiplication factor is given.

$$s_{rm} = \left( 50 + 0.25 k_1 k_2 \frac{\phi_b}{\rho_r} \right) \left( \frac{50}{L / \phi} \right) \quad (5)$$

In the German standard for regular concrete, DIN 1045-2, a similar formula for calculation of crack width as in EN 1992-1-1 [20] is found (Eq.3-4). In the Draft 2005 for DafStb changes in both parts of the formula are proposed, i.e. both in the part referring to crack spacing and in the part referring to strain difference. The characteristic crack width,  $w_k$ , is calculated as:

$$w_k = s_{r,max} \cdot (\varepsilon_{sm}^f - \varepsilon_{cm}) \quad (6)$$

with:

$$\varepsilon_{sm}^f - \varepsilon_{cm} = \frac{\sigma_s - (0.4 + 0.6 \cdot \alpha_f) \frac{f_{ct,eff}}{eff\rho} \cdot (1 + \alpha_c \cdot eff\rho)}{E_s} \geq 0.6 \cdot (1 - \alpha_f) \frac{\sigma_s}{E_s} \quad (7)$$

in which the fibre contribution is represented by  $\alpha_f$ , obtained as:

$$\alpha_f = \frac{f_{ctR,LI}^f}{f_{ctm}} \quad (8)$$

and  $\sigma_s$  is the steel stress at the crack without consideration of the fibre effect. (Also in the term  $s_{r,max}$  the fibres are accounted for. Details are omitted here due to incomplete information.)

Remaining parameters can be found in DafStb Draft 2005 (DIN 1045-1). In DafStb for SFRC structural members without conventional reinforcement (in case the required minimum reinforcement area  $\leq 0$ ), the crack width can be calculated as:

$$w_k = 0.140 \cdot \varepsilon_{ct}^f \quad (9)$$

where  $\varepsilon_{ct}^f$  is the strain in the SFRC.

Another way of calculating crack widths in FRC members is proposed in the Norwegian guideline [11], where the same formulae as found in the Norwegian standard NS 3473 for regular concrete are used, although the stresses and strains should be derived considering the contribution from the fibres.

### 3.7 Bending with or without axial force

For structural members reinforced with fibres only, all of the reviewed recommendations consider the residual strength from the fibres when calculating the flexural capacity. In all but the  $\sigma$ - $w$  method by RILEM [3] and DBV Merkblatt for industrial floors [15], the calculations are then based on simplified stress-strain relationships similar to the one shown in Figure 5a. In the case of members reinforced with a combination of fibres and conventional longitudinal reinforcement, though, the Swedish recommendation [21] does not acknowledge the extra capacity provided by the fibres. In that case the fibres are assumed to be pulled out or fractured long before the reinforcement bars are activated; thus the fibre contribution is omitted and the calculations are based on existing formulas for regular concrete. The majority of the

recommendations bases their calculations on a simplified, uniformly distributed cross-sectional residual stress distribution (in addition to the conventional steel stress if applicable); see e.g. Figures 3 and 6. The stresses and strains are obtained from the specific stress-strain diagram each method has adopted; see e.g. Figure 5 and 9. Among the reviewed recommendations, different heights are assumed for the cracked section over which the residual stresses are distributed. In the Norwegian method, though, in the presence of conventional reinforcement, the height of the compressive zone should be calculated according to Norwegian standards for plain concrete [11].

Following the Italian recommendations [4], the ultimate moment capacity  $M_{Rd}$ , for a fixed value of the applied design axial force  $N_{Sd}$ , can be evaluated by means of the equilibrium equations for translation and rotation. Additionally it may be done with reference to the stress-strain distributions shown in Figure 6 and in accordance either with the Italian standard for regular concrete or with ENV 1992-1-1 [19], by adopting the simplified stress-strain relationship shown in Figure 9, where a simplified stress block method may be used with the stress on the crack surface equal to  $f_{Fu} / \gamma_F$ , where  $f_{Fu}$  is the residual tensile strength.

To determine bending moment and axial force in the ultimate limit state (ULS) according to the  $\sigma$ - $\varepsilon$  approach by RILEM, [2], the stresses in the SFRC member are obtained from the adopted stress-strain diagram (Figure 5a), which is based on the flexural strength and flexural tensile strengths given by the beam bending test. To compensate for unrealistic values related to the size of the test specimen, when calculating with the proposed design method, a size factor  $\kappa_h$  has been introduced (Figure 5b). For the  $\sigma$ - $w$  approach by RILEM [3], the loads and deflections are obtained by describing the cracked area as a non-linear hinge; they prescribe the total angular deformation of the hinge having a length  $s$  and then solve the sectional forces by use of equilibrium equations. The method can be used for members with or without conventional reinforcement.

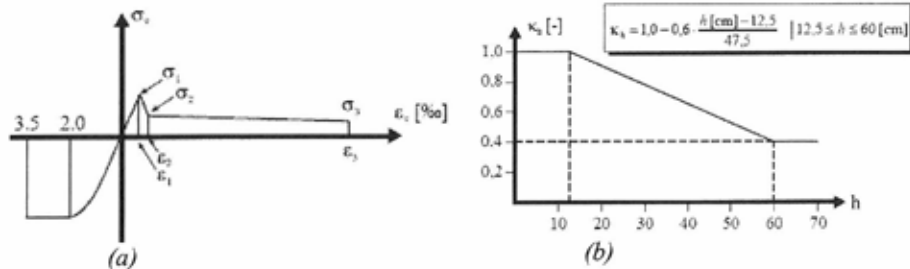


Figure 5 - Stress-strain diagram (a) and size factor  $\kappa_h$  (b). [2]

According to DBV Merkblatt [15] for industrial floors there are two concepts for the design application of SFRC: calculation in the uncracked state and calculation in the cracked state. The former concept is based on elastic theory and it should be verified that the stresses can be sustained by the uncracked concrete section. In this case the occurring stresses must not exceed the calculated value of the characteristic (5%-fractile) flexural tensile strength  $cal \beta_{BZ}$ . For the latter, i.e. calculation in the cracked state, the energy absorption capacity is accounted for and it should be verified that the stresses occurring in the cracked regions do not exceed the value of the characteristic (20%-fractile) equivalent flexural tensile strength,  $nom \beta_{BZ}$ . The stresses have to fulfil:

$$\kappa_N \frac{N_u}{A_0} + \frac{M_u}{W_0} \leq \text{cal} \beta_{BZ} \text{ or } \leq \text{nom} \beta_{BZ}, \text{ depending on the actual state.} \quad (10)$$

$N_u$  = axial force in the ultimate state,  $\kappa_N = 2.0$  for tensile force,  $\kappa_N = 1.0$  for compressive force,  $M_u$  = bending moment in the ultimate state,  $A_0$  = cross-section area of the steel fibre slab and  $W_0$  = section modulus of the steel fibre slab.

For DBV Merkblatt tunnel applications, similar assumptions as seen in Figure 5a and Figure 8 may be used.

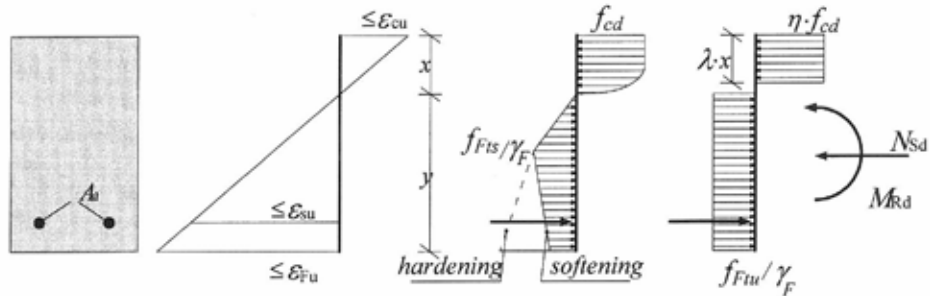


Figure 6 - Assumed cross-sectional strains and stresses for use in the ultimate limit state.  $\epsilon_{su}$  is maximum strain in the reinforcement, and  $\epsilon_{cu}$  is maximum strain in the FRC material; see also Figure 9. Simplified stress/strain relationship; stress-block with coefficients  $\eta$  and  $\lambda$  in accordance with ENV 1992-1-1 [19]. [4]

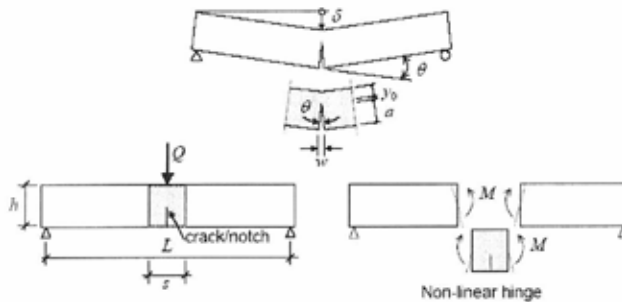


Figure 7 - Non-linear hinge for a beam without reinforcement. [1]

All the recommendations propose that if the member is subjected to both bending and axial force, the loads should be limited according to the  $M-N$  diagram shown in Figure 8, where the principal effect of increasing residual stresses is shown.

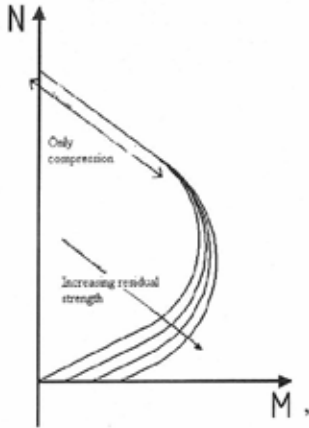


Figure 8 - The effect of steel fibres on an M-N diagram, schematically shown. [11]

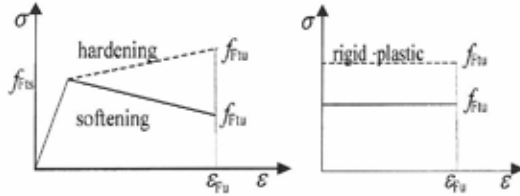


Figure 9 - Simplified stress-strain constitutive relationships. [4]

### 3.8 Shear

Regarding shear, in most of the recommendations the fibre contribution is accounted for by an additional term,  $V_{fd}$ , which is added to the formula used for shear capacity of regular concrete. A majority of the investigated methods base the fibre contribution,  $V_{fd}$ , on a fraction of the residual strength (expressed as  $\tau_{fd}$ ); see RILEM [2], Swedish Betongrapport nr 4 [21], DafStb [13], and DRAMIX [18], as exemplified in Eq.11 from [2]. A similar method is proposed in the Norwegian recommendations [11], only here the residual strength,  $f_{fd, res}$ , is used directly (Eq.12).

$$V_{fd} = 0.7 k_f k_1 \tau_{fd} b_w d \quad (11)$$

$$V_{fd} = 0.8 \cdot f_{fd, res} b d \quad (12)$$

For most of the investigated methods, the contribution of fibres to the shear capacity is only considered for members with fibres in combination with conventional reinforcement. E.g. according to the  $\sigma$ - $\varepsilon$  method by RILEM [2] it is determined as  $\tau_{fd} = 0.12 f_{Rk,4}$ , where  $f_{Rk,4}$  is the characteristic residual strength for the ultimate limit state. Also in the  $\sigma$ - $w$  approach by RILEM [3], the contribution of fibres to the shear capacity is considered only for members with fibres in combination with conventional reinforcement, but here the fibre contribution is calculated from the design stress-crack opening relationship at a certain crack width as:

$$V_{fd} = b z \bar{\sigma}_{pd}(w_m) \quad (13)$$

where  $z$  is internal level arm and  $\bar{\sigma}_{pd}(w_m)$  is the mean design residual stress between crack widths zero and  $w_m$ .

According to the Italian guidelines [4] the fibre contribution may be accounted for also in members without longitudinal reinforcement and without shear reinforcement, although in this case it is recommended that only FRC with hardening tensile behaviour should be used. Here, instead of estimating a separate capacity for the fibre contribution (as in a majority of the reviewed methods) and then adding the extra term to the shear-capacity formula for regular

concrete, the FRC is considered as one material and the formula for shear capacity found in EN 1992-1-1 (Eq.14) is modified with regard to the residual capacity provided by the fibres (Eq.15).

$$V_{Rd,c} = \left\{ \frac{0.18}{\gamma_c} \cdot k \cdot [100 \cdot \rho_1 \cdot f_{ck}]^{1/3} + 0.15 \cdot \sigma_{cp} \right\} \cdot b_w \cdot d \quad [MPa] \quad (14)$$

$$V_{Rd,F} = \left\{ \frac{0.18}{\gamma_c} \cdot k \cdot \left[ 100 \cdot \rho_1 \cdot \left( 1 + 7.5 \cdot \frac{f_{Fmk}}{f_{ck}} \right) \cdot f_{ck} \right]^{1/3} + 0.15 \cdot \sigma_{cp} \right\} \cdot b_w \cdot d \quad [MPa] \quad (15)$$

## 4 DISCUSSION AND SUGGESTIONS

Comparison of different design methods reveals that there are many similarities. Most of them recommend bending tests to determine material properties and then translate the obtained flexural stresses into direct tension (the Swedish recommendation excepted), and all but the  $\sigma$ - $w$  method by RILEM use simplified stress-strain relationships. One of the difficulties with a method based on a stress-strain relationship, with the material parameters obtained from bending tests, is the translation of flexural properties into direct tension properties. Here the Italian recommendation has taken a step forward by the introduction of a so-called characteristic length, which considers the fibre-aspect ratio. However, the question regarding the translation factors as well as the choice of representative strain values, for the SLS and ULS respectively, remain.

### 4.1 Characterization of material parameters

If a bending test is the only option, for the stress-strain approach, the most suitable parameter to characterize the post-cracking strength seems to be the equivalent flexural tensile strength (based on Barros et al. [22]). The question still remains, though, of how to translate a flexural value into a tensile value as well as how to translate deflections or CMODs into strains. There seems to be a need for more research aimed at determining the translation factors and studying how these depend on the material properties. From a strict scientific viewpoint, the optimal method to obtain the material parameters in tension ought to be by performing a tension test, if disregarding the difficulties with the test setup. The stress-crack width relationship can directly be used for calculations if using e.g. the hinge method. If the chosen design method requires a stress-strain relationship, then of course here too the question arises of how to translate the measured crack widths into strain values.

For calculations in the serviceability state, a method which describes the material behavior at small crack widths without large simplifications would be preferable, i.e. in order to best utilize the ability of the fibres to reduce crack widths. Theoretically this could be achieved with the  $\sigma$ - $w$  method.

### 4.2 Design method

The Italian recommendation appears to provide the most comprehensive design tool. Material properties are obtained from beam bending tests, from which values for residual flexural strength may be either chosen as point values, or based on the mean load measured within a specified interval. Alternatively a uniaxial tension test may be used to derive the material properties.

By the introduction of a characteristic length for determination of the strain values from the measured crack openings, this method takes one step forward compared to the other reviewed methods, as it also opens up for calculations using the finite element method. The characteristic length depends on either actual specimen size, crack spacing, or the type of analysis tools used (e.g. FEM and type of constitutive model). It should be kept in mind, though, that for FRC the choice of characteristic length is not as straightforward as for plain concrete and the choice of this parameter greatly affects the calculated load capacity.

Another improvement, compared to the other reviewed methods, is in determining characteristic values for the residual strength. Although the lower 5% fractile is used, the method also considers the size and type of the actual structure. Furthermore, the calculation of crack width/crack spacing for regular concrete is modified to account for the fibre contribution by considering the fibre-aspect ratio,  $l_f / d_f$ . One suggestion, though, is that the method for calculation of the crack spacing/width ought to be modified in accordance with the proposal by Löfgren found in Gustafsson and Karlsson [23].

It should be mentioned that the stress-strain relationships are simplified. This means that FRC with high fibre contents is not represented in the best way. In addition, the simplifications imply that the method is somewhat restricted as regards calculations at small crack widths, i.e. it is better suited for rough calculations (e.g. in the ultimate limit state).

### 4.3 Safety considerations

Due to the quite large scatter in the test results for an FRC material, a different approach (as opposed to regular concrete) should be used when determining the design strength values. Since quite small test specimens are used, in order to utilize the post-cracking strength of FRC, a characteristic value based on the 5% fractile of a test population may be on the conservative side. This is especially true for statically indeterminate structures, where redistribution can occur; here the characteristic value of the post-cracking strength could be chosen closer to the mean value. Regarding the safety coefficient, it seems an acceptable proposal to follow the recommendations given in EC2 for regular concrete. However, to be able to determine a characteristic value in such a way that the capacity of the fibres is utilized as well as possible, more research is needed.

### 4.4 Areas for improvement

Barros et al. [22] analyzed the  $\sigma$ - $\varepsilon$  method proposed by RILEM TC 162-TDF [2] and found poor correlation between experimental values and values predicted by use of the proposed  $\sigma$ - $\varepsilon$  diagram. Three-point bending tests on notched beams were carried out to derive residual and average flexural tensile strengths ( $f_R$  and  $f_{ctm,n}$ ) from the obtained load-deflection curves. By adopting the proposed  $\sigma$ - $\varepsilon$  relationship, attempts were made to simulate the experimental load-deflection curves. Two types of hooked-end steel fibres were used, and the results from both of them showed quite poor correlation between the load-deflection curves predicted by the proposed  $\sigma$ - $\varepsilon$  relationship and those obtained from the beam bending tests. Barros et al. [22] proposed a new set of transformation parameters for obtaining the values of the  $\sigma$ - $\varepsilon$  diagram. It should be mentioned that in [13] these parameters may adopt varying values within each performance class (i.e. serviceability or ultimate limit state).

Furthermore, the procedure to determine the initial slope of the load–deflection curve is subjective and may lead to an incorrect value of the load at the limit of proportionality. This leads to incorrect values of  $f_{ct}$  and possibly incorrect estimation of the post-cracking strengths; see e.g. [24]. In addition, when determining the points/design values for the  $\sigma$ - $\varepsilon$  diagram, the residual stresses are assumed to be distributed uniformly over a cross-section height of  $0.66h_{sp}$  or  $0.9h_{sp}$ , where the residual strengths are  $f_{R1}$  and  $f_{R4}$  respectively; see Figure 3. This assumption might be questioned, since different fibre contents (as well as different specimen heights) lead to different depths of cracked section; see e.g. [25]. It should be mentioned, though, that the  $\sigma$ - $\varepsilon$  approach by RILEM is probably the most evaluated method; hence its drawbacks are well known.

The modifications in calculation of crack spacing/width by [2] and [4] only consider the type of fibre (through  $l_f / d_f$ ). In reality this means that a fibre amount  $V_f = 0.5\%$  would yield the same effect on the crack spacing as  $V_f = 2\%$ , which is quite unlikely. A possibly better approach in the serviceability limit state would be to actually consider the material characteristics, in this case the residual tensile strength, at an approximate crack opening of  $w \approx 0.2$  mm; see [23]. The residual tensile strength depends on fibre content  $V_f$ , aspect ratio, and  $l_f / d_f$  among other factors. Gustavsson and Karlsson [23] investigated and compared the calculation for crack spacing according to [2] with a proposal made by Löfgren (described in the same report).

However, the question of how to calculate the crack spacing / crack width was discussed at the FRC workshop that was held at the Framcos-6 conference in Catania, Italy, on 22 June 2007. [26] It was acknowledged that, in addition to the fibre-aspect ratio, also the fibre amount needs to be considered (i.e. material characteristics).

## 5 REFERENCES

1. Löfgren, I. "Fibre-reinforced Concrete for Industrial Construction-a fracture mechanics approach to material testing and structural analysis". PhD Thesis, Dep. of Civil and Environmental Engineering, Chalmers University of Technology, Göteborg, 2005, 268, pp.
2. RILEM TC 162-TDF. "Test and design methods for steel fibre reinforced concrete,  $\sigma$ - $\varepsilon$  design method.(Chairlady L. Vandewalle)." *Materials and Structures / Matériaux et Constructions*, Vol. 36, 2003, pp. 560-567.
3. RILEM TC 162-TDF. "Design of steel fibre reinforced concrete using the  $\sigma$ - $w$  method – principles and applications (Chairlady L. Vandewalle)." *Materials and Structures*, Vol. 35, No., June 2002, pp. 262-278.
4. CNR-DT 204/2006. "Istruzioni per la Progettazione, l'Esecuzione ed il Controllo di strutture di Calcestruzzo Fibrorinforzato". design recommendation, Rome, Draft 2006, 59, pp.
5. Jansson, A. "Analysis and design methods for fibre reinforced concrete: a state-of-the-art report." Dep. of Civil & Environmental Engineering, Div. of Structural Engineering/Concrete structures, Chalmers University of Technology, 2007:16, Göteborg, 2007, 196.pp.
6. Stang, H. and Aarre, T. "Evaluation of Crack Width in FRC with Conventional Reinforcement." *Cement & Concrete Composites*, Vol. 14, 1992, pp. 143-154.
7. Zhang, J. and Stang, H. "Applications of stress crack width relationship in predicting the

- flexural behaviour of fibre-reinforced concrete." *Cement and Concrete Research*, Vol. 28, No. 3, dec 1998, pp. 439-452.
8. Lok, T. and Xiao, J. "Flexural strength Assessment of steel fiber reinforced concrete." *Journal of Materials in Civil Engineering*, Vol. 11, No. 3, aug 1999, pp. 188-196.
  9. Casanova, P. and Rossi, P. "Analysis and design of steel fiber reinforced concrete beams." *ACI Structural Journal*, Vol. 94, No. 5, 1997, pp. 595-602.
  10. Voo, J. Y. L. and Foster, S. J. "Variable engagement model for fibre reinforced concrete in tension." School of Civil and Environmental Engineering, University of New South Wales, Australia, UNICIV Report R-420, 2003, 87.pp.
  11. Thorenfeldt, E., Sandaker, T., Bosnjak, D., Martinsen, T., Olsen, O., Maage, M., and Fjeld, S. "Veiledning stålfiberarmert betong." Draft 2006, 2006, 42.pp.
  12. Jansson, A. "Fibres in reinforced concrete structures, analysis, experiments and design". Licentiate thesis, Lic 2008:3, Civil and Environmental Engineering, Chalmers University of Technology, Göteborg, 2008, 70, pp.
  13. DAfStb UA SFB N 0146. "DAfStb-Richtlinie Stahlfaserbeton-Draft march." 2005 (In German). 60.pp.
  14. Teutch, M. German Guidelines on Steel Fibre Concrete. International Workshop on advances in Fiber Reinforced Concrete, Bergamo, Italy, 2004. pp. 23-28.
  15. Gettu, R., Schnütgen, B., Erdem, E., and Stang, H. "Test and Design Methods for Steel Fiber Reinforced Concrete: a state-of-the-art report." Report of subtask 1.2. Brite-EuRam Project BRPR-CT98-0813 (DG12-BRPR), 2000, 55.pp.
  16. Lambrechts, A. N. The variation of steel fibre concrete characteristics. Study on toughness results 2002-2003. International Workshop on advances in Fiber Reinforced Concrete, Bergamo, Italy, 2004. pp. 135-148.
  17. Kooiman, A. G. "Modelling steel fibre reinforced concrete for structural design ". Doctoral Thesis, Technical University of Delft, 2000, 184, pp.
  18. BEKAERT. "DRAMIX Guideline for steel fibre reinforced concrete." ([www.bekaert.com](http://www.bekaert.com)), 1995, 20.pp.
  19. ENV-1992-1-1. "Eurocode 2: Design of Concrete Structures, Part 1-1: General Rules and Rules for Buildings.", 1991.
  20. EN-1992-1-1. EUROPEAN STANDARD. Eurocode 2: Design of concrete structures - Part 1-1: General rules and rules for buildings, 2004.
  21. Swedish Concrete Society (Svenska Betongföreningen). Steel-fibre concrete-recommendations for construction, performance and testing. Report no4 -2nd edition (In Swedish: Stålfiberbetong-rekommendationer för konstruktion, utförande och provning. Rapport nr 4 - utgåva 2), 2 ed, 1997.
  22. Barros, J. A. O., Cunha, V. M. C. F., Ribeiro, A. F., and Antunes, J. A. B. "Post-cracking behaviour of steel fibre reinforced concrete." *Materials and Structures*, Vol. 38, No., Jan-Feb 2005, pp. 47-56.
  23. Gustafsson, M. and Karlsson, H. "Fibre-reinforced concrete structures-analysis of crack spacing and crack width (In Swedish: Fiberarmerade betongkonstruktioner-Analys av sprickavstånd och sprickbredd)". MScE, Dep. of Structural Engineering, Chalmers University of Technology, Göteborg, 2006, 102, pp.



24. Tlemat, H., Pilakoutas, K., and Neocleus, K. "Modelling of SFRC using inverse finite element analysis." *Materials and Structures*, Vol. 39, No. 2, 2006, pp. 197-207.
25. Nanakorn, P. and Horii, H. "A fracture-mechanics-based design method for SFRC tunnel linings." *Tunnelling and Underground Space Technology*, Vol. 11, No. 1, 1996, pp. 39-43.
26. FRC workshop. "Fibre-reinforced concrete for strong, durable and cost-saving structures and infrastructures." *FRAMCOS-6*, 2007, pp. 163.

## Industrial concrete construction for a better economy and working environment – possibilities and obstacles with self compacting concrete



Mats Emborg  
Professor LTU / Head R&D Betongindustri AB  
Luleå University of Technology, 971 87 Luleå Sweden  
Betongindustri AB, 100 74 Stockholm  
E-mail: Mats.Emborg@ltu.se

Peter Simonsson  
Ph.D. student  
Luleå University of Technology, 971 87 Luleå Sweden  
E-mail: Peter.Simonsson@ltu.se



### ABSTRACT

The implementation of SCC together with new reinforcement and form techniques make it possible to increase the degree of industrialisation. It has been found in research at LTU that detailed planning and optimization of the building process, are essential utensils to successfully introduce such new techniques. However, also important is to address the technical issues hindering the marketing of SCC. Such issues are the robustness of the concrete and the surface quality. Thus, a discussion is given in the article on the optimization of robust SCC mixes and test results both from laboratory and building site as well as how criteria of SCC can be defined.

**Key words:** Cast in place concrete, industrialization, self compacting concrete, productivity, economy, robust SCC, mix design, aggregate packing

## 1 INTRODUCTION

In the late 1990's it was expected SCC to have more than 50 % of the total concrete market within a five year period, but what happened with the foreseen development? Today, almost ten years later, the market share of SCC in EU nations generally is as small as 1 % (at 2006 according to European Ready Mixed Association, ERMCO) with large variations; e. g. about 2 % in France & Norway, 1 % in Finland, Netherlands & UK and 5 % in Sweden while, on the other hand, the SCC market share in Denmark is as high as 28 %.

An important reason for the low use of SCC is the economy. The need for high quality concrete constituents results in a more expensive product that, according to the general opinion of end-users, not compensates for possible economical benefits. It is also known that several technical issues hinder the introduction of SCC on a broader front like questions regarding the *formwork pressure*, problems related to static and dynamic *segregation resistance*, rapid *loss of slump flow*

and doubtful *robustness*, unaccepted *surface quality*, insufficient *accuracy of production equipment*, *quality control* requirements and a *lack of standards* (see e. g. Shah et al. [1] and Cussigh [2]).

The challenges increasing the share of SCC in RMC (ready mixed concrete) construction in general are closely related to solve the abovementioned problems as well as to clearly document and convince the market on all the direct and indirect benefits using SCC. An overview of some selected issues is given in the paper as well as examples from research and case studies.

The success of SCC in Denmark may be commented on. In Denmark the application of SCC started almost from a zero level at 2000. With support of a large national R&D project ("The SCC consortium", 17 industrial and research institute partners), and certain strategies for initializing and promoting the SCC products, the SCC level increased to about 400 000 m<sup>3</sup> at 2003 and 800 000 m<sup>3</sup> at 2006, i. e. a 30 % share of RMC [25] in the country.

## 2 THE PERFORMANCE OF SCC – CRITERIA AND ROBUSTNESS

### 2.1 Criteria

The lack of robustness and quality assurance system for difficult castings (e. g. narrow structural section and dense reinforcement) are considered to be important obstacles when marketing SCC. Robustness is related to the performance of the product, which can, according to the EU Growth project Testing-SCC [3], [4] be discerned into three main parameters: 1) *Filling ability* 2) *Passing ability* and 3) *Segregation proneness*. For these parameters, criteria should be established depending on geometry of structure to be cast, form type, reinforcement, and, last but not least, method and local tradition on how to pour the concrete. Figure 1 shows possible target values and allowed variations of the *filling ability* (slump flow and T50) for horizontal and vertical bridge structural elements used at some occasions in Sweden. The diagram can be transformed into a corresponding rheology diagram; i. e. slump flow and T50 are related to shear stress and viscosity respectively [4]. It is seen that, for a proper form filling, the concrete for a bridge deck should have slightly less fluid properties as compared to a wall concrete. Criteria on *passing ability* and *segregation proneness* can, of course, be treated in a similar way.

Furthermore, Walraven [6] concludes that SCC can be tailor-made for any kind of construction and suggests nine consistency classes described by slump flow, T50, V-funnel time, passing ability and segregation properties. The consistency classes are dependent on the construction part (e. g. walls, floors) and have been approved in EU SCC guidelines [7], Figure 2.

In Denmark, main applications are horizontal castings (slab on grade, industrial floors and foundations), i. e. fairly uncomplicated geometries and reinforcements [25]- [27] . Therefore, the Danish SCC feature a rather moderated flowability; slump flow in the range of 500 – 600 mm, mainly in order to avoid segregation, i. e. properties rather different the ones of Figures 1 and 3.

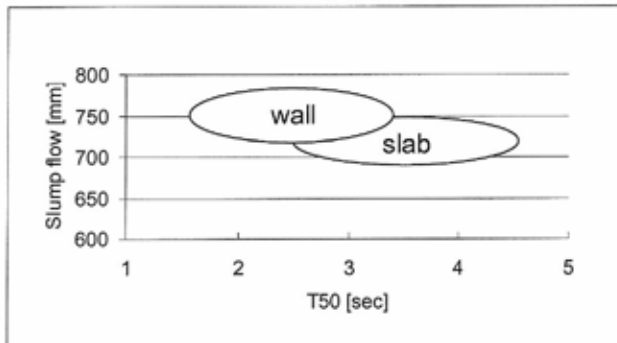


Figure 1 Examples of target values in slump flow - T50 diagram for SCC, wall and slab (here bridge deck), where the areas in the diagram represent the tolerances. Transformation of slump flow into shear stress and T50 into viscosity gives corresponding rheology target values [4],[5].

Viscosity				Segregation resistance/ passing ability
VS 2 VF 2	Ramps			Specify passing ability for SF1 & 2
VS 1 or 2 VF 1 or 2 or a target value.		Walls and piles	Tall and slender	Specify SR for SF 3
VS 1 VF 1	Floors and slabs			Specify SR for SF 2 & 3
	SF 1	SF 2	SF 3	
	Slump-flow			

Figure 2 Properties of SCC for various types of application suggested in EU guidelines of SCC [7] based on [6], VS, VF – viscosity classes obtained by T50 or V-funnel respectively. SF-slump flow classes, SR – segregation resistance.

Criteria for all SCC-casting should be defined by the contractor, to be met by a robust SCC that is controlled by an agreed quality assurance system (by testing at building site and/or concrete plant). Examples of results from such a SCC site testing are shown in Figure 3.

Concerning the quality assurance system, crucial is to document reliable values at the plant or site testing, which focus on the precision of test methods chosen. According to the Growth EU project Testing SCC, precision consists of two elements – repeatability and reproducibility which thus are statistical measures of the error inherent in a test method [3] [4]. The first measures is the likely error of tests on identical material performed by a single operator, and the second that of tests performed by different operators also on identical material. It is necessary to know the magnitude of these errors in order to properly understand and interpret test results and to establish the tolerances of SCC criteria.

Within the project Testing SCC, a comprehensive inter-laboratory study was performed establishing precisions of the most common test methods for SCC, see [4]. For example, slump flow and T50 test methods implied precisions according to Table 1. It was observed almost no significant difference between repeatability and reproducibility, indicating that the operator (or within-laboratory) variance dominated the precision. Rather large values of precision are observed and, hence, it is concluded that acceptable tolerances of SCC criteria not imply too narrow limits.

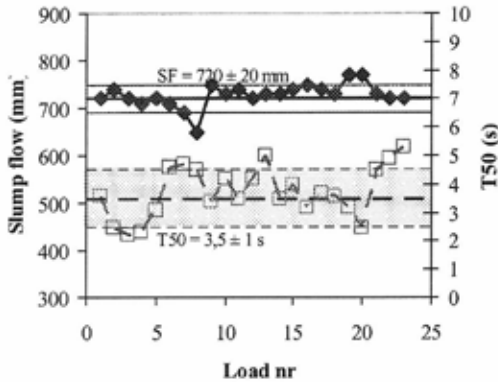


Figure 3 Slump flow (solid dots) and T50 tests at bridge deck casting meeting target values of Figure 1 [5].

Table 1. Precision of slump flow and T50 expressed in reproducibility obtained at an inter-laboratory study within the Growth EU project Testing SCC [3], [4].

Test method	Range	Reproducibility
Slump flow	SF: 600 – 750 mm	43 mm
	SF: > 750 mm	28 mm
T50	≤ 3,5 sec	0,88 sec
	3,5 – 6 sec	1,18 sec

## 2.2 Robustness

Generally speaking, *robustness* is defined as insensitive against disturbance [8] and for SCC the disturbance appears in the form of fluctuations of the concrete constituents properties, mixing procedure and transport conditions. An important feature of SCC is thus the ability of the concrete to maintain its fresh properties and structure during transport and casting of a single batch or multiple batches, [5], [9].

To develop a robust concrete mix is as important for a successful result as it is complex to accomplish. It is believed that *both* theoretical analysis (by e. g. packing theories) *and* laboratory tests on cement paste, mortar and/or concrete are required in order to design reliable mixes [5]. In Sweden it is now striven to establish such a mix design system for SCC, considering e. g. the aggregate fluctuations.

The SCC should thus allow for certain variations of influencing variables. For the properties of the concrete immediately after mixing, variables like aggregate uneven grading and uneven humidity of aggregate as well as unequal qualities of constituents can be discerned. According to the European SCC guidelines [7] a well designed and robust SCC can typically tolerate a variation of 5 -10 liters/m<sup>3</sup> in mix water content which in practice is about 3 – 6 % of the total water content per m<sup>3</sup>. This variation corresponds to a 0,5 – 1,0 % humidity variation of the sand fraction (0 – 8 mm), a level of sudden changes in moisture that can be handled at the concrete production in Sweden.

### 2.3 Examples of activities studying the robustness of SCC

Ongoing projects in Sweden address the robustness. One project reflects the influences of aggregate and filler on the variation of SCC properties. The reason is that an important challenge is to abandon the natural sand as main aggregate type entirely using crushed aggregate instead. In order to fulfil demands from the society regarding more sustainable environment, the use of natural gravel must be considerably reduced or even stopped in the nearest future. Crushed rock is the only alternative implying that proportioning tools must be further developed to consider the certain feature of the crushed rock – and variation of it. In the project, main variables to be examined have been identified to: aggregate type (natural, crushed), aggregate grading and distribution of particle shape, humidity of the sand and effects of industrial or natural filler.

Figure 4 shows typical influences of humidity variation of sand (+/- 1 %), not compensated for, when natural aggregate is replaced by crushed rock [10]. It is evident that the crushed rock, especially at a total replacement (KK in the figure), implies a more sensitive system i. e. the robustness is much lower than for natural aggregate (NN). Increasing the cement content or paste volume seems to be one effective measure to enhance the robustness for crushed aggregate concretes when varying the water content, see Figure 5. This is often done in reality but is however costly and implies negative effects like high shrinkage, high temperature increase and cracking as well as a negative environmental impact – important in the climate debate of today.

As known, several other methods are available increasing the robustness of the concrete. For example, viscosity agents and industrial filler often imply a more water insensitive system. Ongoing research at e. g. CBI in cooperation with the University of Sherbrook shows promising attempts of developing a variation stabile concrete.

Figures 6 and 7 depict tests results for variations of Civil Engineering SCC mix properties (different aggregate grading, filler content and cement paste content) when water content were varied similarly to Figs 4 and 5. The impact of filler content and grading curve is clear. Some influence of mix on robustness was detected.

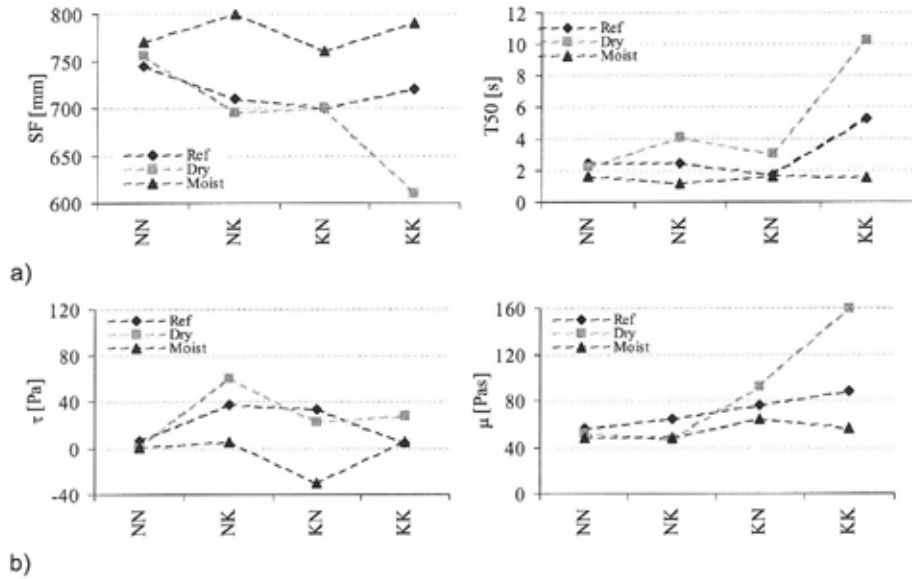


Figure 4. Slump flow and T50 (a) and shear stress and viscosity (b) when 0–8 mm and 8–16 mm natural aggregates (NN) are replaced by crushed 8–16 mm (NK), crushed 0–8 mm (KN) and at a total replacement (KK). Moist = + 0,5% humidity of sand, dry = - 0,5%) from reference sand moisture without compensation, cement: Std Portland Type II, 42,5 A-LL (Byggcement, Cements) 350 kg/m<sup>3</sup>, w/C = 0,5, [10] Rheology testing by ConTec 3 viscometer [22]

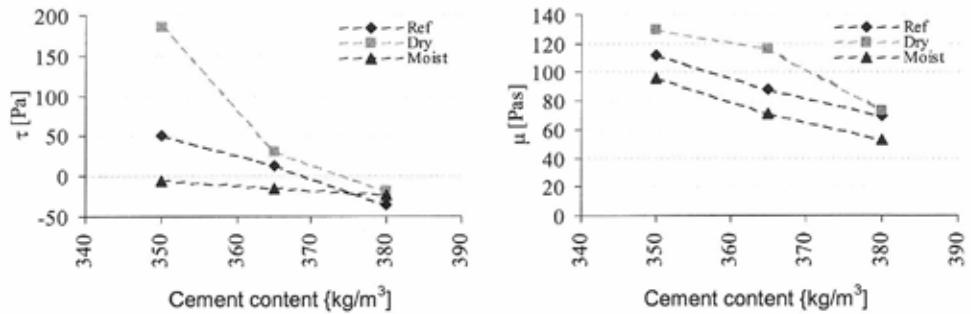


Figure 5. Shear stress,  $\tau$ , and viscosity,  $\mu$ , (ConTec 3 viscometer [22]) for SCC with entirely crushed aggregate for an increase of cement content. Moist = +0,5% moisture of sand, dry = -0,5%), (see also Figure 4) [10].

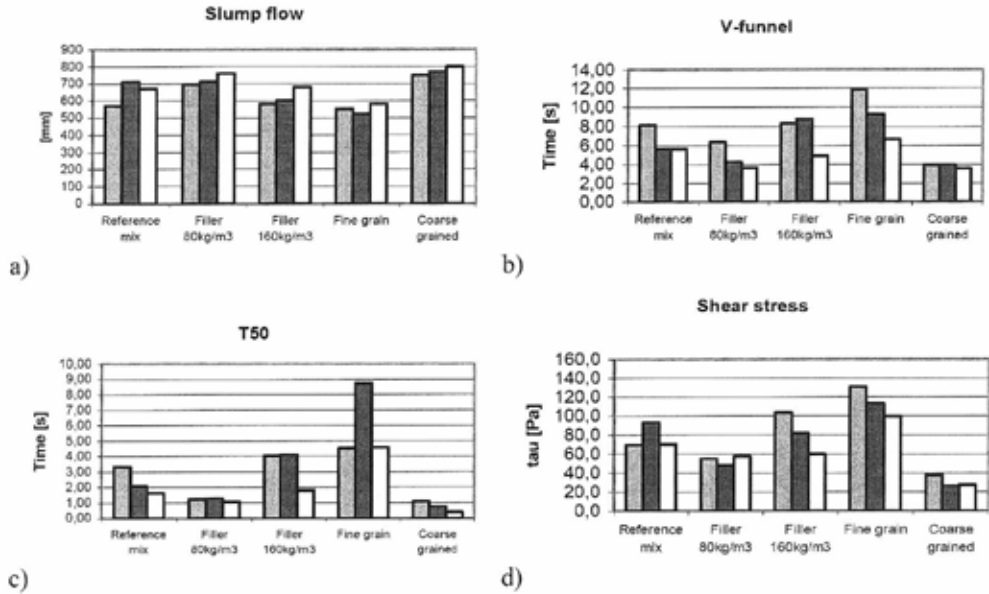


Figure 6. Example of influences on workability (slump flow, V-funnel flow time, T50) and rheology (shear stress,  $\tau$ ) of moisture variations of fine aggregate (left: +1 %, middle: reference moisture, right: -1 %). Laboratory tests with concrete used at the full scale bridge casting of Section 5, variations of filler content and grading curve. Cement: Std Portland Type I, 42,5 N MH/SR/LA (Degerhamn, Cements), 450 kg/m<sup>3</sup>, w/C=0,40, reference limestone filler content: 120 kg/m<sup>3</sup>, from [11].

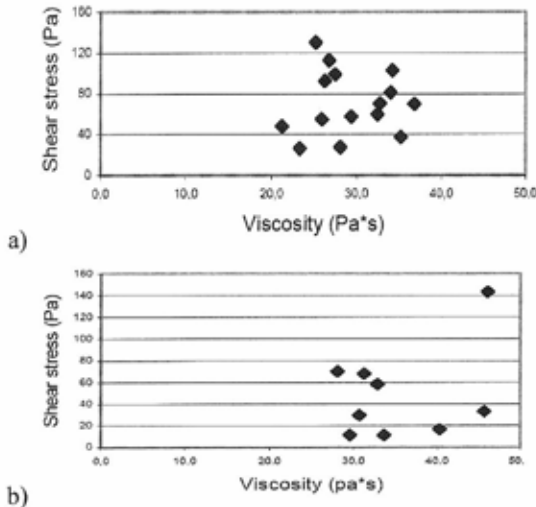


Figure 7. Example of influences on rheology (shear stress and viscosity) for fine aggregate moisture variations. Tests with different lime stone filler content and grading curve, (see Fig 6), (a) and (b) represent different concrete mixes made with the same aggregate [11].



### 3 METHODS TO DESIGN A ROBUST SCC

It is clear that the design of SCC shall fulfil various types of target values that, in fact, can imply contradictory strategies in material optimization. Therefore, it is important to carefully check with the client and the contractor the overall set of criteria, both as written “on the drawings” but also regarding casting conditions etc. (This is nothing new in this matter but the question has become more critical with SCC). It is thus important that the tolerances of the criteria are defined (the size of the area in the workability/rheology diagrams, Figure 1) which is met by a certain robustness of the material.

One philosophy regarding mix design of SCC is to consider the air voids of the aggregate. For an optimum flow, the air void volume of a certain fraction when packed should be filled by finer fractions of the material - and somewhat more i. e. an excess of finer particles is established. Similar conditions are valid for the finer fractions and the filling of the air voids of each fraction, achieving an optimum mobility, is repeated down to the smallest filler ending up by obtaining an excess of the cement paste volume. A correct mix of aggregate fractions thus gives the optimum grading curve and volume of cement paste. The rheology behaviour of the cement paste defines parameters like flowability and segregating proneness and can be controlled by superplasticiser, viscosity agent, cement and fine grained filler etc.

It is however observed that, in reality, for a concrete producer, the aggregate is often given i. e. one sand and one stone fraction is at disposal.

Several mix design methods of SCC utilize the theory above (see e. g. [13] – [18]) like the early proportioning system [13] where the coarse aggregate volume was fixed at 50 % of its packing density (50 % void volume). The properties of the mortar were adjusted in order to provide significant viscosity and flowability. The early excess paste theory explained the fact, to attaining workability, it is necessary to not only cover the surface of the aggregate with cement paste to reduce the friction but also to add more “excess” paste. The theory has been further developed to SCC by several researchers [14] [15]. At LCPC, France, a more refined method was developed based on the Compressive Packing Model (CPM) in which it is possible to consider grading and particle shape of each fraction more generally and to optimize the overall particle size distribution [16], [17].

Input to the CPM and other packing based models is the aggregate packing, see Figure 8, showing results from packing tests (loose packing i. e. not exposed to vibration) on fractions of 0,125 – 2 mm materials. Clear differences between natural and crushed aggregate are shown. Pilot calculations have been performed earlier [10] with the SCC-mix software based on the Compressive Packing Model [17] that was one output of the Brite-Euram project SCC [18]. Mainly, the influence of aggregate was studied by replacing natural aggregate with crushed similarly to the tests of Figures 4 and 5, see Figure 9. Except values in wrong level with regard to rheology (i. e. the values should be lower) due to insufficient calibration of superplasticiser influence in the program, the trends are logic and the agreements with test results are markedly good. With crushed rock and 380 kg/m<sup>3</sup> cement, about the same flowability was achieved as with natural aggregate, both theoretically (shear stress and viscosity) and at tests (slump flow tests), see Figure 9.

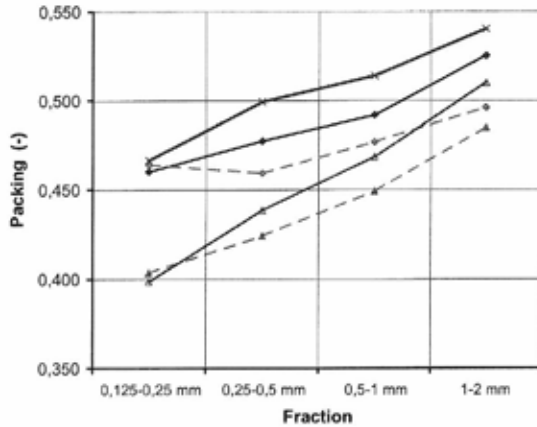


Figure 8. Packing densities documented for four fractions of one natural (thick solid line) and two crushed aggregates (dashed line) as well as two crushed aggregate treated to achieve a more cubic particle shape (thin solid) (tests at RMC company Betongindustri, local aggregates Stockholm)

Furthermore, Figure 10 shows the robustness for moisture changes of sand without compensation for natural and crushed aggregate, with calculated values by the SCC-mix software. The positive influence on robustness is demonstrated when adjusting the sieve curve of crushed aggregate to be similar to the one of the natural aggregate.

The mix design system for normal vibrated concrete and SCC, that is now to be developed in Sweden, will to some extent use the packing theories. This seems to be a promising approach as shown by the pilot calculations of Figs 9 and 10.

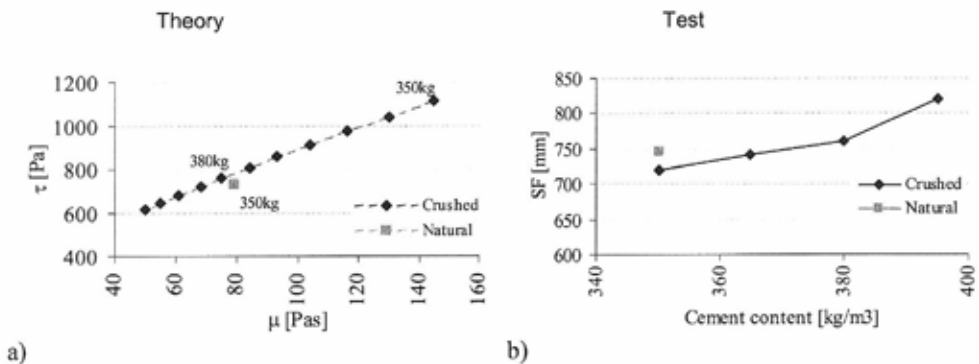


Figure 9a) Influence of cement content on rheology parameters (theoretically calculations with the Compressive Packing Model) and b) slump flow tests. Natural and crushed aggregate. In the calculations, the cement content was increased from 350 kg/m<sup>3</sup> to C ≈ 380 kg/m<sup>3</sup> for the concrete with crushed aggregate to obtain same shear stress (i. e. flowability) as natural aggregate. This was similar to the behaviour at the workability slump flow test [10].

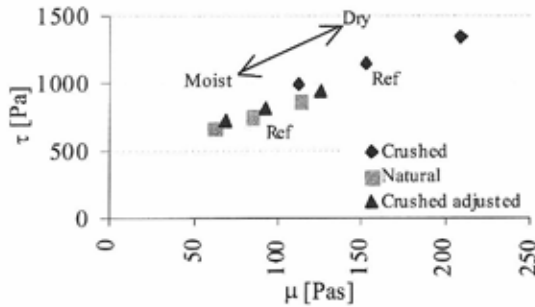


Figure 10. Rheology parameters as calculated with SCC-mix program [17] for crushed and natural aggregates at moisture changes of sand. Moist = +0,5% moisture of sand, dry = - 0,5% (see Figure 4). Calculations were also performed when crushed aggregate curve was adjusted to be exactly the same as the one of the natural aggregate [10].

#### 4 SURFACE QUALITY

Initially, at the introduction of SCC, the concrete was marketed to give perfect surfaces, free of pores or other defects. As known, despite some very successful cases (e. g. Figure 11), this target has rather seldom been achieved during the ten years of SCC use and several investigations have been initiated to examine the reasons of the absence of excellent surfaces.

If the SCC meets the three criteria of filling ability, passing ability and stability, it is assumed that it is possible to produce homogenous structural elements with high quality surfaces [19]. However, like the case with ordinary vibrated concrete, the surface of a SCC structure, in addition to the concrete material as such, also is influenced by the (surface) quality of the form, the form releasing agent, the way of casting, filling rate, weather condition and more. A perfect

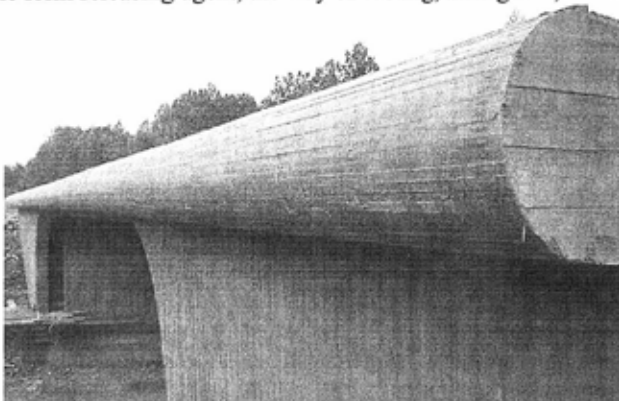


Figure 11. Perfect concrete (also inward) surfaces without pores or any other defects of a Swedish bridge cast 1999 with high performance SCC.

surface cannot be guaranteed unless the concrete fulfils the three criteria. But the defects, which can be subdivided into air pores, water pores and inward bends, can be mitigated.

Moreover, often, the source of a surface failure can be explained in a sudden inadequate delivery, which according to above, can be related to a low robustness of the concrete.

In Gram [19] and Emborg [20] some recent findings are found on the surface defects and how to avoid them. It can also be mentioned that several projects have been started in the Nordic countries to optimize concrete for perfect surfaces and to recommend practical measures to avoid the defects.

## 5 PRODUCTIVITY AND ECONOMY

One of the drawbacks with SCC is, as mentioned above, its high prize due to the quality demands on the concrete constituents and higher manufacturing costs. Hence, it is important to make SCC profitable also for the end user i. e. the contractor, which means that the construction system needs to be adapted to the “new” concrete, by that increasing the productivity.

Although several “technical” benefits of SCC can be expected, e. g. increased durability and strength, implying lower future maintenance cost and possible reduction of shear force reinforcement as well as structural cross sections, it is the productivity related gains that are of importance. Today, contractors however usually do not take these benefits into consideration. Instead, when casting SCC they use the same casting methods and amount of workers as with traditional vibrated concrete resulting in “normal” productivity and a poor production economy as the material costs and initial costs are higher. Fortunately, some exceptions from this are present in the Nordic countries.

One example is demonstrated in a PhD research project, “Industrialized Construction of RMC Bridges” [11]. SCC has been combined with effective reinforcement mounting (prefabricated cage reinforcement for foundations and carpet rolled reinforcement for bridge deck) as well as with production planning according to so called Lean Construction Philosophies [12], [21].

Two examples of full scale bridges were included in the study. Cost assessments clearly demonstrate the economical potential using SCC, especially if on-site man-power is reorganized. Marked reductions of man-power were obtained for e. g. the superstructures of the bridges using SCC. The total concrete costs for the superstructure (including the higher prize of the concrete) were equal or below the estimated costs if traditional concrete had been used. If reorganization of concrete workers had been accomplished (e. g. by means of two casting teams instead of one at the second case) the reductions would have been even larger i. e. the man-power need was considerably less the ones for a traditional casting,

## 6 WORKING ENVIRONMENT AND RELATED COSTS

Although the Swedish construction working environment is regarded as on of the safest in the world on the subject of physical health, working conditions, illnesses and accidents, still working environment related health problems exist that needs to be tackled [23]. Regarding concrete workers, 279 cases of Work-related Muscular Skeletal Disorders (WMSDs) were reported in Sweden 2004 and their sick leave compensations was estimated up to *1,3 millions €*

*for the taxpayers.* It is noted that this is valid for Sweden with, as compared to other EU nation, a small consumption of RMC per capita (resulting in 3 million m<sup>3</sup> per year in total). For ERMCO nations (European Ready Mixed Organisation), if the working environment is assumed to be equal to that of Sweden, the number could be extrapolated to 214 millions € for the EU taxpayers (492 millions m<sup>3</sup> of total annual RMC production). Moreover, for the contractors, of course other direct and indirect costs than sick leave compensation exists such as productivity loss and hiring substitute workers, probably *equal or higher* than the numbers above, which should be included in the injury cost estimations.

According to a study at the Danish Technological University [24] some 26 % of a workers average day consists of concrete casting and reinforcement fixing - a work that often is done in awkward postures with heavy equipment such as the poker vibrators for the traditional concrete or with heavy material when placing the reinforcement piece by piece. It is argued by the author of [24] that construction workers is one of the most exposed groups of employees in the society today when it comes to noise level, heavy lifts, poor ergonomics and varying weather conditions. The difference in working environment between traditional casting of concrete and casting SCC has been debated in recent publishing, and all argues for the importance of introducing SCC for the workers point of view. Unfortunately, there are few investigations which actually grade the working environment when casting traditional concrete as compared to SCC. One interesting example is however presented in the above mentioned PhD research project, [11], [12], [21].

Pilot studies were performed using the so called ErgoSAM and Cube models on site observations to acquire the risk of abovementioned WMSDs. At one of the full scale studies in the project, a mean value of work cycle load exposure level was documented and compared with the use of traditional vibrated concrete. Very large load exposure level reductions were obtained; the exposure level was in general about 1/3 as compared with casting of traditional vibrated concrete.

It was concluded that the effect of SCC on working environment is fundamental, constituting a base for strong economical benefits both for the society and, in fact, also for the building industry that cannot only concern about the short term site related benefits.

## 7 SUMMARY AND CONCLUSIONS

Besides solving technical problems, the possibility of increasing the market share of SCC is closely related to how all the direct and indirect benefits using the concrete are demonstrated. The challenge of the concrete sector is to market these benefits!

In Swedish studies it has been observed that, when estimating productivity and costs, it is important to adapt the site organization to the potential of the SCC. With a smart production planning, large reductions in unit time and total project time can be achieved. Some 20 – 25 % reductions of unit and project times as well as costs have been realized in pilot full scale tests.

Moreover, long term benefits of SCC should be addressed and demonstrated i. e. by reducing the costs for sick leave and injury related to an unhealthy working environment. The important benefit on working environment observed when using SCC will be followed up by new site examinations. Unfortunately, the chance of improving the working environment often is denied in the Nordic countries as the contractor only considers the short term prize for material and

man power and not the total possible long gain from e.g. the enhanced working environment. This attitude must be changed!

Of course, the technical obstacles hindering the marketing of SCC also should be directed in future actions. Activities are now focused on establishing criteria for the SCC on site, designing robust concrete mixes (using e. g. packing theories) meeting the criteria and finding a proper quality assurance system documenting the concrete delivered. When establishing criteria, important is to take into consideration the maximum precision of test method chosen as defined by e. g. the EU Growth project Testing SCC.

Although concrete manufacturers in recent time have improved the quality and hence the robustness of SCC, still deviations are present with the negative influence that the contractor calculates the risk when using SCC to be too high. Therefore, often the contractors simply *do not use the product even though both costs and time evidently can be saved*. Hence, the casting at site is performed with no reductions in man-power to be on the safe side, i. e. no large benefits in productivity are achieved.

If it is intended to increase the market of SCC, also the phenomena beyond the surface defects must be understood and reliable concrete mixes for perfect surfaces as well as casting methods in conjunction with form qualities should be established and documented in guidelines.

## 8 REFERENCES

- 1 Shah S, Ferron R, Ferrara L, Tregger N, Kwon S "Research on SCC: some emerging themes", 5<sup>th</sup> international RILEM symposium on SCC 3-5 sept 2007, Ghent. pp 3-15
- 2 Cussigh F: SCC in practice: opportunities and bottlenecks, .5<sup>th</sup> Rilem SCC Conf (see [1]), pp 21-29
- 3 Bartos P J M: Assessment of Key Characteristics of Fresh Self-Compacting Concrete: A European Approach to Standardisation of Tests. 4<sup>th</sup> International Rilem Symposium on Self Compacting Concrete, Oct, 2005, Chicago, pp 807-831
- 4 Testing SCC, Technical report of the Growth project: Testing SCC Measurement of properties of fresh self-compacting concrete, 2001 - 2004. Co-ordinator ACM Centre, University of Paisley, UK CONTRACT N° G6RD-CT-2001-00580, 66 pp
- 5 Emborg M, Simonsson P, Carlswärd J, Nilsson M: Industrial casting of bridges combining new production methods and materials, like a robust SCC, utilizing Lean Construction Principles, 5<sup>th</sup> Rilem SCC Conf (see [1]), pp 485 - 491
- 6 Walraven J, Structural aspects of self compacting concrete, 3<sup>rd</sup> international RILEM Symposium on SCC 2003, Reykjavik, pp 15-22.
- 7 The European Guidelines for Self Compacting Concrete, specification, production and use, BIBM, CEMBUREA, EFCA, ERNARC, ERMCO, 2005, 68 pp
- 8 Taguchi Shin: Robust engineering, Genichi Taguchi, Subir Chowdhury, ISBN 0- 07-134782-8, 2000
- 9 Bonen D, Deshpande Y, Olek J, Shen L, Struble L, Lange D, Khayat K: Robustness of self-consolidating concrete. 5<sup>th</sup> Rilem SCC Conf (see [1]), pp 33-42.
- 10 Emborg M, Jonasson J-E, Nilsson M, Utsi S and Simonsson S (2005): Designing robust SCC for industrial construction with cast in place concrete, 4<sup>th</sup> International Rilem Symposium, see [3], pp 1251-1259

- 11 Simonsson P: Industrialized construction with SCC with new production techniques and Lean Construction, Division of Structural Engineering, Luleå University of Technology, Licentiate thesis 2008:17, 140 pp
- 12 Simonsson P and Emborg M: Industrialized construction: Benefits using SCC and innovative productions methods, The Third North American Conference on the Design and Use of Self-Consolidating Concrete, Chicago, Nov 2008, 8 pp
- 13 Okamura H and Ozawa K: Mix design for Self-Compacting Concrete, Concrete Library of JSCE, No. 25. June 1995
- 14 Oh S. G., Noguchi T, Tomosawa F: Towards Mix Design for Rheology of Self-Compacting Concrete, Proc 1<sup>st</sup> Int RILEM-Symp on Self-Compacting Concrete, Stockholm, 1999, pp 361-372
- 15 Petersson Ö, Billberg P, Van B. K.: A Model for Self-Compacting Concrete, RILEM Int Conf on Production Methods and Workability of Concrete, Glasgow, June 3–5, 1996, pp 483-492
- 16 Sedran T, de Larrard F: Optimisation of Self Compacting Concrete Thanks to Packing Model, Proc 1<sup>st</sup> Int RILEM-Symposium, see [14] pp 321-332
- 17 Sedran T: Mix Design of SCC, Task 5 report of the SCC project, see [4]), 80 pp
- 18 SCC, Technical report of the Brite EU project: Rational production and improved working environment through using self compacting concrete, 1997 - 2001. Co-ordinator NCC AB, Sweden (Dr Marianne Grauers), CONTRACT N° BRPR-CT96-0366, 86 pp
- 19 Gram H-E "Oberflächenschäden bei Selbstverdichtendem Beton (Surface defects of SCC", In German/English), Betongwerk+Fertigteil-Technik, No 8, 2004, pp 28-32
- 20 Emborg M: How to increase the market of ready mixed SCC – experiences from Nordic countries, The Third North American Conference on the Design and Use of Self-Consolidating Concrete, Chicago, Nov 2008, 11 pp
- 21 Simonsson P and Emborg M: Industrialized construction: benefits using SCC, the XX<sup>th</sup> Symposium on Nordic Concrete Research & Development, Bålsta (SE), June 2008, 20 pp (also published in the Nordic Concrete Research journal)
- 22 [www.contec.is](http://www.contec.is)
- 23 Swedish Social Insurance Agency (Riksförsäkringsverket) (2004): What are the costs for sick leaves for women and men (In Swedish: Vad kostar sjukdomarna för kvinnor och män? Sjukpenningkostnaderna fördelade efter kön och sjukskrivningsdiagnos. Riksförsäkringsverket 2004:5.
- 24 Nielsen, C 2007, Does SCC really improve the working environment? 5<sup>th</sup> Rilem SCC Conf (see [1]), pp 967-974
- 25 Nielsen, C, Thrane L, Pade C, Danish experience with self compacting concrete, Journal of Concrete Plant International, no 1, 2008, [www.cpi-wordwide.com](http://www.cpi-wordwide.com), pp 60 -68.
- 26 SCC-consortium, Mix design and Execution of SCC, and Danish Techn Inst, Aug 2007, 22 pp + 48 pp (in Danish)
- 27 Nielsen C, Glavind M, Gredsted L, Hansen C N, SCC- A technical breakthrough and a success of the Danish Concrete Industry, 5<sup>th</sup> Rilem SCC Conf (see [1]), pp 993-999
- 28 Thrane L, Pade C, Svensson T, Estimation of Bingham rheological parameters of SCC from slump flow measurements, 5<sup>th</sup> Rilem SCC Conf (see [1]), pp 353-358

## Test methods and a theoretical model to assess shrinkage cracking of steel fibre reinforced concrete overlays



Jonas Carlswård  
 PhD, Research engineer  
 Betongindustri AB  
 Box 47 312 Stockholm  
 E-mail: jonas.carlsward@betongindustri.se

### ABSTRACT

Shrinkage cracking of concrete overlays with and without steel fibres has been assessed through laboratory testing and theoretical analysis. Test results showed that steel fibres limit crack widths although the contribution was not found to be sufficient to distribute cracks in areas of poor or non-existent bond to the substrate. Results further verified that a distributed pattern of fine cracks is obtained even for un-reinforced concrete when the bond is high, i.e. steel fibres, or other reinforcement, is not required to limit crack widths for this situation. An analytical model, developed to assess the risk of cracking and to predict crack widths of steel fibre reinforced concrete (SFRC) overlays, was found to give reasonable correlation with experimental results.

**Keywords:** Shrinkage, Restraint, Cracks, Steel fibres, Bond, Overlay, Theoretical model.

## 1. INTRODUCTION

### 1.1 Background

The technique of applying thin bonded overlays on concrete substrates is frequently applied in order to repair or strengthen deteriorated bridge and parking decks, damaged industrial floors or as finishing layers on prefabricated elements. In order to ensure that the overlaid system maintains durable and fully functioning during the intended service life it is essential to limit crack widths and to prevent de-lamination.

Many researchers and building clients have pointed out that the single most important factor determining the service life of an overlaid structure is the shrinkage of the newly cast overlay, e.g. [1-4]. Cracking, de-lamination and edge lifting (Figure 1) are typical consequences of the shrinkage, or rather the difference in shrinkage between the overlay and sub-structure.



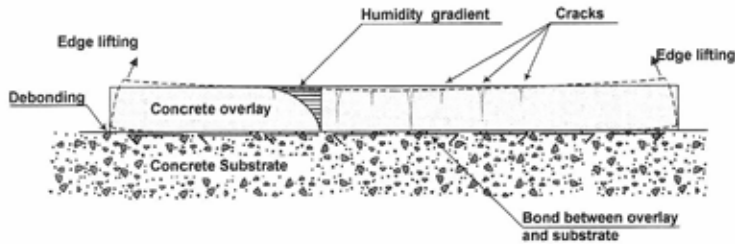


Figure 1 – Cracking and edge lifting of a bonded overlay exposed to shrinkage.

Two measures may be undertaken to minimise the negative effects of cracking: reduce the material shrinkage or provide reinforcement to distribute cracks. Shrinkage reduction may be accomplished by e.g. introducing a Shrinkage Reducing Admixture (SRA). The effect of SRA has been studied quite extensively over the last 15-20 years, e.g. [5-9], and the technique may be regarded as an accepted method to control concrete shrinkage.

Reinforcement is provided either by welded mesh or steel bars or by mixing steel fibres into the concrete matrix. Attractive features of SFRC are that the demanding handling of traditional reinforcement is eliminated and that more rational production techniques can be adopted.

## 1.2 Aims of the research

Main incentives of the research presented in the article are: (1) to experimentally verify the effect of steel fibres on widths and distribution of shrinkage cracks in thin overlays, (2) to investigate how the bond strength is influenced by quality and preparation of substrate concrete and (3) to establish a theoretical model for the estimation of crack risk due to restrained shrinkage and to assess the contribution of steel fibres on crack widths.

The results presented in this article summarise work conducted within a recent doctoral thesis [10].

## 2. RESTRAINED SHRINKAGE TESTING

### 2.1 General

Three main categories of test set-ups are frequently used to study shrinkage cracking: (1) end-restrained, (2) base restrained and (3) ring tests (see Figure 2). Category (2) tests, i.e. overlays cast on a substrate, are clearly the most suitable from the viewpoint that the restraint condition represents the real overlay conditions. A drawback is that it is difficult to control the bond conditions, which means that the cracking response will rely on the particular restraint situation (bond quality) obtained in each test.

From this viewpoint it is favourable to use end-restrained set-ups or ring tests, as they offer a direct evaluation of the effect of for instance type or amount of fibre. The ring test, in which the shrinkage of an external concrete ring is restrained by an inner steel ring, is certainly the most popular test method. Favourable properties are the simplicity of the set-up and that the degree of

restraint is well defined. A review of test results reported on the ring test method (see [10]) indicates however that the ring test overestimates the influence of fibres. Multiple cracking is regularly obtained already at steel fibre dosages as low as  $20 \text{ kg/m}^3$ . In fact, more than one crack has even been observed for plain concrete, e.g. [6, 9, 11-13]. As crack distribution would clearly not take place in un-reinforced concrete this leads to speculations regarding the validity of the method for assessing the fibre effect.

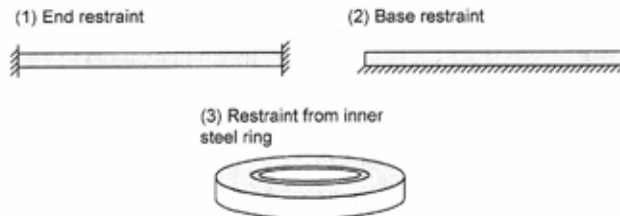


Figure 2 – Common types of test methods used to study the effect of restrained shrinkage.

In the present research two types of test methods were adopted to simulate the effect of restrained shrinkage, an end-restrained and a base-restrained type of set-up. Some main results from the last mentioned test method are summarised below. For more details on the end-restrained test, reference is made to [10].

### 2.3 Base-restrained test

#### *Test set-up and material details*

The base restrained tests consisted of (out-stretched) overlay strips ( $50 \times 150 \times 2500 \text{ mm}$ ) cast on large concrete bottom slabs ( $300 \times 2000 \times 3000 \text{ mm}$ ), see Figure 3. Four bottom slabs were produced approximately a year in advance to minimise the remaining shrinkage, i.e. in order to maximise the differential shrinkage between overlays and slab. Different substrate preparations were applied in order to achieve a variation in bond quality. One of the slabs was grinded and dry at the time of overlaying, one was grinded and wet, one was milled and wet and the last slab was milled and primed. Grinding procedure gave a rather smooth texture while milling resulted in a rough texture.

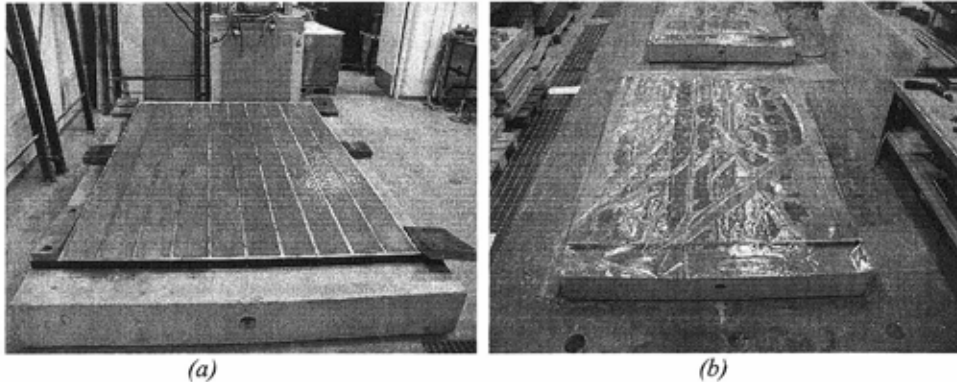
Ten overlay strips were cast on each slab; 2 strips of un-reinforced concrete (PC), 2 steel bar reinforced strips (a centrally placed  $10 \text{ mm}$  steel bar) referred to as SBRC, 2 with shrinkage reduced concrete ( $1.5 \%$  SRA type Sika Control 40) and 4 SFRC strips (2 with  $30 \text{ kg/m}^3$  of fibres and 2 with  $60 \text{ kg/m}^3$  of the type Dramix RC-65/35-BN).

The same basic concrete recipe was used for all tests (Table 1), corresponding to self compacting concrete (SCC) of class C28/35  $D_{\text{max}} 8 \text{ mm}$  and a  $w/c$ -ratio of 0.58 with a target slump flow of  $700 \text{ mm}$ . The cement was Slite Byggcement (CEM II/A-L 42,5 R) and the sand was of a natural occurring type from Riksten. Limestone filler of the type Limus 40 by Nordkalk was further added in order to ensure stability for the SCC. The superplasticizer was Sikament 56 by Sika, a chemical compound based on poly-carboxylate-ether.

*Table 1 – Basic concrete mix composition used in the base-restrained test series.*

Materials	Cement kg/m <sup>3</sup>	Sand 0/8 kg/m <sup>3</sup>	Filler kg/m <sup>3</sup>	Sika 56 kg/m <sup>3</sup>	Water kg/m <sup>3</sup>	w/c
Basic recipe	370	1613	100	4.1	215	0.58

The overlays were cured underneath plastic coverage for five days before exposed to a rather harsh laboratory environment (15-20 % relative humidity and 20°C) resulting in a rapid drying shrinkage development and associated overlay cracking within a rather short period of time (prior to 30 days). Cracking and de-bonding were followed for a period of approximately 3 months.



*Figure 3 – (a) Overlay strips on slab 3 directly after casting has been finalised. (b) The concrete was covered by air-tight plastic sheeting approximately four hours later.*

#### *Material properties and free shrinkage*

The tests conducted to assess the properties of the actual concrete produced for the overlays were limited to compressive strength testing as a more extensive material investigation had been performed previously within the end-restrained test series on concrete with similar composition (see [10]). Previously controlled material properties included splitting tensile strength at different ages to determine strength development, flexural beam tests to establish residual strength factors (*R*-values) in accordance to instructions given in [14] and creep tests. Details on results from the material tests can be found in [10].

Free shrinkage was obtained from thin concrete prisms sealed at the bottom and along the sides to allow drying only through the upper face, see Figure 4. In order to simulate the overlay strips a thickness of 50 mm was adopted. Deformations were measured at the bottom and upper faces of the specimens, using a handheld mechanical measuring device, to capture the shrinkage gradient through the overlays. The prisms were placed aside the overlays to evaluate the unrestrained deformation under identical drying conditions.

Measured free shrinkage development for the concrete types within the study is shown in Figure 4. Noticeable is the extensive difference in strain between the top and bottom faces of the specimens, resulting from the one sided drying conditions. It can further be seen that the addition of SRA reduced the average shrinkage by approximately 25 %.

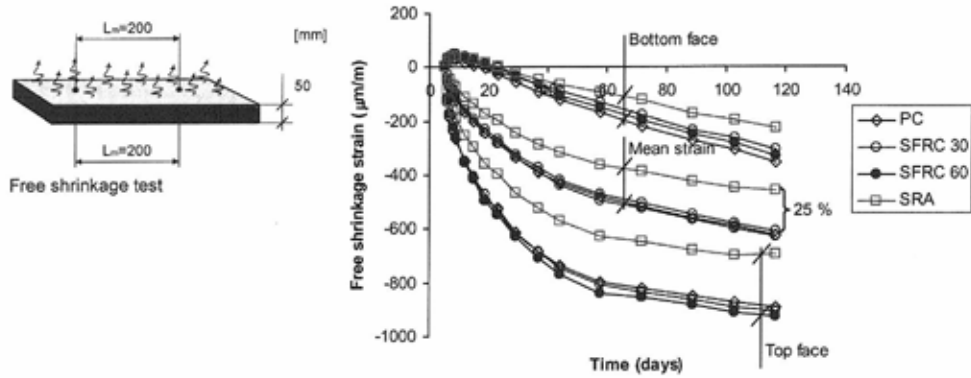


Figure 4 – Test method to determine shrinkage development and measured shrinkage at the upper and lower faces as well as the mean shrinkage.

#### Cracking and de-bonding

The first visible cracks were observed between 1 and 3 weeks after the start of drying from most of the overlay strips and new cracks were then established until the end of the test period 3-4 months later. From the crack width summary given in Figure 5 it can be seen that most of the cracks had a width of only between 0.05 and 0.2 mm at the end of the measuring period while a few cracks with more significant widths developed in overlays strips of slabs 2, 3 and 4.

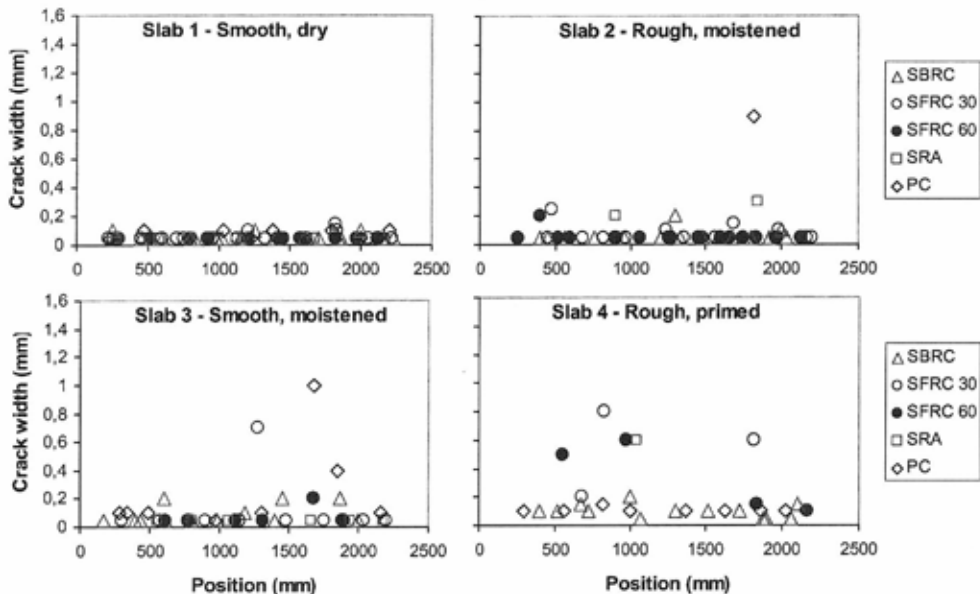


Figure 5 - Measured crack widths at the end of the measuring period approximately 4 months after initiation of drying. (Smooth = grinded, rough = milled).

Cracks with more significant width always coincided with the development of a major, internal de-bonded zone. A crack mapping of the overlays on slab 3 is given as an example in Figure 6. For overlays with a major internal de-bonded zone (shaded area) a single crack developed within this zone for PC, SRA and SFRC with 30 and 60 kg/m<sup>3</sup> (see PC II, SRA II, SFRC 30 II and SFRC 60 II). This indicates that distribution of cracks, and corresponding crack control, was not achieved for the SFRC used in the tests. For SBRC on the other hand an additional crack developed within the major de-bonded zone (see SBRC II), thus implying that the steel bar was sufficient to give some crack distribution.

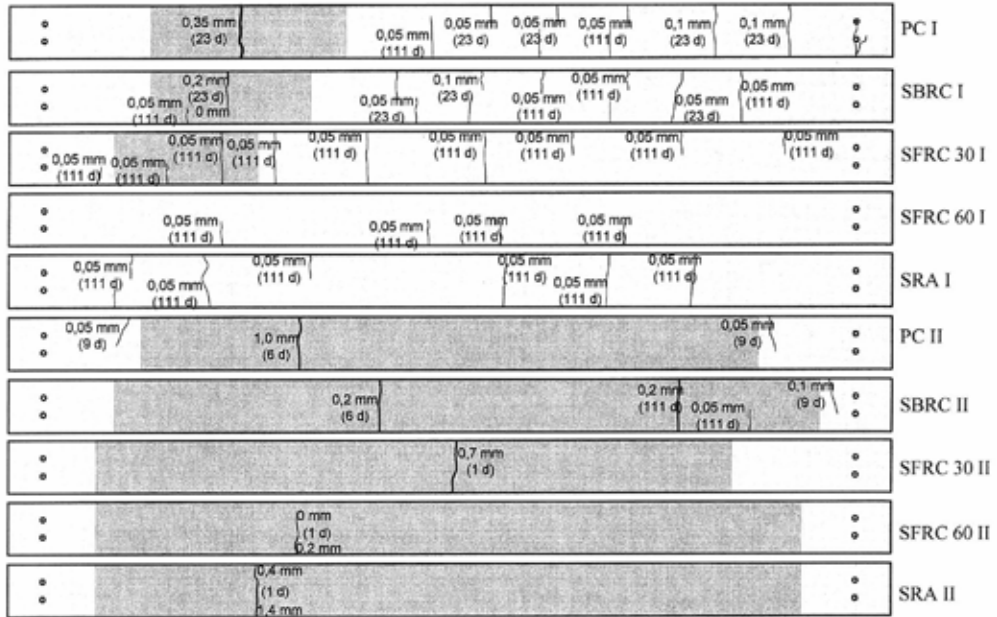


Figure 6 – Cracks in overlays on slab 3. Shaded areas indicate that the overlays have de-bonded. Values within parenthesis correspond to the time at which the crack was first observed.

The reason as to why none of the cracks observed in overlays on slab 1 had a width that exceeded 0.15 mm (see Figure 5) is that the bond strength obtained was high and evenly distributed, i.e. no de-bonding occurred. The result was somewhat un-expected as a smooth and dry substrate is generally believed to be unfavourable from a bond perspective. The effect of the moisture condition of the substrate on the bond strength is further discussed in Section 3.

#### Effect of steel fibres on cracks

Based on the results presented above it can be concluded that steel fibres, or conventional steel bar reinforcement, are not required in cases when the bond strength is adequate to prevent de-bonding. In order to validate a possible effect of fibres it is thus necessary to consider the case where a major de-bonded area has developed.

A summary of crack widths obtained for PC and SFRC overlays in which a major de-bonded zone was established can be seen in Figure 7. The crack widths have been normalised with respect to the de-bonded length in order to enable comparisons. It should also be mentioned that

the actual fibre contents were calculated based on the counted number of fibres crossing the crack and by utilising fibre orientation theory (e.g. [15, 16]). An interesting observation is that the actual fibre content was lower (3 cases) or equal (1 case) to the expected amount. This shows that the fibre content varied in the SFRC overlays and that a major crack is more likely to develop in a section with low fibre content.

From the results it is quite clear that increasing the fibre content resulted in a decreased crack width. Based on the trend line it can be seen that a content of  $40 \text{ kg/m}^3$  reduced the crack width from 0.6 to 0.3 mm/m while  $60 \text{ kg/m}^3$  of steel fibres reduced the crack width to approximately 0.1 mm/m. Important to recognise is however that as long as only a single crack develops (which was the case for PC and SFRC overlays) the actual crack width will be proportional to the size of the de-bonded zone, i.e. it is not possible to determine a content of steel fibres required to limit crack widths. A distributed crack pattern would be required in order to enable crack limitation within a de-bonded zone. It is believed that the content of steel fibres required to initiate multiple cracking is approximately  $80\text{-}100 \text{ kg/m}^3$  or even higher depending on fibre type and concrete composition.

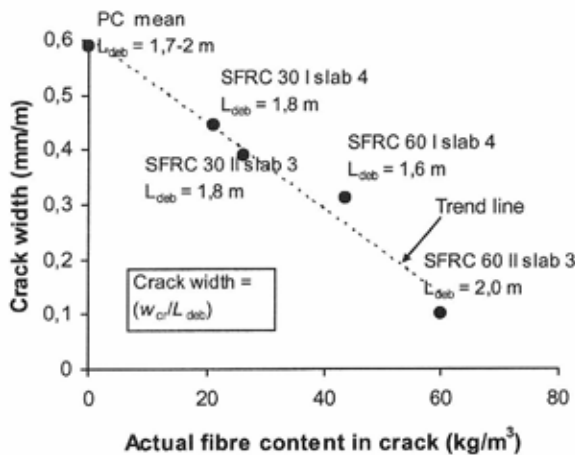


Figure 7 – Crack width divided by de-bonded length as a function of steel fibre amount. Only the cracks that developed within major de-bonded areas have been considered.

### 3. BOND TESTS

#### 3.1 General

The bond situation is, as is evident from the base-restrained test series above, quite important for the limitation of overlay cracking. A rather interesting result was that the highest bond strength was achieved for the slab that was grinded (smooth) and dry at the time of overlaying despite the fact that a rough and pre-moistened surface is often believed to give the best bond. Some bond tests were therefore conducted to investigate the significance of the roughness and moisture condition of the substrate.

### 3.2 Test set-up and material details

Two test series were conducted where the effect of pre-moistening, priming and roughness of the substrate were studied in series I while test series II focused on the influence of the substrate concrete quality or  $w/c$ -ratio.

Thus, 70 mm thick overlays of self compacting concrete (SCC) were cast on bottom slabs that had been produced some months in advance to allow for some drying (see Figure 8). Pull-out tests were used for the bond strength evaluation, conducted approximately a month after casting. The overlays were covered by plastic foil during the entire storage period in order to prevent potential negative effects of drying shrinkage (e.g. edge lifting).

A rough texture for some of the slabs of the first test series was obtained by milling the slabs by hand while the remaining slabs of series I and all slabs of series II were just levelled off to obtain a smooth texture.

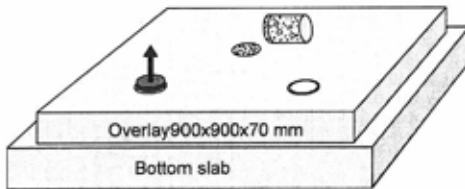


Figure 8 – Set-up used to assess the pull-out bond strength.

Material details are given in Table 2. Cement Bygg has the type notification CEM II/A-L 42,5 R while cement Anl is denoted CEM I N 42,5 MH/SR/LA. The limestone filler was of the type Limus 100 by Nordkalk and sand and coarse aggregates were of a natural occurring type. Furthermore, two different plasticisers were used, a melamine based product called Cementsa 92 M and a poly-carboxylate ether from Sika (Sikament 56).

Table 2 – Concrete mix composition used in the bond tests.

Materials	Test series I		Test series II			
	Bottom slabs	Overlays	Bottom slabs A	B	C	Overlays
Cement Bygg, kg/m <sup>3</sup>		350	340	400	500	350
Cement Anl, kg/m <sup>3</sup>	350					
Filler, kg/m <sup>3</sup>		150				150
Sand 0-8 mm, kg/m <sup>3</sup>	1007	1077	1046	974	883	1077
Coarse agg 8-16, kg/m <sup>3</sup>	824	580	757	797	815	580
Cementsa 92 M	3,7					
Sikament 56, kg/m <sup>3</sup>		?	1.5	3.0	5.0	6.0
Water, kg/m <sup>3</sup>	170	185	187	180	175	185
$w/c$	0.49	0.53	0.55	0.45	0.35	0.53

### 3.3 Results

Results from series I (Figure 9 (a)) showed that the bond strength was rather poor for dry

substrates, while priming and pre-moistening were found to give positive effects. Thus, different from the base restrained tests it seems as if a moistening or primer was required to obtain good bond quality. It can also be seen that roughening the substrate did not increase the bond strength in this series (except for the dry substrate situation).

For series II it can be seen that the bond strength in general was higher than that obtained in series I. It is suspected that this is due to the different concrete compositions used for the bottom slabs as this is the only parameter that differ between the two series (see Table 2).

It is also interesting to see that a somewhat different experience was obtained in test series II regarding the need for pre-moistening (Figure 9 (b)). Different from series I, dry substrates gave almost as high bond strength as pre-moistened substrates. There is, however, a tendency of increasing difference between dry and pre-moistened substrate for slab type A, with  $w/c$ -ratio of 0.55.

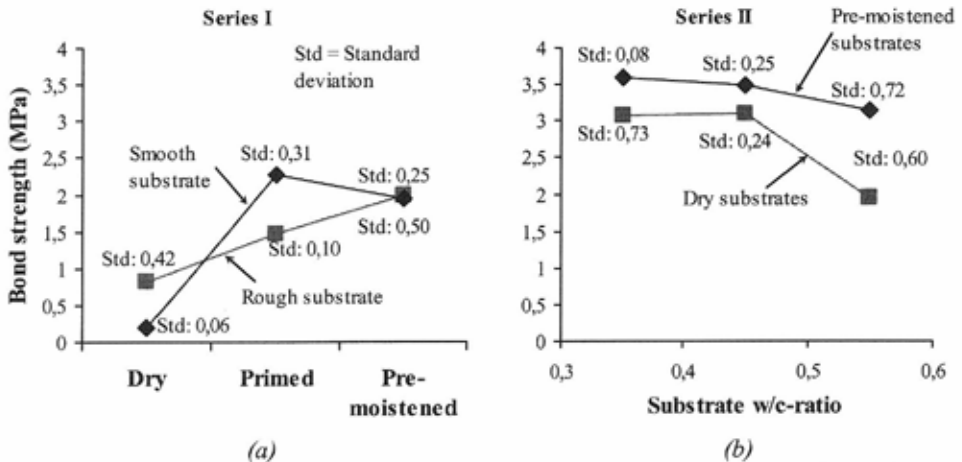


Figure 9 – (a) Pull-out bond strength obtained in test series I. (b) Bond strength obtained in series II.

Considering that the development of bond strength is strongly related to the moisture exchange or situation at the transition zone between overlay and substrate, it is believed that the results of series II reflect the differences in permeability of the substrates. For high  $w/c$  concrete the permeability will be high, which means that excessive amounts of water may be absorbed from the overlay, resulting in a deficiency of water available for the cement reactions in a layer near the interface. It is believed that the decrease in permeability, following on a reduction in  $w/c$ -ratio, is the reason as to why pre-moistening did not give a significant contribution for low  $w/c$  concrete substrates in series II.

This would also explain the high bond strength obtained in the base restrained tests of a dry substrate considering that the substrate slabs were produced with a very high quality concrete ( $w/c$  0.38). It is however somewhat strange that the bond strength was substantially lower for dry substrates in series I (see Figure 9 (a)) despite the rather low  $w/c$ -ratio of 0.49. One possibility is that the use of a coarser cement in these slabs (Blaine of  $310 \text{ m}^2/\text{kg}$  for an cement compared to  $460 \text{ m}^2/\text{kg}$  for Byggcement) gave a higher permeability. More tests are conducted



at the moment to study the relation between the moisture state in the substrate and the bond strength further.

## **4. THEORETICAL MODELLING OF SHRINKAGE CRACKING**

### **4.1 General**

Despite the fact that SFRC is regularly adopted for the purpose of limiting crack widths and distribute cracks in overlays there is no reliable method available for the design on this regard. Hence, fibre concrete is typically designed/selected based on recommendations relying on experience. A number of experience based design proposals are available according to [17] and a Swedish example of such approach is the formula given in [18], which makes it possible to calculate a steel fibre amount based on a given fraction of steel bar reinforcement. Although these methods occasionally may prove to result in “crack-free” overlays it is obvious that more reliable approaches need to be developed for the future use of SFRC in overlays.

An analytical model to determine the risk of cracking and the crack width of SFRC overlays exposed to shrinkage was proposed in [10]. The basic principles as well as some examples of application are given below.

### **4.2 Proposed model**

The analysis is divided into two stages (Figure 10); (1) an initial analysis in the un-cracked stage, and (2) crack width analysis. In the first stage the tensile stress development is calculated based on beam theory for a composite member, i.e. assuming full bond between the two layers. The analysis includes the rate of shrinkage and creep, the development of stiffness and tensile strength and the situation of restraint.

Two situations are distinguished in the cracked stage (2), assumed to be reached when the tensile stress exceeds the overlay strength. The first is that substantial de-bonding occurs and the second that the overlay is still bonded after cracking. In case of de-bonding it is assumed that just a single crack occurs in the un-bonded region while a distributed crack pattern is expected for a bonded overlay.

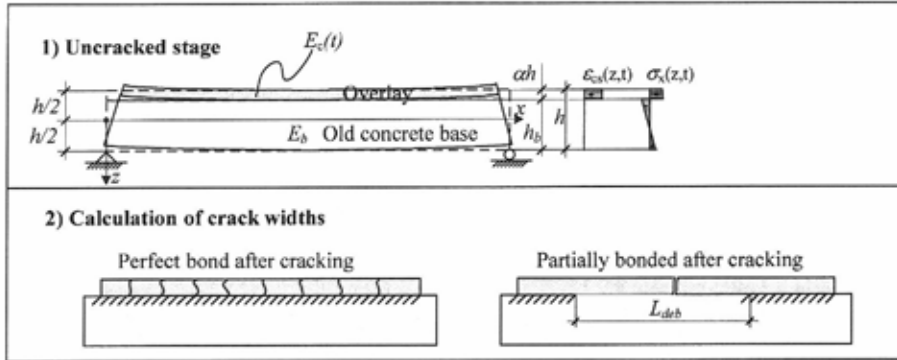


Figure 10 – The proposed analytical model divided into two stages; (1) initial stress analysis in the un-cracked stage and (2) crack width analysis.

### Un-cracked stage

The stress state in the composite structure is evaluated using beam theory for a statically determined system, see (1) in Figure 10. Such analysis has previously been used by e.g. [19, 20] to predict the risk of shrinkage related cracking in overlaid structures. An incremental procedure is adopted to calculate the shrinkage stress development including the favourable effect of creep, or rather stress relaxation (Figure 11 (a) and (b)).

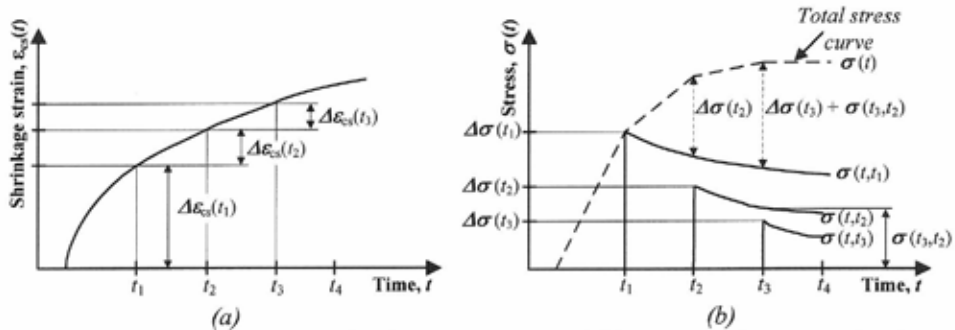


Figure 11 – (a) Shrinkage strain development in time and (b) corresponding stress development in a restrained structure incorporating the effect of relaxation.

If the overlay shrinkage is approximated with an even distribution over the section, see (1) in Figure 10, the following expression may be derived for the stress in the overlay (average stress) at time  $t$  due to the increment of shrinkage strain applied at  $t_i$ ,  $\Delta\epsilon_{cs}(t_i)$ :

$$\sigma_{\text{mean}}(t, t_i) = \frac{m(t, t_i) \cdot (1 - \alpha) \cdot (m(t, t_i) \cdot (1 - \alpha)^2 + \alpha^3)}{m(t, t_i) + (m(t, t_i) - 1) \cdot (m(t, t_i) \cdot (1 - \alpha)^4 - \alpha^4)} \cdot R_c(t, t_i) \cdot \Delta\epsilon_{cs}(t_i) \quad (1)$$

It should be mentioned that a similar equation has previously been developed by Silfwerbrand, see e.g. [19]. A difference is that the proposal of Silfwerbrand is a one-step calculation, i.e. a single stress value is calculated based on the final shrinkage.  $\alpha$  in the above equation

corresponds to the relative overlay depth (see Figure 10 for definition) and  $m(t, t_i)$  is the stiffness relation between overlay and substrate calculated as:

$$m(t, t_i) = \frac{E_b}{R_c(t, t_i)} \quad (2)$$

where  $E_b$  is the elastic modulus of the substrate concrete and  $R_c(t, t_i)$  is the relaxation function corresponding to the shrinkage load applied at  $t = t_i$ . Creep in the substrate is neglected. The total stress at any time  $t$  is calculated by summing the contribution from each increment as:

$$\sigma(t) = \sum_{i=1}^i \sigma(t, t_i) \quad (3)$$

It should be pointed out that Eq. (1) gives the average stress in the overlay, i.e. the stress at mid-section, although it is recognised that the maximum stress will be obtained at the interface for the assumption of an even shrinkage distribution. The reason for the choice of the average stress value is that the shrinkage in reality will be highly non-linear due to the one-sided drying condition. This means that the stress at mid-section will be more representative.

#### *Cracked stage*

The cracked stage is considered to be reached if the tensile stress in the overlay reaches the tensile strength. Two situations may be distinguished after crack initiation: (1) the bond between the two layers is sufficient to prevent major de-bonding starting from a crack and (2) the bond is insufficient to prevent major de-bonding. For the case of sufficient bond it has been verified that a distributed pattern of fine cracks develops even for un-reinforced concrete, i.e. reinforcement is not required for this situation (at least not for overlay thickness up to 50 mm).

For case (2) it is assumed that a single crack develops within a de-bonded area, which has been verified to be valid for SFRC with steel fibre amounts up to 60 kg/m<sup>3</sup> in the base restrained tests. The fact that just a single crack develops implies that the crack width is related to the length of the de-bonded zone, or rather the free distance between bonded parts of the overlay ( $L_{deb}$ ) in addition to the residual strength of the SFRC.

It is of course not a simple task to determine a relevant value for the de-bonded zone and no recommendations are given in the present report on this regard. However, the following formulation has been found to give a reasonable approximation of the crack width development  $w_{cr}(t)$  in situations where the distance between bonded parts is known:

$$w_{cr}(t) = (\Delta \varepsilon_c(t_{cr}) + \Delta \varepsilon_{cs}(t, t_{cr})) \cdot (1 - R_{10,20}) \cdot L_{deb} \quad (4)$$

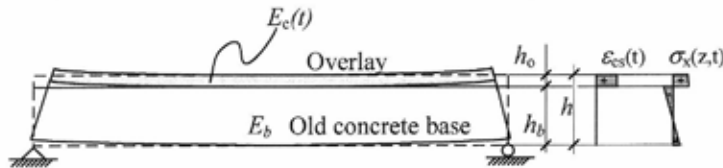
where  $\Delta \varepsilon_c(t_{cr})$  is the change in elastic concrete strain (sum of shrinkage strain and creep strain) at the time of cracking  $t_{cr}$ ,  $\Delta \varepsilon_{cs}(t, t_{cr})$  is the shrinkage strain applied after the time of cracking (shrinkage strain positive) and  $R_{10,20}$  is a residual strength factor for SFRC obtained from flexural beam tests.

The formulation given in Eq. (4) implies that the concrete will be completely relieved at the time of cracking in case of plain concrete, for which  $R_{10,20}$  is zero. In other words, the complete elastic strain developed in the concrete prior to cracking will contribute to the crack width as

well as the total shrinkage applied after cracking. In case of SFRC on the other hand, fibres will transfer some load across the crack, which means that the strain release at cracking will not be complete, and furthermore, that all of the shrinkage applied after cracking will not contribute to crack opening. It can be seen that the crack width will approach zero in case the residual strength factor reaches a value of 1 (or 100 %). This is not entirely correct as reinforcement will not prevent cracking. However, multiple cracking is foreseen for  $R_{10,20}$  values in the region of 1, which means that the crack width may be expected to be close to zero.

### 4.3 Factors influencing the cracking potential of overlays

Some examples of calculation results are given below to demonstrate how different factors influence the stress build up in bonded overlays. The basic prerequisites for the calculations are given in Figure 12. Shrinkage was calculated using a theoretical model described in [21] while creep and relaxation was estimated with a method given in [22] (see [10] for more details).



<b>Old concrete base</b>	<b>Overlay</b>
$h_b = 240$ mm	Overlay depth $h_o$ : varied
$E_b = 30$ GPa	Concrete quality: C25/30
<b>Drying environment</b>	<b>Curing time</b>
$RH = 60$ %	1 day
$T = 15^\circ\text{C}$	

Figure 12 – Main prerequisites for the calculations are that the overlaid structure is simply supported and that the overlay is exposed to an even shrinkage. Self weight is neglected.

A factor that significantly influences the crackability of concrete overlays is the depth of the layer. There are two reasons for this. The first is that the degree of restraint increases as the relative overlay depth ( $\alpha = h_o/h$ ) decreases and the second reason is that the shrinkage rate increases with decreasing depth. Some results are given in Figure 13 for 30, 60 and 120 mm overlays to illustrate the effect, where calculated free shrinkage is given in (a) and corresponding stress development in (b). Also shown in (b) is the estimated tensile strength for concrete type C25/30. Results imply that cracking is likely to occur already within a few weeks for overlay depth 30 mm while cracking may be completely avoided in a 120 mm overlay for this situation.

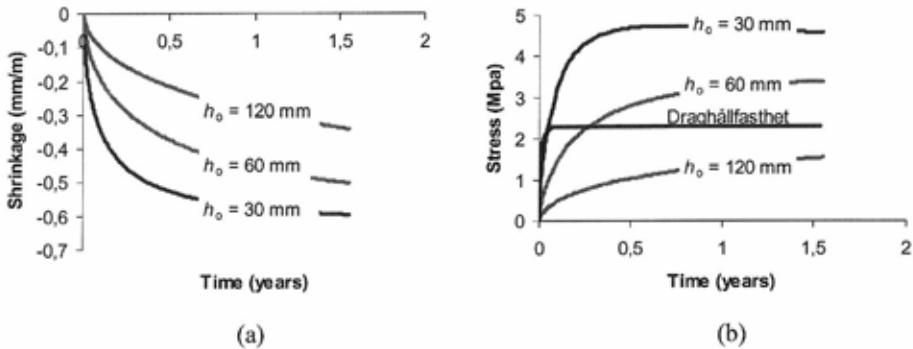


Figure 13 – Effect of overlay depth on the overlay stress development. Basic prerequisites for the calculations are given in Figure 12. (a) Free shrinkage development. (b) Overlay stress development.

Calculations were further conducted to demonstrate the effect of the concrete type. Results are given in Figure 14 for a comparison between C25/30 and C45/55 for three relative overlay depths  $\alpha$  of 0,1, 0,2 and 0,3. It can be seen that the stress development and the maximum stress values will be higher for concrete quality C45/55. Nevertheless, the cracking potential does not necessarily have to be higher for this concrete due to the higher tensile strength.

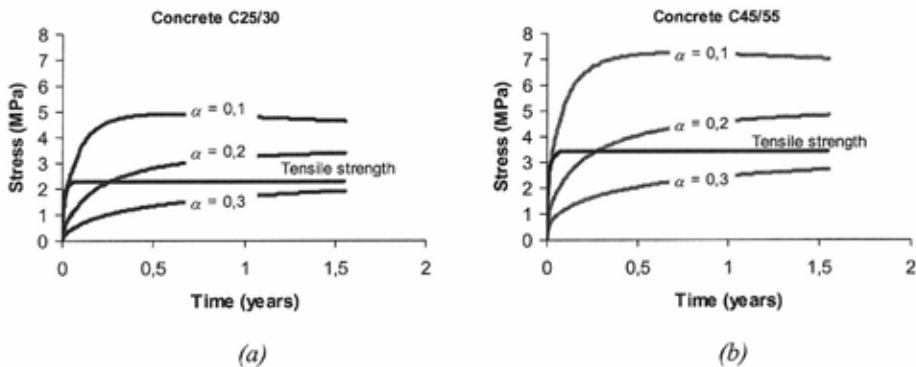


Figure 14 – Effect of concrete type and relative overlay depth on the stress development. (a) Concrete type C25/30. (b) Concrete type C45/55.

Another factor that has a significant influence on the stress development is the stiffness, or deformability, of the overlay. It can be seen in Figure 15 that stress relaxation due to creep reduces the stress in the overlay quite significantly. A reduction of the elastic modulus of the overlay is also positive.

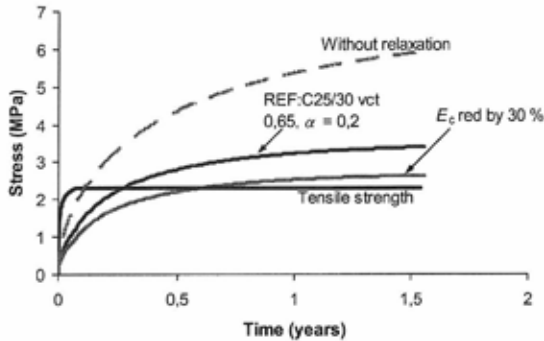


Figure 15 – Influence of relaxation (creep) and elastic modulus of the overlay concrete on the stress development.

#### 4.4 Crack width prediction

Some examples from the crack width analysis proposed in case of substantial de-bonding are presented in Figure 16 for an overlay depth of 60 mm,  $\alpha$  (relative depth) factor of 0,2 and a de-bonded length  $L_{deb}$  of 3 m. The shrinkage and relaxation was the same as used in the previously described analysis in the un-cracked stage.

From the stress development shown in Figure 16 (a) it can be seen that the stress drops immediately to zero when the tensile strength is reached for un-reinforced concrete. For SFRC on the other hand, the residual strength limits the magnitude of the abrupt stress decrease.

It may further be seen in Figure 16 (b) that the predicted crack width decreases with increasing  $R_{10,20}$ -value. The results imply that it is necessary to apply SFRC with a rather high  $R_{10,20}$ -value in order to maintain crack widths at an acceptable width if extensive de-bonded areas develop.

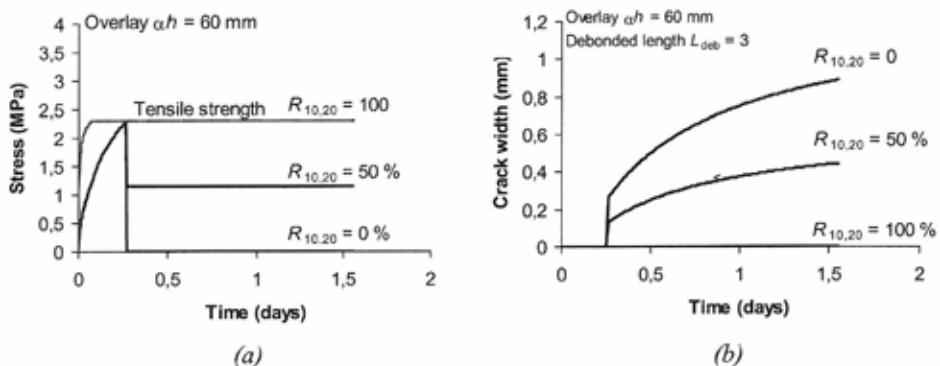


Figure 16 – (a) Tensile (Normal) stress development for an overlay depth of 60 mm and  $\alpha = 0,2$  for different residual strength factors  $R_{10,20}$ . (b) Crack width development for the corresponding residual strength factors.

Thus, provided that the theoretical approach is appropriate, it may be concluded that in order to ensure that crack width requirements are not exceeded for plain or fibre reinforced concrete overlays the best alternative is to make sure that de-lamination over substantial areas is avoided.

#### 4.5 Comparison of model predictions with test results

The theoretical model was used to predict the age at cracking and the crack widths of the base restrained overlay strips described in Section 2.3. Age at cracking is determined as the time when the predicted stress reaches the tensile strength. This situation is obtained at an age of approximately 19 days for PC and 32 days for SRA according to Figure 17 (a). In the real bonded overlay strips the first cracks were generally observed between 2 and 4 weeks after casting, which means that the correlation was satisfactory. It was, however, difficult to discern a clear difference in crack age between SRA and the other concrete types in the real tests.

A comparison of predicted and measured crack widths is given in Figure 17 (b). The results only cover cracks that appeared within de-bonded zones. It can be seen that the correlation was acceptable. This implies that the model can be used to predict crack widths of overlays within de-bonded areas. A condition is however that the de-bonded length is known in advance, which is of course seldom the case in reality.

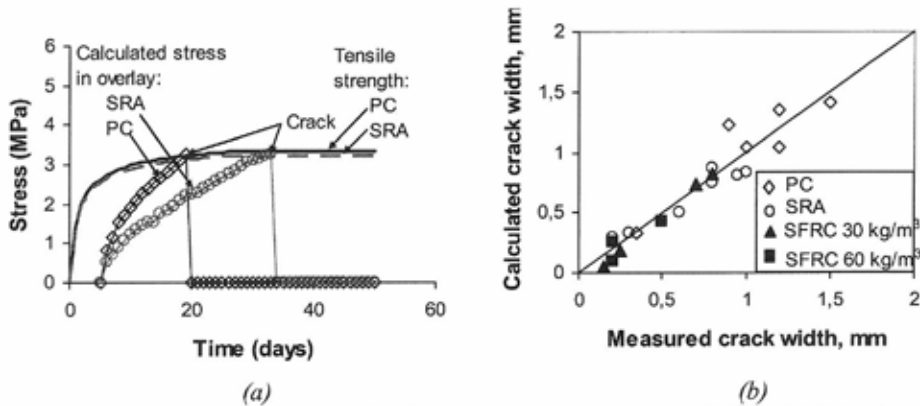


Figure 17 – (a) Predicted stress development for concrete types PC and SRA of the base restrained test series (Section 2.3). (b) Predicted and measured crack widths in base restrained test series.

## 5. CONCLUSIONS

Test results revealed that the cracking response of thin concrete overlays exposed to differential shrinkage to a significant extent relies on the bond situation. A distributed pattern of fine cracks (0,05-0,1 mm) developed in overlays with high bond strength to the substrate. For overlays with insufficient bond, on the other hand, major de-bonded areas occurred with a single major crack in case of inadequate reinforcement.

It was found that steel fibre contents up to 60 kg/m<sup>3</sup> were not enough to provide crack distribution within an internal de-bonded area even though crack widths were reduced due to the

fibre addition. A general recommendation on the required amount of fibres for crack control can thus not be given, as the crack width will also be related to the extent of the de-bonded area.

A main conclusion from the base restrained test series is, thus, that in order to ensure crack control for thin SFRC overlays it is essential that sufficient bond strength is achieved. Results of pull-out bond tests have shown that roughening the substrate is not critical for high bond strength to be achieved although a treatment may be required nonetheless in order to eliminate weak laitance layers or damaged concrete in case of repairs. Pre-moistening the substrate was on the other hand found to be beneficial, particularly for high  $w/c$  substrates. If overlays are placed on low  $w/c$  substrates, on the other hand, pre-moistening seems to be less important.

A theoretical model to predict overlay cracking and crack widths was also developed within the doctoral study [10] and comparisons with experimental results show a reasonable correlation.

## REFERENCES

1. Granju, J.L., Sabathier, V., Turatsinze, A. and Toumi, A., "Interface Between an Old Concrete and a Bonded Overlay: Debonding Mechanism," *Interface Science*, Vol. 12, No. 4, 2004, pp. 381-388.
2. Rahman, M.K., Baluch, M.H. and Al-Gadhib, A.H., "Simulation of shrinkage distress and creep relief in concrete repair," *Composites*, Part B31, 2000, pp. 541-553
3. Weiss, J., Yang, W. and Shah, S.P., "Shrinkage Cracking of Restrained Concrete Slabs," *Journal of Engineering Mechanics*, Vol. 124, No. 7, 1998, pp. 765-774
4. Yuan, Y., Li, G. and Cai, Y., "Modeling for prediction of restrained shrinkage effect in concrete repair," *Cement & Concrete Research*, Vol. 33, 2002, pp. 347-352
5. Ohama, Y., Demura, K. and Satoh, Y., "Drying shrinkage of steel fiber reinforced polymer-modified mortars containing shrinkage-reducing agent," In: *Proceedings of the 31<sup>st</sup> Japan Congress on Materials Research*, Kyoto, Japan, 1988, pp. 81-86
6. Shah, S.P., Karaguler, M.E. and Sarigaphuti, M., "Effects of Shrinkage-Reducing Admixtures on Restrained Shrinkage Cracking of Concrete," *ACI Materials Journal*, Vol. 89, No. 3, 1992, pp. 289-295
7. Grzybowski, M. and Ohama, Y., "Properties of cementitious composites containing shrinkage reducing agents," *Report 36*, Structural Design and Bridges, Royal Institute of Technology, Stockholm, Sweden, 1996.
8. Weiss, J. and Shah, S.P., "Restrained shrinkage cracking: the role of shrinkage reducing admixtures and specimen geometry," *Materials and Structures*, Vol. 35, 2002, pp. 85-91
9. Petersson, Ö. "Jointless concrete floors and shrinkage reducing admixtures for the repair of concrete structures," Report of SBUF projects 11529 and 11683, Aug. 2007 (In Swedish).
10. Carlswärd, J. "Shrinkage cracking of steel fibre reinforced self compacting concrete overlays – Test methods and theoretical analysis," *Doctoral thesis 2006:55*, Division of Structural Engineering, Luleå University of Technology, 2006.
11. Groth, P., "Fibre Reinforced Concrete – Fracture mechanics methods applied on self-compacting concrete and energetically modified binders," *Doctoral Thesis 2000:04*, Division of Structural Engineering, Luleå University of Technology, Luleå, Sweden, 2000.
12. Shah, H.R., Hossain, A.B., Mazzotta, G. and Weiss, J., "Time-dependent fracture in restrained concrete: The influence of notches and fibers," In: *Proceedings of Advances in Cement and Concrete IX: Volume Change, Cracking and Durability*, Aug., 2003, Copper Mountain, Colorado, USA.



13. Bissonnette, B., Morency, M., Von Fay, K., Vaysburd, A.M. and Brown, C.D. (2006) "Development of test method for cracking tendency of repair materials," In: *Proceedings of the Conference on Concrete Repair, Rehabilitation and Retrofitting*, Nov. 2005, Cape Town, South Africa, pp. 1045-1051.
14. Concrete Report No 4, "Steel fibre concrete – Recommendations for the design, construction and testing," *Swedish Concrete Association*, 1995, 132 pp. (In Swedish).
15. Soroushian, P. and Lee, C.H., "Distribution and Orientation of Fibers in Steel Fiber Reinforced Concrete," *ACI Materials Journal*, Vol. 87, No. 5, 1990, pp. 433-439.
16. Löfgren, I., "Fibre-reinforced Concrete for Industrial Construction – a fracture mechanics approach to material testing and structural analysis," *Doctoral Thesis*, Dep of Civil and Env Eng, Struct Eng, Chalmers University of Technology, Göteborg, Sweden, 2005.
17. Granju, J.L. and Turatsinze, A., "Repairs by the thin bonded overlay technique: the RILEM TC 193-RLS and last findings about the debonding mechanism," In: *Proceedings of the Conference on Concrete Repair, Rehabilitation and Retrofitting*, Nov. 2005, Cape Town, South Africa, pp. 43-52
18. Swedish National Road Administration, "Regulations for bridges, Part 6: Coatings and pavements," *VV Publ 2004:56*, Borlänge, Sweden, 2004. (In Swedish).
19. Silfwerbrand, J., "Concrete overlays," *Report No 10*, 2<sup>nd</sup> ed, Dep of Struct Eng, Royal Institute of Technology, Stockholm, Sweden, 1996, pp. 41. (In Swedish).
20. Denarić, E. and Silfwerbrand, J., "Structural behaviour of bonded concrete overlays," In: *Proceedings of the International RILEM Workshop "Bonded Concrete Overlays"*, June 2004, Stockholm, Sweden, pp. 38-45.
21. Svensk Byggtjänst "Concrete Handbook – Material," Stockholm, Sweden, 2<sup>nd</sup> ed, 1997. (In Swedish).
22. Eurocode 2, "European pre-standard ENV 1992-1-1: Design of concrete structures. Part 1: General rules and Rules for Buildings, draft version, 2001.

## Modelling of Thermally Induced Cracking of a Concrete Buttress Dam



Anders Ansell  
Ph.D., Associate Professor  
Department of Civil and Architectural Engineering, KTH  
SE-100 44 Stockholm, Sweden  
E-mail: anders.ansell@byv.kth.se



Richard Malm  
Tech. Lic., Ph.D. student  
Department of Civil and Architectural Engineering, KTH  
SE-100 44 Stockholm, Sweden  
E-mail: richard.malm@byv.kth.se

### ABSTRACT

Some of the larger hydropower dams in Sweden are buttress dams, consisting of up to 100 concrete monoliths formed by a front plate with a supporting buttress. Cracks have been observed in some dams, through the buttresses and at the base close to the rock foundation. The combined effects of restrained thermal displacements and loads caused by water are studied through finite element analysis. The results demonstrate the use of a non-linear material model and show that it is possible to follow the formation and propagation of the cracks. The analyses indicate that thermal stresses in combination with the loads caused by external water pressure are the reason for the cracking.

**Key words:** Buttress dam, cracking, finite element model, non-linear material properties.

## 1. INTRODUCTION

### 1.1 Background

Many of the major Swedish dams are concrete dams and in some of them, cracks have been observed. The type of cracks, the causes of cracking and their influence on the dam safety vary for different types of dams. Cracks appear due to restrained thermal strain during cooling after casting, but also due to large stresses from loads in the serviceability state, for example from water pressure, ice load and seasonal temperature changes. The cracks are often unstable as the creep effects, caused by long-term loads, lead to cracking at stresses lower than the concrete short-term strength. A cracked concrete structure is more likely to be damaged by environmental agents, which in turn can lead to further cracking or widening of the existing ones.

It is often difficult to predict the cause of cracking in concrete dams and therefore it is important to use analytical methods that allow the engineer to incorporate complex geometries, loads and material models. This is possible with the finite element method (FEM) which also makes the use of non-linear material models possible. Such a non-linear analysis does, however, rely on advanced numerical routines and may suffer from problems with convergence and numerical stability. The guidelines in the field of hydropower are adapted to old design and calculation models based on simplified assumptions and therefore effective use of numerical models are not permitted. There is thus a need to evaluate the use of FEM for analysis of large concrete dams and to show possibilities and restrictions associated with the method. A first step was taken through linear elastic analyses aiming at showing whether or not deformations and stresses caused by seasonal variation of temperatures could initiate cracks in a concrete dam, [1]. The main purpose was to demonstrate the use of FEM as a tool for analysis. The results revealed areas of stress concentrations and high stress levels in parts of a dam from where cracks could initiate. The analysis was performed with a large three-dimensional model of solid elements that could not be practically used in a non-linear analysis. The present paper summarizes two following projects that included non-linear analysis, see [2–3].

## 1.2 In situ observations

The studied dam is a buttress dam consisting of tall concrete monoliths, each with a front-plate facing the water and supported by a buttress. A section of such a dam is shown in Figure 1 where three adjacent monoliths are seen, each with a front-plate supported by a buttress. There is an inspection gallery that passes through each buttress and there is also a vertical insulating wall that together with the front-plate encloses a space where temperature and humidity can be controlled. A large buttress dam can be over 1000 m long and 40 m high, consisting of up to 100 large monoliths that can be over 30 m wide at the base, see [1–4]. The gap between the front-plates of two adjacent monoliths has a water tight seal.

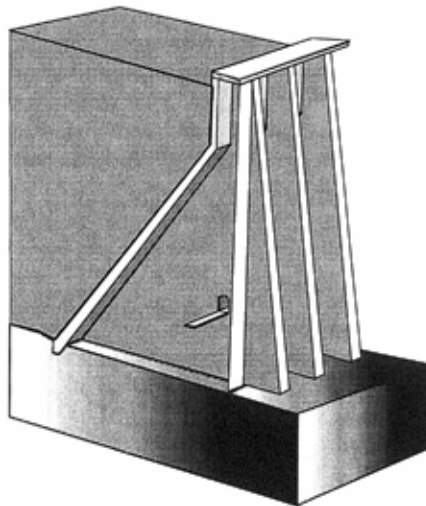


Figure 1 – A section of a concrete buttress dam. From [1].

In some large dams cracks have been observed in the lower part of the front-plate, which often leads to water leakage from the reservoir. A summary of typical observed cracks are given in [1], and here in Figure 2. It is possible that some of the cracks have partly arisen, or at least been initiated, during the cooling phase that follows casting of the concrete. Previous studies have mentioned cooling stresses during the moulding stage as the cause of cracking and calculations of such stresses are presented in [4] and [5]. The Storfinnforsen hydropower dam in northern Sweden was originally constructed in 1954, without a heat insulation wall. Inspections made in 1961 and 1986 revealed several cracks in the front-plates and that that ice formed on the upstream side of it below the water surface, see [4]. To protect the concrete against frost attack a heat insulation wall was installed in 1994. An inspection of the dam in 2004 revealed that the cracks in the front plates had increased even further since the previous mapping in 1986. The inspection also revealed that inclined cracks had appeared in the buttress. These cracks, (2)–(4) in Figure 2, were not reported in 1986 which implies that these cracks developed after the insulation wall was installed. Two of the tallest monoliths of the dam are now monitored regarding crack width and temperature changes since March 2006, [1–3]. It is therefore of great interest to model a dam of similar type and dimensions and to compare the results with these observations.

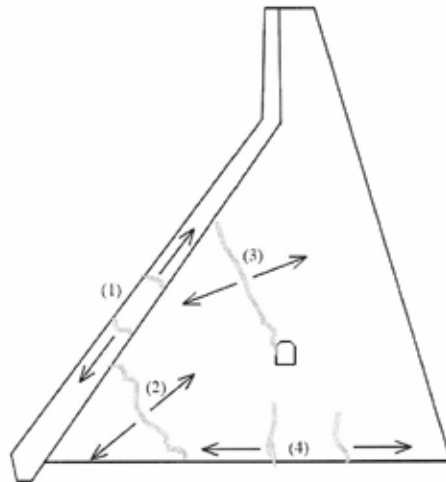


Figure 2 – Location of cracks observed in situ. From [1].

## 2. MODELLING OF A BUTTRESS DAM

Finite element analysis of a concrete dam subjected to water pressure and transient seasonal temperature variation was done using a non-linear fracture mechanical model. Pressure from ice, water pressure in concrete pores and shrinkage due to cooling at early ages was not considered. A fictitious buttress dam structure is studied, with measurements typical of large buttress dams in Sweden. Two different modelling approaches were tested, using a three-dimensional model and a less accurate but more computationally effective two-dimensional model. The analyses were used to determine the direction and the extension of thermally induced cracks.

## 2.1 Geometry and material properties

The analysed structure is a 40 m high section of a buttress dam, as shown in Figure 3. One concrete monolith of typical dimensions is considered, consisting of a 2 m thick and 8 m wide front-plate facing the water, and a triangular supporting buttress. The upper 10 m of the front plate is vertical while the lower part is inclined, with an angle of  $56.3^\circ$  versus the horizontal axis. The front-plate is rigidly connected to the buttress, but free at its outer ends that are in contact with the front-plates of the adjacent monoliths. The buttress is 2 m thick and rigidly connected to the rock underground, which is assumed to be of good quality granite. The dam crest, the horizontal upper part of the buttress and front-plate, has a width of 4 m. There is an inspection gallery through a  $2 \times 1.5 \text{ m}^2$  rectangular opening in the buttress, situated 9 m above the ground. The downstream edge of the buttress slopes  $68.2^\circ$  versus the horizontal. The water surface is assumed to be situated 1.5 m below the dam crest.

In some analyzed models the effect of steel reinforcement is included. The steel is here assumed to be elasto-plastic with a bi-linear definition and standard ribbed steel bars of Swedish type Ks 40 is assumed, all with a diameter of  $\phi 18 \text{ mm}$ . Two layers of reinforcement are placed in the entire monolith, each positioned 50 mm below the concrete surface. The reinforcement is arranged as shown in Figure 3. Physical and mechanical material parameters for steel, rock and concrete included in the analysis are given in Table 1. The table also gives parameters for thermal analysis but for rock and steel some of these are not needed in the numerical analysis and have therefore been noted with an \* in the table. It is assumed that only one quality of concrete have been used in all parts of the monolith.

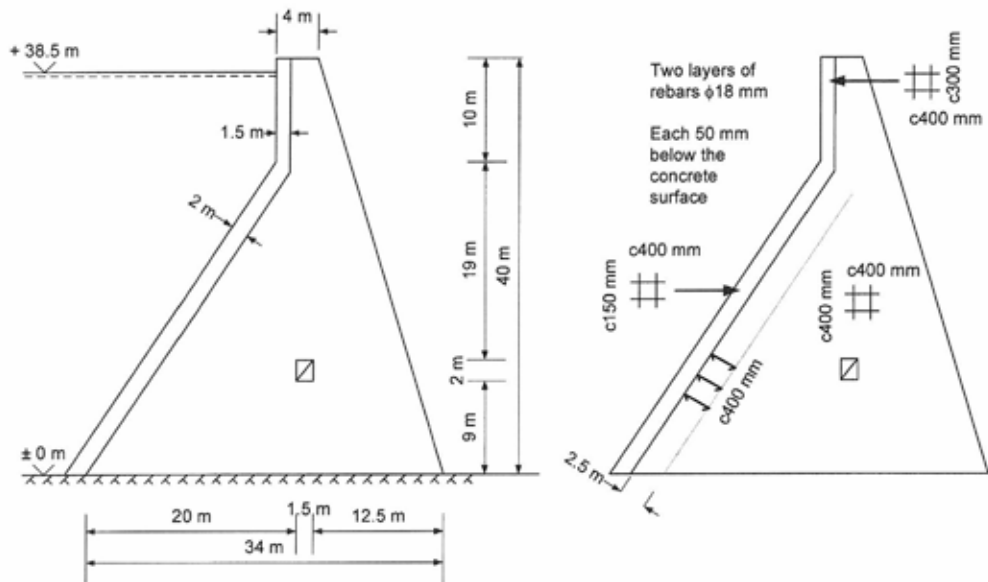


Figure 3 – Geometry of the analysed monolith. Arrangement of steel reinforcement.

*Table 1 – Physical, mechanical and thermal data for concrete, rock and reinforcement steel. Parameters not utilized in the analysis are noted with \*.*

	Concrete	Rock	Steel
Density (kg/m <sup>3</sup> )	2300	2300	7800
Modulus of elasticity (GPa)	25	60	206
Poisson ratio	0.2	0.2	0.3
Compressive strength (MPa)	28.5	*	*
Tensile strength (MPa)	2.5	*	*
Fracture energy (Nm/m <sup>2</sup> )	120	*	*
Expansion	0.00001	0.00001	0.00001
Heat conductivity (W/mK)	2.5	2.5	*
Heat capacity (J/kgK)	1000	1000	*
Heat transfer between solid and air (W/m <sup>2</sup> K)	13	*	*

## 2.2 Temperatures and loads

The maximum and minimum outside air temperatures that the dam-structure experience also give rise to the largest temperature differences, since the temperature variation in the water is much less than in the air. This means that the maximum stresses in the concrete structure induced by temperature occur under high summer or mid-winter, when the outside temperatures reach the maximum and minimum of the year. Stresses in the concrete occur due to restraint deformations caused by the bond to the underground and temperature gradients within the structure. The concrete is assumed to be unstrained at its initial temperature +10° C, corresponding to the zero stress condition at casting. The numerical calculations are performed as steady-state analyses where the various temperature fields are reached step-wise from the initial temperature of the concrete.

The two maximum temperatures during summer and winter are shown in Figure 4. The 8.5 m of water closest to the surface is assumed to have small seasonal temperature variation while water at greater depth is assigned a constant temperature over the year. The temperature variation of the rock is identical to that of the surface water. Two different cases are studied, with and without an insulating wall that divides the area of the buttress in contact with the outside air into two separate zones. The space between the front-plate and the wall will have temperatures much closer to that of the water.

For some of the modelling cases the temperatures shown in Figure 5 are used as input. As opposed to Figure 4 are not the air temperatures given, but instead the temperatures within the concrete structure, divided into four zones. The two cases summer and winter should be seen as possible extreme temperature distributions. The surface water is given the same temperature as water at greater depth and there is no need to insert rock temperatures for the cases studied with these temperature distributions. In both cases the temperature of the centre of the buttress is kept close to +10°C, the initial temperature of the concrete that corresponds to zero temperature strain. The part facing downstream, i.e. away from the front plate, is given high positive and negative temperatures, depending on season.

In addition to temperature loads are also gravity and water pressure considered, but not the pressures from wind and ice. The water is the most important of the loads and one monolith is

assumed to be designed to carry the load from 38.5 m of water acting on the 8 m width of the front-plate. The water pressure gives a resulting force of approximately 58 MN in the horizontal direction.

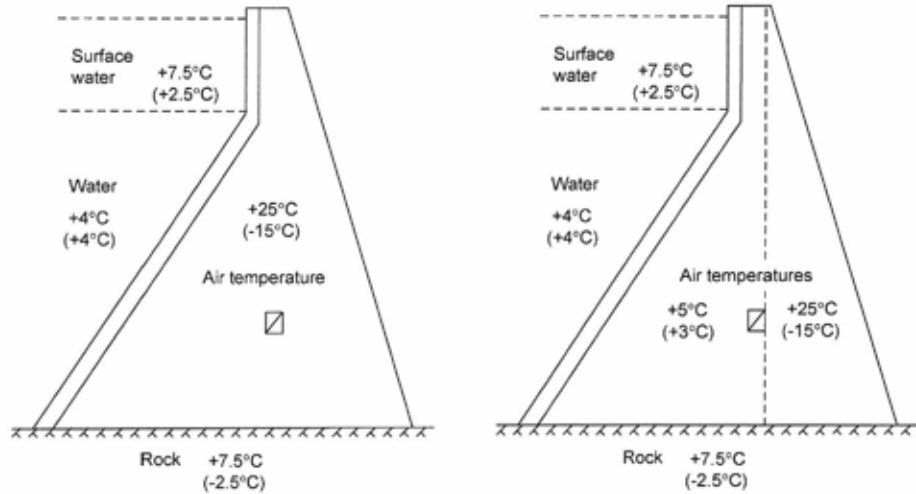


Figure 4 – Maximum temperatures in air, water and rock during summer (and winter) for a monolith with and without an insulating wall.

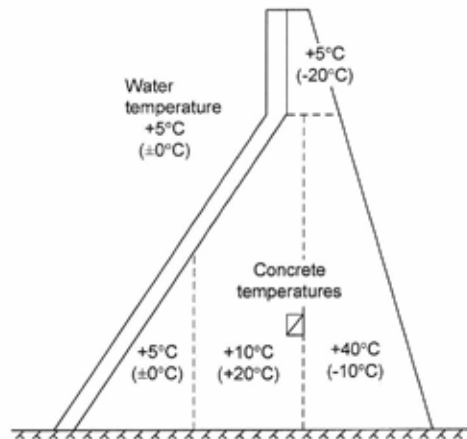


Figure 5 – Assumed extreme temperatures in water and concrete during summer (and winter).

### 2.3 Finite element modelling – in general

The studied concrete dam has been modelled using the *Abaqus/Standard* [6] finite element software. Two modelling approaches are used, three-dimensionally using shell elements and

two-dimensionally using plane stress elements which are a less accurate but more computationally effective model. A numerical analysis with the program is divided in steps, each corresponding to a load change from one magnitude to another. For the analysis of a dam the first steps can be the addition of gravity load and water pressure, followed by one or more temperature loads. For each step a procedure is chosen that corresponds to the type of analysis to be performed, and a full analysis may thus include various numerical procedures. The state of the model in terms of stress, strain, temperature, etc. is updated throughout all analysis steps. The effects of previous steps are always included in each new step. It is therefore important to use a sequence of steps that accurately describes the actual load situation for the structure analysed. It is possible to do both linear and non-linear analysis with respect to predefined properties, such as stress-strain relations for included materials. Solving non-linear problems are much more computationally demanding than linear problems and the objective in such cases is often to obtain a convergent solution at a minimum effort. For solving the non-linear equilibrium equations Newton's method is the general numerical technique due to its convergence rate for the often studied types of problems.

The *Abaqus* program contains a large number of various finite elements for two- and three-dimensional analyses. The two-dimensional elements allow modelling of plane and axisymmetric problems and also include the possibility to model generalized plane strain situations. The latter assumes that the model exists between two planes that may move with respect to each other. This gives strains that are constant with respect to thickness position but may vary with position in the plane of the model. It is recommended (see [6]) that isoparametric elements are used, if possible, as these often are the more computationally effective of the provided elements. For three-dimensional analyses the elements are hexahedrons (brick-shaped), while their two-dimensional counterparts are quadrilaterals. When it is impossible to use isoparametric elements throughout a model it is recommended that triangular, tetrahedrons, and wedge elements are used instead. For the analysis of a triangular structure, such as the studied buttress dam, these types of element may be used to model the entire structure. An accurate description of the geometry is especially important when detailed predictions of strains are required. Elements that describe plane strain situations are often used for two dimensional analyses of long and massive structures, such as gravity dams. For the studied concrete monolith, that basically consist of two connecting plates, elements for plane stress-situations will be a better choice. This type of elements is recommended (see [6]) when the thickness of the analysed structure is much smaller relative to the other directions, thereby assuming that all stresses outside the observed plane are zero. For the studied dam the best choice of such a plane is that of the buttress, with the front-plate included as a stiff edge, modelled by deep two-dimensional elements. It will not be possible to define temperature gradients on surfaces parallel to the plane of observation. All temperatures will thus correspond to the centre of the buttress and not the outside surfaces in contact with the surrounding air.

Modelling of curved, intersecting plates and shells is possible with shell elements in a three-dimensional analysis. These elements can undergo large overall translational and rotational motions. The shell elements in *Abaqus* are divided into three categories, depending on theoretical formulations. Thin elements provide solutions that are adequately described by Kirchhoff shell theory, while thick elements yield solutions for structures that are best modelled by shear flexible Mindlin theory. The third category is general-purpose elements that can provide accurate solutions to both thin and thick shell problems. For the studied dam triangular general-purpose elements used, which give an accurate model of both the triangular buttress and the front-plate that consist of two rectangular plates. With shell elements, temperature distributions over all shell surfaces can be described, as well as for the centre of the shell.



## 2.4 Non-linear material model

Material models are an integrated part of *Abaqus*, also including models specially developed for concrete and quasi-brittle materials. There are three material models for the non-linear behaviour of concrete [6]. Two are based on the smeared crack approach, the *concrete smeared cracking* and *brittle cracking* models. The third model, used in this analysis of the buttress dam, is based on plasticity theory and called *concrete damaged plasticity* model, see also [7] and [8]. With this model it is possible to define the material degradation in compression as well as tension, so that its tensile softening behaviour is based on a crack-opening law and fracture energy. Damage is associated with the failure mechanisms of the concrete and therefore results in a reduction in the elastic stiffness. The *concrete damaged plasticity* model is intended for analysis of reinforced concrete structures but can also be used for plain concrete. Concrete reinforcement can be modelled as discrete rebars or as reinforcement layers embedded in concrete. The model is also suitable for the analysis of other quasi-brittle materials such as rock, mortar and ceramics. Under low confining pressures, concrete behaves in a brittle manner and the main failure mechanisms are cracking in tension and crushing in compression. The brittle behaviour of concrete disappears when the confining pressure is sufficiently large to prevent crack propagation. Under these circumstances, failure is driven by the consolidation and collapse of the micro-porous structure in the concrete [6].

The following short summary of theoretical relations associated with the *concrete damaged plasticity* model is based on [9], where a more detailed description is given. Within the context of the scalar-damage theory, the stiffness degradation is isotropic and characterised by degradation variables  $d_t$  and  $d_c$ , for tension and compression respectively. The stress-strain relationship under uniaxial tension ( $\sigma_t, \varepsilon_t$ ) and compression ( $\sigma_c, \varepsilon_c$ ) are:

$$\sigma_t = (1 - d_t) E_0 (\varepsilon_t - \tilde{\varepsilon}_t^p) \quad (1)$$

$$\sigma_c = (1 - d_c) E_0 (\varepsilon_c - \tilde{\varepsilon}_c^p) \quad (2)$$

where  $E_0$  is the initial undamaged elastic modulus with  $\tilde{\varepsilon}_t^p$  and  $\tilde{\varepsilon}_c^p$  denote the equivalent plastic strain in tension and compression, respectively. The yield function used is a combined geometric form of two different Drucker-Prager type functions, illustrated in Figure 6. The yield criterion is based on an invariant function of the stress state, i.e. independent of the choice of the coordinate systems. In Figure 6  $\bar{q}$  is the Mises equivalent stress,  $\bar{p}$  is the equivalent pressure and  $\alpha$  and  $\beta$  are dimensionless coefficients.

The Drucker-Prager hyperbolic plastic potential function used in the *concrete damaged plasticity* model is illustrated in Figure 7 and defined according to:

$$G = \sqrt{(\varepsilon \sigma_{t0} \tan \psi)^2 + \bar{q}^2} - \bar{p} \tan \psi \quad (3)$$

where  $\varepsilon$  is the eccentricity, which defines the rate at which the plastic potential function approaches the asymptote, and  $\psi$  the dilation angle measured in the  $\bar{p}-\bar{q}$  plane at high confining pressure. The flow in the Drucker-Prager function is non-associative (not identical with the yield surface) in the meridional plane if the dilation angle and the material friction angle are different. The experimental observation in most quasi-brittle materials, including

concrete, is that the compressive stiffness is recovered upon crack closure as the load changes from tension to compression. On the other hand, the tensile stiffness is not recovered as the load changes from compression to tension once micro-cracks from crushing have developed. This behaviour is illustrated in Figure 8, where  $\Gamma_t = 0$  corresponds to no recovery as load changes from compression to tension and  $\Gamma_c = 1$  to complete recovery as the loading changes from tensile to compressive [6].

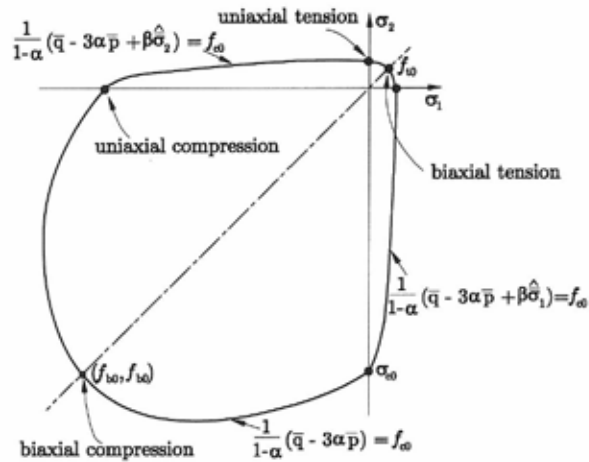


Figure 6 – Biaxial yield surface in the constitutive model concrete damaged plasticity. From [9].

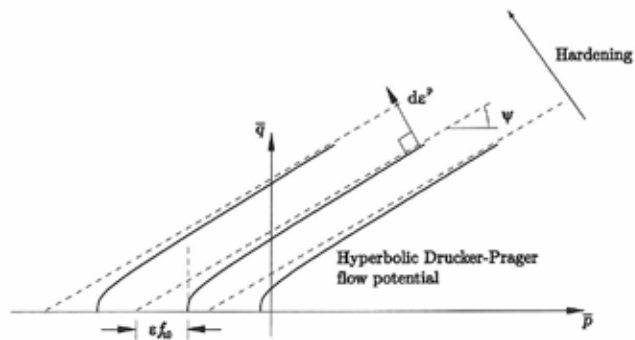


Figure 7 – The Drucker-Prager hyperbolic plastic potential function in the meridional plane. From [9].

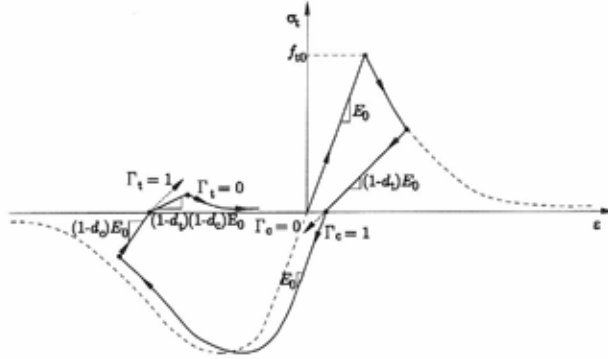


Figure 8 – Uniaxial load cycle (tension-compression-tension) assuming default values for the stiffness recovery factors  $\Gamma_t = 0$  and  $\Gamma_c = 1$ . From [9].

For the non-linear analysis of the buttress dam the coefficients for Eqs. (1–3) were chosen as  $\varepsilon = 0.1$ ,  $\psi = 38^\circ$  and  $\alpha = 0.12$ . The compressive behaviour is given as follows:

$$\sigma_c = 1.33 \cdot 10^{10} \varepsilon_c^{in} + 1.71 \cdot 10^7 \quad \text{for } \varepsilon_c^{in} \leq 8.6 \cdot 10^{-4} \quad (4)$$

and in tension is:

$$\sigma_t = -2.60 \cdot 10^{10} u_t^{ck} + 2.50 \cdot 10^6 \quad \text{for } u_t^{ck} \leq 9.6 \cdot 10^{-5} \quad (5)$$

Tension damage is defined by:

$$d_t = 9000 u_t^{ck} \quad \text{for } u_t^{ck} \leq 9.6 \cdot 10^{-5} \quad (6)$$

In the equations  $\varepsilon_c^{in}$  and  $u_t^{ck}$  are the inelastic strain and the direct cracking displacement, respectively, given in (m) whereas the stresses  $\sigma_c$  and  $\sigma_t$  are in (Pa).

### 3. TWO-DIMENSIONAL ANALYSIS

In a first modelling approach two-dimensional models and non-linear material properties for the concrete are used. The front-plate and the buttress are relatively thin in comparison with the height and width of the dam and therefore plane stress conditions were assumed, in contrast to plane strain conditions that are often used for two-dimensional models of massive structures, such as gravity dams.

#### 3.1 Finite element model

Two-dimensional triangular continuum elements were used, but also quadrilateral elements were tested in some models. For the combined analysis of displacements, stresses and temperatures thermally coupled elements were chosen. A typical model of the dam consisted of 5776

triangular elements with 52620 degrees of freedom, as shown in Figure 9. The depth (thickness) of the model is 2 m, apart from a 2 m wide band closest to the water where the depth is 8 m. The monolith is assumed to be rigidly connected to the underground. The effect of reinforcement is not included in this case.

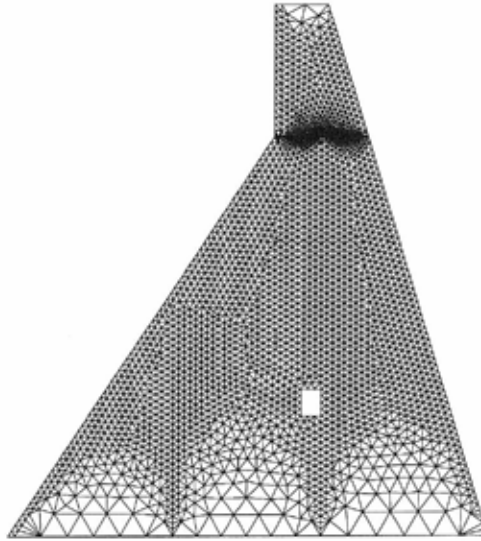


Figure 9 – Finite element model with 5776 triangular elements.

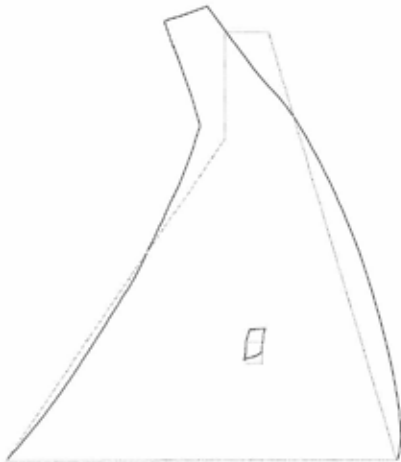


Figure 10 – Deformation due to extreme summer temperatures. Deformation scale factor 1000.

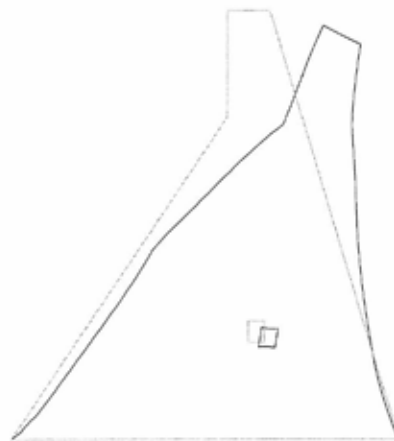


Figure 11 – Deformation due to extreme winter temperatures. Deformation scale factor 1000.

### 3.2 Deformation due to extreme temperatures

Stresses and deformations have been calculated on basis of the extreme summer and winter temperatures given in Figure 5. The deformed shapes are shown in Figures 10–11 where it is evident that the buttress deforms towards the side with extreme temperatures, towards the relatively cold water during the summer and vice versa during the winter. The horizontal displacement of the crest is approximately 5 mm during summer and 9 mm during winter.

### 3.3 Stresses and concrete damage

The stresses and zones with damaged concrete in the front-plate and buttress are shown in Figures 12–13. The left figures (a) show the distribution of maximum principal stresses while the right figures (b) indicate cracked zones where the tensile strength of the concrete is exceeded. The extreme summer temperatures give rise to large stresses inside the structure, as seen in Figure 12. Tensile cracks have propagated from the opening towards the front plate, in a direction perpendicular to the front-plate, and towards the lower right corner of the structure. Note that the cracks can be traced in the stress plot (a) and that there are high stresses around the tip of the cracks. For the winter conditions there are low or zero stresses within the interior zone with temperatures close to the initial temperature of the concrete, as shown in Figure 13. A vertical band of stresses appear to the right, along the interface between positive and negative temperature zones. There are high stresses along the front-plate, which is heavily strained as seen in Figure 11. There is one crack that runs through the front plate and further towards the rectangular opening. It should be noted that the full coupling to the underground in both cases gives rise to large stresses and some damage at the lower corners of the structure.

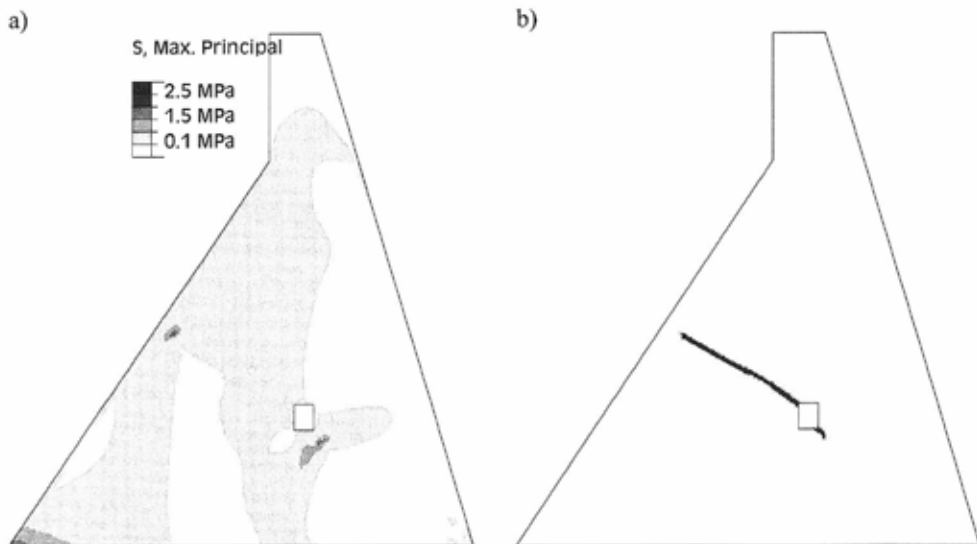


Figure 12 – Maximum principal tensile stresses (a) and cracked concrete (b) during extreme summer.

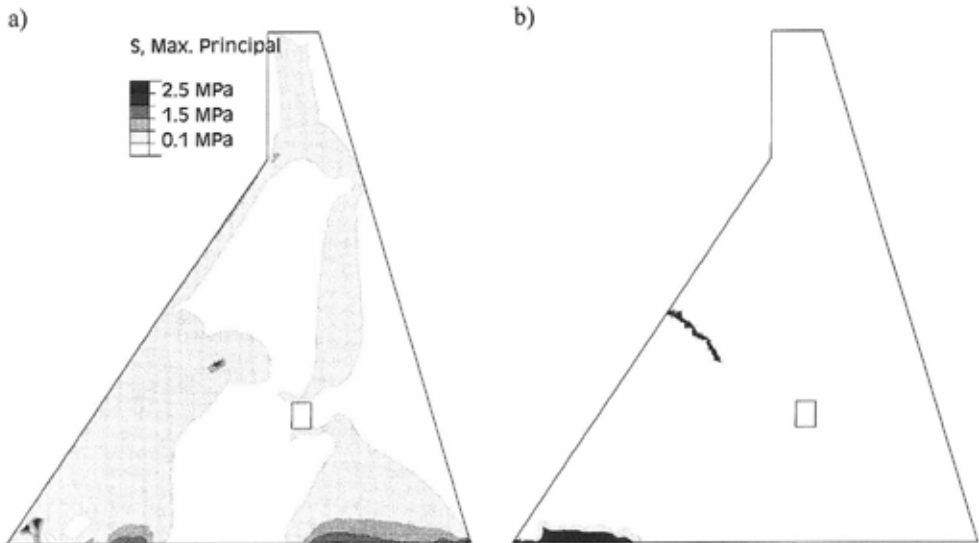


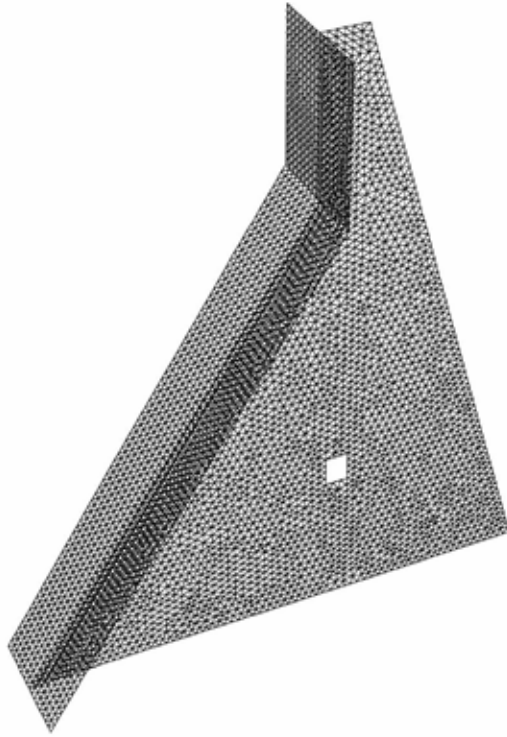
Figure 13 – Maximum principal tensile stresses (a) and cracked concrete (b) during extreme winter.

#### 4. THREE-DIMENSIONAL ANALYSIS

The concrete monolith was modelled with shell elements for this analysis, also including the effect of steel reinforcement. The three-dimensional model makes it possible to assign temperatures to each surface of the shells. A finite element analysis with non-linear material properties was performed to determine temperature distributions in both the maximum summer and winter temperature case. The temperature distributions were thereafter used as input for calculation of displacements and stresses in the monolith. The effect of the insulating wall described in section 2.2 was studied as a separate case.

##### 4.1 Finite element model

The three-dimensional model was built up with 9418 triangular shell elements with 32916 degrees of freedom, as shown in Figure 14. The monolith is also in this case assumed to be rigidly connected to the underground, which is not included in the figure. The rock is here modelled as an elastic 2 m thick plate, with material properties as given in Table 1. This will lead to less stress build-up at the concrete-rock interface, compared to a case where the rock is un-deformable. In this way an elastic coupling to the ground is obtained, which approximates the function of anchorage of dam structures in situ. Reinforcement bars are included in the model for the second analysis step, stresses due to unevenly distributed temperatures from the first step is calculated. The bars are coupled to the shells as embedded elements, situated as described in section 2.1.



*Figure 14 – Finite element model with 9418 triangular shell elements.*

#### **4.2 Stresses and concrete damage**

The deformed shapes due to extreme temperatures are similar to those of the two-dimensional model, with the buttress bending towards the coldest side. The magnitudes of the deformations are also comparable and the deformed shapes of the shell model are therefore not shown here. Stresses and concrete damage due to maximum temperatures as given to the left in Figure 4 are shown in Figures 15–16. The summer temperatures give rise to high stresses in the front-plate but only minor stresses in the buttress, as seen in Figure 15(a). The plate is cracked (b) at the lower 15 m, with a vertical crack along the connection to the buttress, ending with a horizontal crack across the plate. There are also large stresses at the connection between the upper vertical and the lower front-plates. The stresses due to winter temperatures show less stress in the front-plate but high stress fields in the lower part of the buttress, as seen in Figure 16(a). There are in this case also large stresses at the centre of the front-plate. The stresses do not initiate cracking, apart from at the edges of the concrete-rock interface as shown in Figure 16(b).

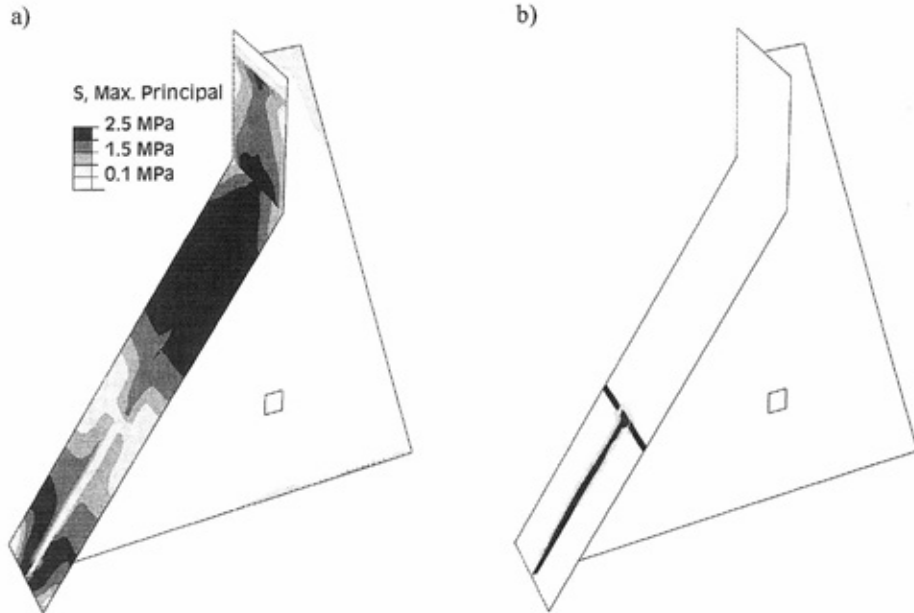


Figure 15 – Maximum principal stresses (a) and damaged concrete (b) due to summer temperatures.

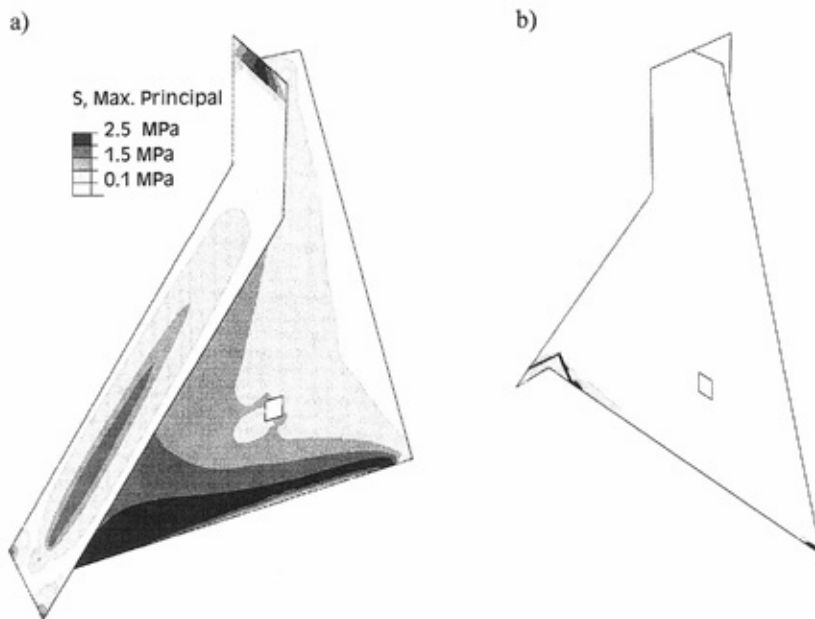


Figure 16 – Maximum principal stresses (a) and damaged concrete (b) due to winter temperatures.



### 4.3 The effect of an insulating wall

The inclusion of the insulating wall results in a division of the surfaces of the buttress into two temperature zones, as shown to the right in Figure 4. The sharp line between the moderate temperatures between the wall and the front-plate and low outside temperature during winter give rise to large stresses in the buttress, in the zone with the lowest temperatures, as seen in Figure 18(a). The stress situation in the front-plate during the winter is comparable to that of the cases without the wall, as in Figure 16(a). Comparing the case with and without the insulating wall for the summer case, it can be seen that the high tensile stress in the front-plate of the original dam reduces after the instalment of an insulating wall, see Figures 15(a) and 17(a). This shows that the insulating wall is working as intended regarding decreasing the tensile stresses in the front-plate, but instead introducing large tensile stresses in the buttress. In this case the summer temperatures will also initiate cracks at the rectangular opening which propagates diagonally towards the front-plate and in the opposite direction, as seen in Figure 17(b). The cracks are initiated at an outside temperature of  $+20^{\circ}\text{C}$ , but will propagate first when this has reached  $+25^{\circ}\text{C}$ . There are cracks in the front-plate, also present in the winter case shown in Figure 18.

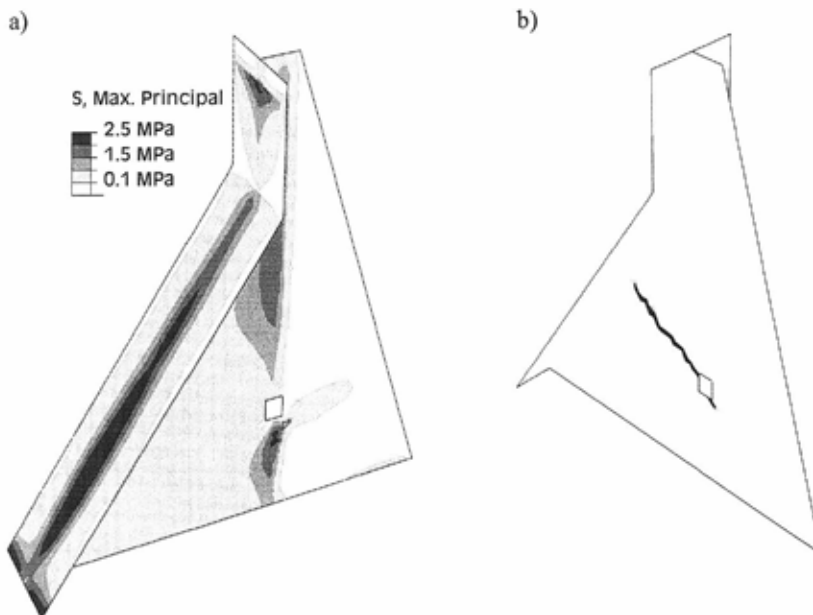


Figure 17 – Maximum principal stresses (a) and damaged concrete (b) due to summer temperatures.

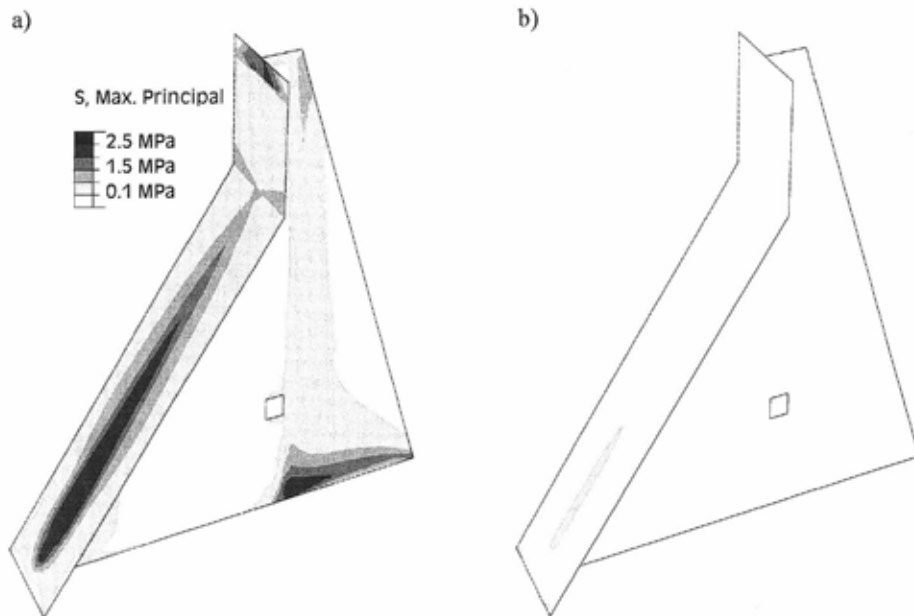


Figure 18 – Maximum principal stresses (a) and damaged concrete (b) due to winter temperatures.

## 5. DISCUSSION

### 5.1 Comments

The use of a non-linear material model gives a much more correct description of the post-elastic behaviour of the large concrete dam than a strictly elastic analysis, but it is considerably more computationally demanding. The convergence of a non-linear analysis must be ensured by carefully selecting the type of finite elements, mesh density and numerical tolerances. These choices are also significantly more important when using a three-dimensional model compared to one in two dimensions. Two-dimensional models will always be computationally more efficient than three-dimensional equivalents, with respect to cost in time and computer capacity.

As the modelled concrete monolith basically consists of two orthogonal plates a finite element analysis with a two-dimensional model in the plane of the buttress will give fairly accurate results. One drawback is that it is not possible to assign temperatures to surfaces that are parallel with the plane considered in the analysis. It is thus impossible to describe temperature variations across the thickness of the front-plate and the buttress. Regarding the stress and displacement analysis temperature variations within the concrete structure must be given as input. Numerical tests showed that extreme temperatures, positive and negative, must be applied to parts of the structure before cracks were initiated. It was possible to accurately describe cracking of the concrete monolith with the two-dimensional model which in this respect was superior to the

earlier approach [1] with a three-dimensional solid element model with only linear material properties.

A three-dimensional model will, however, always give a more accurate description of a structure such as the analysed dam than a two-dimensional model. As an example deformations and cracking due to transverse bending of the front-plate can not be described with the two-dimensional model. A model based on shell elements was therefore tested, having much less degrees of freedoms than a comparable model with solid elements. It is possible to accurately describe the two plates of the monolith as plane shells, thereby also facilitating the application of surface temperatures as input for the analysis. With shell elements it is also possible to obtain information on the temperature variation through the thickness. Another important feature is that steel reinforcement can be included as embedded bars within the shells, which increases the accuracy of the analysis. The method of two-step analysis proved to be efficient. In a first step the temperature distribution within the structure is calculated on basis of the surface temperature input. This relatively fast analysis step is then followed by a relatively slow non-linear calculation of stresses and displacements.

The calculated results show that all four types of cracks observed in situ were obtained in the non-linear analyses. Horizontal cracks in the front-plate, type (1) according to Figure 2, occur due to high tensile forces during the summer, which can be seen in Figure 15. The winter temperatures results in cracking of type (1) and (2) on the downstream side of the front-plate and in the lower part of the buttress respectively, as can be seen in Figure 16 and in Figure 13 from the two-dimensional analysis. Diagonal cracks in the lower part of the buttress, type (2), are visible in Figure 16 but not in the results from the two-dimensional analysis. This type of cracks is probably caused by a combination of static load from the water and restrained shrinkage due to low temperatures. The third type of cracks (3) goes diagonally from the rectangular opening orthogonally towards the front-plate. Such a crack is clearly visible in Figure 12 and a crack propagating in the opposite direction is found in Figure 13, caused by extreme summer and winter temperatures, respectively. This crack type did not appear with the three-dimensional model, unless the insulating wall was accounted for, as seen in Figure 17. A detailed analysis showed that such cracks propagates when the temperature within the space enclosed by the front-plate and the insulating wall is colder than approximately  $+10^{\circ}\text{C}$  at the same time as the outside temperature exceeds  $+25^{\circ}\text{C}$ . Vertical cracks from the concrete-rock interface, type (4), are caused by restrained movement due to low temperatures, and possibly also concrete shrinkage. High tensile stresses and some concrete damage in this area are visible in Figures 12–13 and 16. The magnitude of the stresses within the area close to the concrete-rock interface depends on the rigidity of the rock underground.

## 5.2 Conclusions

The numerical results show that it is possible, by means of numerical non-linear analysis, to describe and follow the initiation and propagation of cracks found in situ on the studied type of concrete buttress dams. The use of three-dimensional shell models proved to be more accurate than two-dimensional models. Although the shell models were computationally more demanding than the simpler two-dimensional models, they were still much more efficient than three-dimensional solid element models. The results show that the seasonal temperature variation may cause high tensile stresses at different locations on the dam, and that the cracks can be initiated from at least four locations on the dam. All types of cracks can also be initiated and propagate simultaneously. The analyses indicate that the addition of an insulating wall,

which together with the front-plate encloses a space that includes the rectangular opening, may be one of the causes for cracking of the dam.

### 5.3 Further research

The future research will aim at calculation of deformations and stresses within the dam for combinations of various temperatures, water pressure and ice pressure. The risk of possible widening of existing cracks due to temperature cycles repeating yearly will be investigated. The effect of using non-linear material models for the steel reinforcement must be studied further. The long term effect of concrete creep and water pressure within concrete cracks are also of interest. The temperature distribution and propagation within the concrete must be studied in detail and verified with measurements and observations in situ. The movement of the dam crest due to seasonal temperature changes must be measured on a full size dam and used for verification of the finite element models. It is of great interest to first predict the effect of possible repair methods for cracked dams by calculations, and then evaluate this by in situ observations.

### ACKNOWLEDGEMENTS

The work was performed during 2006–07, in collaboration with *Vattenfall* and *Grontmij*, with financial support from *Elforsk AB*, the Swedish Power Companies R&D association. The authors thank Dr. Manouchehr Hassanzadeh, Dr. Tomas Ekström, Dr. Mattias Unosson and Mr. Jonas Björnström for their valuable participation in the project.

### REFERENCES

1. Björnström, J., Ekström T., Hassanzadeh M., “Cracked concrete dams – overview and calculation methods”, Report 06:29, Elforsk AB, Stockholm, 2006 (in Swedish).
2. Ansell, A., Björnström, J., Ekström, T., Hassanzadeh, M., Unosson, M., “Thermally induced crack propagation in a buttress dam”, Paper 56, International Symposium on Dam Safety Management, NN25, Icold, St Petersburg, 2007.
3. Ansell, A., Björnström, J., Ekström, T., Hassanzadeh, M., Unosson, M., “Cracked concrete buttress dams. FE analysis – Part 1”, Report 08:21, Elforsk AB, Stockholm, 2008 (in Swedish).
4. Fahlén, A., Näslund, L., “Cracks at Storfinnforsen concrete dam – mapping and analysis”, Division of Structural Engineering, LTU, Luleå, 1991 (in Swedish).
5. Melander, R., “Concrete dams condition and durability”, Division of Hydraulic Engineering, KTH, Stockholm, 1997.
6. “Theory manual. Abaqus 6.6”, Online manual, Simulia, Providence, RI, USA, 2006.
7. Lubliner, J., Oliver, J., Oller, S., Oñate, E., “A plastic-damage model for concrete”, *International Journal of Solids and Structures*, 25:3, 1989, pp. 229–326.

8. Lee J., Fenves, G. L., "Plastic-damage model for cyclic loading of concrete structures", *Journal of Engineering Mechanics*, 124:8, 1998, pp. 892–900.
9. Malm, R., "Shear cracks in concrete structures subjected to in-plane stresses", Bulletin 88, Department of Civil and Architectural Engineering, KTH, Stockholm, 2006.

## Structural assessment of concrete bridges

Mario Plos Ph.D., Lecturer,  
Chalmers University of Technology, Göteborg, Sweden  
e-mail: mario.plos@chalmers.se

Kent Gylltoft, Professor  
Chalmers University of Technology, Göteborg, Sweden  
e-mail: kent.gylltoft@chalmers.se

Karin Lundgren, Assoc. Prof.  
Chalmers University of Technology, Göteborg, Sweden  
e-mail: karin.lundgren@chalmers.se

Jan Cervenka, Dr.  
Cervenka Consulting, Praha; Czech republic  
e-mail: cervenka@cervenka.cz

Andrin Herwig, Dr.  
Ecole Polytechnique Fédérale de Lausanne(EPFL), Lausanne,  
Switzerland, e-mail: andrin.herwig@epfl.ch

Eugen Brühwiler, Professor  
Ecole Polytechnique Fédérale de Lausanne(EPFL), Lausanne,  
Switzerland, e-mail: eugen.bruehwiler@epfl.ch

Sven Thelandersson, Professor  
Lund University of Technology, Lund, Sweden  
e-mail: sven.thelandersson@kstr.lth.se

Lennart Elfgren, Professor  
Luleå University of Technology, Luleå, Sweden  
e-mail: lennart.elfgren@ltu.se

Ebbe Rosell, M.Sc.  
Swedish Road Administration, Borlänge, Sweden  
e-mail: ebbe.rosell@vv.se

### ABSTRACT

The paper summarises the work on concrete bridges performed in the EU project Sustainable Bridges. The work provides enhanced assessment methods that are able to prove higher load-carrying capacities and longer fatigue lives for existing concrete railway bridges, and is implemented in a Guideline [1]. Methods for determination of in-situ material properties and advanced methods for structural analysis were developed. One main focus was non-linear analysis, since these provides the greatest potential for discovering of additional sources for load-carrying capacity. Furthermore, methods to assess the remaining structural resistance of deteriorated concrete bridges with respect to corrosion and fatigue were developed.

**Key words:** Structural assessment, concrete, railway, bridge, non-linear analysis, fatigue, corrosion.

## 1. INTRODUCTION

For a sustainable development of Europe, there is a need to at least double the railway transports in the coming 20 years. In order to reach this goal, the residual service lives of existing concrete railway bridges need to be extended, at the same time as they are subjected to higher axle loads, higher railway speeds and heavier traffic intensity. Today, many concrete bridges are replaced or strengthened because their reliability cannot be guaranteed based on the structural assessments made. The objective of the work presented here was to provide enhanced assessment methods that are able to prove higher load-carrying capacities and longer service lives for existing concrete railway bridges.

The work was a part of the EU-project Sustainable Bridges. The results are implemented in the *Guideline for Load and Resistance Assessment of existing European Railway Bridges* [1] that was developed within the project. The guideline is based on the current state-of-the-art, but improved knowledge was developed in a few prioritised areas: material properties in existing bridges, advanced methods for structural analysis and assessment of deteriorated bridges with respect to fatigue and corrosion. This paper focus on the research performed, which is reported more in detail in a background document to the guideline [2]. In the Sustainable Bridges project, guidelines were developed also for inspection and condition assessment [3], for monitoring [4] and for repair and strengthening [5] of railway bridges.

Improved methods for the determination of in-situ material properties in existing concrete bridges were developed, for deterministic as well as for fully probabilistic assessments. To facilitate structural analysis on different levels, recommendations for redistribution of sectional moments and forces from linear finite element (FE) analysis were developed. Furthermore, advanced methods for local resistance analysis were developed, e.g. regarding combined shear, torsion and bending interaction.

To facilitate the usage of non-linear analysis for structural assessment, recommendations for practical use were developed. Non-linear analysis provides the greatest potential to discover any additional sources for load-carrying capacity, and gives a better understanding of the structural response, forming an improved basis for assessment decisions.

Another main objective was to provide methods for assessing the remaining structural resistance of deteriorated concrete bridges. Recommendations on the effect of corrosion on the anchorage capacity of reinforcement were developed. Furthermore, a methodology was presented for improved assessment of the fatigue safety for existing concrete bridges. Here, the emphasis was on evaluation of the remaining fatigue life of short-span bridges and secondary elements, since these often cause fatigue problems for railway bridges.

## 2. EVALUATION OF MATERIAL PROPERTIES

The purpose of assessment of material properties is to obtain the best possible information about the relevant resistance parameters for a specific bridge. It is also important to describe the uncertainties associated with each parameter e.g. in terms of expected variability. Important bases for evaluation are the material specifications from the original construction as well as testing of current in-situ properties for the materials in the existing bridge structure. For railway bridges dynamic effects on strength and stiffness properties are of interest. Relevant data for modelling

of such effects are given in the *Guideline for Load and Resistance Assessment of existing European Railway Bridges* [1], for the materials mentioned above.

A proper description of mechanical properties for concrete as a basis for structural analysis is a complex matter for the following reasons:

- A number of different strength parameters are needed.
- Material properties change with age, due to continuous hardening and deterioration.
- Results from testing of strength depend on size and design of the test specimens used.
- The in-situ strength in the finished structure is different from that obtained by standard specimen testing of the same concrete.

In the guideline [1], recommendations for assessment of concrete properties are presented. A methodology to estimate the properties based on the original strength class specifications combined with the effect of continued hydration was developed. The long-time hydration leads for most bridges to increased strength at higher age, see Figure 1. Recommendations are also given about interpretation of in-situ testing to obtain reliable updated information about strength in the existing structure. The basic reference property for concrete is uniaxial compressive strength. Other properties of interest in non-linear structural analyses are elastic modulus, uniaxial tensile strength, fracture energy, bond strength, ultimate compressive strain and strain at peak compressive stress. These can often be estimated from empirical relations between the property and the compressive strength.

Recommendations on how the yield strength can be estimated given the specified grade of reinforcing steel, usually with rather good precision, are given in the guideline [1]. The variability can be reduced if test results are available for samples taken from the structure, in particular if it is known that the steel in the structure originates from the same producer and/or batch. Other properties of interest for reinforcing steels are tensile strength and strain at ultimate load. These are defined in relation to the yield strength and depend on the ductility class for the steel.

For prestressing steels, recommendations are given on relevant mechanical properties, i.e. tensile strength, proof strength, effective elastic modulus and strain at maximum stress. Nominal strength values are generally specified by manufacturers of prestressing steel products. The variability is different for different types of products such as wires, bars and strands, and such information may in a given case be available from the suppliers. In some cases results from

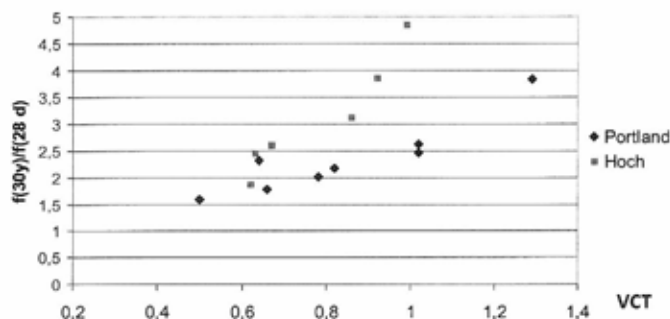


Figure 1 – Example of relative compressive strength growth for old concrete qualities, from 28 days to 30 years, for different water cement ratios.



strength tests of the prestressing steels used during construction are available. Such results can be used to estimate the mean values of strength, proof stress and ultimate strain. The variability may also be estimated from such data. Generic information about variability of prestressing steel properties is to some extent given in the guidelines.

### 3. REDISTRIBUTION OF MOMENTS AND FORCES FROM LINEAR ANALYSIS

FE structural analysis can rationalise and improve bridge assessment and design, in particular for complicated geometries where modelling in three dimensions is required. Due to moving loads and the large amount of different load cases, linear analysis is normally used for bridges. Linear analysis often leads to high stress concentrations, e.g. at point supports or slab-column connections. These are often expressed as concentrated cross-sectional moments and shear forces.

However, the stress concentrations obtained through linear analyses of concrete bridges do often not exist in reality. This is due to the cracking of the concrete, often already for service loads, and the yielding of the reinforcement in the ultimate limit state, leading to even larger redistribution of moments and shear forces. Another reason for unrealistic stress concentrations in linear analysis can be due to idealisations of the geometry when structural elements like slabs and beams are used to model the bridge.

In this part of the project, recommendations were developed for redistribution of concentrated cross-sectional moments and shear forces, obtained by linear FE analysis, for assessment of concrete bridges. The study focused on slab bridges and on the moments and shear forces at concentrated supports. A state-of-the-art investigation was made and different recommendations regarding distribution of reinforcement in slabs were studied. A typical slab bridge was designed with different methods, following different recommendations for reinforcement distribution, and the structural responses of the different solutions were analysed using non-linear FE analysis, see Figure 2.

It was found that unrealistic moment and shear force concentrations emanating from different sources need to be treated differently. Concentrations due to geometrical idealisations can be overcome by using sufficiently dense FE mesh and by using the cross-sectional forces and moments in the critical cross-sections. The cross-sectional moments and shear forces in a slab will tend to go to infinity, when the element mesh is being refined, if it is supported in a single point. However, in reality, the largest stresses are obtained in the critical cross-sections around the support (or slab-column connection). Moments and shear forces in the critical cross-sections are unaffected by the geometrical simplification if the FE mesh is dense enough. At least two first-order (or one second-order) shell elements between the support point and the critical cross-section was found to be needed. The peak values inside the critical cross-sections can then be ignored since their physical interpretation is unclear and they are not connected to any possible failure mode.

Concentrations of cross-sectional moments and shear forces due to material simplifications, i.e. from the assumption of linear response, need to be redistributed. In the ultimate limit state, the moment distribution in an existing bridge will be governed by the reinforcement provided. When assessing a slab bridge, lateral redistribution of the moment within a slab cross-section is necessary to avoid excessive under-estimation of the load-carrying capacity. The

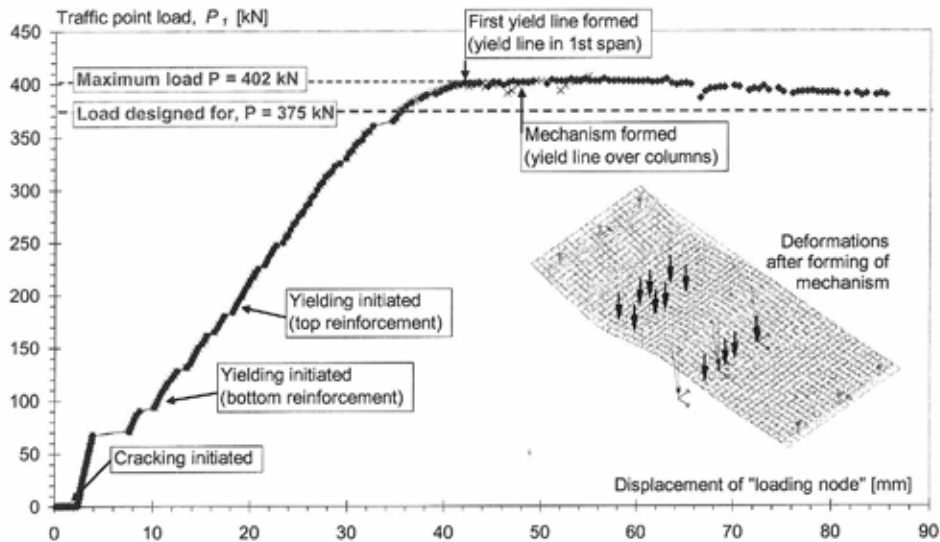


Figure 2 – Example of results from one of the non-linear FE analysis of the slab bridge studied. The graph shows the total of traffic point loads (in addition to dead load and distributed traffic load) versus the displacement of a load distribution node (for distribution of the point loads).

moment should be redistributed so that the moment distribution corresponds to the available reinforcement in the existing bridge. Recommendations in handbooks regarding strip widths for redistributions should not be used, since this would mean that too rigorous limitations on the redistributions are introduced. Instead, the study indicates that substantial lateral redistribution can be allowed compared to the linear distribution, if the slab has sufficient capacity for plastic rotations. Consequently, the ductility should be checked with respect to the requirements in Eurocode 2 [6].

#### 4. BENDING-SHEAR-TORSION INTERACTION

Earlier, bending, torsion and shear was treated as separate actions in the design of a cross section. With the advent of the truss analogy and the modified compression field theory it became clear that the forces interact, see e.g. Collin and Mitchell [7]. This way of thinking is now introduced in the Eurocodes. In the *Guideline for Load and Resistance Assessment of existing European Railway Bridges* [1], recommendations for the use of such methods are given, and several examples of applications for bridge assessment are reported in the background document [2].

Using the theory of plasticity and the assumption of yielding of all longitudinal and transverse reinforcement before concrete compression failure, simple closed interaction surfaces can be obtained, e.g. Elfgrén *et al.* [8]. For a common case with compression in the top of a member, an interaction formula may be derived as

$$\frac{M}{M_0} + \left(\frac{V}{V_0}\right)^2 + \left(\frac{T}{T_0}\right)^2 = 1 \quad (1)$$

Here  $M$ ,  $V$ , and  $T$  represent the bending moment, the shear force and the torsion moment respectively, while  $M_0$ ,  $V_0$ , and  $T_0$  are the capacities of a section loaded in pure bending, pure shear or pure torsion respectively.

More detailed results can be obtained with the modified compression field theory where the successive increase of stresses can be studied in a section with the program Response-2000, see Bentz [9]. The torsion stresses are usually added to the stresses of the vertical shear forces. The torsion-bending-shear interaction has been studied for several Swedish bridges, see e.g. Puurula *et al.* [10].

## 5. ASSESSMENT OF CONCRETE BRIDGES BY NON-LINEAR ANALYSIS

Non-linear analysis is the most realistic method for improved assessment of existing structures. It removes the inconsistency included in standard design approaches where the check of cross-section is done using non-linear material assumptions while the cross-sectional forces are determined based on linear analysis. However, in contrary to linear analysis, it puts higher demand on the engineer and it may require considerable computational resources. For practical applications, numerical computational methods such as the finite element method (FEM) must be used. In the *Guideline for Load and Resistance Assessment of existing European Railway Bridges* [1], recommendations are given for the use of non-linear analysis, but also regarding in which cases non-linear analysis has potential for discovering additional load-carrying capacity of concrete bridges. In the background document [2], validation of the suggested methods and their applicability are given on material as well as on structural level.

Non-linear analysis is a rather general term that encompasses many methods and approaches.

- Geometric non-linearity takes into account large deformation or strains. In most civil engineering structures this is not a dominant source of non-linearity with the exception of various buckling problems.
- Material non-linearity considers the non-linear material response such as: steel and reinforcement yielding, concrete or masonry cracking, and concrete crushing.
- A complete response of a structure to a given imposed loading can be obtained by such an analysis including stages of crack propagation in the pre-peak serviceability state, the failure load and failure mode and the post-peak behaviour. The model can be described on three levels, as shown in Figure 3, each involving certain approximations:

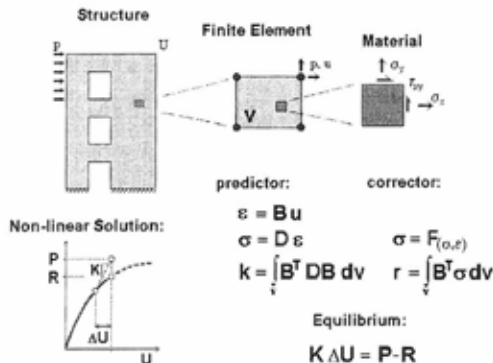


Figure 3 – Main steps of a non-linear analysis.

- Structure. In the stiffness approach the structural geometry is reduced into a system of finite elements, boundary conditions and loading. The structural response is described by the equilibrium matrix equation, where  $\mathbf{U}$  are discrete displacements,  $\mathbf{K}$  is a stiffness matrix and  $\mathbf{P}$  are loading forces.
- Finite element. A shape of the displacement function in terms of nodal displacements (reflected in the matrix  $\mathbf{B}$ ) is assumed and used together with the material stiffness  $\mathbf{D}$  to calculate the element stiffness matrix  $\mathbf{k}$ .
- Constitutive relations. They define the behaviour of the material in terms of stress-strain relations, function  $\mathbf{F}_{(\sigma,\epsilon)}$ , in a material point and corresponding material stiffness  $\mathbf{D}$ . They reflect the non-linear material effects and failure, such as the concrete cracking or the reinforcement yielding.

The above formulation is typically incremental. The forces, displacements, strains and stresses are linearized increments within each load step.

The first two levels of the structural model in Figure 3 are well known from applications in other fields of engineering, and can be solved with required accuracy, just providing sufficiently fine meshes and adopting reasonable shape functions in finite elements. The third level, the constitutive modelling of specific properties of reinforced concrete, especially their derivation from experiments, represents a difficult task, because material behaviour can not be easily separated from its structural context. In order to verify the validity of nonlinear models, the performance of programs is often confronted with experiments in bench mark tests, e.g. Bonnard & Gardel [11], Margoldova *et al.* [12].

Since cracking is the most important property of brittle materials such as masonry, concrete or rock, a variety of crack models have been proposed: the discrete crack, the embedded crack and the smeared crack model. The smeared crack model is present in some form in most commercial finite element codes. A real discrete crack is simulated by a band of localized strains as illustrated in Figure 3. Due to the energy formulation, this model is objective and its dependency on the finite element mesh size is substantially reduced, Cervenka *et al.* [13]. This was confirmed by numerous studies, for example by those about shear failure published in Cervenka [14]. Nowadays, nonlinear analysis represents a powerful tool for the estimation of remaining load-carrying capacity of existing structures. Typical result from such a non-linear finite element analysis with localized failure zone is shown in Figure 4.

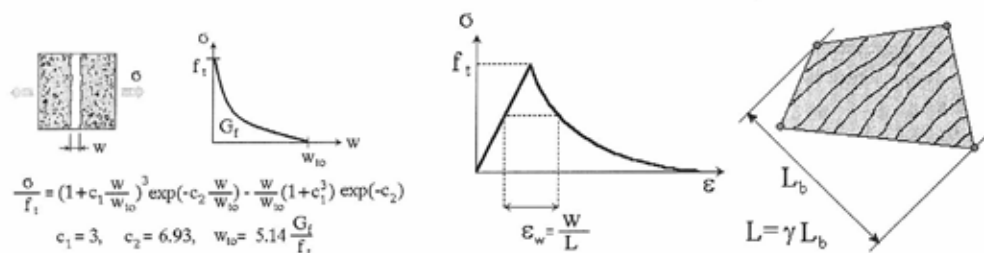


Figure 3 – Crack opening law (left). Strain softening law (middle). Crack band  $L$  (right).

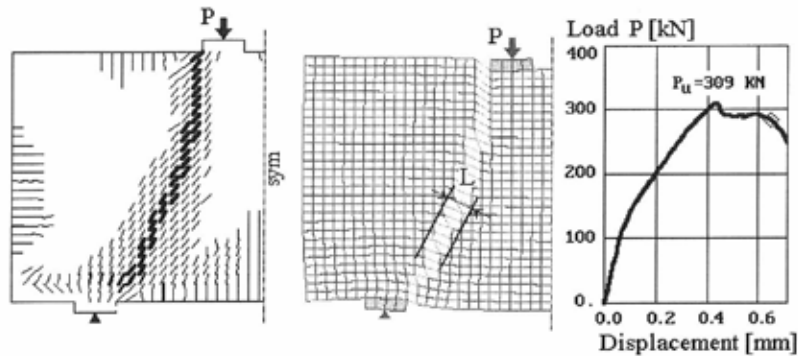


Figure 4 – Example of a typical crack localization in a non-linear finite element analysis.

## 6. EFFECT OF REINFORCEMENT CORROSION ON BOND AND ANCHORAGE

The volume increase that takes place when reinforcement in concrete corrodes causes splitting stresses in the concrete. Thereby, the bond between the reinforcement and the concrete is influenced. This effect has been studied both experimentally and theoretically by many researchers. In this project, the effect of corrosion on the bond between reinforcement and concrete was investigated and described in a systematic way. Literature studies of experimental work were combined with axisymmetric finite element analyses, for details see Lundgren [15]. A frictional model for the bond between reinforcement and concrete was used, together with a model describing the volume increase due to the corrosion, see Lundgren [16], [17].

The same basic bond mechanisms are active for both ribbed and smooth bars. However, they are of different magnitude, and therefore different mechanisms determine the behaviour. Generally, the bond capacity of smooth bars is smaller, mainly since smooth bars have limited ability to generate normal stresses at slip. Therefore corrosion, as long as it does not crack the cover, can increase the bond capacity of smooth bars to about the level of ribbed bars. For ribbed bars, corrosion might increase the bond capacity, but only to a minor extent. High corrosion levels will damage the bond, especially if there is no confining transverse reinforcement.

Based on the conclusions from the overview made, recommendations for maintenance of bridges were developed. These are included in the *Guideline for Load and Resistance Assessment of existing European Railway Bridges* [1], and are summarised below:

- Ribbed bars without confining transverse reinforcement are most sensitive to corrosion. For bridges where the anchorage capacity may be critical for the load carrying capacity, it is advised to monitor the risk of corrosion and to take measures when there is any corrosion risk.
- Smooth bars will normally have end hooks. However, smooth bars without end hooks oriented into the structure, and without transverse reinforcement, will also be critical. If the anchorage capacity may become critical for the load carrying capacity, it is advised to detect the onset of corrosion, and take measures when there is any indication of corrosion.

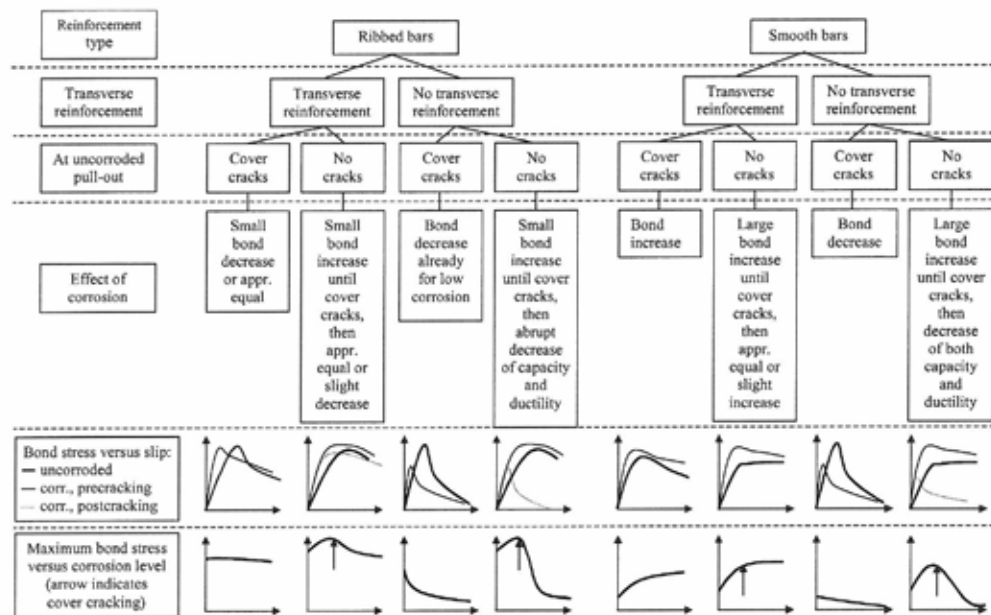


Figure 5 – Overview of the effect of corrosion on bond. The scales in the bond-slip curves are varying, to make all graphs clearly visible. However, the scales in the maximum bond stress versus corrosion level graphs are the same, to enable comparisons.

- Ribbed bars with sufficient amount of confining transverse reinforcement are less sensitive. Here, it is advised to do regular inspections, and to take measures before the cover spalls off in order not to lose the anchorage capacity.
- Smooth bars with sufficient and effective transverse reinforcement are not very sensitive, but measures need to be taken when the concrete spalls off.

## 7. REMAINING FATIGUE LIFE OF REINFORCED CONCRETE BRIDGES

The aim of performing a proof of fatigue safety is to demonstrate that the fatigue effects of (higher) rail traffic loads will not impair the safety of the structure during its intended service life. For railway bridges, proof of fatigue safety is generally required for all structural elements, and in particular for those subjected directly to wheel loads.

Current knowledge of fatigue behaviour of reinforced concrete suggests that the fatigue safety examination of reinforced concrete elements of existing railway bridges includes in principle a fatigue safety check of the steel reinforcement, and existing knowledge in fatigue behaviour of steel structures can be adopted. Fatigue failure of concrete is very unlikely to occur if the concrete is in good condition, i.e. concrete is not suffering from any deterioration mechanism (cracking) due to bar corrosion, frost or alkali-aggregate reaction.

Consequently, a rational methodology for the assessment of fatigue safety was developed and implemented in the *Guideline for Load and Resistance Assessment of existing European Railway Bridges* [1]. The methodology is based on the three following study areas taking

advantage of the fact that the bridge is existing: (1) study of the bridge structure and evaluation of reinforcement detailing, (2) inspection of the existing bridge and study of the past performance, and (3) fatigue safety check. In the following, each of the three study areas is briefly discussed.

If the principles of good fatigue design practice were followed when the bridge was built and if the bridge is in good condition, then the check of structural safety will be usually determinat. However, in cases where low fatigue strength can be expected for the steel reinforcement, this is possibly not the case, and a fatigue safety check may limit the use of the bridge.

The main objective of the study of the bridge structure and the detailing of the reinforcement is thus to detect fatigue vulnerable spots. Such fatigue vulnerable spots are predominantly pre-sent at locations where the rules of "good" fatigue resistant design have not been respected.

Grouping types of reinforcement into fatigue categories in accordance with code provisions allows recognizing types of reinforcement with low fatigue strength. Fatigue vulnerable reinforcement details include, for example, all welded reinforcement, mechanically connected reinforcing bars, anchorages for and coupler between prestressing elements or reinforcement bars showing significant corrosion.

Fatigue fracture of reinforcement bars may be preceded by cracking of the concrete cover. For example, the fatigue failure of a deck slab is characterized by a distinct crack pattern that is formed depending on the state of the fatigue damaged reinforcement bars. Also, the deflection of fatigue damaged reinforced concrete elements may significantly increase when important fatigue damage has occurred. As a consequence, bridge inspection and monitoring of fatigue vulnerable elements should focus on the detection of crack patterns and deformations.

The fatigue safety of a structure is proven if the following condition is satisfied:

$$n = \frac{R_{d,fat}}{E_{d,fat}} \geq 1.0 \quad (2)$$

where  $n$  is the fatigue safety index,  $R_{d,fat}$  is the examination value for the fatigue resistance (including a partial safety factor), and  $E_{d,fat}$  is the examination value for the fatigue action effect (without partial safety factor). The fatigue safety check is made separately for reinforcing steel and concrete, but may also be performed using the overall structural response of a fatigue vulnerable element.

Proof for reinforcing steel: The fatigue safety check is performed first with respect to the fatigue limit and then with respect to the equivalent stress range.

Proof for concrete: In the determination of stresses in concrete due to fatigue loading it must be considered that such calculated stress values only represent an approximation of effective stresses. Also, reliable fatigue damage accumulation method is still lacking. Consequently, it is not possible to perform a rigorous and reliable fatigue safety check for concrete. Fortunately, proof of fatigue safety by calculation is not required for normal stresses in concrete if inspection shows that the concrete is in good condition.

Proof with respect to ultimate load: Fatigue testing revealed that relevant fatigue damage only occurs if the level of fatigue solicitation is beyond 50% and 40% of the ultimate load for

predominant bending and shear fatigue loading respectively. From this follows that no fatigue failure of the structural element will occur if the following condition is fulfilled under predominant bending and shear fatigue, respectively:

$$n_{fat} = \frac{0.5 \cdot F_{ult}}{F_{fat,max}} \geq 1.0 \quad n_{fat} = \frac{0.4 \cdot F_{ult}}{F_{fat,max}} \geq 1.0 \quad (3a, 3b)$$

$F_{ult}$  is the ultimate load of the structural element as obtained. It is determined by means of a non-linear structural analysis using nominal values of material properties and considering partial safety factors (resistance coefficients).

Proof considering the crack pattern: In bending fatigue tests on slab-like beams, Schläfli *et al.* [18], it was observed that only beams with an *entirely developed crack pattern* failed under cyclic loading. If the distances between the cracks are larger or even a multiple of the upper bound value given below, the cracking is not stabilised yet and *no fatigue effective stress ranges* occur in the reinforcement and will not occur as long as the crack pattern does not change. The degree of cracking is a function of the average observed crack distance. An upper bound for the crack distance  $s_r$  for a stable crack pattern may be assessed according to Oehlhafen [19]:

$$s_r = 2l_r \quad (4)$$

Here,  $l_r = 60 + \lambda \cdot \kappa \cdot s$  [mm] is the transition length for the force transfer between rebar and concrete.  $\lambda = 0.25(1 + 2c/\phi)$  is a factor depending on the ratio between the rebar cover  $c$  and diameter  $\phi$ .  $\kappa$  is a coefficient which depends on the nature of the solicitation (it is equal to 1.0 for pure traction and 0.5 for pure bending), and  $s$  is the spacing between the reinforcement bars.

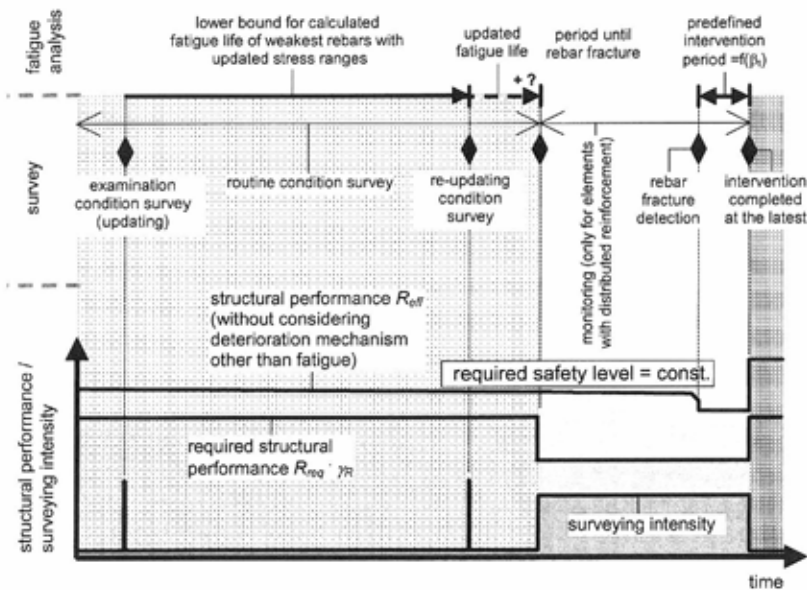


Figure 4 – Scheme illustrating the fatigue safety concept for existing reinforced concrete bridges (monitoring may be considered only for elements with distributed reinforcement).



The fatigue safety concept shown in Figure 4 is based on fatigue life calculation. It considers the extension of the service life with safe operation through monitoring by periodic visual inspections and/or continuous measurements of structural behaviour. Reinforcement is triggered only in case the monitoring results show the beginning of significant fatigue damaging.

## 8. CONCLUSIONS

The research activities summarised here were performed as a part of the European research project Sustainable Bridges in order to obtain an improved basis for the *Guideline for Load and Resistance Assessment of existing European Railway Bridges* [1], which was developed within the project. The work provides methods for enhanced assessment of existing railway bridges. The use of more advanced analysis methods, such as non-linear analysis, will lead to that higher load carrying capacities can be proven, but also to an improved understanding of the structural response, forming a better basis for decisions in the assessment. Recommendations are given for assessment of corroded concrete bridges, and the improved methods for fatigue assessment will lead to increased remaining service lives.

## REFERENCES

1. Sustainable Bridges (2007): *Guideline for Load and Resistance Assessment of existing European Railway Bridges*. Report D4.2. Prepared by Sustainable Bridges - a project within EU FP6. Available from: [www.sustainablebridges.net](http://www.sustainablebridges.net).
2. Sustainable Bridges (2007): *Non-Linear Analysis and Remaining Fatigue Life of Reinforced Concrete Bridges*. Report D4.4.2. (Background document to "Guideline for Load and Resistance Assessment of Railway Bridges"). Prepared by Sustainable Bridges - a project within EU FP6. Available from: [www.sustainablebridges.net](http://www.sustainablebridges.net).
3. Sustainable Bridges (2007): *Guideline for Inspection and Condition Assessment of Railway Bridges*. Report D3.15. Prepared by Sustainable Bridges - a project within EU FP6. Available from: [www.sustainablebridges.net](http://www.sustainablebridges.net).
4. Sustainable Bridges (2007): *Monitoring Guidelines for Railway Bridges*. Report D5.2. Prepared by Sustainable Bridges - a project within EU FP6. Available from: [www.sustainablebridges.net](http://www.sustainablebridges.net).
5. Sustainable Bridges (2007): *Repair and Strengthening of Railway Bridges - Guideline*. Report D6.1. Prepared by Sustainable Bridges - a project within EU FP6. Available from: [www.sustainablebridges.net](http://www.sustainablebridges.net).
6. EN 1992-2 (2004): Eurocode 2: Design of concrete structures - Part 1-1: General rules and rules for buildings. European Standard, Brussels: CEN.
7. Collins, Michael P and Mitchell, Denis (1991): *Prestressed Concrete Structures*. Prentice Hall, Englewood Cliffs, N.J., USA, 1991, 766 pp. ISBN 0-13-691635-x. Reprinted by Response Publications, Toronto 1997, 766 pp, ISBN 0-9681958-0-6.
8. Elfgrén, Lennart, Karlsson, Inge and Losberg, Anders (1974): Torsion - bending - shear interaction for reinforced concrete beams. *Journal of the Structural Division*, American Society of Civil Engineers (ASCE), Vol 100, No ST 8, Proc Paper 10749, New York, August 1974, p. 1657-1676
9. Bentz, Evan C. (2000): *Sectional Analysis of Reinforced Concrete Members*. A thesis submitted in conformity with the requirements for the degree of Doctor of Philosophy, Graduate Department of Civil Engineering, University of Toronto, Toronto 2000, 187 + 118 pp. [www.ecf.utoronto.ca/~bentz](http://www.ecf.utoronto.ca/~bentz)

10. Puurula, A. (2004): *Assessment of Prestressed Concrete Bridges Loaded in Combined Shear, Torsion and Bending*. Licentiate Thesis 2004:43, Luleå: Division of Structural Engineering, Luleå University of Technology, 103 + 144 pp. Available from: <http://epubl.ltu.se/1402-1757/2004/43/index.html> [cited 31 November 2006].
11. Bonnard and Gardel (1994): *Bench Mark on Numerical Analysis of Concrete Structures*. Bonnard&Gardel, Neuchatel, Switzerland, 1994.
12. Margoldova J., Cervenka V. and Pukl R. (1998): Applied Brittle Analysis. *Concrete Engineering International* 8 (2) 1998, 65-69.
13. Cervenka V. and Margoldova J. (1995): Tension Stiffening Effect in Smeared Crack Model. In: *Engineering Mechanics*, Ed. S. Sture, ACSE, New York, USA, ISBN 0-7844-0083-0, 1995, 655-658
14. Cervenka V. (1998): Simulation of shear failure modes of R/C structures. In: *Computational Modelling of Concrete Structures (Euro-C 98)*, eds. R. de Borst, N. Bicanic, H. Mang, G. Meschke, A.A.Balkema, Rotterdam, The Netherlands, 1998, 833-838.
15. Lundgren, K. (2007): Effect of corrosion on the bond between steel and concrete: an overview. *Magazine of Concrete Research*, Vol. 59, No 6, pp. 447-461.
16. Lundgren K. (2005a): Bond between ribbed bars and concrete. Part 1: Modified model. *Magazine of Concrete Research*, Vol. 57, No. 7, September, pp. 371-382.
17. Lundgren K. (2005b): Bond between ribbed bars and concrete. Part 2: The effect of corrosion. *Magazine of Concrete Research*, Vol. 57, No. 7, September, pp. 383-396.
18. Schläfli M. (1999) *Ermüdung von Brückenfahrbahnplatten aus Stahlbeton* ("Fatigue of Bridge Deck Slabs of Reinforced Concrete", Doctoral thesis. In German), Thèse N° 1998, Ecole Polytechnique Fédérale de Lausanne.
19. Oehlhafen U. (1984) *Rissnachweis*, Conférence aux journées d'études des 12 et 13 octobre 1984 à Lausanne sur le thème « principes et conception de la nouvelle norme SIA 162 » Documentation SIA No. 77 (in German).



## Robustness of Fresh VMA-modified SCC to Varying Aggregate Moisture



Peter Billberg  
 Ph.D., Postdoctoral Researcher  
 University of Sherbrooke, Department of Civil Engineering  
 Sherbrooke, Quebec, J1K 2R1, Canada  
 E-mail: peter.billberg@usherbrooke.ca



Mikael Westerholm  
 Tech. Lic., Researcher  
 Swedish Cement and Concrete Research Institute, CBI  
 SE- 100 44 Stockholm, Sweden  
 E-mail: mikael.westerholm@cbi.se

### Abstract

One of the most important factors limiting SCC from becoming a major part of the ready-mixed concrete industry is the difficulties involved in steady and variation-free production in terms of fresh properties. The aim of this project is to find a concept enabling increase in robustness of SCC. Micro mortar studies show that misjudged aggregate moisture is the parameter causing the most variation in rheology response. The ability for different viscosity-modifying admixtures (VMAs) to increase robustness to variation in aggregate moisture is studied using concrete-equivalent mortar (CEM). It is shown that depending on VMA type, robustness can indeed be achieved.

**Keywords:** aggregate moisture, concrete-equivalent mortar, micro mortar, rheology, robustness, self-compacting concrete, temperature, viscosity-modifying admixture

## 1. INTRODUCTION

Some 15 years ago, Sweden became one of the pioneering countries in developing and using self-compacting concrete (SCC) outside Japan. It is therefore quite remarkable to observe that SCC's share of the ready-mix concrete produced annually in Sweden is, to this day, still only about 5%-10%, despite the possibilities to significantly increase productivity using this class of high-performance concrete. The same applies to many other countries where the use of SCC has mostly been fully adopted by the precast industry, which benefits greatly from this change in concrete production concept. This low share of the ready-mix production market is in part due to considerably larger difficulties involved in producing SCC than exist for conventional vibrated concrete. In order to reach the target slump time after time a higher degree of precision and more frequent control of e.g., the aggregate moisture content is required. For the precast industry, where the whole production cycle is kept in-house and the extent of concrete formulations, transport time, and handling are limited, production is considerably simplified.

SCC is required to meet three workability criteria: high filling ability, passing ability, and resistance to segregation [1]. If the acceptance intervals of these criterias are not met, the results will inevitably lead to some kind of failure in casting results. These intervals are often relatively small, and thus the fresh properties of SCC should not vary too much. Since SCC is sensitive to variations in properties of its constituent materials, e.g., aggregate moisture and gradation, SCC delivered to the job site often displays variations in fresh properties. This leads to extensive quality assurance, which requires substantial manpower resources and, thus, result in increased labour costs. This is an important factor limiting SCC from taking a major share of the ready-mixed concrete market.

## 2. RESEARCH SIGNIFICANCE

The production of robust SCC mixtures will enable reduction of costs related to quality and acceptance control at site, i.e., reduced labour costs. It will also lead to more secure planning of the casting procedure for the contractor. Altogether it has the potential to increase the overall use of SCC, which in turn will lead to increased productivity of the whole concrete construction industry. Furthermore a predictable SCC will also lead to such delicate matters as improved forecast of form pressure and thus, optimized formwork system and/or casting process (casting rate). Another aspect of SCC where research is in progress is that of numerical simulation of SCC flow which has grown in interest in the last few years [2]. Also, for this interesting and important topic, it is very crucial that the modelled flow behaviour is obtained at the time of casting, without severe variations.

## 3. SCOPE OF INVESTIGATION

This on-going project is divided into three parts, 1) micro mortar study, 2) study of concrete-equivalent mortar (CEM) and 3) a detailed study on SCC. This article reports on findings within the two first parts. The third part is still on-going. The first part, micromortar study, is based on the hypothesis that concrete is a particle suspension with aggregate particles greater than 125  $\mu\text{m}$  suspended in the micromortar, i.e., micro mortar being the concrete fluid phase [3]. Further on, the hypothesis states that the rheology of concrete is a function of its fluid phase rheology, and thus, the focus is here set on evaluating the influence of varying parameters on micro mortar rheology. The parameters selected for study are those that commonly occur in the ready-mix process, i.e., variation of aggregate moisture and aggregate fines content, as well as temperature. In this work, aggregate fines is defined as aggregate particles smaller than 125  $\mu\text{m}$ .

The use of viscosity modifying agents (VMA) is reported in a number of papers to increase the robustness of SCC [4–7]. Thus, the second part of the project focuses on the ability of different VMAs to reduce the rheological response of mortar in terms of yield stress and plastic viscosity caused by variations in aggregate moisture content. In addition, the response in terms of mini-slump flow is also measured. In this part the mortars were designed using the concept of CEM. Consequently, the mortar design is based on a SCC mixture with coarse aggregate replaced by a certain mass of sand required to maintain the same total specific surface. Thus, the total aggregate surface per mixture volume of the SCC and CEM is equal; therefore the degree of water and admixtures adsorbed onto aggregate surface is unchanged. Good correlation between the rheology [8] and thixotropy [9] of CEM and SCC has been established.

## 4. PART 1 – MICRO MORTAR STUDIES

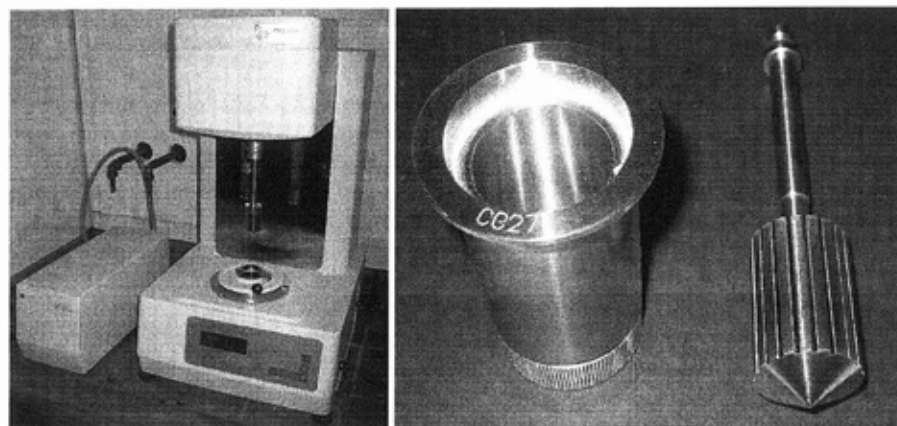
### 4.1 Test methods

The mixing of the micro mortars was done in 1-litre batches with a Hobart mixer and the mixing sequence consists of the steps shown in Table 1. When VMA was added to the mixture, it was intermixed with the dry materials in step 1 while the SP was added after the water in step 4. Steps Nos. 3, 5 and 7 are manually performed in order to fully secure that homogenisation is achieved.

*Table 1. Mixing sequence*

Step	Action	Duration (s)
1	All dry materials (including VMA when used) are mixed at low speed	10
2	Water added while mixing at low speed	10
3	Homogenisation by hand	10
4	SP added + mixing at medium speed	60
5	Homogenisation by hand	10
6	Mixing at medium speed	60
7	Homogenisation by hand	10
8	Mixing at medium speed	60
1-8	Total	3 min 50 s

The rheology was evaluated using the Physica MCR 300 rheometer shown in Figure 1 (left). This rheometer can be set to control both the rate of deformation (CR) and the rate of stress (CS); the CR option was used in this investigation. The selected measuring system consists of concentric cylinders where the inner cylinder is profiled to reduce the risk of surface slippage, Figure 1 (right). The geometry of the cylinder system is given in Table 2.



*Figure 1. Physica MCR 300 rheometer (left) and concentric cylinder measuring system (right)*

*Table 2. Geometry of the cylinder system.*

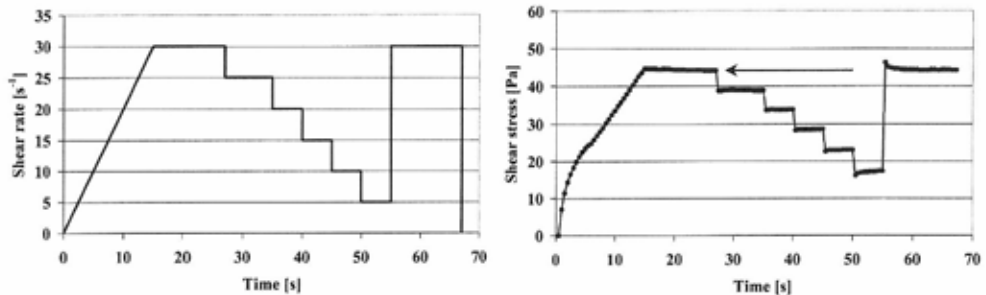
Inner cylinder radius, $R_i$ (mm)	13.33
Inner cylinder height (mm)	40.00
Outer cylinder radius, $R_o$ (mm)	14.46
Gap (mm)	1.13
$R_o/R_i$	1.085

The configuration of shear rate vs. time is shown in Figure 2 (left). The equilibrium shear stresses at each  $5 \text{ s}^{-1}$  downward step of shear rate are used to evaluate rheology according to the Bingham model (Eq. 1).

$$\tau = \tau_0 + \mu_{pl} \cdot \dot{\gamma} \quad (1)$$

where,  $\tau$  is the shear stress,  $\tau_0$  (Pa) is the dynamic yield stress,  $\mu_{pl}$  (Pa s) is the plastic viscosity, and  $\dot{\gamma}$  ( $\text{s}^{-1}$ ) is the shear rate.

A typical response showing the equilibrium stresses obtained at each shear rate level is shown in Figure 2 (right). Note the arrow (Figure 2 right) highlighting that the level of shear stress at the last repeated maximum shear rate equals that at the first plateau (same shear rate), indicating that no segregation has occurred.



*Figure 2. The shear sequence used for rheology measurements (left) and an example of a typical resulting shear stress response (right).*

## 4.2 Materials and mixture designs

The fine aggregate used is of glaciofluvial origin having a granitic mineral composition. The water absorption values are in the range of 0.5 to 0.7%. The aggregate was sieved to obtain a maximum particle size of  $125 \mu\text{m}$ . Since micro mortar is regarded as the fluid phase of concrete, the amount of sand added to the mixtures was varied to simulate variation in concrete aggregate fines content. Simulation of varying aggregate moisture is done by adding different amounts of mixing water to the mixtures.

The cement used is a relatively coarsely ground (Blaine  $310 \text{ m}^2/\text{kg}$ ) and sulphate resistant low-heat cement, of low alkali content. According to SS-EN 197-1, it is designated Cem I 42.5 N BV/SR/LA. Crystalline limestone powder, (LF) was used as filler. The compact density is  $2720 \text{ kg}/\text{m}^3$  (Blaine  $470 \text{ m}^2/\text{kg}$ ) and the median particle size is approximately  $25 \mu\text{m}$ .

Two types of superplasticizers (SP) were used in the work, polycarboxylate ether-based (PCE) and melamine formaldehyde condensate (Melamine). The PCE superplasticizer was diluted (1:10) in order to avoid any possible weighing error. The viscosity-modifying admixture (VMA) is based on natural polysaccharide and is added as dry material to the micro mortar mixtures.

To control and reach the used span of micro mortar temperature, either ice cubes were used to cool the mixing water temperature to 3-4 °C or the mixing water was heated to 45 °C. When mixing the micro mortars, use of cold water resulted in 12 °C mixtures, while hot water resulted in 30 °C mixtures. The temperature of the micro mortars was measured in the rheometer prior to the measurements. In order to remain a constant temperature during the measurement, the temperature system of the rheometer was set at the same temperature as the mortar.

In all 32 mixes were tested. These mixtures were split into three series designated series I-T (temperature variation), series II-M (moisture variation), and series III-F (aggregate fines content), respectively. The mixture proportions are shown in Table 3 (series I-T) and Table 4 (series II-M and III-F).

In series II-M and III-F, the amount of constituents besides the material being varied, i.e., water in series II-M and sand in series III-F, respectively, is not changed since the variation itself simulates unknown deviations from the aimed proportion.

*Table 3. Mixture proportions for micro mortars in series I-T with temperature variation; amounts in g*

Material	Series I-T		
	PCE	Melamine	PCE+VMA
Cement	1024	1019	1026
Water	461	459	462
Sand < 125 µm	150	149	151
LF (30% of binder)	444	442	445
PCE*	0.72	-	2.47
Melamine*	-	4.34	-
VMA	-	-	0.462
W/C	0.45	0.45	0.45
W/(C+F)	0.31	0.31	0.31

\* Active component

*Table 4. Mixture designs for micro mortars in series II-M with aggregate moisture variation and series III-F with variation in aggregate fines content; amounts in g*

Material	Series II-M		Series III-F
	PCE	PCE+VMA	PCE
Cement	1024	1024	1024
Water	397 – 525	408 – 516	461
Sand < 125 µm	150	150	0-300
LF (30% of binder)	444	444	444
PCE*	0.72	1.08	0.72
VMA	-	0.462	-
W/C	0.45	0.45	0.45
W/(C+F)	0.31	0.31	0.31

\* Active component



### 4.3 Results and discussion

#### Temperature variation (Serie I-T)

The rheological results from the micro mortar series where the temperature was varied are shown in Figures 3 and 4. It is evident that the yield stress increases linearly for all three series of micro mortars with increasing temperature (Figure 3). The temperature dependence is strongest for the micro mortars with PCE, both with and without VMA, relative to those with Melamine. Even though the response in terms of plastic viscosity is not linear for all series, these values also increase with increasing temperature (Figure 4).

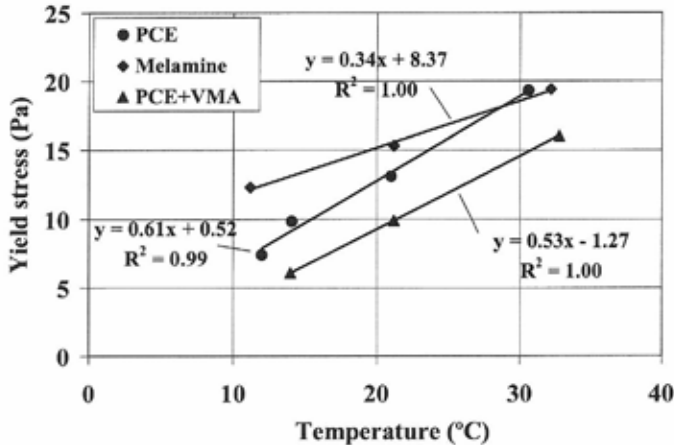


Figure 3. The yield stress response to variation in temperature

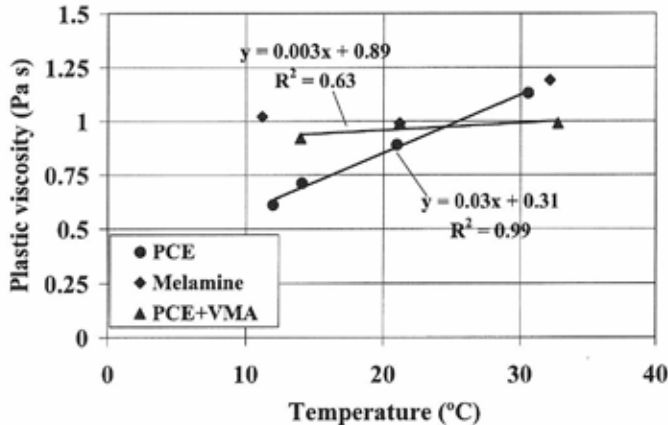


Figure 4. The plastic viscosity response to variation in temperature

The plastic viscosity of the micro mortars respond differently to temperature changes compared to the yield stress of the micro mortars. The PCE mixtures respond more strongly to the temperature than those with Melamine. Also, the addition of VMA to PCE mortars reduces this dependence to nearly none. The plastic viscosity response of the Melamine mortars displays

relatively low difference with increase in temperature from 20 to 30 °C and no change with the decrease in temperature from 20 to 10 °C.

The rheology of a particle suspension is always a function of the fluid phase rheology, i.e., in the case of micro mortar, the rheology of water. For water, like for most materials with a Newtonian behaviour, viscosity decreases with increasing temperature, simultaneously, the flocculation of the suspended phase often increases due to increased thermal energy [10]. The rheology of cementitious suspensions is also affected by temperature, since the chemical reactions of the cement is strongly depended on temperature. Similar results on the temperature dependence of PCE based mortar have been reported previously in the literature [11]. The authors relate to [12] and discuss the influence being due to the fact that high concentrations of sulphate ions in the aqueous phase can prevent the adsorption of the PCE polymers onto cement particles. The temperature influences this sulphate ion concentration in the solution in that a higher temperature results in a high concentration, and consequently, a lower temperature in a lower concentration. Thus, a lower dispersion degree at higher temperatures relates to higher yield stress.

#### *Aggregate moisture variation (Serie II-M)*

The results from the series where the variation of sand moisture content is simulated are shown in Figure 5 for yield stress and Figure 6 for plastic viscosity. When the total amount of water is varied in a particle suspension such as micro mortar, the solid volume concentration of particles,  $\emptyset$  (%) is affected. This parameter,  $\emptyset$ , is traditionally used in many models to predict the viscosity of particle suspensions, where an increase in particle concentration leads to increased viscosity, which is also the case here. The same also applies for the yield stress, which is well known to vary significantly with water content in cementitious systems. Even though the range in terms of variation is relatively large (i.e.,  $\pm 3$  %-units which corresponds to approximately  $\pm 30$  litre per  $m^3$  of concrete), it is a fact that the yield stress increases from 20 Pa to 30 Pa when the moisture is overestimated by the more realistic 1 %-unit and reduced from 20 Pa to 15 Pa when underestimated by 1 %-unit, thus, a two-fold change in yield stress in the range of  $\pm 1$  %-units of aggregate moisture content.

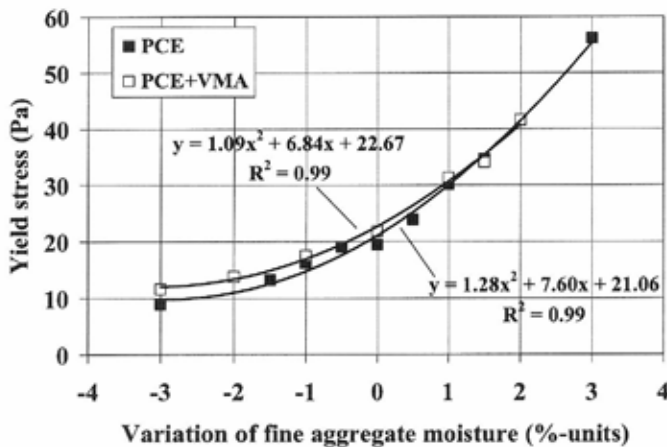


Figure 5. The yield stress response to simulation of fine aggregate moisture variation

The addition of VMA reduces the variation in terms of yield stress (Figure 5) slightly, and only on the underestimated moisture side. The VMA increases the level of plastic viscosity, however, the relative change in plastic viscosity with the moisture content is basically unchanged, Figure 6.

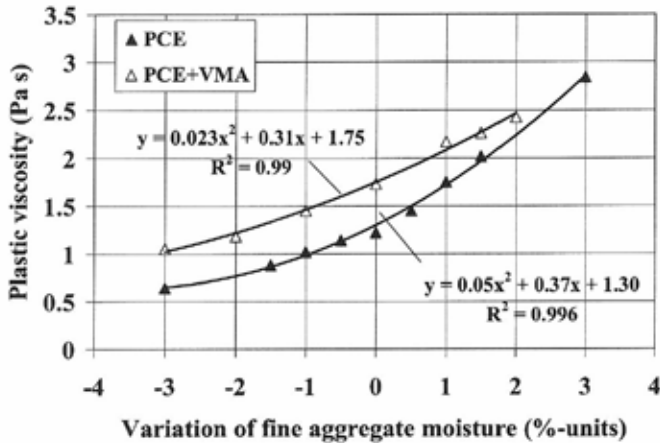


Figure 6. The plastic viscosity response to simulation of fine aggregate moisture variation

#### Variation in aggregate fines content (Serie III-F)

The range of variation for the simulation of incorrectly assumed aggregate fines content ( $\pm 7$  %-units) is also exaggerated relative to everyday situations in concrete production. The “correct” amount of aggregate  $< 0.125$  mm is assumed to be 7% of the sand (0-8 mm fraction) in the corresponding concrete. Thus, an overestimation of 7 %-units is equal to having all aggregate below 0.125 mm missing in the concrete sand fraction. However, it is evident from the results shown in Figure 7 (yield stress) and Figure 8 (plastic viscosity), that regardless of variation span, the rheological response to varying aggregate fines content is less than that for moisture variation.

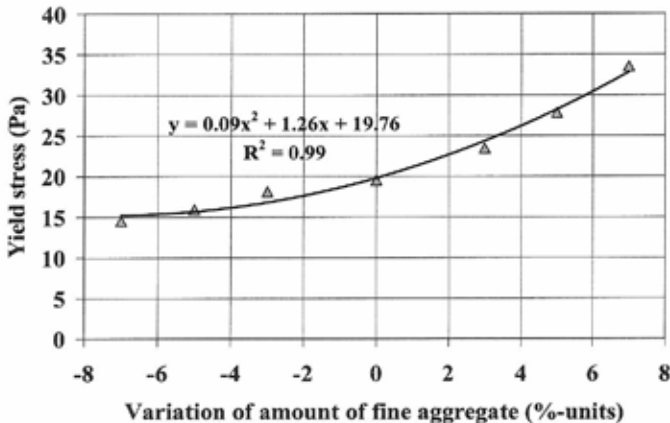


Figure 7. The yield stress response to simulation of varying fine aggregate amount

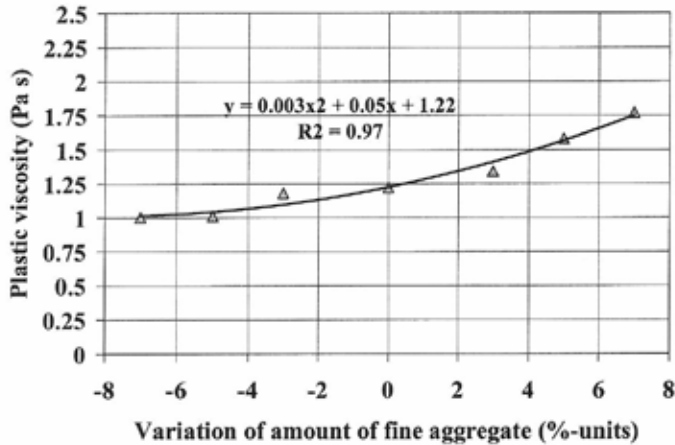


Figure 8. The plastic viscosity response to simulation of varying fine aggregate amount

#### Comparison of varying parameters

In Figure 9 (yield stress) and Figure 10 (plastic viscosity), the results are compared for the three varied parameters. Here only the series without VMA and with PCE is presented. Varying moisture content of aggregate is clearly shown to have the most significant effect on the variation in rheological response of micro mortar.

The rheological response can also be discussed relating to the solid volume concentration of particles ( $\emptyset$ ) in the micro mortars. In this case, a moisture variation of  $\pm 1$  %-units equal to  $\emptyset = \pm 1.1\%$ . The same  $\emptyset$ -variation for the aggregate fines content variation would result in a misjudged fine aggregate content of approximately  $\pm 2.9$  %-units. The total variance in yield stress in the case of  $\pm 1$  %-units aggregate moisture (as already mentioned) is 15 Pa, while for the  $\pm 2.9$  %-units of fine aggregate, it is only 5 Pa (Figure 7 and Figure 9).

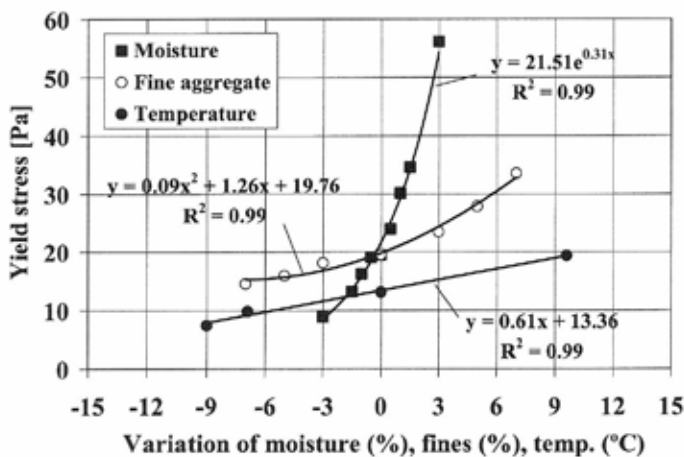


Figure 9. Comparison of the yield stress response to variation in temperature, fine aggregate content and aggregate moisture

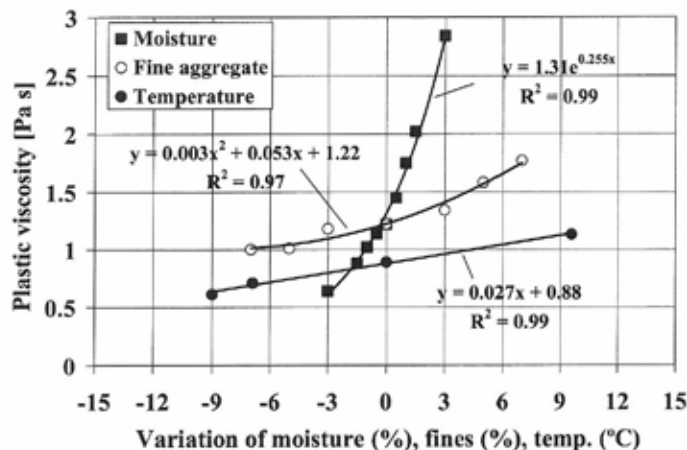


Figure 10. Comparison of the plastic viscosity response to variation in temperature, amount of fine aggregate and aggregate moisture

The difference is due to the fact that, even though the solid volume concentration of particles varies equally in both cases (i.e., for moisture variation of  $\pm 1$  %-units and fine aggregate variation of  $\pm 2.9$  %-units, respectively), the surface area of the coarser aggregate particles (coarser relative to the total particle system including cement and limestone filler) leads to a ratio of water to total particle surface area that varies less in the case of varying aggregate fines content relative to variation in aggregate moisture. In other words, the amount of free water varies more if the aggregate moisture (water content) is varied relative to a fixed total particle system than if a part of the particle system (coarser part) varies relative to a fixed suspension of water, cement, and limestone filler. Thus, the parameter to focus on regarding robustness is primarily the variation in aggregate moisture content.

## 5. PART 2 – CONCRETE-EQUIVALENT MORTAR APPROACH

### 5.1 Test methods

The rheological measurements of concrete-equivalent mortar (CEM) were performed using a ConTec 6 viscometer, as shown in Figure 11 (left). This instrument is equipped with concentric-cylinders geometry with a gap of 10 mm (inner and outer cylinder radii of 50 and 60 mm, respectively). The viscometer is configured to perform stepwise downward shear rates as shown in Figure 11 (right), and the equilibrium shear stresses at corresponding shear rates are used to correlate to the linear Bingham model (Eq. 1). Thus, the rheology of the mixtures is characterized by the yield stress and plastic viscosity. At each level, the shear rate is kept constant for 12 seconds where 50 measuring points are collected during the last 5 seconds. The last point at 2/3 of the maximum shear rate is used to evaluate any possible segregation of the mixture. All rheological results are the mean values of two consecutive measurements.

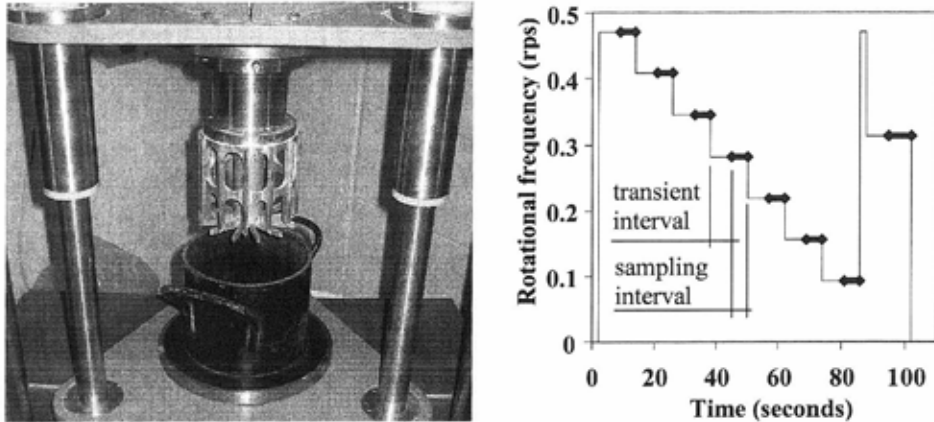


Figure 11. Viscometer used: ConTec 6 (left) and the measurement configuration (right)

The ability of the VMAs to reduce variations in rheological parameters due to sand moisture is evaluated for control mixtures with correctly assumed sand moisture and with a fixed yield stress of 25 Pa, i.e., the superplasticizer content is adjusted to secure 25 Pa value for control mixtures. The purpose for this is to simulate each VMA-containing CEM to represent SCCs with approximately the same slump-flow.

## 5.2 Materials and mix designs

The reference CEM was designed to represent a SCC used for residential construction, as shown in Table 5. Batches of 1.0 litre were prepared. Limestone-blended cement, Cem II/A-LL 42.5 R (Blaine 460 m<sup>2</sup>/kg) and crystalline limestone filler, Betocarb 8 (Blaine 400 m<sup>2</sup>/kg), were used. A modified polycarboxylate with 21.5% solid content was used as SP. The maximum particle size of the aggregate was 2.5 mm. In order to estimate the effect of sand moisture content in SCC, the part of the sand of CEM mixtures representing the sand content in SCC was pre-conditioned to vary the total moisture content by approximately  $\pm 1\%$ .

Table 5. Mix design of the reference CEM mixture (no VMA)

Material	Unit	SCC	Unit	CEM
Cement		350		456.5
Limestone filler		150		195.6
Water		193		251
Aggregate 0-8 mm	kg/m <sup>3</sup>	981	g/l	1324*
Aggregate 8-16 mm		654		-
SP**		2.42		3.15
W/C	-	0.55	-	0.55
W/powder	-	0.385	-	0.385

\* Sand 0-2.5 mm. \*\* Active component

In total, seven different VMAs were evaluated; their characteristics are shown in Table 6. The dosage of the VMAs were based on manufacturers recommendations.

Table 6. Characteristics of evaluated VMAs

Designation	Active component	Solids (%)	Dosage	Unit
VMA1	Nano-silica	15	1.0	% by mass of cement
VMA2	Aluminium modified nano-silica	8	1.0	% by mass of cement
VMA3	Starch derivate	100	250	mg/l, (batch)
VMA4	Modified polysaccharide	1.6	0.8	% by mass of (cem+Lf)
VMA5	Modified biopolymer	5	0.11	% by mass of cement
VMA6	Anionic polysaccharide	100	100	ppm of water
VMA7	Natural polysaccharide	100	100	ppm of water

### 5.3 Results and discussion

The incorporation of VMA to the reference CEM mixture with correctly assumed sand moisture led primarily to an increase of yield stress from 25 Pa to values as low as 40 Pa in the case of VMA7 and as high as 180 Pa in the case of VMA3, as shown in Figure 12. The same trend is reported in [13-14]. As a consequence, the SP dosage needed to regain the 25 Pa yield stress level for the reference mixture was increased by more than 50% (from 2.25% to 3.6% by mass of cement + filler). Indeed, the slope representing the response to varying SP dosages is also a measure of robustness [15], and here VMA7 is found to perform best. When the yield stress of the reference mixture, i.e., approximately 25 Pa is reached, the aggregate with respectively lower and higher moisture contents relative to the reference mixture is used, and the rheology is measured, as well as the mini-slump.

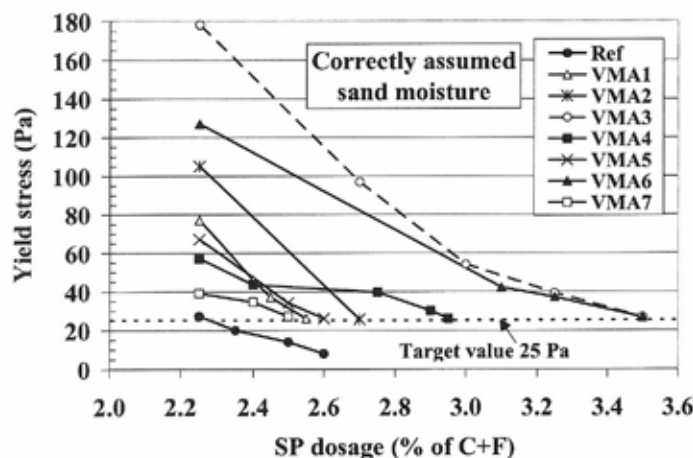


Figure 12. Variation in yield stress with SP dosage of mixtures with different VMAs at correctly assumed sand moisture

The response in terms of mini-slump is shown in Figure 13. The results indicate that the fixed yield stress level at correctly assumed moisture corresponds to mini-slump flow values between 180 and 195 mm. When the aggregate moisture is varied depending on VMA type, the mixtures act slightly different. On the underestimated moisture side (moisture of +1.0%) they all show lower spread values than the reference, which is favourable in terms of robustness. But on the overestimated moisture side (moisture of -1.3%), the reaction is different. Most robustness is

shown by the mixtures containing VMA3, VMA 6, and VMA 7, in that they react less than the reference CEM to either under- or overestimated aggregate moisture.

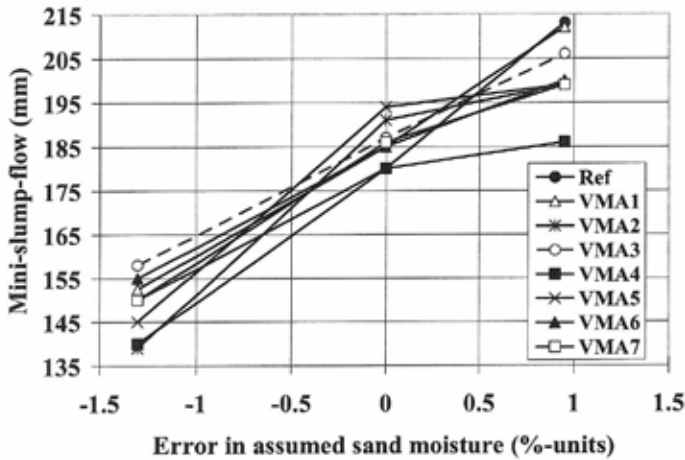


Figure 13. Mini-slump response to incorrectly assumed sand moisture

In Figure 14, the rheological response to aggregate moisture variations is shown. The same trend as for the mini-slump flow results can be identified in that, except for the mixture with VMA1, all mixtures are less sensitive to underestimated aggregate moisture. On the overestimated aggregate moisture side, however, only VMA3, VMA6, and VMA7 (again) are capable of reducing sensitivity relative to the reference CEM.

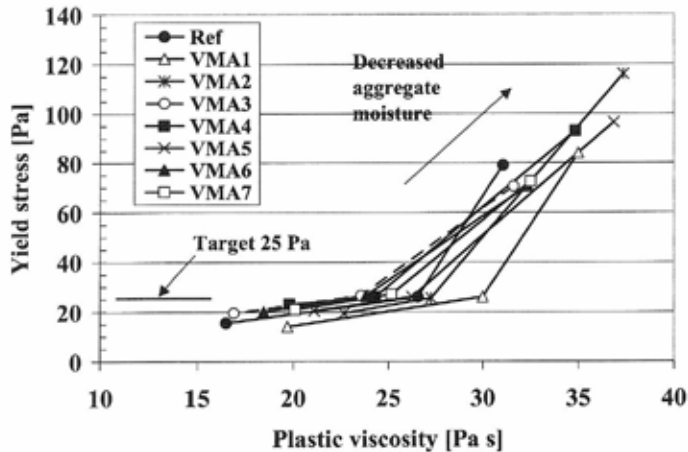


Figure 14. Rheological response to simulated incorrectly assumed aggregate moisture

In an attempt to quantify robustness, two different methods are schematically described in Figure 15. One method calculates the area equal to total spread in response of yield stress times the total response in terms of plastic viscosity.



The other calculates the respective coefficient of variation of rheological parameters (Eq. 2).

$$\text{COV} = \sigma / \bar{x} \quad (2)$$

where  $\sigma$  is the standard deviation, and  $\bar{x}$  is the mean value of yield stress and plastic viscosity.

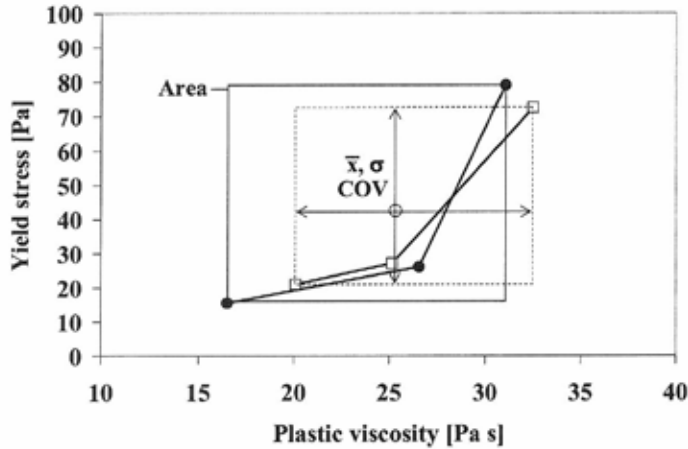


Figure 15. The principle for calculation of robustness areas and COV

In Figure 16 and Figure 17, respectively, the results in terms of relative area and relative COV are compared. The results are shown as relative (%) of the reference mixture. In the case of relative area (Figure 16), the same trend is found for rheology as was earlier shown for mini-slump, i.e., that the most promising VMAs to increase robustness of SCC are the starch-derivate-based VMA3, and anionic and natural-polysaccharides-based VMA6 and VMA7, respectively. Their relative areas are the only ones smaller than that of the reference CEM mixture.

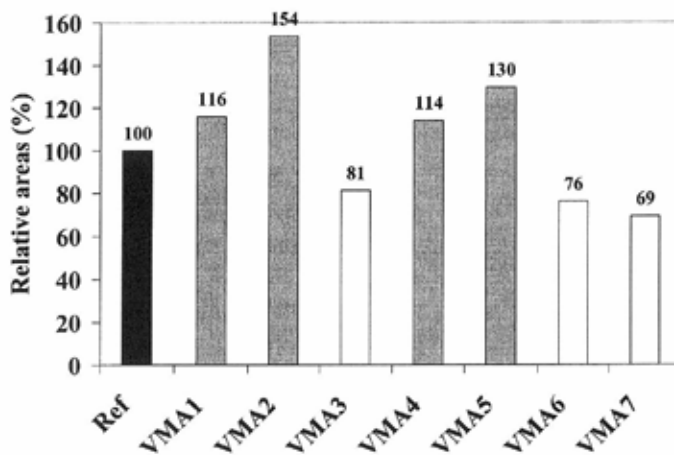


Figure 16. Validation of robustness using the method of relative areas

However, a clearer picture of robustness is offered in Figure 17 where the rheological parameters ( $\tau_0$  and  $\mu_{pl}$ ) are displayed separately. It then becomes more obvious that all the VMAs beside VMA3 have the ability to reduce the variation expressed by plastic viscosity, but only VMA3, VMA6, and VMA7 can reduce the variation expressed by yield stress. Thus, focusing on robustness in relation to the slump-flow of SCC (corresponding to the yield stress), these three VMAs are the only ones possibly offering this property. In [16], similar results are found with regard to VMAs based on the same basic materials as VMA3 and VMA7, i.e., to make SCC less sensitive to variation in the W/B.

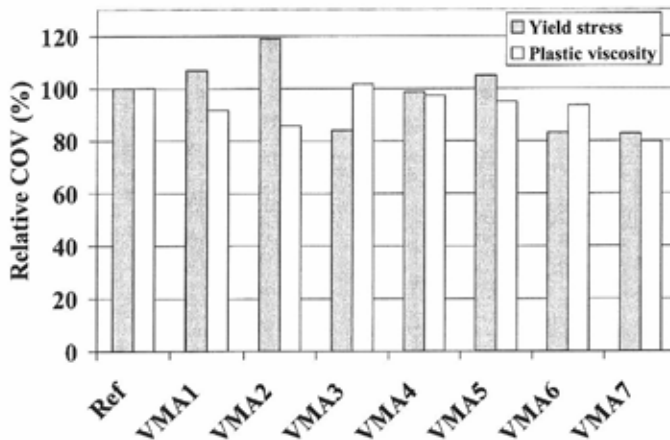


Figure 17. Validation of robustness using the method of relative coefficients of variation

## 6. CONCLUSIONS

From this on-going investigation, bearing in mind the obvious limitations in range due to the materials used and the range of variations used, the following conclusions can be drawn:

- When temperature is varied, the yield stress is affected more than the plastic viscosity, and the yield stress dependence for all tested series is linear. For the micro mortars dispersed with PCE, the influence of temperature variation on rheology is greater than for the ones where Melamine was used.
- For the evaluated and varied parameters; temperature, aggregate fines content, and aggregate moisture, the most significant influence on the rheological response of the micro mortar was associated with the variation of aggregate moisture content.
- The addition of VMA to the reference CEM resulted in increased yield stress of up to more than 7 times higher than the reference CEM, depending on VMA type. This is, of course, strictly dependent on VMA dosage used in this investigation, which was set based on manufacturers recommendations. However, to regain the yield stress of the reference mixture, adjustment of SP dosage is necessary, sometimes leading to more than 50% increase in dosage demand.

- The lowest sensitivity, i.e., highest robustness, to variations in SP content was shown by the natural polysaccharide VMA7 in that its yield stress vs. SP response is the lowest.
- The incorporation of VMA can increase the robustness of the tested CEMs vis-à-vis moisture content of sand; however, this depends on the type of VMA in use. The best performing VMA, natural polysaccharide VMA7, reduces the relative rheology area to 69% of that of the reference CEM made without VMA; the relative COV decreased to 80% (for both yield stress and plastic viscosity) compared to the reference CEM.

## 7. ACKNOWLEDGEMENTS

The financial support by the Swedish Consortium for Financing Basic Research in the Concrete Field is gratefully acknowledged.

## REFERENCES

1. Skarendahl, Å., Billberg, P. (Eds.), "Casting of Self Compacting Concrete," RILEM Report 35, RILEM Publications S.A.R.L., Bagnaux, France, 2006, 42 p.
2. RILEM Technical Committee 222-SCF, <http://www.rilem.net/tcDetails.php?tc=222-SCF>
3. Billberg, P., "Some Rheology Aspects on Fine Mortar Part of Concrete," Part of Licentiate thesis, Royal Institute of Technology, Department of Structural Engineering, ISSN 1103-4270, Stockholm, Sweden, 1999, 32 p.
4. Yurugi, M., Sakai, G., Sakata, N., "Viscosity Agent and Mineral Admixtures for Highly Fluidized Concrete," Proceedings International Conference on Concrete under Severe Conditions, Sapporo, 1995, pp. 995-1004.
5. Kashima, S., Kanazawa, K., Okada, R., Yoshikawa, S., "Application of Self Compacting Concrete Made with Low Heat Cement for Bridge Substructures of Honshu-shikoku Bridge Authority," International Workshop on Self-Compacting Concrete, Kochi University of Technology, Tosa-Yamada, Kochi, Japan, 23-26 August 1998, pp. 255-261.
6. Nawa, T., Izumi, T., Edamatsu, Y., "State-of-the-art Report on Materials and Design of Self-Compacting Concrete," International Workshop on Self-Compacting Concrete, Kochi University of Technology, Tosa-Yamada, Kochi, Japan, 23-26 August 1998. pp. 160-190.
7. Bramshuber, W., Uebachs, S., "Practical Experience with the Application of Self-Compacting Concrete in Germany," Second International Symposium on Self-Compacting Concrete, Tokyo, Japan, 23-25 October, 2001, pp. 687-696.
8. Erdem, T.K., Khayat, K.H., Yahia, A., "Correlating Rheology of SCC to that of Corresponding Concrete-Equivalent Mortar," *ACI Materials Journal* (submitted), 2008, 24 p.
9. Assaad, J., Khayat K.H., "Assessment of Thixotropy of Self-Consolidating Concrete and Concrete-Equivalent-Mortar—Effect of Binder Composition and Content," *ACI Materials Journal*, V. 101, No. 5, 2004, pp. 400-408.
10. Ferguson, J., Kembrowski, Z., "Applied Fluid Rheology," Elsevier Applied Science, Amsterdam, the Netherlands, 1991, 340 p.
11. Petit, J.-Y., Khayat, K. H., Wirquin, E., "Coupled Effect of Time and Temperature on Variations of Yield Value of Highly Flowable Mortar," *Cement and Concrete Research*, 36, 2006, pp. 832-841.
12. Yamada, K., Tanagisawa, T., Hanehara, S., "Influence of Temperature on the Dispersibility of Polycarboxylate Type Superplasticizer for Highly Fluid Concrete," 1<sup>st</sup>

International RILEM Symposium on Self-Compacting Concrete, Stockholm, Sweden, 1999, pp. 437-448.

13. Saric-Coric, M., Khayat, K.H., Tagnit-Hamou, A., "Performance Characteristics of Cement Grouts Made with Various Combinations of High-Range Water Reducer and Cellulose-Based Viscosity Modifier," *Cement and Concrete Research Jr.*, **33**, (12), 2003, pp. 1999-2008.
14. Khayat, K.H., "Use of Viscosity-Enhancing Admixtures in Cement-Based Systems – An Overview", *Cement and Concrete Composites*, **20**, 1998, pp. 171-188.
15. Hwang, S.-D., Khayat, K. H, "Effect of Various Admixture-Binder Combinations on Workability of Ready-Mix Self-Consolidating Concrete," *ACI, SP-233*, 178 p.
16. Leemann, A., Winnefeld, F., "The effect of Viscosity Modifying Agents on Mortar and Concrete," *Cement and Concrete Composites*, **29**, 2007, pp. 341-349.



## Full-Scale Test to Failure of a Strengthened Reinforced Concrete Bridge. Calibration of Assessment Models for Load-bearing Capacities of Existing Bridges



Arto Puurula, Tekn. Lic.  
Ola Enochsson, Tekn. Lic.  
Håkan Thun, Tekn. Dr.  
Håkan Nordin, Tekn. Lic.  
Björn Täljsten, Tekn. Dr., Prof.  
Lennart Elfgrén, Tekn. Dr., Prof.  
Division of Structural Engineering  
Luleå University of Technology  
SE-971 87 Luleå, Sweden  
Email: [Name.Name@ltu.se](mailto:Name.Name@ltu.se);  
[hakan.nordin@wspgroup.se](mailto:hakan.nordin@wspgroup.se)



Björn Paulsson, Banverket  
SE-781 85 Borlänge, Sweden  
Email: [bjorn.paulsson@banverket.se](mailto:bjorn.paulsson@banverket.se)

Jan Olofsson  
Skanska Sverige AB, Skanska Teknik  
SE-405 18 Göteborg, Sweden  
Email: [jan.olofsson@skanska.se](mailto:jan.olofsson@skanska.se)



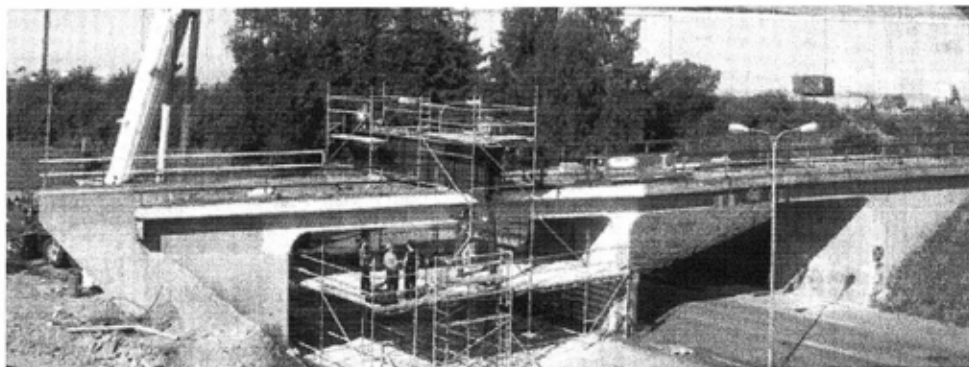
### ABSTRACT

A reinforced concrete railway trough bridge has been strengthened and loaded to failure. The aim was to test and calibrate methods developed in the European Research Project "Sustainable Bridges" regarding: (a) condition appraisal and inspection, (b) load carrying capacity analysis, (c) monitoring and (d) strengthening of existing bridges.

The tested methods proved to be useful and to give accurate predictions. A failure in combined shear, bending and torsion was reached for an applied mid span load of 11,7 MN. This was well predicted by enhanced methods but 20 to 50 % higher than ultimate load evaluated according to predictions based on common codes and models.



**Key words:** Bridge, Shear, Strengthening,  
Ultimate load carrying capacity, Failure



*Figure 1 - View from NE of tested bridge in Örnsköldsvik in northern Sweden. A plan, an elevation and cross sections of the bridge are given in Figures 2 and 3.*

## 1. INTRODUCTION

Field tests have been carried out on an existing reinforced concrete railway bridge in a European Research Project “Sustainable Bridges”. The aim of the project was to develop improved procedures and methods for inspection, testing, monitoring and condition assessment, of railway bridges. Furthermore, the project aimed to develop methodologies for assessing the safe carrying capacity of bridges and better engineering solutions for repair and strengthening. A consortium, consisting of 32 partners drawn from railway bridge owners, consultants, contractors, research institutes and universities carried out the Project during 2003 – 2008, see SB [1] and [www.sustainablebridges.net](http://www.sustainablebridges.net).

The bridge presented in this paper was loaded to failure to demonstrate and test methods developed in the project regarding procedures for (a) condition assessment and inspection, (b) load and resistance assessment, (c) monitoring, and (d) strengthening. For cost reasons, not many full scale tests to failure are carried out on bridges; a few examples are reported by Täljsten [2] and Plos [3].

The bridge was a reinforced concrete railway trough bridge in the form of a frame with two spans 12+12 m, see Figures 1-4. It was located in Örnsköldsvik in northern Sweden. It was built in 1955 and was taken out of service in 2005 due to the building of a new high-speed railway, the Botnia Line. The bridge was planned to be demolished in 2006 and this gave the opportunity to test it to failure before that.

## 2. GEOMETRY AND LOADS

The geometry is given in Figures 2-3. The bridge is slightly curved. It is founded on piles with a length up to 6 m driven down to the bedrock. The bridge was designed for an axle load of 200 kN, SB7.3 [4]. In 1990 the allowable axle load was increased to 225 kN. The line was electrified in 1995/96. Timber and pulp have been transported by railway into the city and scrap iron, paper and limestone out of it. The number of axle passages of 225 kN during 1990-2005 can be estimated to maximally 25 000.

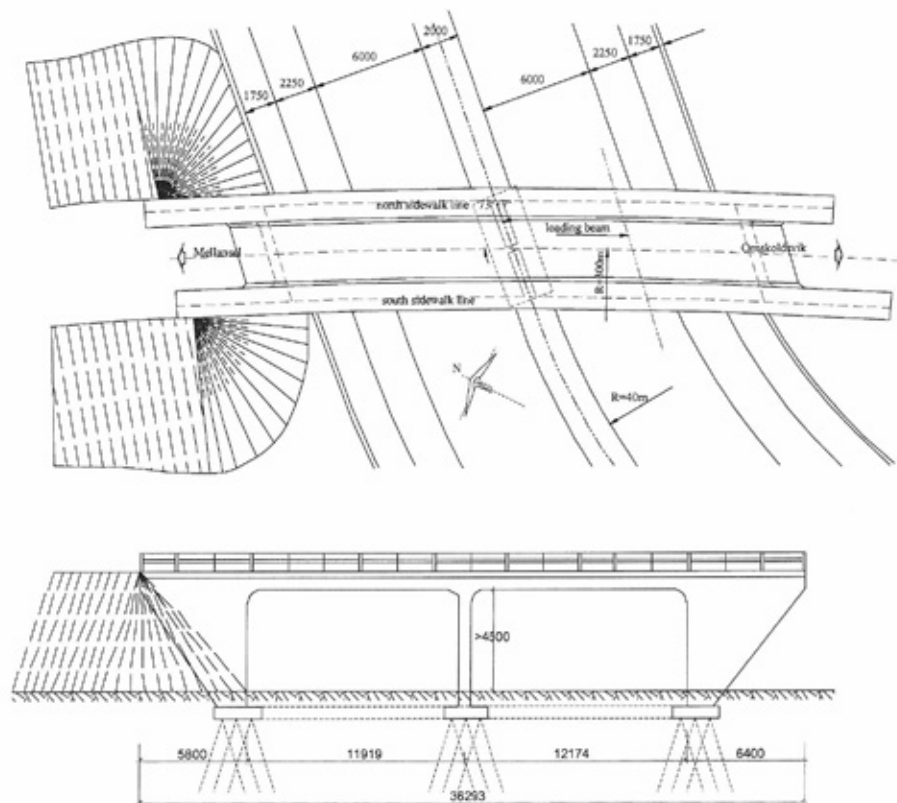


Figure 2 - Plan and elevation of tested bridge with landfill removed at SE wings

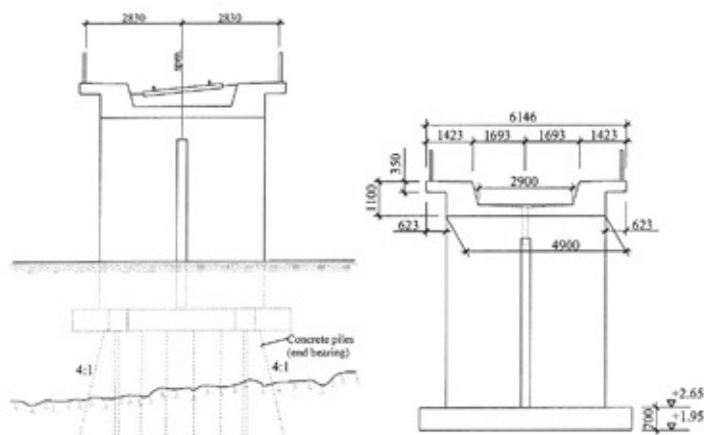


Figure 3 – Sections of tested bridge.



Maximum design bending moments and shear forces according to the original calculations from 1954 give section forces according to Figure 4. The maximum shear force is  $V = 2.3$  MN whereof 0.7 MN from dead load as shown in figure 4. The maximum mid span moment is  $M = 3.6$  MNm, whereof 0.8 MNm from dead load. The support moment is  $-4.7$  MNm, whereof  $-1.5$  MNm due to dead load.

The bending resistance in the mid span can roughly be evaluated to 10 MNm. The shear force is mainly carried by inclined bars close to the supports and by stirrups in the central parts.

The bridge was proposed to be tested with a vertical point load  $P$  in the middle of the SE span, see Figure 5. This loading may lead to a combined bending and shear failure which is interesting to evaluate and compare with code predictions from BBK04 [5], CEB-FIP [6], EN 1992-2 [7], and with more refined models in SB [1], Bentz [8], Enochsson et al [9], and Puurula [10]. In order to avoid a premature bending failure and to check newly developed strengthening methods, the bridge was strengthened in bending before the final test with bars of Carbon Fibre Reinforced Polymers, CFRP.

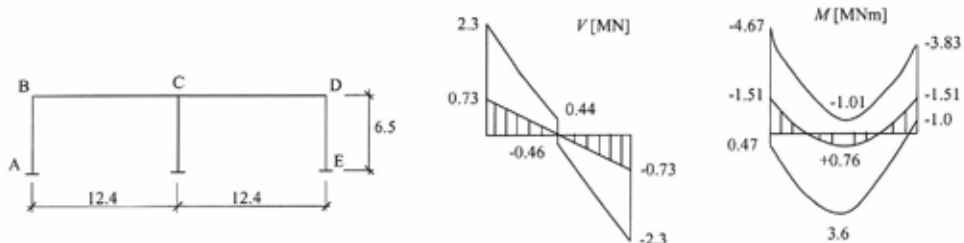


Figure 4 – Design section forces for one span of the bridge.

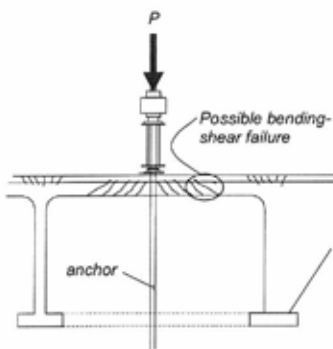


Figure 5 - Proposed loading arrangement with a jack supported by anchors injected into the rock (some 10 m below the bridge foundation slabs). A possible combined bending-shear failure close to the load point is indicated.

### 3. MATERIAL PROPERTIES AND MONITORING

The bridge was inspected in 2005 before it was decided to carry out the full-scale loading test. When the decision had been taken to test it, the bridge was inspected again, first by Luleå

University of Technology and later by the Federal Institute for Materials Research and Testing (BAM) in Berlin and COWI A/S in Copenhagen, with methods developed in the Sustainable Bridges project using ultrasonic radar, impulse response, electrochemical potential and Laser Induced Breakdown Spectroscopy (LIBS), [1], [4], [15]. In general it can be said that the bridge was in a good condition with few cracks and no reinforcement corrosion.

The bridge was designed for strength class K400 according to the Swedish code with a compressive strength of 40 MPa (400 kp/cm<sup>2</sup>) measured on 200 mm cubes. This corresponds roughly to EC class C28/35. By 2006 the strength had increased to C55/67 (measured on drilled out cores, [4]). The reinforcement was mostly  $\phi$  16 and  $\phi$  25 mm of grade Ks40 with nominal yield strength of 400 MPa.

In order to prevent the unwanted flexural failure, the bridge slab was strengthened with 9 + 9 = 18 rectangular bars of Carbon Fibre Reinforced Polymers (CFRP) Sto FRP Bar M10C with a length of 10 m, a cross section of 10 x 10 mm, a modulus of Elasticity  $E_f = 250$  GPa and a rupture strain  $\epsilon_r = 11\%$ . The rods were mounted as Near Surface Mounted Reinforcement (NSMR) in sawn out grooves spaced at 100 mm distances at the soffit of the decking slab, see Nordin and Täljsten [16], [17]. The strengthening provided an enhanced flexural resistance of approximately 4 MNm, which means about 40 % increase.

Several methods have been used to test and evaluate the different material parameters to form a basis for load-carrying capacity evaluations. In Table 1 a summary of the results is presented which is used in the analysis of the bridge. First *initial* properties are given based on the original drawings and simple estimations. *Characteristic* values refer to the 95% percentile of the strength values and to about a 50 % percentile of the elasticity values. The *design* values for the ultimate limit state (ULS) are based on the characteristic values divided by partial coefficients given in the table. *Mean* properties are given based on tests during 2006.

First the concrete properties are given: the compressive strength,  $f_c$  [MPa], the modulus of elasticity,  $E_c$  [GPa], the tensile strength,  $f_t$  [MPa], and the fracture energy,  $G_F$  [Nm/m]. Then the steel properties are given: the yield stress,  $f_{sy} = R_{eh}$  [MPa], the ultimate strength,  $f_{su} = R_m$  [MPa], and the modulus of elasticity,  $E_s$  [GPa]. Definitions and test details are given in SB 7.3 [4].

The bridge was first tested in the serviceability limit state before strengthening and before the final loading to failure.



*Figure 6 – Grooves were sawn in the bottom of the slab (15 x15 mm) and then filled with a resin and rods of CFRP (10 x 10 mm) in order to enhance the flexural resistance of the slab, [16], [17].*

Table 1 - Summary of material properties.

Stage	Type of value	Concrete				Steel		
		$f_c$ [MPa]	$E_c$ [GPa]	$f_t$ [MPa]	$G_F$ [Nm/m <sup>2</sup> ]	$f_{sy} = R_{ch}$ [MPa]	$f_{tm} = R_m$ [MPa]	$E_s$ [GPa]
Initial properties <small>(These values are assumed or taken from original drawings)</small>	Characteristic	31 <sup>a)</sup>	32 <sup>a)</sup>	1.8 <sup>a)</sup>	-	φ16: 410 <sup>b)</sup> φ25: 390 <sup>b)</sup>	φ16: 500 <sup>c)</sup> φ25: 500 <sup>c)</sup>	φ16: 200 <sup>c)</sup> φ25: 200 <sup>c)</sup>
		Design ULS <sup>d)</sup>	17.2	25.4	1.0	-	φ16: 297.1 φ25: 282.6	φ16: 362 φ25: 362
	Mean <small>(Standard deviations are given in parenthesis)</small>	68.5 (8)	25.4 (1.7)	2.2 (0.5)	154 (82)	φ16: 441 (12)	φ16: 738 (2.4)	φ16: 192.1 (23.3)
			tension	uni- axial		φ25: 411 (8.2)	φ25: 706 (22.6)	φ25: 198.3 (31.5)

a) The concrete compressive strength is according to BVH [11] obtained from the concrete class used in the bridge, i.e. 400 (K400), which corresponds to the concrete class K40. K40 is approximate equivalent to the strength class C28/35 in Eurocode which has a characteristic compressive strength of 27 MPa, a tensile strength of 1.8 MPa and a E-modulus of 32 GPa, BBK04 [5]. Since the bridge is more than 10 years old the compressive strength can according to BVH [11] be increased with 15 % from 27 MPa to  $1.15 \times 27 = 31$  MPa, see also Thun [21].

b) The characteristic yield strengths are taken from BVH [11], section 4.3.3. The bridge also contained some Ø10 mm bars. Their properties are assumed to be the same as the Ø16 mm bars.

c) According to BHB-M [12] the minimum ultimate stress is 500 MPa. According to BBK04 [5] the characteristic value of the E-modulus is 200 GPa.

d) The design value = characteristic value / ( $\eta\gamma_m\gamma_n$ ), where  $\eta\gamma_m$  is 1.5 for concrete and  $\gamma_n$  is the safety factor with regard to injury to people, in this case safety class 3, which gives the factor 1.2. For reinforcement steel  $\eta\gamma_m$  is 1.15 and for the E-modulus  $\eta\gamma_m$  is 1.05 according to BBK04 [5].

The monitoring system used during testing of the bridge consisted mainly of (a) strain gauges spot welded to the reinforcement, (b) an optical laser displacement sensor (Noptel PSM 200) and (c) Linear Varying Differential Transducers (LVDTs) for deflection measurements. Measurements were mainly made at the sections of point loads and close to the supports. Examples of measured deflections are given in Figure 7. The University of Minho and City University also successfully tested newly developed fibre-optic sensors for crack detection and accelerometers for modal identification and damage detection, SB7.3 [4].

## 4. ASSESSMENT METHODS AND PREDICTED CAPACITY

### 4.1 Eurocode 2

The bridge was first assessed with the traditional truss model according to Eurocode 2, EN 1992-2 [7]. The shear resistance  $V_{Rd}$  is calculated as the strength of the reinforcement crossing an inclined shear crack (Equation 6.8)

$$V_{Rd,s} = A_{sw} f_{ywd} (z \cot \theta) / s$$

where

$A_{sw}$  is the cross sectional area of the reinforcement (804 mm<sup>2</sup>, 4 Ø16, two hoops)

$f_{ywd}$  is the design yield strength of the shear reinforcement (see Table 1)

$z$  is the inner level arm (900 mm = 0,9 d)

$\theta$  is the angle between the concrete compression strut and the beam axis (min 21.8°)

$s$  is the spacing of the stirrups (300 mm)

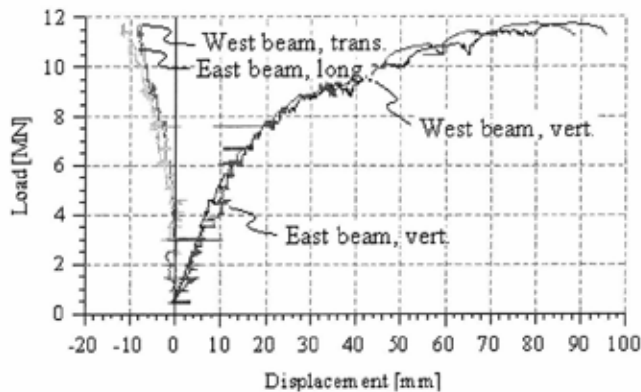


Figure 7 - Vertical and horizontal displacements of the east and west beams in the mid span during the final loading to failure of the bridge. To the left two curves are shown for horizontal displacements. One shows that the mid span moves transversely south-westwards some 8 mm along the loading line and longitudinally north-westwards some 12 mm. To the right the vertical deflections of the two beams are shown with a maximum mid span deflection of 88 mm for the east beam and 96 mm for the west beam.

Initial design values from Table 1 for one of the two beams give  $V_{Rd} = 1,79$  MN and mean values give  $V_{Rd} = 2,66$  MN. If a somewhat steeper angle is used ( $\theta = 30^\circ$  instead of the minimum value of  $21.8^\circ$ ) mean values give  $V_{Rd} = 1,84$  MN. Corresponding results are obtained with BBK 04 [5]

#### 4.2 Modified Compression Field Theory

The bridge was next assessed with the Modified Compression Field Theory, MCFT, which was developed at the University of Toronto by Michael Collins and co-workers, [13], [14]. The method is based on experimental studies of large reinforced concrete panels from which constitutive relationships were derived for cracked reinforced concrete. Response 2000, a program based on MCFT, developed by Bentz [8] was employed for the assessment.

Employment of mean values for material properties results in  $V_{Rd} = 2,53$  MN for a low normal force and 3,01 MN for a higher normal force [4].

#### 4.3 Linear Elastic 3D-model

The bridge has also been analyzed by Skanska with a finite element method using the computer program Lusas [18]. Three dimensional linear beam elements (BMS3) and thick quadrilateral linear shell elements (QTS4) have been used. In this way the influence of the curvature of the bridge could be modeled as well as the corresponding torsion moments. The model and some results are shown in Figure 8. As a comparison the bridge has also been modeled with the computer program Brigade [19] giving similar results [4].

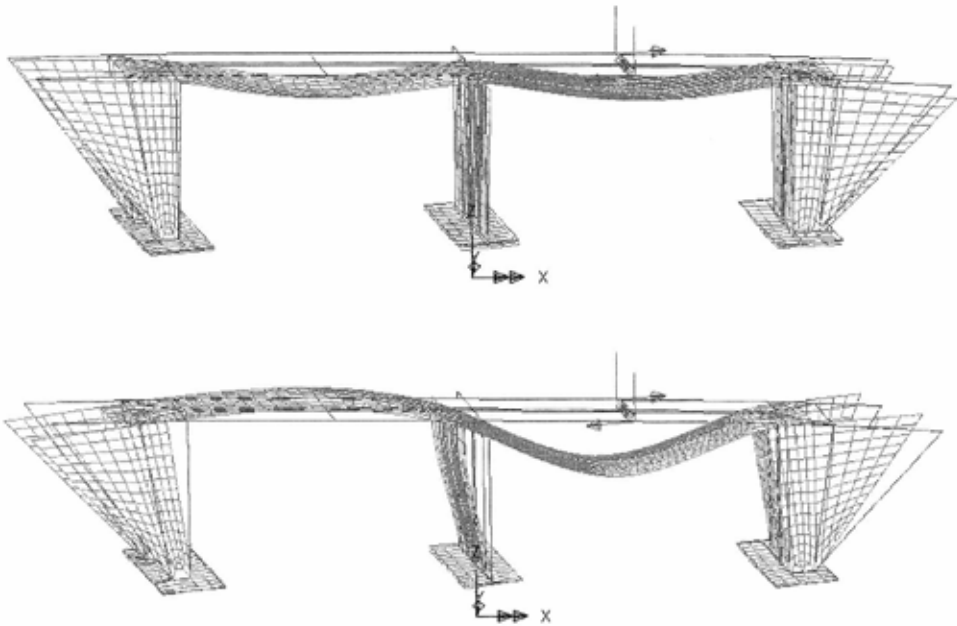


Figure 8 – Deflections due to permanent loads (top) and to a point load according to Lusas [18]. The three supports are numbered 1 to 3 starting from the left NW support.

The most critical beam for a shear failure according to the linear elastic analysis according to Lusas is the NE beam just outside the concentrated load towards the mid support (NE 2). However, almost as critical is the SW beam just outside the concentrated load towards the end support (SW 3).

The other beams, NE3 and SW2, are much less loaded in a linear elastic analysis, which means that before a real failure can take place (with the test set-up including both beams) there must be non-linear load redistributions in the structure. In the real test the “non-linear” shear failure came towards end support 3 and included both beams (NE3 and SW3).

Using the capacities from the Eurocode calculation in section 4.1 the *initial material properties* give, together with the Lusas results, that the maximum capacity is reached when the two concentrated loads are about  $P = 2.95$  MN, or a total of  $2P = 5.91$  MN. This turned out to be about 50 % of the failure load 11.7 MN.

With *mean material properties* the maximum capacity according to the analysis is reached when the concentrated loads  $P$  are about 4.39 MN, or a total of  $2P = 8.78$  MN.

#### 4.4 Nonlinear 2D-model

A non-linear analysis was performed by Cervenka Consulting using the finite element computer program Atena [20]. Some results can be seen in Figure 9. The analysis predicted an ultimate load of 10,5 MN after yielding in the longitudinal reinforcement.



Figure 9 - Detailed crack patterns at final loading state predicted by Atena [20]. The cracks illustrated are of widths  $> 0,1$  mm].

#### 4.5 Comparison

The results from the different models are compared in Table 2 together with the test result. In the test, the longitudinal bottom steel bars and the vertical stirrups started to yield close to the ultimate load. The final failure was caused by rupture in the stirrups crossing the inclined shear crack in Figure 10. The strengthening with near surface mounted reinforcement functioned and no premature bending failure did occur. Instead, a failure in combined shear, bending and torsion took place.

In the table, the shear capacity  $V_R$  of each of the two longitudinal beams are first given. The value also includes the influence of torsion. Then the live load capacity for the applied two point loads  $2P$  is given. It can be seen that the standard linear finite element methods together with Eurocode 2 give quite conservative predictions. A part of this may be caused by arch actions in the beam which is not considered in the calculations. It can also be seen that it is important to use a correct value of the inclination  $\theta$  for the compressive strut. When the minimum strut inclination ( $\theta = 21,8^\circ$ ) is used, a hypothetical situation will arise that a higher number shear reinforcing units is activated than in reality.

Enhanced non-linear methods as Atena and Response predict higher values for the resistance, which are closer to the tested value. Their stress and strain predictions are also closer to what has been observed in the bridge, SB7.3 [4].

Table 2 – Load carrying capacity for the bridge as predicted by different models.  $V_R$  is the shear capacity for one of the two longitudinal beams and  $2P$  is the live load capacity when the bridge is loaded with the load  $P$  in the middle of the span on each of the two longitudinal beams.

Method	$f_{yd}$ [MPa]	$\theta$ [°]	$V_R$ [MN]	$2P$ [MN]
EC2, design, $\theta_{min}$ + Lusas, 3D linear FEM	297	21,8	1,79	5,9
EC2, mean, $\theta_{min}$ + Lusas, 3D linear FEM	441	21,8	2,66	8,8
EC2, mean, $\theta_{real}$ + Lusas, 3D linear FEM	441	30	1,84	6,1
Response, nonlinear section analysis + low axial force	441		2,53	≈9
Response, nonlinear section analysis + high axial force	441		3,01	≈12
Atena, 2D nonlinear FEM	430	20-30	3,07	10,5
Test to failure	441	~30		11,7

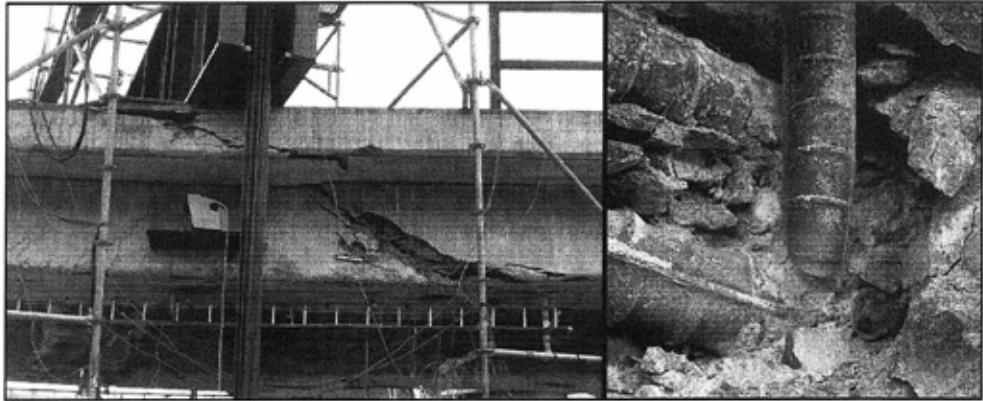


Figure 10 – Ultimate shear-bending failure with detail of stirrup rupture after yielding.

## 5. SUMMARY AND CONCLUSIONS

Procedures have been tested for inspection and condition assessment, load carrying capacity, monitoring, and strengthening of a 50 year old reinforced concrete railway trough bridge. In this paper focus has been on the assessment of the load carrying capacity. In the final test, a failure in combined shear, bending and torsion was reached for an applied mid span load of 11,7 MN. This was close to what was predicted by the methods developed in the project and is 20 to 50 % higher than predicted by design codes and other general models. All the predictions were on the safe side and the failure was initiated by rupture of a stirrup after yielding in both stirrups and longitudinal reinforcement. There is a need for additional full-scale test where advanced load carrying models can be calibrated to real failure mechanisms.

## ACKNOWLEDGEMENTS

The authors gratefully acknowledge support and contributions from: the European Union 6<sup>th</sup> Framework Program; Banverket, Sweden; The Federal Institute for Materials Research and Testing (BAM), Germany; Botniabanan, Sweden; City University, England; Cervenka Consulting, Czech Republic; COWI A/S, Denmark; Denmark Technical University (DTU), Denmark; Luleå University of Technology (LTU), Sweden; Nordisk Spännarmering, Sweden; Savonia University, Finland; Skanska Sverige AB, Sweden; STO Skandinavia AB, Sweden; Örnsköldsviks kommun, Sweden; and University of Minho (UMINHO), Portugal..

## REFERENCES

1. SB (2007): *Sustainable Bridges – Assessment for Future Traffic Demands and Longer Lives*, A European Integrated Research Project during 2003-2008 within FP6, No TIP3-CT-2003-001653, see [www.sustainablebridges.net](http://www.sustainablebridges.net). Four guidelines have been prepared: - *Inspection and Condition Assessment (SB-ICA)*, 259 pp;

- *Load and Resistance Assessment of Railway Bridges (SB-LRA)*, 428 pp;
  - *Guideline for Monitoring of Railway Bridges (SB-MON)*, 93 pp; and
  - *Guide for use of Repair and Strengthening methods for Railway Bridges (SB-STR)*, 139 pp.
- Background documents with state-of-art reports, analytical and numerical analyses and test results are also provided. [cited 2008-07-25].
2. Täljsten, Björn: *Plate Bonding. Strengthening of Existing Concrete Structures with Epoxy Bonded Plates of Steel or Fibre Reinforced Plastics*. PhD thesis 1994:152 D. Division of Structural Engineering, Luleå University of Technology, 2<sup>nd</sup> Ed 1994, 308 p.
  3. Plos, Mario: *Application of Fracture Mechanics to Concrete Bridges. Finite Element Analysis and Experiments*. Ph D Thesis. Publication 95:3, Chalmers university of Technology, Division of Concrete Structures, Göteborg 1995, 57 + 70 p.
  4. SB 7.3 (2007): *Field Test of a Concrete Bridge in Örnköldsvik, Sweden*. Prepared by Sustainable Bridges – a project within EU FP6. 63 + 333 pp. Available from: [www.sustainablebridges.net](http://www.sustainablebridges.net). [cited 2008-11-25].
  5. *Boverkets Handbok om Betongkonstruktion BBK04*. (Design Rules for Concrete Structures. In Swedish) Updated version Boverket, Karlskrona 2007, 271 p. [www.boverket.se/upload/publicerat/bifogade%20filer/2004/boverkets\\_handbok\\_om\\_betongkonstruktioner\\_BBK\\_04.pdf](http://www.boverket.se/upload/publicerat/bifogade%20filer/2004/boverkets_handbok_om_betongkonstruktioner_BBK_04.pdf). ISBN 91-7332-687-9 [cited 2007-08-25].
  6. *CEB-FIP Model Code 1990*. Design Code, Comité Euro-International du Béton, Sprint-Druck, Stuttgart 1999, 324 p. ISBN 2-88394-042-8.
  7. *Eurocode 2: Design of concrete structures - Part 2: Concrete bridges - Design and detailing rules*. EN 1992-2. European Standard, Brussels: CEN, 2005..
  8. Bentz, Evan C.: *Sectional Analysis of Reinforced Concrete Members*. A thesis submitted in conformity with the requirements for the degree of Doctor of Philosophy, Graduate Department of Civil Engineering, University of Toronto, Toronto 2000, 187 + 118 p. Four programs are presented in the thesis: Membrane –2000 for plates; Response-2000 for beams and columns; Triax-20000 for 3D blocks; and Shell-2000 for shells with out-of-plane forces. [www.ccf.utoronto.ca/~bentz](http://www.ccf.utoronto.ca/~bentz) [cited 2007-08-25].
  9. Enochsson, Ola; Puurula, Arto & Elfgren, Lennart: *Beräkning av betongbroars bärförmåga. Interaktion mellan tvärkraft, vridmoment och böjning i Källösundsbron* (Assessment of the Load Carrying Capacity of Concrete Bridges. Interaction between torsion, shear and bending in the Källösund Bridge. In Swedish) *Technical Report 2004:15*, Luleå: Division of Structural Engineering, Luleå University of Technology, 116 p. <http://epubl.ltu.se/1402-1536/2004/15/LTU-TR-0415-SE.pdf> [cited 2007-08-25].
  10. Puurula, Arto: *Assessment of Prestressed Concrete Bridges Loaded in Combined Shear, Torsion and Bending*. Licentiate Thesis 2004:43, Luleå: Division of Structural Engineering, Luleå University of Technology. <http://epubl.ltu.se/1402-1757/2004/43/index.html>. [cited 2007-08-25].



11. BVH (2005): *Evaluation of Concrete Railway Bridges*. (Bärighetsberäkning av järnvägsbroar. In Swedish). Handbok BVH 583.11. Banverket, CB, Borlänge 2005-06-01. 108 p + 9 app.
12. BHB-M (1994): *Betonghandbok – Material* (Concrete Handbook – Materials. In Swedish). 2<sup>nd</sup> Ed. Svensk Byggtjänst, Stockholm. 1127 p. ISBN 91-7332-709-3.
13. Collins M.P. and Michell D (1987, 1991): *Prestressed Concrete Basics*. Canadian Prestressed Concrete Institute, Canada, 1987, ISBN 0-9691816-6-3 Collins, Revised version (1991): *Prestressed Concrete Structures*. Prentice Hall, Englewood Cliffs, N.J., USA 1991, 766 pp. ISBN 0-13-691635-x. Reprinted by Response Publications, Toronto 1997, 766 p, ISBN 0-9681958-0-6.
14. Collins, Michael P; Mitchell, Denis; Adebar, Perry; and Vecchio, Frank J: A General Shear Design Method. *ACI Structural Journal*, Detoit, Vol 93, No 1, Paper 93-S5, January-February 1996, pp 36-45. Regarding code development see also Elstner, R C and Hognestad, E (1957): Laboratory investigation of rigid frame failure. *ACI Journal*, Vol 53, No 1, Jan 1957, pp. 637-668.
15. Hejll Arvid: *Civil Structural Health Monitoring – Strategy, Methods and Applications*, Doctoral Thesis 2007:10, Luleå University of Technology, ISBN: 978-91-85685-08-0, 189 p. <http://epubl.ltu.se/1402-1544/2007/10/index.html> [cited 2008-07-30].
16. Nordin Håkan: “Fibre Reinforced Polymers in Civil Engineering – Flexural Strengthening of Concrete Structures with Prestressed Near Surface Mounted CFRP Rods, Licentiate Thesis, Luleå University of Technology, ISBN: 91-89580-08-7, 145 p
17. Nordin H. and Täljsten B., (2006), “*Concrete Beams Strengthened with Prestressed Near Surface Mounted CFRP*”, *Journal of Composites for Construction*, Vol 10, No. 1, February 1, 2006, pp 60-68.
18. Lusas, software version 14.0-5. Lusas is a flexible software for finite element analysis of structures developed by LUSAS, Forge House, 66 High Street, Kingston upon Thames, Surrey, KT1 1HN, United Kingdom, see [www.lusas.com](http://www.lusas.com) [cited 2008-11-20].
19. Brigade, software version Brigade 2.1-4. Brigade is a suite of finite element analysis tools for the field of structural and civil engineering developed by Scanscot Technology, Ideon Research Park, SE-223 70 Lund, Sweden, see <http://www.scanscot.com/software/software.html> [cited 2008-11-20].
20. Atena is a non-linear finite element program for simulation of the real behavior of concrete and reinforced concrete structures developed by Cervenka Consulting, Predvoje 22, 160 00 Praha 6, Czech Republic, see <http://www.cervenka.cz/> [cited 2008-11-20].
21. Thun, Håkan (2006): *Assessment of Fatigue Resistance and Strength in Existing Concrete Structures*. Ph D Thesis 2006:65, Div. of Structural Engineering, Luleå University of Technology, 169 pp. ISBN 978-91-85685-03-5. Can be downloaded from: <http://epubl.ltu.se/1402-1544/2006/65/index.html> [cited 2008-11-20].

## Strengthening of concrete structures with cement based bonded composites



Thomas Blanksvård  
Lic. Tech., Ph.D. Student  
Luleå University of Technology  
971 87 Luleå, Sweden  
E-mail: thomas.blanksvard@ltu.se



Björn Täljsten  
Ph.D., Professor  
Technical University of Denmark  
Brovej Building 118, 2800 Kgs. Denmark  
E-mail: bt@byg.dtu.dk

### ABSTRACT

Due to demands on higher loads, degradation, re-construction etc. there is a constant need for repair or strengthening of existing concrete structures. Many varying methods exist to strengthen concrete structures, one such commonly used technique utilizes surface epoxy bonded FRPs (Fibre Reinforced Polymers). The method is very efficient and has achieved world wide attention. However, there are some drawbacks with the use of epoxy, e.g. working environment, compatibility and permeability. Substituting the epoxy adherent with a cement based bonding agent will render a strengthening system with improved working environment and better compatibility to the base concrete structure. This study gives an overview of different cement based systems, all with very promising results for structural upgrading. Studied parameters are structural retrofit for bending, shear and confinement. It is concluded that the use of carbon FRPs provides the highest strengthening effect and that the fibres should be imbedded into a matrix for enhanced utilisation of inherent strain capacity.

**Key words:** Strengthening, Concrete, FRP, CFRP, Mortar, Fabric, Textiles, Grids, MBC.

## INTRODUCTION

### 1.1 General

The use of reinforced concrete as a material for building structures is widely spread over the world due to its versatile applications. In general the construction industry is not known for development and technical innovations, at least not in comparison with industries such as the car and aerospace industries. Despite this, a considerably amount of research, development and innovations are carried out in construction and the society is highly dependent on these innovations. For example, systems or products that can lower the cost of maintenance and

prolong the structural life do not only save some of our beautiful heritage to future generations, but can also save a considerably amount of money.

The research and development of high performance and multifunctional construction materials have been improved to meet up with new demands and innovations. Advanced technologies have recently been focused on repair or upgrading of existing structures. The anticipated design life of steel reinforced concrete structures is frequently shortened due to alternation of the load situation on structures or deterioration, e.g. steel reinforcement corrosion. Traditional upgrading systems can consist of widening the cross section, external pre-stressing, span shortening etc. An alternative method to these traditional retrofitting methods is to bond a non corrosive material, such as FRP (Fibre Reinforced Polymers), to the surface of the structure. FRP materials have significant retrofitting potential and possess three physical properties of interest; high tensile strength, high elastic modulus and elastic-brittle stress-strain behaviour. One of the critical parameters in upgrading existing structures is the choice of bonding agent between the FRP and concrete surface, [1]. Strengthening systems with the use of continuous carbon fibres in an epoxy matrix bonded to concrete structures has proven to be successful, [2]. However, these methods present some important disadvantages regarding the use of organic resins (especially epoxies) which involve a hazardous working environment for the manual worker and have a low permeability, diffusion tightness and poor thermal compatibility with concrete, [3]. Upgrading civil structures with cement based bonding agents and high performance fibre materials give a more compatible repair or strengthening system with the base concrete. Consequently the use of cementitious bonding agents should prevent some of the disadvantages with the organic resins mentioned above. This study gives an overview of existing strengthening systems that use cement based bonding agents to adhere advanced fibre materials in order to upgrade existing concrete structures.

## 1.2 Materials

In this section only a brief introduction to the materials used in cement based strengthening systems is presented. It should be addressed that it is not the individual material properties that characterise the cement based composite, but the materials in combination and the synergy between them. A rough approach divides most of the cement based strengthening systems into two categories, fine grade *mortar* (bonding agent) and *fibre composites* (reinforcing for high tensile stresses).

*Mortar*: The bonding agents used in a cement based strengthening system are often fine grade (1 mm maximum grain size) mortars. To enhance the properties, e.g. workability, flowability, mechanical properties etc, of the mortars different mixtures and additives are used. Different additives can be polymers, superplasticizers and reinforcing fibres. The addition of different polymers enhances the properties of ordinary Portland cement. There are also a number of chemical admixtures, such as water reducing agents, ashes, aluminosilicate, superplasticizers, etc., that further improve the quality of mortar. All of the above mentioned improvements can enhance strength, shorten setting time, decrease autogenous shrinkage, control the alkali aggregate reaction and improve the durability, [4]. To increase the fluidity of fresh mortar and concrete for pumping, increase the strength and prolong the durability of hardened mortar and concrete, a small quantity of superplasticizers is often added to the mortar and concrete mixture. However, the single application of some superplasticizers can develop complications in the form of excessive bleeding, segregation and early loss of workability. Using them in combination with latex polymers could minimize these complications [5]. Other polymeric compounds can be re-dispersible polymer powder, water soluble polymer or liquid polymer.

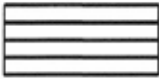

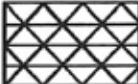
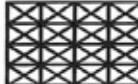
Another parameter that has a significant influence on the properties of the mortar is the mixture of ingredients. Compared with ordinary cement mortar, the properties of polymer modified mortar depend more on the polymer content or polymer to cement ratio (P/C) than the water to cement ratio (W/C) [6]. For example, three-point bending tests show that the maximum load is fairly constant for mortars with a P/C ratio 7.5 wt.% or lower. Increasing the P/C ratio between 10-15 % wt.% has shown to increase the flexural strength. However, a P/C ratio higher than 15 wt.% decreases the mechanical strength [7],[8].

Other ways to improve the performance of the mortars can be by adding reinforcing fibres. Especially for applications such as shotcreting, concrete upgrading and mining. The reason for adding fibres is primary to stabilize the micro-cracking. There are two main types of incorporating the fibres to the cement matrix, by the use of chopped or milled fibres or by the use of continuous fibres. The latter is more expensive and not easily mixed into the cement matrix. Chopped or milled fibres have less mechanical efficiency compared to continuous fibres but are more easily mixed in the mortar. Different types of fibres can be used, such as steel, alkali resistant glass, carbon, PP (polypropylene), PVA (polyvinyl alcohol) and natural fibres [9]-[13]. Drying shrinkage can be reduced by adding fibres in cement based materials. However, incorporating fibres in the material will generally reduce the compressive strength, thus increasing the permeability [14]. These insufficiencies can be bridged through the use of supplementary materials that will lead to a densification of the cement matrix. In the case of polypropylene reinforcing fibres, a suitable proportion of 2.0% is recommended; with an addition of 0.5% melamine formaldehyde dispersion, [15]. Adding silica fume will also improve the mechanical properties, such as compressive strength and flexural strength for cement matrices with steel and glass fibres [14]. When incorporating carbon fibres into the mortar a content of 0.5% of cement weight will give an optimum increase in flexural strength (general purpose pitch based carbon fibres), [13].

*Fibre composites:* The most common fibre composites consist of polymer fibres in matrices and additives. Different types of fibres consist of different materials, such as aramid, glass and carbon. The choice of material depends on the desirable properties of the composite, where carbon fibres have the highest strength and stiffness followed by aramid and glass fibres. The main function of the matrix is to transfer forces between fibres and to a lesser degree protect the fibres from the surrounding environment. The properties of the composite can be enhanced with the addition of additives, e.g. improve the bond between the composite and the strengthened material by a sizing compound, [16].

The fibres or fibre composites can be placed in different directions in the composite and thus form a large amount of FRP geometries with different mechanical properties. If the fibres are oriented in one direction the FRP becomes unidirectional. The fibres can also be woven or bonded in many directions, thus creating a bi or multi directional FRP. Table 1 shows different geometries for fibre composite strengthening materials. It should also be mentioned that 3D geometries are available. Depending on the type of fibre used, the FRP material can be referred to as CRFP (Carbon Fibre Reinforced Polymer), GFRP (Glass Fibre Reinforced Polymer) and AFRP (Aramid Fibre Reinforced Polymer). It is also possible combine these materials into a composite and then tailor-make the mechanical properties to correspond to the preferred characteristics.

Table 1. Different geometries for composite materials.

	Mono-axial	Biaxial	Triaxial	Multi-axial
1 Dimensions	Pultruded rod	-	-	-
2 Dimensions				
	Sheet	Weave/grid	Weave/grid	Weave/grid

## MINERAL BASED STRENGTHENING SYSTEMS

Strengthening concrete structures with continuous fibres or FRPs and cement based bonding agents must be done in well-defined steps. The process of optimising each and all of the incorporated materials into a composite with the most favourable strengthening properties are very complex. The components in the mineral based bonding agent as well as the materials and geometry of the fibres, or FRPs, play a significant role in the performance of the strengthening system. It is very hard to achieve a perfect penetration of the fibres or bond to FRPs in the mineral based matrix. Enhanced bonding of the fibre or FRP should be obtained when a non-linear geometry is introduced into the mineral based matrix. A special geometry may provide mechanical anchoring to the cement based matrix. As supported by many studies, in mineral based composites, the matrix does not fully penetrate in the spaces surrounding the fibre or FRP [13],[15]. In the following sections, four different approaches when designing cement based strengthening systems for concrete structures are described. The first system is Textile Reinforced Concrete (TRC) developed at the collaborative research centre at Dresden and Aachen University, Germany, in 1998. This strengthening system basically consists of woven fabrics bonded to the concrete surface with modified cement. The second system is called Fibre Reinforced Cement (FRC) and is being developed at Wayne State University, USA. This strengthening system consists of fibres impregnated with a cement matrix that results in a thin composite sheet. The third evaluated strengthening system is called Textile Reinforced Mortar (TRM), which is similar to the TRC system because it uses fibre textiles and mortar as a bonding agent. TRM is developed at the University of Patras, Greece. The fourth system and another way to strengthen concrete structures with FRPs and cementitious bonding agents is called Mineral Based Composites (MBC). This system has been developed at Luleå University of Technology, Sweden and presented in detail in this paper. This system uses a fibre composite grid bonded to the surface of a concrete structure to enhance its strength, stiffness or both. Common for all strengthening systems is the use of a cement based bonding agent. The main difference lies within the design of the fibre composites the manufacturing process and application technique.

### 2.1 Textile Reinforced Concrete (TRC)

The TRC strengthening technique is comprised of a cementitious matrix as the bonding agent and a textile fabric as reinforcement. The TRC system is mounted with a fine-grained, high strength concrete as the bonding agent. This high strength concrete has a maximum aggregate size of 1 mm. The reinforcing fibres are predominately made of AR-glass (alkali resistant glass fibres) produced into to a woven fabric, the use of carbon fibres or a combination with AR-glass has also been utilized. There can be many designs of the textile fabrics depending on the load

case and positioning of the fabric. A maximum of four different fibre orientations can be obtained in the same multiaxial fabric; see also Figure 1. Fabrics with relatively complicated yarn shapes, such as short weft knit, enhance the bonding and improve the composite performance [18]. Figure 1 shows a multiaxial textile fabric with filament bundles and stitching fibres.



Figure 1. Multiaxial textile fabric used in textile reinforced concrete, tow spacing  $\sim 10$  mm.

### Strengthening in Shear

Shear strengthening of concrete beams with the TRC strengthening system has been performed at the Dresden University of Technology [19], [20]. The concrete beam specimens had a T-section and the test set-up was three point beam bending with a support span of 200 cm, see Figure 2. The concrete T-beams were symmetrically strengthened with the TRC system three sided wrapped around the bottom of the web extending 900 mm on each side from the middle of the beam. The TRC strengthening system was applied layer by layer. Fine-grained cement was used as the bonding agent and the fabric was laminated with a spatula in the wet cement matrix. The application of the TRC system is shown in Figure 3. The steel shear reinforcement was designed to ensure the redistribution of internal forces in the state of cracking and to simulate a reinforced concrete beam in need of strengthening. The flexural steel reinforcement was designed for a higher load than the shear reinforcement to avoid bending failure in the T-beam.

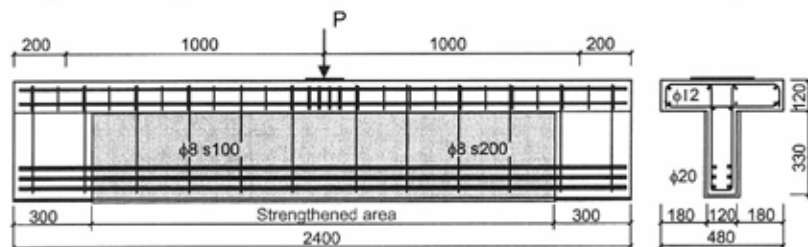


Figure 2. Test set-up and geometry of T-beams, strengthened area situated in the middle. Units in cm. after [19].

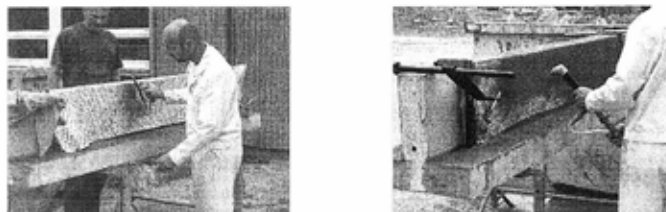
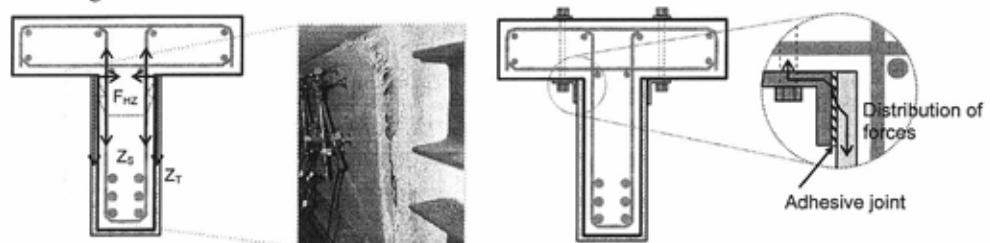


Figure 3. Mounting of the TRC strengthening system. To the left, the fabric is laminated onto the side of the beam. To the right, a layer of cement matrix is sprayed on to the surface of the fabric. Courtesy of A. Brueckner, Dresden University of Technology.

As seen in Figure 3, the fabric is wrapped around the web of the beam up to the underside of the flange. This strengthening methodology may cause insufficient anchorage of the TRC system,

since there is no anchorage in the compressive zone. A mechanical anchorage would then be advantageous. In [19], the mechanical anchorage was designed with a steel L-section that was bonded on both sides of the TRC system surface with an epoxy adhesive. Both anchored and unanchored strengthening was performed. Anchorage failure of a strengthened beam and strengthened T-beam cross sections with and without mechanical anchoring are recorded in Figure 4. The fabric used in these tests was a multiaxial textile with a weight per unit area of  $470 \text{ g/m}^2$ . The AR-glass fibre inclination was  $\pm 45^\circ$  to the load direction with the aim to be aligned with the principal stresses in the web. The applied textile fabric used in the system is shown in Figure 1. In total five concrete beams were strengthened with the TRC system. Two concrete beams were strengthened with two textile layers and one with four textile layers, all without mechanical anchoring. Two additional beam specimens were strengthened, one with three layers of fabric and one specimen with four layers of fabric, both with mechanical anchoring.



A. Without mechanical anchoring B. Anchorage failure

C. With mechanical anchoring

Figure 4. Strengthened T-section without mechanical anchoring. To the right, delamination failure of strengthening layer, from [19].

Strengthening of the T-beam cross section with TRC significantly increased the shear load capacity. However, when the number of textile fabric layers increases, so does the need for mechanical anchoring. The results indicate that the ultimate bearing capacity will roughly be the same for a T-beam strengthened with two layers compared to a specimen strengthened with four layers. The difference between two and four layers of textile fabric is in the initial stage of loading, where the four-layered strengthening displays higher stiffness until the propagation of the anchorage failure initiate. Typical anchorage failure is recorded in Figure 4 B. With mechanical anchoring, an increased stiffness and higher bearing capacity of the strengthened T-beam specimens are noticed. The strengthening effect of a TRC strengthened concrete beam compared to the average value of three non-strengthened reference T-beam is recorded in Table 2. The deformation rate of the loading in this study was set to  $0.01 \text{ mm/sec}$ . Table 2 shows that the strengthening effects are low and that debonding failure dominates if the textile is not anchored. However, by using anchoring a higher utilisation of the textile will be achieved and thus a higher strengthening effect. It should be noted that the strengthening effect is not drastically influenced by adding more textile layers. It should also be noted that the overall strengthening effect with or without anchoring is not that high (maximum 16%). The maximum strengthening effect was accomplished by using high amounts of fibres and mechanical anchorage. When using less layers of textiles and no mechanical anchorage the strengthening effect would be insignificant, taking into consideration the stochastic scattering of the failure loads.



It should be pointed out that the fibres were aligned in a  $\pm 45^\circ$  and therefore are having a better utilisation of the fibres. Despite this, significant strengthening effect is absent although using mechanical anchorage.

*Table 2. Strengthening effect of TRC, ultimate failure load divided by the average failure load of the reference beams, from [19].*

	2 textile layers (without anchoring)	4 textile layers (without anchoring)	6 textile layers (without anchoring)	2 textile layers (with anchoring)	4 textile layers (with anchoring)	6 textile layers (with anchoring)
Strengthening effect	1.01	1.01	1.07	1.06	1.09	1.16
Failure mode	Fracture	Debonding	Debonding	Fracture	Fracture	Fracture

### *Strengthening in flexure*

It is also possible to use TRC for flexural strengthening, as reported in [21]. This study contains flexural strengthening of pre-deformed concrete slabs. For the flexural strengthening, a biaxial geometry of the fabrics was used. Three different fabric designs were evaluated. All of the textile reinforcement was mounted in three layers. The three fabric designs were AR-glass with a fibre area of  $143 \text{ mm}^2$ , AR-glass fibre with polymer coating and a fibre area of  $143 \text{ mm}^2$ , and carbon fibre with polymer coating and a fibre area of  $50 \text{ mm}^2$ . The biaxial geometry of the fabrics was longitudinal and cross directional of the strengthened concrete beam. Mounting of the reinforcement can be seen in Figure 5. The test set-up was four-point beam bending with an effective span of 1.6 m. The height of the concrete slab was 100 mm and the concrete slab had flexural steel reinforcement. The results on the strengthened concrete specimen show that higher ultimate load carrying capacity and higher stiffness can be achieved. And also that a polymer coating of the fabrics increases the effectiveness of the textile fabric. It is also shown that for the same load carrying capacity only one-third of the carbon fibre area is needed compared to the AR-glass fibre area. The strengthening effects of the different TRC systems are recorded in Table 3. Strengthening of pre-damaged concrete structures utilizes the effectiveness of the fabrics more than strengthening of an undamaged concrete structure. The effectiveness of the fibres in pre-damaged cross sections is based on the nature of bridging stresses over cracks in damaged zones. However, the effectiveness of the fibres with polymer coating is not concurrent to pre-damaged cross sections but is related to the strains and slip development in the textile and mechanical interlocking during loading, see also the discussion in the last chapter.



*Figure 5. Mounting of the TRC strengthening system. Courtesy of A. Brueckner, Dresden University of Technology.*

*Table 3. Strengthening effect of flexural strengthened concrete beam with TRC system. Ultimate failure load divided by failure load of unstrengthened beam, from [21].*

	AR-glass, $A_f = 143 \text{ mm}^2$ . No coating	AR-glass, $A_f = 143 \text{ mm}^2$ . Polymer coating	Carbon fibre, $A_f = 50 \text{ mm}^2$ . Polymer coating
Strengthening effect	1.51	1.86	1.86



There are numerous references on the development of TRC and for example computational models can be found in [22], analytical solutions of tensile response of the TRC in [17], stochastic modelling in [23] and bond mechanisms in [24].

## 2.2 Fibre Reinforced Cement (FRC)

This strengthening system is comprised of a fibre sheet or fabric that is impregnated with a cement based matrix. Combining the cement slurry and the different fibre geometries results in a thin composite sheet. Depending on the geometry of the fibres and the strengthening purpose, the composite plates can be made as thin as 2 mm, see Figure 6 C. Composites of ultra high performance, fibre reinforced cement plates have excellent durability and ductility properties during flexural tests, see Figure 6 A and B. The mounting of this strengthening system differs from the MBC and TRC strengthening systems. The sheet or fabric is cut into chosen dimensions and the fibre geometry is submerged into a cement slurry (matrix) for full penetration. The impregnated sheet or fabric is then removed from the slurry and immediately bonded to the concrete surface. The performance of this system is investigated in both confinement and flexural strengthening of concrete specimens [25], [26], and [27]. In the latter, the high tensile strength comes from the carbon fibre sheet and the ductility from multiple cracking of the cement based matrix, similar to the Engineered Cementitious Composites (ECC) [28]. The competitive product to cement based strengthening is epoxy bonded fibres; hence, comparing epoxy bonded products to the cement based composites would be of interest. In [26] and [27], both confinement and flexural strengthening were performed. The fibre material used in both studies was based on continuous carbon fibres without matrix.

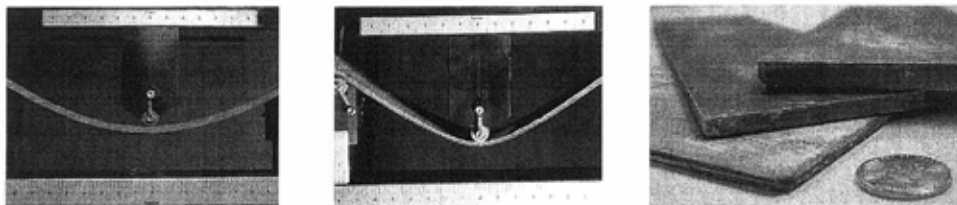


Figure 6. Composite plate with a thickness: A. 4.8 mm, B. 3.2 mm. C. Cement based composite plates with mono-axial fibre sheets, from bottom, 2, 3 and 4 mm of thickness. Courtesy of H.C. Wu.

### Strengthening for Confinement

By using a carbon fibre sheet, concrete cylinders can be strengthened for confinement. The height of the cylinders was 203 mm with a diameter of 102 mm. The test set-up of the cylinders was in accordance to ASTM C39-96 (compression strength test on cylindrical specimens). The epoxy based strengthening system (CFRP) was wrapped around the cylinders and anchored with a bond length of 51 mm, the total thickness of this strengthening system was 2-3 mm. The cement based strengthening system (CFRC) was applied as described above with two layers of carbon fibre. The CFRC composite sheet was wrapped around the cylinder as with the CFRP strengthened specimens. However, the bond length of this system was 76 mm with an average thickness of 3 mm. Gaps of 38 mm were left at the bottom and top of the concrete cylinders for both strengthening systems, see Figure 7. The results indicate a higher compressive strength and higher ductility for the CFRP specimens. However, no major differences between the CFRP and the CFRC systems were noticed. The unconfined concrete cylinders had a compressive failure

of 54 MPa and a deflection of 2 mm, whereas the compressive strength for CFRC strengthened specimens were 105 MPa with a deflection of 8 mm. Anchorage of the fibres is improved when wrapped. In this comparison it is much the properties of the carbon fibres that are shown, for fully anchored fibres.

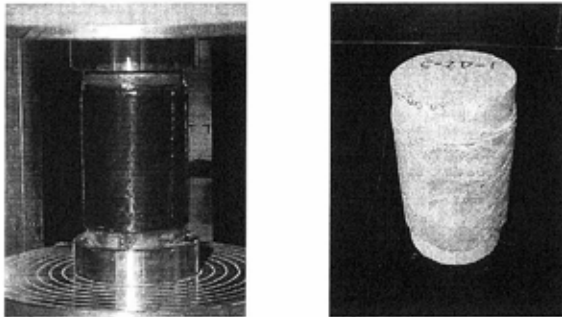


Figure 7. Confinement of concrete cylinders, to the left epoxy bonded CFRP and to the right CFRC wrapped specimen, courtesy of H.C. Wu.

#### *Strengthening for flexure*

Concrete beams have also been strengthened for flexure with the FRC system. Here, a comparison with epoxy bonded carbon fibres was conducted. The flexural test set-up is three-point bending according to ASTM C78-75 (rectangular beam specimen subjected to a three point load case with two shear spans and a maximum bending moment in the mid-point of the beam specimen). In comparison to the confinement strengthening, the fibre geometry changed from a sheet to a two dimensional/biaxial carbon fibre grid without any matrix. The volume content of fibres in the composite is 4.2% for both strengthening systems. Both CFRP and CFRC composites were bonded to the tensile side of the concrete beam. The test set-up for the CFRC beam can be seen in Figure 8. The non-reinforced and non-strengthened concrete reference beam displayed brittle failure due to lack of tensile reinforcement. An increase in both flexural strength and deflection occurred in both of the strengthening systems. However, the epoxy bonded strengthening system exhibited the highest increase in flexural strength. Failure of the beams with the epoxy bonded carbon fibres started with the formation of several cracks in the concrete as the load increased. The crack formulation gradually propagated to the bond zone between the concrete and epoxy adhesive. A typical peeling phenomenon then propagated through the transition zone between the base concrete and adhesive, with failure finally occurring as crushing of the concrete under the line load. Concrete beams strengthened with the CFRC system behaved differently with primarily one flexural crack and final failure due to rupture of the CFRP composite, see Figure 8. No bond problems were noticed in the transition zone between the base concrete and cement based bonding agent. The flexural strength of the CFRC system is inferior compared to the CFRP system, though larger than the non-strengthened reference beam. The strengthening effect, i.e. ultimate failure load of the strengthened specimen divided by the failure load of the reference beam for both confinement and flexural strengthening, is recorded in Table 4. It is not stated in [27], but the large difference in strengthening effects between the cement based and epoxy based flexural strengthening could be due to slippage of the fibres in the cement matrix. This better bond is also shown by one crack in the CFRC system and multiple cracking in the CFRP system. The fibres can be anchored by wrapping for the confinement strengthening. Fully anchoring the fibres will lead to similar strengthening effects when comparing the two strengthening systems for confinement. Slippage of the fibres originates from the poor bond/penetration of the cement matrix. A better bond to

the fibres can be achieved when using epoxy bonding agents. This shows the importance of anchorage of the fibres in the cement based bonding agent. However in this case another aspect is not dealt with and that is the peeling stresses that occur in at the cut of end of the adhered system. In this case the system is applied beyond the supports and peeling stresses are prohibited.

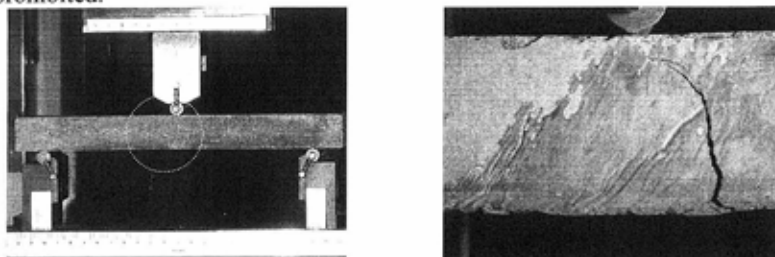


Figure 8. To the left, three point flexural test set-up and to the right, failure of CFRC beam, courtesy of H.C. Wu.

Table 4. Strengthening effect of both the FRC system and similar epoxy bonded strengthening system, ultimate failure values from [27].

	Confinement/ Cement	Confinement/Epoxy	Flexural/Cement	Flexural/Epoxy
Strengthening effect	1.85	1.94	2.03	4.65

### 2.3 Textile Reinforced Mortar (TRM)

This system is similar to the TRC strengthening system. The fibre textiles used for strengthening purposes are made of carbon fibre and the bonding agent is a polymer modified mortar. In this study, the evaluation of shear strengthened concrete beams was undertaken based on [29]. The base concrete beam specimens to be strengthened were 2600 mm long and with a cross section of 150 x 300 mm<sup>2</sup>. The base concrete specimens were reinforced with steel rebars, both flexural and in the shear span. The steel reinforcement scheme is recorded in Figure 9 together with the four point bending test set-up. In [29], both epoxy and a cementitious bonding agent were used. This study had three variables; bonding agent (epoxy or mortar based), number of layers of textile (1 or 2 layers) and the alignment of the textiles. The alignment of the textiles was vertical or spirally applied at an angle of 10°.

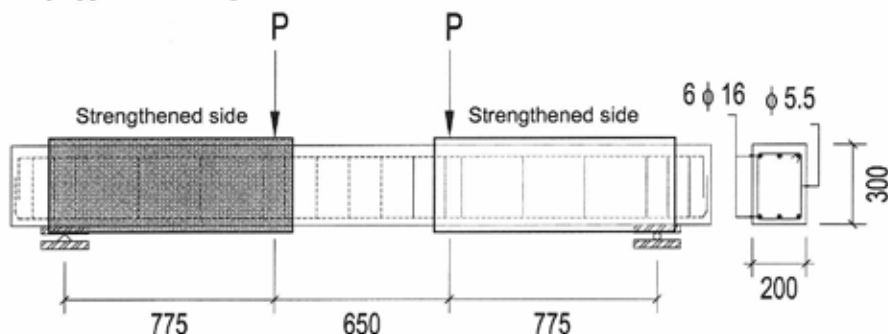


Figure 9. Reinforcement scheme for the base concrete specimens after [29].

The carbon fibre textile used in the strengthening system equalled the quantity of high strength rovings in the two orthogonal directions. Each roving is stitched together by a secondary polypropylene grid, similar to Figure 1. The width of the roving is 4 mm and the distance between them is 10 mm. The total weight of carbon fibres in the textile are  $168 \text{ g/m}^2$ , elastic modulus 225 GPa and tensile strength 3350 MPa.

Bonding agents used in the study were a structural epoxy adhesive and a polymer modified mortar. The two component epoxy adhesive had a tensile strength of 30 MPa and an elastic modulus of 3.8 GPa. The mortar consisted of a cementitious binder with the addition of polymers (10:1). Application of the mortar was done by a hand lay-up technique using a trowel to apply the mortar layers onto the base concrete surface and the textiles. The thickness of the mortar layers ranged from 1.5-2 mm, with the number of layers depending on the number of textile layers used.

All of the evaluated concrete beam specimens were statically loaded until failure with a displacement rate of 0.01 mm/sec. One non strengthened control beam was used as a reference. The beam specimens evaluated in this literature study are recorded in Table 5. Note that specimens R2, M2, M2-s and R1 indicated that the shear failure was suppressed and the ultimate failure was dominated by flexure. Common for all of the previously mentioned specimens is that the shear resistance was increased by a factor of approximately 2. Specimen M1, a strengthened reinforced concrete beam using one layer of carbon fibre textile bonded with mortar, failed in shear similar to the reference beam, but with a strengthening effect of 1.71. This was somewhat lower than the strengthened specimens using epoxy bonding agents. The shear failure using mortar bonded carbon fibres could be detected visually, which is not possible when using epoxy bonded fibres. This is a desirable property as it permits onsite damage control assessment when strengthening real structures [29]. It should also be noted that all of the strengthened specimens were wrapped and thus prohibited to fail by debonding of the strengthening system. If only side bonded, then anchorage problems and internal bond of the fibres could be evident. Especially for specimens with limited heights and therefore limited anchorage lengths, see also section 2.1.

*Table 5. Summary of evaluated beam specimens, after [29].*

Specimen	Strengthening	Bonding agent	Peak force [kN]	Failure mode	Strengthening effect <sup>^</sup>
C	-	-	116.5	Shear	-
R2	2 layers of textile vertically wrapped	Epoxy	233.4	Flexure	2.00
M2	2 layers of textile vertically wrapped	Mortar	243.8	Flexure	2.09
M2-s	2 layers of textile spirally wrapped	Mortar	237.7	Flexure	2.04
R1	1 layers of textile vertically wrapped	Epoxy	261.9	Flexure	2.24
M1	1 layers of textile vertically wrapped	Mortar	200.1	Shear	1.71

<sup>^</sup> Calculated as maximum peak load divided by peak load of the reference beam

### 2.3 Mineral Based Composites (MBC)

The MBC system used in this research contains basically three material components – a cementitious binder, a CFRP grid and a concrete surface primer. To achieve a good bond between the base concrete and the mortar, the surface of the base concrete needs to be roughened, e.g. sandblasting or water jetting, in order to remove the cement laitance. The surface preparation method for all presented test specimens was sandblasting. In laboratory environment a hand lay-up method was used to apply the MBC. This method includes pre-wetting the base concrete with water for 1-3 days depending on the conditions of the base concrete and the surrounding climate. The moisture conditions in the transition zone between the base concrete and mortar are further discussed in [30], where it is found that the best bond is obtained when the base concrete has just dried back from a saturated surface. Prior to mounting the MBC system the base concrete surface has to be primed using a silt-up product (primer) to prevent moisture transport from the wet mortar to the base concrete. A first layer of mortar is immediately applied to the primed surface. Next, the CFRP grid is placed on the first layer of mortar followed by an additional layer of mortar being applied on top of the grid. The thickness of the mortar depends on the maximum grain size in the mortar. The hand-lay up method, after sandblasting, is shown in four steps in Figure 10. All of the evaluated specimens are strengthened with the MBC system using the hand lay-up method in laboratory conditions of 20°C and 60% relative humidity (RH).

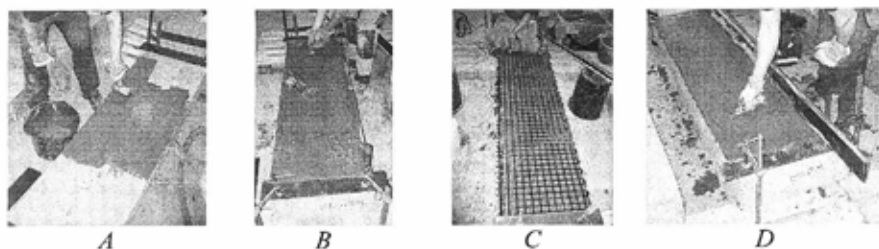


Figure 10. Hand lay-up of the MBC strengthening system. A) surface primer, B) first layer of mortar, C) placement of CFRP grid and D) last layer of mortar.

When strengthening large structures, the hand lay-up method might be too time consuming and uneconomical depending on the size of the project. Figure 11 shows the strengthening of a balcony for flexure. The mortar is applied by shotcreting. These balconies were strengthened on the bottom side of the slab. This involves mounting the MBC system vertically from below. The production method generally consists of the same procedure as the laboratory hand lay-up method. However, to prevent the CFRP grid from falling down, a number of steel studs were nailed to the surface of the base concrete. The grid is fastened to these studs after the first layer of mortar has been applied. The first mortar layer is applied by spraying and the peak of the studs act as a maximum distance measurement to ensure that the right mortar layer thickness is being obtained. After attachment of the CFRP grid, a second layer of mortar is sprayed on. Prior to applying the mortar the surface was roughened by sandblasting and then primed. It is also possible to mount the grid to the studs and then apply the mortar by spraying directly onto the grid in one layer, thus reducing the workmanship by one step.

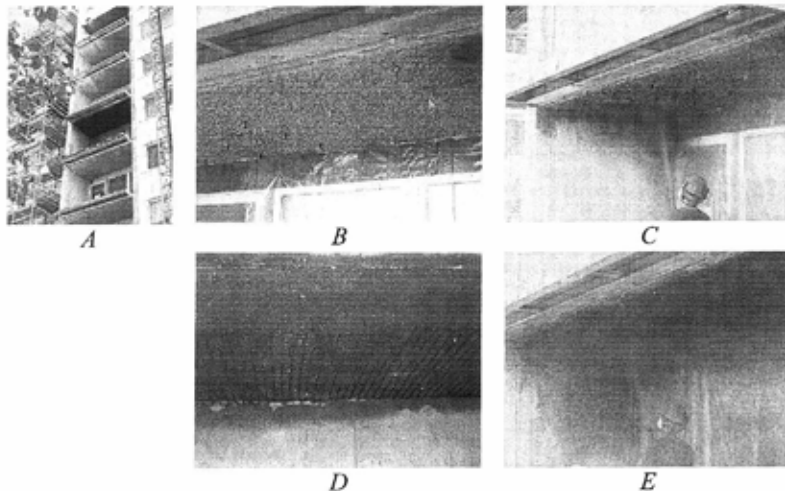


Figure 11. In-situ production method for the MBC strengthening system. A) Balconies to be strengthened, B) Concrete surface to be strengthened, studs applied, C) first layer of mortar is being sprayed, D) Mounting of the CFRP grid to the studs and E) Last layer of mortar is being sprayed.

#### Strengthening for shear

In this study, 8 concrete beams were evaluated for shear strengthening purposes, comprising unstrengthened and strengthened concrete beam specimens. The strengthening consists of using epoxy bonded CFRP sheets, a cementitious bonding agent only and the MBC system. Beams strengthened with the use of epoxy bonding agents and CFRP sheets were performed by [31]. Set-up for all beam specimens were four-point bending. The geometries and reinforcement scheme are recorded in Figure 12. The concrete beams are reinforced in such a way that shear failure is directed to one of the shear spans. The design of the steel reinforcement is detailed below. This design of the reinforcement is motivated by the fact that due to the lack of shear reinforcement in one span, the beams only need to be strengthened in this span. Thus, the other shear span is heavily reinforced with steel stirrups. Common to all of the concrete beams is that they are reinforced with 12  $\text{\O}16$  steel bars at the bottom and 2  $\text{\O}16$  at the top of the beam as flexural and compression reinforcement. The shear reinforcement contains  $\text{\O}12$  steel bars with a distance 50 mm at the supports and  $\text{\O}12$  with the distance 100 mm in the heavily reinforced shear span. The densification of the shear reinforcement over the supports is supposed to prevent crushing and peeling failures and secure the anchorage of the longitudinal reinforcement. All of the steel reinforcements have the characteristic yield strength of 500 MPa. For a more comprehensive study the reader is referred to [32]. The latter includes a vast monitoring set-up using strain gauges and photometric measurement. [33] and [32] also contain the interaction between the MBC system and steel shear reinforcement and crack propagation for different magnitudes of shear load. The beam specimen strengthened with the epoxy based system utilizes vertically applied unidirectional carbon fibre sheets ( $200\text{g/m}^2$ ). Beams strengthened with the MBC system utilize three different CFRP grids, see Table 6. One of the beam specimens was strengthened using only mortar. The mortar used in this study had a maximum grain size of 1 mm, tensile strength of 5.4 MPa, modulus of elasticity 26.5 and compression strength of 45.0 MPa. The failure mode and strengthening effect for the studied beam is reported in Table 7.

Four specimens were loaded by a deformation control of 0.01 mm/sec and specimens noted with a \* which were load controlled at 10 kN/min.

Table 6. Manufacturer provided properties of the fibres in vertical CFRP tows.

CFRP grid	Total fibre amount (g/m <sup>2</sup> )	Transverse fibre amount (g/m <sup>2</sup> )	Elastic modulus (MPa)	Tensile strength (MPa)	Tow distance (mm)
1	66	32	589	4300	24
2	98	51	288	3800	70
3	154	84	284	3800	44

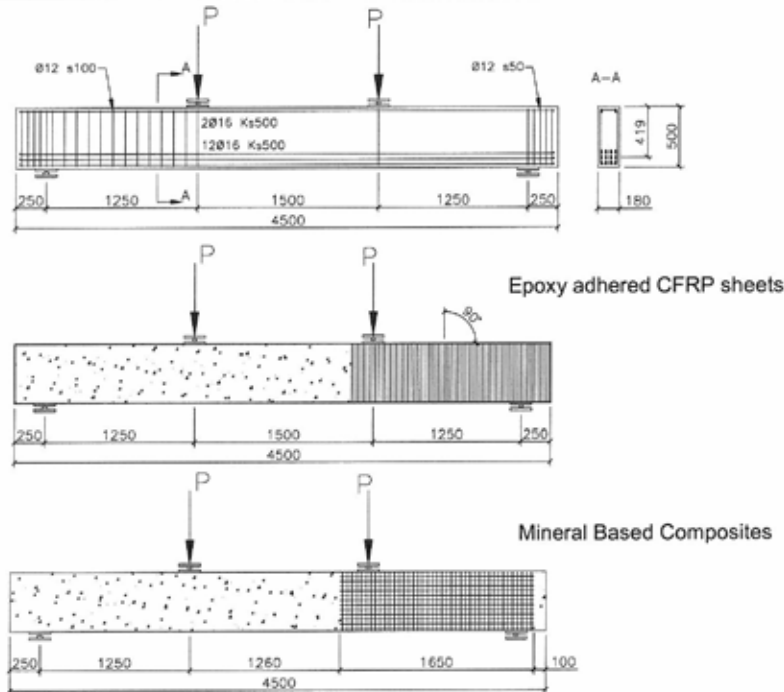


Figure 12. Test set-up and geometry for the reference and strengthened beams.

Table 7. Summary of beams strengthened for shear with MBC

Specimen	Strengthening	Bonding agent	Peak force (kN)	Failure mode	Strengthening effect <sup>A</sup>
R	-	-	123.5	Shear	-
R*	-	-	126.7	Shear	-
M	Only mortar	Mortar	141.9	Shear	1.15
MG3	MBC with grid 3	Mortar	244.9	Rupture of fibres	1.98
ES	Epoxy with sheet	Mortar	259.9	Debonding	2.10
MG1*	MBC with grid 1	Mortar	208.1	Rupture of fibres	1.68
MG2*	MBC with grid 2	Mortar	206.4	Rupture of fibres	1.67
MG3*	MBC with grid 3	Mortar	251.9	Rupture of fibres	1.99

<sup>A</sup> Calculated as maximum peak load divided by peak load of the reference beam

Using mortar only to increase the cross section will contribute to the shear capacity with 15%. Using a grid with a higher fibre amount will generate a higher strengthening effect. The geometry of the studied grid seems to have little influence of the crack formation. However, using a grid with small tow distance will generate a higher first crack load. This should probably depend on the faster redistribution of tensile stresses. There is no large variation in strengthening effect when comparing the MBC system to the epoxy bonded carbon fibre sheet. It should be noticed that the fibre amount in the epoxy bonded sheets is almost 138% higher in the vertical direction compared to the MBC system. However, the failure mode for the sheets was debonding and ultimate strength of the fibres was not fully utilized.

#### *Strengthening for flexure*

The CFRP grid used in this study is the same as grid 3 in Table 6. Six slabs were tested, one reference slab, one with additional steel reinforcement, one with a carbon fibre sheet and three with the MBC system. Three different designs regarding the CFRP grid in the MBC strengthening were utilized. In one of the strengthened specimens an ordinary design of the grid was used, see section 2.3. In another, sand was adhered to the surface of the grid to enhance the mechanical interlocking to the mortar. In the last specimen, two layers of grid were used to increase the total fibre amount. The experimental set-up for the slabs was four point beam bending, with a distance of 3860 mm between the supports and 1333 mm to the line loads from the supports. Strengthening schemes and experimental set-up are shown in Figure 13. All the slabs have the same dimensions (4000 x 1000 mm), though they have been strengthened by different methods. The slabs were flexural reinforced with 10  $\phi$  8 Ks 500 standard steel reinforcement. Table 6 shows the manufacturer provided material properties of the CFRP grid and carbon fibre sheet together the laboratory tested quality of the steel reinforcement.

Slab No 1 was a reference, steel reinforced concrete beam without any strengthening. Slab No 2 was strengthened with 4 extra steel reinforcement bars,  $\phi$  8. Slabs No 3, 4 and 6 were strengthened with the MBC system. The internal tow distance of the grid was 44 x 44 mm with a total cross sectional area corresponding to 21 mm<sup>2</sup>/m in the tensile bending direction. Note slab No 3 had a sanded surface on the grid and that slab No 6 had dual layers of CFRP grid. The total thickness of the cementitious layer and the CFRP grid was approximately 10 mm. Slab No 5 was strengthened with three carbon fibre sheets with a cross sectional area corresponding to 62 mm<sup>2</sup>/m of the slab in the bending tensile direction.



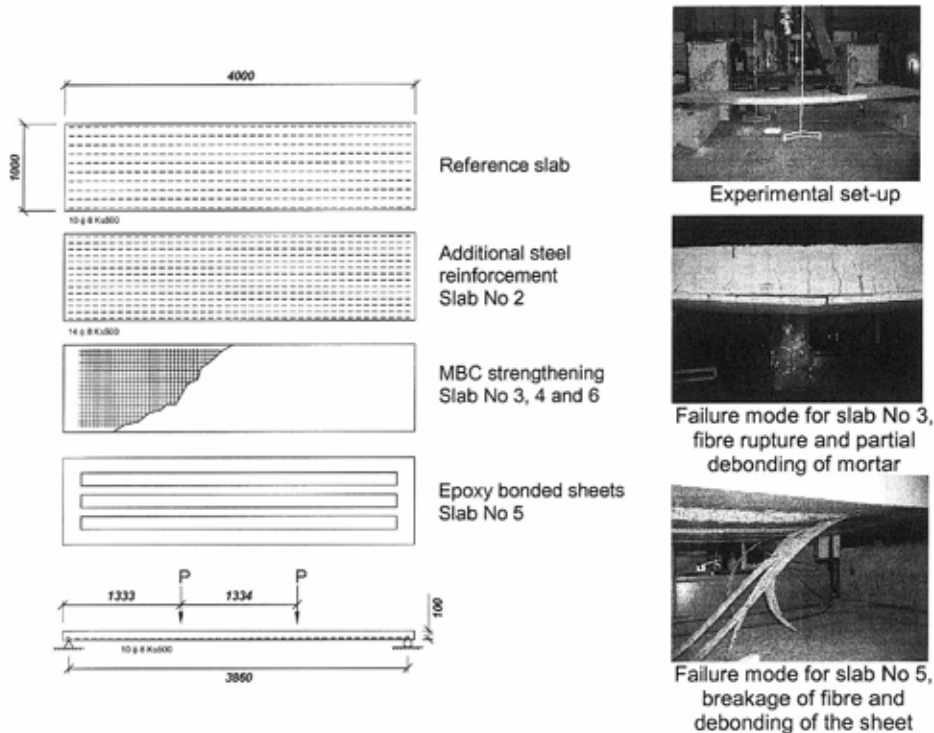


Figure 13. Experimental set-up of evaluated beam specimens.

Table 8. Material properties for steel and composites.

Material	Tensile strength (MPa)	Elastic modulus (GPa)
Steel $\phi$ 8	483	209
CFRP grid	3800	253
Carbon fibre sheet	3600	228

The slabs were loaded with two line loads up to failure and the loading was deformation controlled with a load rate of 0.03 mm/s. This rate was doubled when the steel in the slab reached yielding. A summary of the beam specimens is shown in Table 9, note that the slab with two layers of carbon fibre grid (No 6), sustained the highest load at failure. Slab No. 3 reached failure earlier than the other slabs due to fibre breakage, which was due to the bond between the sanded grid and the cementitious bonding agent probably being too high, resulting in high stress concentrations. As a consequence, a failure arose at a crack in the cementitious bonding material. In slab No. 4, debonding between the CFRP grid created a small slippage between the cementitious bonding materials. This provided for a higher load since the stress concentrations were smeared out over a short distance, i.e. discrete stress concentrations could be avoided. Slabs No. 2, 4 and 5 reached approximately the same failure load. The slab with extra steel reinforcement, No. 2, showed stiffer behaviour than slabs No. 3, 4 and 5. The right-hand side in Figure 13 shows a photo of failure modes for slabs No 3 and No 5. For both of these slabs, debonding occurred after fibre breakage. This was not the case for slabs No. 2, 4 and 6, where extensive cracking and large deflections preceded fibre breakage. This may also be noticed in Figure 13, where large deflections were obtained for all these slabs. In addition slab No 6

obtained the highest failure load and was also the stiffest slab of the ones tested. Also the cracking and steel yielding loads were considerably higher for slab No 6 compared to the other slabs. Here it should also be noted that slab No 6 had a lower fibre content at the cross sectional area in the tensile direction. For a more detailed analysis of this study the reader is referred to [34].

*Table 9. Summary of flexural strengthened beam specimens.*

Slab	Strengthening	Bonding agent	Peak force (kN)	Failure mode	Strengthening effect
1	----	----	25		-
2	Extra steel 4 no $\phi$ 8 <sup>2</sup>	----	38	Large deflection/yielding	1.52
3	MBC, sanded grid	Mortar	35	Fibre rupture	1.40
4	MBC, ordinary grid	Mortar	40	Large deflection/Fibre rupture	1.60
5	Epoxy bonded sheet	Epoxy	41	Fibre rupture/debonding	1.64
6	MBC, 2 layers of grid	MBC	51	Large deflection/Fibre rupture	2.04

## DISCUSSION AND CONCLUSION

It is not entirely reasonable to compare the different achieved strengthening effects between the different cement based strengthening systems. The reason for this originates in the experimental set-up design and size of the specimens. One major influencing parameter is the design of the steel reinforcement in the base concrete. But, it can clearly be stated that these strengthening systems all give a contribution to the load bearing capacity but with different strengthening effects. All evaluated tests on large scale specimens were deformation controlled and the deformation rate ensured similar redistribution of stresses and strains in the specimens. Nevertheless, a summary of flexural and shear strengthened specimens for all systems are shown in Table 10. The summarised specimens and strengthening system are all based on the best performing specimens with fibre rupture as failure mode. However, the failure mode was not stated for the flexural strengthened specimen using the TRC system. From Table 10 it can be concluded that for flexural strengthening all systems generated similar strengthening effects using approximately the same amount of carbon fibres in the tensile direction. However the FRC system was applied on small scale specimens with no steel reinforcement, for these specimens the size effect is not considered. Regarding the shear strengthening the TRM and MBC systems provided almost similar strengthening effects, for failure mode in shear, with the use of almost the same amount of carbon fibres. It should also be noted that the TRM system was wrapped around the beam and therefore prohibited to fail by debonding while the MBC system was side bonded. In retrofitting of existing structures fully wrapping is often not possible. For the TRC system in shear using glass fibres, an excessive amount of glass fibres is needed to generate a very small strengthening effect.

When using textile fabrics, there is a limitation on how many layers that can be used effectively. Using too many layers will create anchorage problems and generate debonding. This is especially apparent for shear strengthening with insufficient anchorage length in the compressed zone. However, using mechanical anchorage can delay and even avoid debonding. Using non impregnated sheets, grids or textiles will generate larger slips and inferior effective strain over the roving cross section. The reason for this is that total penetration of the cement based bonding agent in the fibre roving is difficult or even impossible to achieve. Using impregnated fibres (fibres imbedded in a matrix) will create a more effective strain distribution in the FRP tow. A better utilisation of the fibres will be achieved by stress transfer of the matrix and a mechanical interlocking in the mortar. Also the connection points between tows/rovings become more rigid which ensures less slippage and thus further enhance the mechanical interlocking. Another aspect of full utilisation of the fibres is the inclination of the fibres to the cracks. If the direction of fibre rovings or tows are applied perpendicular to the principal stress direction (crack inclination) a better utilisation should be achieved. This should have been the case for the shear strengthened TRC specimens. But in this case the choice of fabrics was the limiting parameter.

By wrapping the non impregnated fibres around the beam (as the case for shear strengthening using the TRM system) will create an infinite anchorage for the textiles and therefore a higher strengthening effect. This complete wrapping of the beam may become difficult to achieve in retrofitting an in-situ structural beam. By comparing the use of different fibre material then it is clear that the use of carbon fibre has the greatest structural advantage and the total amount of fibres to reach the same bearing capacity will be much lower. However, wrapping is not possible when using an epoxy impregnated carbon fibre grid due to the rigidity and brittleness of the matrix. Using textiles makes wrapping around corners much easier. Using a semi elastic matrix, e.g. latex, which still ensures rigid connection points but allows wrapping around corners could be a beneficial solution for ensuring rigidity, anchorage and effectiveness of the fibres.

The epoxy based systems have a slightly better performance compared to the cement based system, due to the superior bond between epoxy and the fibres. However, the MBC system for flexural strengthening needed a smaller carbon fibre area, in the tensile direction, to generate a higher bearing capacity compared to the epoxy bonded sheets. Increasing the bond between mortar and fibres by the use of sand, bonded to the surface of the CFRP grid, will cause high stress concentration and premature fibre rupture for flexural strengthening.

It should also be mentioned that none of the mortars used in the presented cement based systems for shear strengthening had any chopped or milled fibres, e.g. PVA, PP, glass, carbon etc. By using a mortar with chopped or milled reinforcing fibres should postpone large crack openings by the crack bridging ability of these fibres and thus create a more durable structure in service limit state. If the base concrete has a large chloride penetration depth then these cement based bonding agents should provide a more sustainable repair or upgrading system due to their permeability and the chloride peak would therefore equilibrate. For fully covered concrete surfaces the use of impermeable epoxy based systems may create durability problems for the steel reinforcement. Regarding the long term behaviour for the case of using the MBC strengthening, commercially available mortars with proven sustainability were employed. CFRPs have good long term behaviour if protected against UV radiation, which is the case when embedded into a cement matrix. Note, that it may be difficult to achieve fully resistant glass fibres in an alkaline environment. Another important aspect to be considered is the bond between cement based bonding agent and base concrete. Here, the preparation of the surface of the base concrete is crucial thus removing all poor concrete to ensure ultimate bonding

characteristics. Complicated or poor anchoring details could also be a source of shortened service life of the strengthening systems.

Cost and labour effective application techniques have to be established to be able to successfully implement the strengthening system for structural retrofit. One example of effective application techniques are shotcreting the system, which can be done for the MBC and TRC systems. No industrialised application techniques have been recorded for the TRM and FRC systems.

*Table 10. Summary of strengthening effects for evaluated systems.*

Strengthening system	Strengthening	Failure mode	Fibre type	Fibre amount	Strengthening effect
TRC	Flexural	-	Carbon	50 mm <sup>2</sup>	1.86
FRC	Flexural	Fibre rupture	Carbon	40 mm <sup>2</sup>	2.03
MBC	Flexural	Fibre rupture	Carbon	42 mm <sup>2</sup>	2.04
TRC	Shear	Fibre rupture	Glass	2820 g/m <sup>2</sup>	1.16
TRM	Shear	Fibre rupture	Carbon	168 g/m <sup>2</sup>	1.71
MBC	Shear	Fibre rupture	Carbon	154 g/m <sup>2</sup>	1.99

## REFERENCES

- Rizkalla, S. Hassan, N & Hassan, T. "Design recommendations for the use of FRP for reinforcement and strengthening of concrete structures". *Progress in Structural Engineering and Materials*, Vol. 5, No. 1, February 2003, pp. 16–28.
- Nordin, H., & Täljsten, B. "Concrete beams strengthened with prestressed near surface mounted CFRP". *Composites for Construction*, Vol. 10, No. 1, January 2006, pp. 60-68.
- Holmgren, J., & Badanoui, A. "Cementitious composites reinforced with continuous carbon fibres for strengthening of concrete structures". *Cement and Concrete Composites*, Vol. 25, No. 3, April 2003, pp. 387-394.
- Li, Z., & Ding, Z. "Property improvement of Portland cement by incorporating with metakaolin and slag". *Cement and Concrete Research*, Vol. 33, No. 4, 2003, pp. 579-584.
- Hewlett, P.C. "Cement Admixtures, Uses and Applications". Longman Scientific and Technical (2<sup>nd</sup> ed), 1988, pp 85-101.
- Ohama, Y. "Polymer-based admixtures". *Cement and Concrete Composites*, Vol. 20, No. 2, April 1998, pp. 189-212.
- Van Gemert, D., Czarnecki, L., Maultzsch, M., Schorn, H., Beeldens, A., Lukowski, P., & Knapen, E. "Cement concrete and concrete-polymer composites: Two merging worlds: A report from 11<sup>th</sup> ICPIC Congress in Berlin, 2004". *Cement and Concrete Composites*, Vol. 27, No. 9-10, October 2005, pp. 926-935.
- Pascal, S., Alliche, A., & Pilvin, Ph. "Mechanical behaviour of polymer modified mortars". *Materials Science and Engineering A*. Vol. 380, No. 1-2, August 2004, pp. 1-8.
- Groth, P. "Fibre Reinforced Concrete". Doctoral thesis, Luleå University of Technology, division of structural engineering. 2000.
- Cuyper, H., Wastiels, J., Van Itterbeeck, P., De Bolster, Orlowsky, E. J., & Raupach, M. "Durability of glass fibre reinforced composites experimental methods and results". *Composites Part A: Applied Science and Manufacturing*, Vol. 37, 2006, pp. 207-215.
- Agopyan, V., Savastano, H., V.M., & Cincotto, M.A. "Developments on vegetable fibre-cement based materials in São Paulo, Brazil: an overview". *Cement and Concrete*

- Composites*, Vol 27, 2005, pp. 527-536.
12. Li, V.C., & Fisher, G. "Reinforced ECC – An evolution in from materials to structures". *In the first FIB Congress*, Osaka, Japan, October 2002, pp. 105-122.
  13. Garcés, P., Fraile, J., Vilaplana-Ortego, E., Cazorla-Amorós, D., Alcocel, E. G., & Andión, L. G. "Effect of carbon fibres on the mechanical properties and corrosion levels of reinforced odellin cement mortars". *Cement and Concrete Research*, Vol. 35, 2005, pp. 324-331.
  14. Gutiérrez, R.M., Díaz, L.N., & Delvasto, S. "Effect of pozzolans on the performance of fibre –reinforced mortars". *Cement and Concrete Composites*, Vol. 27, 2005, pp. 593-598.
  15. García Santos, A., Rincón, J. M., Romero, M., & Talero, R. "Characterization of a polypropylene fibered cement composite using ESEM, FESEM and mechanical testing". *Construction and Building Materials*, Vol. 19, 2005, pp. 396-403.
  16. Paipetis, A., & Galiotis, C. "Effect of fibre sizing on the stress transfer efficiency in carbon/epoxy model composites". *Composites Part A: Applied Science and Manufacturing*, 27, 1996, pp. 255-267.
  17. Mobasher, B., Pahilajani, J., & Peled, A. "Analytical simulation of tensile response of fabric reinforced cement based composites". *Cement and Concrete Composites*, Vol. 28, 2006, pp. 77-89.
  18. Peled, A. "Textile cement based composites, effects of fabric geometry, fabric type and processing". *Composites in Construction 2005 – Third International Conference*, Lyon, France, July 2005.
  19. Brueckner, A., Ortlepp, R., & Curbach, M. "Anchoring of shear strengthening for T-beams made of textile reinforced concrete (TRC)". *Materials and Structures*, Vol 41, No 2, March 2008, pp. 407-418.
  20. Brueckner, A., Ortlepp, R., & Curbach, M. "Textile reinforced concrete for strengthening in bending and shear". *Materials and Structures*, Vol 39, No 8, October 2006, pp. 741-748.
  21. Weiland, S., Ortlepp, R., & Curbach, M. (2006) "Strengthening of predeformed slabs with textile reinforced concrete". *Proceedings of the second International fib-Congress CEB-FIP*, Naples, June 2006.
  22. Holler, S., Butenweg, C., Noh, S. Y., & Meskouris, K. "Computational model of textile-reinforced concrete structures". *Computers & Structures*, Vol. 82, 2004, pp. 1971-1979.
  23. Chudoba, R., Vořechovský, M., & Konrad, M. "Stochastic modelling of multi-filament yarns. I. Random properties within the cross-section and size effect". *Solids and Structures*, Vol. 43, 2006, pp. 413-434.
  24. Häussler-Combe, U., & Hartig, J. "Bond and failure mechanisms of textile reinforced concrete (TRC) under uniaxial tensile loading". *Cement & Concrete Composites*, Vol 29, No 4, April 2007, pp. 279-289.
  25. Wu, H.C., & Teng, J. "Innovative Cement Based Thin Sheet Composites for Retrofit". *Third International Conference on Composites in Infrastructures*, San Francisco, US, June 2002.
  26. Wu, H.C. "Design Flexibility of Composites for Construction". *In International Conference on Fiber Composites, High Performance Concretes and Smart Materials*. Parameswaran, India, 2004, pp. 421-432.
  27. Wu, H.C., & Sun, P. (2005) "Fiber Reinforced Cement Based Composite Sheets for Structural Retrofit". *International Symposium on Bond Behavior of FRP in Structures*, Hong Kong, December 2005, pp. 351-356.
  28. Li, V.C. "On engineered cementitious composites". *Advanced Concrete Technology*, Vol 1, No 3, August 2003, pp. 215-230,

29. Triantafillou, T.C., & Papanicolaou, C.G. "Shear strengthening of reinforced concrete members with textile reinforced mortar (TRM) jackets". *Materials and Structures*, Vol 39, No 1, April 2006, pp. 93-103.
30. Carlsvärd, J. "Shrinkage cracking of steel fibre reinforced self compacting concrete overlays – Test methods and theoretical modelling". Doctoral thesis, Luleå University of Technology, Division of Structural Engineering, 2006.
31. Carolin, A. (2003) "Carbon Fibre Reinforced Polymers for Strengthening of Structural Elements". Doctoral thesis, Luleå University of Technology, 2003
32. Blanksvärd, T. "Strengthening of concrete structures by the use of mineral based composites". Licentiate thesis, Dept. of Structural Engineering, Luleå University of Technology, Luleå, 2007, 300 pp.
33. Blanksvärd T., Carolin A. and Täljsten B., (2008), "*Shear crack propagation in MBC strengthened concrete beams*". Proceeding of the fourth International Conference on FRP Composites in Civil Engineering, Zurich, Switzerland, 22-24 July 2008, CD-Publication and extended abstracts.
34. Täljsten, B., & Blanksvärd, T. "Mineral based bonding of carbon FRP to strengthen concrete structures". *Composites for Construction*, Vol 11, No 2, March 2007, pp. 120-128.



## Modelling of Concrete in Tension – Energy Dissipation in Cyclic Loops



Rasmus Rempling <sup>1</sup>  
Ph.D. student  
rasmus.rempling@chalmers.se

Karin Lundgren <sup>1</sup>  
Ass. Professor

Kent Gylltoft <sup>1</sup>  
Professor

<sup>1</sup> Department of Civil and Environmental Engineering  
Structural Engineering, Concrete Structures  
Chalmers University of Technology  
Gothenburg, Sweden



### ABSTRACT

This paper deals with modelling of concrete subjected to cyclic loading in tension. A model based on the theory of plasticity combined with the theory of damage mechanics was developed. To describe the non-linearity that concrete exhibits during cyclic loading, the concept of bounding surface is used as a hardening function. An evolution law for the elastic domain is proposed that depends on the consumption of fracture energy in hysteresis loops. In addition, an energy balance equation is proposed, which deals with the consumption of fracture energy by completing hysteresis loops. Finally, a drawback in the smeared crack approach for combined damage and plasticity is identified and presented.

**Keywords:** plasticity theory; damage mechanics; bounding surface; concrete; fracture; cyclic loading; fatigue

## 1 INTRODUCTION

Cyclic loading is one of the deterioration processes of great importance for concrete structures such as piles, sleepers, machinery foundations, parts of bridges, etc. The deterioration of concrete structures entails heavy costs for the society. These costs can be cut down by an increased understanding of the cyclic-loading phenomenon and by the development of constitutive models with an increased accuracy.

Due to the non-linear stress-strain response that concrete exhibits, cyclic loading can be divided



into two main characteristic responses: pre-peak cyclic loading and post-peak cyclic loading. Pre-peak cyclic loading is cyclic loading before maximum load is reached, while post-peak cyclic loading is cyclic loading after maximum load and localization of deformation. These phenomena are equally important as parts of cyclic loaded structures may be in pre-peak state, while other parts are in post-peak state.

The work presented here deals with concrete subjected to cyclic loading in biaxial tension with focus on improving the analysis methods for such cases and increasing the understanding of the deterioration processes related to repeated loading.

Plasticity, damage mechanics, and the combination of both, are often used to describe the non-linear response of concrete, e.g. models [1]-[3]. Moreover, the concept of bounding surface, introduced by [4], has been proved to be useful to describe the hysteresis loops that concrete exhibits when subjected to cyclic loading: [5]-[10]. Research that identifies the characteristic hysteresis loops has been conducted by [11]-[30]. The combination of plasticity and damage mechanics used in this investigation was previously investigated by e.g. [31]-[33] and [34], and shows good results for complex crack patterns.

The model presented here is based on the theory of plasticity combined with the theory of damage mechanics, using the concept of bounding surface to describe the non-linearity seen when hysteresis loops from experiments are examined. The basic equations for the plasticity-damage model are presented together with the hardening rule that is based on the bounding surface concept. An evolution law for the elastic domain is proposed that describes the increasing non-linearity with increasing damage. Moreover, an energy balance equation is stated and motivated, which considers the dissipated fracture energy while completing a loading cycle in biaxial tension (Figure 1).

The crack band approach of [35] is used to control the mesh dependence of the softening branch of the stress-strain curve. The crack band approach makes it possible to consider the crack strain as the average over a characteristic crack band width  $w_c$  of the fracture process zone.

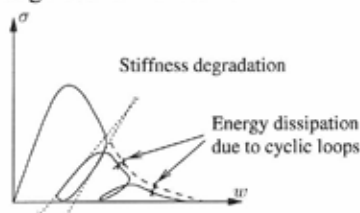


Figure 1: Illustration of the observed mechanisms related to fatigue.

## 2 THE CONCEPT OF BOUNDING SURFACE

Plasticity models with two yield surfaces were introduced by [36] to describe the non-linear hardening behaviour for ductile solids with continuum models. Two surface models have later been renamed as bounding surface models due to the enclosing nature of the bounding surface with regard to the yield surface. The concept of bounding surface models is to describe the non-linear hardening and softening behaviour by prescribing the variation of the plastic modulus  $K_p$ , i.e. another way of describing strain hardening. The plastic modulus is determined by the

distance between the position of the actual plastic loading point and the mirror point on the bounding surface  $\hat{\sigma}$ . A general definition of  $\hat{\sigma}$  is

$$\hat{\sigma} = \sqrt{(\bar{\sigma} - \hat{\sigma})^2} \quad (1)$$

where  $\hat{\sigma}$  contains the coordinates of the mirror point on the bounding surface and  $\bar{\sigma}$  is the actual plastic stress point; in this study the actual plastic stress is the effective stress, i.e. the stress in the undamaged stress space.  $\hat{\sigma}$  is determined along the normal to the yield surface (Figure 2).

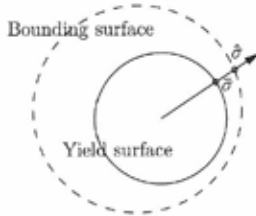


Figure 2: Illustration of the enclosing nature of the bounding surface with regard to the yield surface and the actual stress  $\bar{\sigma}$ , with the corresponding mirror stress  $\hat{\sigma}$ .

The computation of  $\hat{\sigma}$ , is done with a function,  $M$ , called the mapping rule:

$$\hat{\sigma} = M(\bar{\sigma}). \quad (2)$$

The bounding surface is constructed in the same way as a yield surface; thus the bounding surface and the flow rule are generally described, respectively as

$$F = 0, \quad \dot{L} = \dot{\lambda} \frac{\partial F}{\partial \sigma} \quad (3)$$

where  $\dot{\lambda}$  is the rate of the plastic multiplier. The identity condition,  $\bar{\sigma}$  on  $F = 0$  so that  $\bar{\sigma} = \hat{\sigma}$  and  $\frac{\partial F}{\partial \bar{\sigma}} = \frac{\partial F}{\partial \hat{\sigma}}$ , introduces restrictions on the relative evolution of the surfaces due to the fact that they can never intersect with each other.

Bounding surface models make it possible for the plastic response to evolve depending on the distance from the actual stress state  $\bar{\sigma}$  to the bounding surface itself. An evolution law  $K_{pf}$  for the plastic modulus  $K_p$  can be stated as

$$K_p = K_{pf}(\hat{\sigma}). \quad (4)$$

Equation (4) expresses the main feature of the bounding surface, i.e. the plastic deformation is calculated by  $K_p$ , with a magnitude based on  $\hat{\sigma}$ .

### 3 THE PLASTICITY-DAMAGE MODEL

Experimental observation of concrete subjected to cyclic loading reveals a non-linear stress-strain response with increasing plastic deformation during loading, as well as a degradation of the material due to damage. Therefore, it is convenient when developing a constitutive model to

use the theory of plasticity to describe the plastic deformation and at the same time describe the evolution of damage with damage mechanics.

The model presented here is a combination of plasticity and damage with a kinematic hardening rule based on the theory of bounding surface. The damage is determined by the accumulated plastic strain and a fracture energy consumption law. To deal with localization the deformation in the softening regime, the crack width  $w_c$ , is smeared over the element length. The stress-strain relationship is given as

$$\sigma = (1 - \omega)\bar{\sigma} = (1 - \omega)E_p(\varepsilon - \varepsilon_p + \varepsilon_{p,0}). \quad (5)$$

#### Plasticity model

The plasticity model is based on the effective stress and consists of: a yield function based on the Rankine criterion, a flow rule, a hardening rule, an evolution law for the elastic domain and the loading-unloading conditions.

The elastic domain is a crucial issue for concrete subjected to cyclic loading. In experimental observations it is observed that during cyclic loading a non-linear state is exhibited during loading as well as unloading. In between these non-linear states the response is elastic with a stiffness that corresponds to the level of damage. This can be understood as the elastic domain moves with the non-linear response without changing shape. This rigid body movement is described by the hardening function of the model presented below. At the same time, energy is released by the completion of a hysteresis loop, which can be observed in experiments as an increase of the non-linear response. This increase of non-linearity is done at the cost of the elastic domain, i.e. the elastic domain decreases in size during cyclic loading. This is considered in the model by the evolution law for the elastic domain that is based on the energy balance equation stated below.

#### Loading

For loading in plane stress the yield function becomes

$$f(\bar{\sigma}_1, \delta) = \bar{\sigma}_1 - \sigma_{y,1}^{N,n}(\delta) \quad (6)$$

where  $\bar{\sigma}_1$  is the maximum principal value of the effective stress tensor  $\bar{\sigma}$ ,  $\sigma_{y,1}^{N,n} = \sigma_{y,1}^{N,(n-1)} + H(\delta)$  is the yield stress, updated from the previous step ( $n - 1$ ) and  $H(\delta)$  is the hardening rule.

When the stress state violates the yield condition  $f = 0$ , plastic flow is initiated. The flow rule is associated and given as

$$\varepsilon_p = \dot{\lambda} \frac{\partial f}{\partial \bar{\sigma}} \quad (7)$$

where  $\dot{\lambda}$  is the rate of the plastic multiplier.

The evolution of the yield surface during plastic flow, Figure 3, is controlled by the hardening rule. The hardening rule  $H(\delta)$  is linearly dependent on the maximum principal effective stress ( $\delta = \bar{\sigma}_1 - \bar{\sigma}_1$ ) and to achieve a practical hardening rule,  $\delta$  is normalized with  $\bar{\sigma}_1 - \sigma_{y,1}^{N,n} \cdot \sigma_{y,1}^{N,n}$  is the yield stress at the initiation of plastic flow for the actual cycle  $N$ , which initially is set at input with the parameter  $\sigma_{y,n}$ . Then, the hardening rule yields

$$H(\delta) = E \frac{\bar{\sigma}_2 - \bar{\sigma}_2}{\bar{\sigma}_2 - \sigma_{y,2}^{N,n}} \quad (8)$$

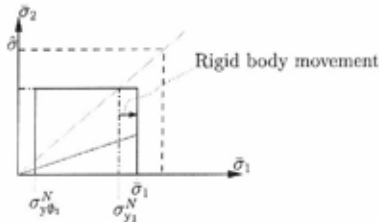


Figure 3: Evolution of the yield surface due to plastic loading.

where  $\bar{\sigma}_1$  is the mirror stress of the actual stress.

For loading the elastic domain is constant, though it translates in stress space during plastic flow. Therefore, the lower yield surface  $\sigma_{y,\delta,1}^{N,n}$  must be updated for  $\delta \geq 0$  (Figure 4). The updating is done according to

$$\sigma_{y,\delta,1}^{N,n} = \sigma_{y,\delta,1}^{N,(n-1)} + H(\delta). \quad (9)$$

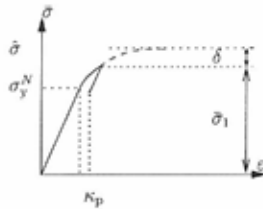


Figure 4: The hardening is kinematic which represents a rigid body movement of the elastic domain.

#### Unloading

For unloading the equations differ slightly.

The yield function is stated as

$$f_D(\bar{\sigma}_1, \delta_D) = -\bar{\sigma}_1 + \sigma_{y,\delta,1}^{N,n}(\delta_D) \quad (10)$$

where  $\bar{\sigma}_1$  is the maximum principal value of the effective stress  $\bar{\sigma}$  and

$$\sigma_{y,\delta,1}^{N,n} = \sigma_{y,\delta,1}^{N,(n-1)} - H_D(\delta_D) \quad (11)$$

is the yield stress, updated from the previous step ( $n-1$ ), for the lower bound and  $H_D(\delta_D)$  is the unloading hardening rule.

The flow rule is

$$\varepsilon_{p,D} = \dot{\lambda}_D \frac{\partial f_D}{\partial \bar{\sigma}} \quad (12)$$

where  $\dot{\lambda}_D$  is the rate of the plastic multiplier for unloading.

The evolution law for the unloading plastic multiplier is calculated as

$$\dot{\kappa}_{p,D} = \|\boldsymbol{\varepsilon}_{p,D}\| = \dot{\lambda}_D \quad (13)$$

The hardening rule together with the normalization of  $\hat{\sigma}_D$  ( $\hat{\sigma}_D = \bar{\sigma}_1 - \hat{\sigma}_{D,1}$ ) give the unloading hardening rule

$$H_D(\hat{\sigma}_D) = E \frac{\bar{\sigma}_1 - \hat{\sigma}_{D,1}}{\sigma_{y,D,1}^{N,n} - \hat{\sigma}_{D,1}} \quad (14)$$

where  $\hat{\sigma}_{D,1}$  is the unloading mirror stress, considered as a material parameter.

According to the rigid body movement of the elastic domain the upper yield surface is updated during plastic flow. This is considered by the consistent equation for the elastic domain at unloading and is defined according to

$$\sigma_{y,1}^{N,n} = \sigma_{y,1}^{N,(n-1)} - H_D(\hat{\sigma}_D) \quad (15)$$

#### *Loading-unloading conditions*

The loading-unloading conditions conclude the plasticity part. The yield function must remain negative in the elastic regime at the same time as the rate of the plastic multiplier initially must be zero, or remain constant at reloading. In the plastic regime the yield function must be zero and the rate of the plastic multiplier must be positive. The conditions are stated as follows:

• Loading:

$$f \leq 0 \quad \dot{\lambda} \geq 0 \quad \dot{\lambda} f = 0 \quad (16)$$

• Unloading:

$$f_D \leq 0 \quad \dot{\lambda}_D \geq 0 \quad \dot{\lambda}_D f_D = 0 \quad (17)$$

These last conditions in Equations (16) and (17) are the conditions that separate the elastic regime from the plastic regime. The conditions state that when  $f = 0$  then  $\dot{\lambda} \geq 0$ , and if  $f \leq 0$  then  $\dot{\lambda} = 0$  (for loading and unloading).

#### *Damage model*

The damage model consists of a fracture surface determined by the damage function and an isotropic damage variable  $\omega(\kappa_D)$ . The damage variable is determined so that the resulting stress-strain relation for monotonic loading will be an exponential function for loading in the softening region. Damage evolves with two different cases:

1. When the maximum principal value of the effective stress reaches the bounding surface: this is checked by the damage function.

$$f_D = \bar{\sigma}_1 - \hat{\sigma}_1 \quad (18)$$

2. When the damage history variable increases the damage history variable is computed by the current plastic strain  $\varepsilon_{p,1}$  and the plastic strain at initiation of damage  $\varepsilon_{0,p}$ .

$$\kappa_D = \max(\varepsilon_{p,1} - \varepsilon_{0,p}). \quad (19)$$

If damage is present the isotropic damage parameter is calculated according to

$$\omega(\kappa_D) = \frac{1 - \frac{\varepsilon_0}{\varepsilon_f}}{1 - \frac{\kappa_D}{\varepsilon_f}} \quad (20)$$

where  $\varepsilon_0 = f_u/E$  is the strain that corresponds to the initiation of damage,  $\varepsilon_f$  is the final strain and  $f_u$  is the ultimate strength given at input.

Because the yield surface initially is separated from the bounding surface, strain hardening of the effective stress  $\bar{\sigma}$  is present after yielding has been initiated; but only to some extent as the effective stress converges rapidly with the bounding surface. In addition, the amount of strain hardening is small compared to the total crack strain.

### Energy dissipation

In cyclic loading the loading pattern produces hysteresis loops which make energy dissipate. There are three main mechanisms that dissipate energy: temperature, the cohesive zone, and shear friction. In the biaxial tension region, crack sliding is a minor issue. Thus, the energy dissipation in the cohesive zone and the temperature increase are in main focus. Based on the discussions about energy dissipation at cyclic loading found in [37], [24], [38], and [14], there should be an energy dissipation when a load cycle is completed, considering the total energy that should be released as constant regardless of the loading history. From this statement it is possible to set up a balance equation: between the energy inside a loop  $E_1$  and the dissipated fracture energy  $E_2$  so that the fracture energy  $G_f$  remains constant (Figure 1). If plasticity is initiated while unloading, energy is released; this dissipation of energy appears for pre-peak- as well as post-peak unloading. In the model the energy release for post-peak hysteresis loops is accounted for by reducing the softening branch, related to the energy dissipated by the cyclic loop  $E_1$ . The energy released by the cyclic loop can be estimated in a simplified way by computing the area that is bound by the current loading yield stress and the actual effective stress during unloading-plastic flow

$$E_1 = (\sigma_{y,1}^N - \bar{\sigma}_1) \kappa_{p,0}. \quad (21)$$

In Equation (21) and the following equations equilibrium is assumed and therefore  $n$  is omitted.

The fracture energy is depending on the current yield surface as the fracture energy is known as the area under the softening curve. Therefore, the decrease in fracture energy can be calculated as an evolution of the elastic domain, i.e. the yield surfaces are adjusted with  $E_1$  and a factor  $B$ . The material parameter  $B$  reflects the fact that the two areas are not equal due to temperature release, i.e.  $E_2 = B E_1$  ( $0 \leq B \leq 1$ ). The reason for dealing with this in the effective stress space is related to the hypothesis that the energy release due to hysteresis loops is related to plastic flow. Even though this is done in the effective-stress space, a corresponding response in the nominal-stress space is achieved.

$$\sigma_{y,1}^{N+1} = \sigma_{y,1}^N - B \frac{E_s}{G_f} \sigma_{y,1}^N \quad (22)$$

$$\sigma_{y,0.1}^{N+1} = \sigma_{y,0.1}^N + B \frac{E_2}{G_f} \sigma_{y,1}^N \quad (23)$$

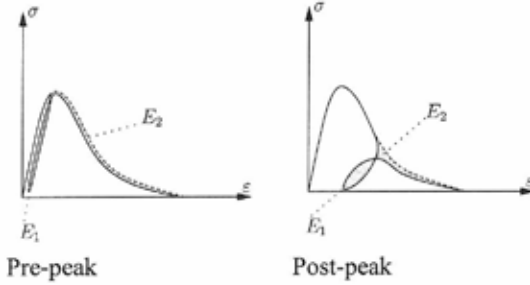


Figure 1: Illustration of the energy balance between a produced hysteresis loop and the released energy.

To consider energy release for pre-peak cyclic loading the bounding surface is decreased during unloading plastic flow:

$$\hat{\sigma}^{N+1} = \hat{\sigma}^N - A \frac{E_2}{G_f} \sigma_{y,1}^N \quad (24)$$

where  $\hat{\sigma}^N$  is the mirror stress related to the previous cycle ( $\hat{\sigma}^N$  is initially set to  $f_u$ ). The bounding surface is updated for every loading cycle  $N$ . The material parameter  $A$  is similar to  $B$ , besides that it controls the energy balance of pre-peak cyclic loading.

#### 4 ANALYSIS OF DIRECT TENSION TEST

A finite element simulation of a tension test is described in the present section. The example is a tension test of a double-edge-notched plate, conducted by [12], shown in Figure 5. The specimen is discretized by a fine mesh of triangular three-node elements, Figure 6, assuming plane stress. For simplicity, the specimen is modelled as a quarter of the real specimen, fixing the boundaries of symmetry in the normal direction. The deformation of the specimen is applied along the edge at the right hand side in Figure 6. Until the first unloading, the deformation is applied by controlling the deformation over the notch. Thereafter, deformation is controlled at the same point where it is applied. The crack band approach is used to obtain a mesh independent description of the dissipated energy. For the element row at the notch, the smearing distance is chosen as the width of the notch, 3mm, and for the rest of the elements as the size of the elements. The given material parameters, from the experiment, are presented in Table 1 and the chosen material parameters for the model are presented in Table 2.

Table 1: Material parameters given from experiment by [12].

$E$	30 GPa	$\nu$	0.18
$G_f$	58 Nm/m <sup>2</sup>	$f_u$	3.7 MPa

Table 2: Material parameters chosen for the model.

$\sigma_{y,ip}$	3.7 MPa
$A$	0.05
$B$	0.05

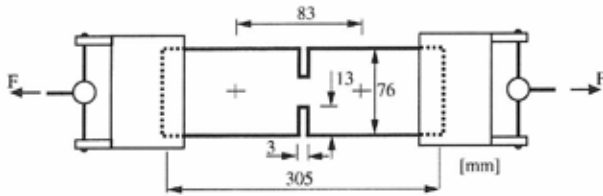


Figure 5: Experimental setup for the direct tension test. The thickness of the specimen is 19mm.

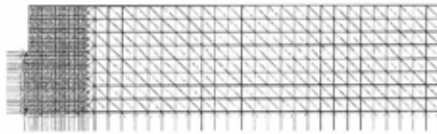


Figure 6: Finite element mesh and boundary conditions of the specimen.

#### Discussion of the results

The result from the analysis is compared to test results by [12] in Figure 7. The simulation shows a loading pattern of three cycles in the post-peak regime. The general response of the experiment is well described by the numerical simulation. The important hysteresis loops are well represented, as is the reduction of the softening branch. However, the simulated hysteresis loops show a slightly increasing deviation in unloading-reloading stiffness with increasing damage, which can be explained as a limitation of the chosen localization model, explained in the following.



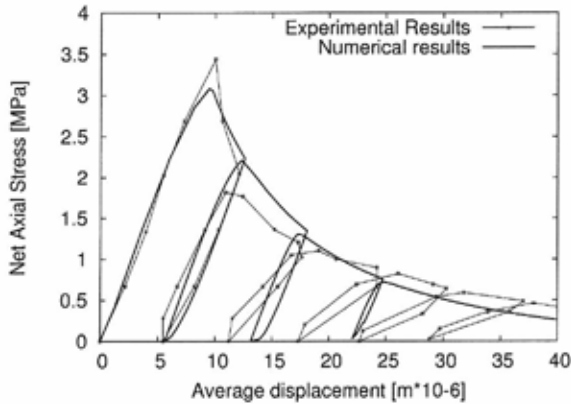


Figure 7: Simulated result of the direct tension test by [10]. The net axial stress, i.e. the load over the net area in the notch plane, is plotted over an average displacement over the notch by a length of 83 mm.

By looking at the unloading stiffness of a bar of length  $L$  the limitation can be identified (see Figure 8). The decrease of the deformation is defined as

$$\Delta u = (L - L_e)\Delta\varepsilon_{\text{unloc}} + L_e\Delta\varepsilon_{\text{loc}} \quad (25)$$

where  $\Delta\varepsilon_{\text{unloc}}$  is the strain decrement in the zones without strain localization and  $\Delta\varepsilon_{\text{loc}}$  is the strain decrement in the zone with localized deformation. The localization zone is for the chosen localization model chosen as the element length  $L_e$ .

The corresponding stress decrements can be expressed as

$$\Delta\sigma_{\text{unloc}} = E\Delta\varepsilon_{\text{unloc}} \quad (26)$$

$$\Delta\sigma_{\text{loc}} = E(1 - \omega)\Delta\varepsilon_{\text{loc}} \quad (27)$$

where  $\Delta\sigma_{\text{unloc}}$  is the stress decrement in the zone without localization and  $\Delta\sigma_{\text{loc}}$  is the stress decrement in the zone with localization (Figure 8).

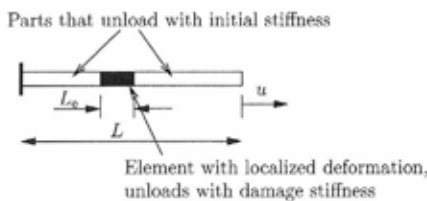


Figure 8: Definition of the stresses outside and inside the element with localized deformation.

As equilibrium applies, these stresses shall be equal. Thus, the decrease of deformation, Equation (25), can be expressed as

$$\begin{aligned}\Delta u &= (L - L_e) \frac{\Delta \sigma}{E} + L_e \frac{\Delta \sigma}{E(1-\omega)} \\ &= \frac{\Delta \sigma L(1-\omega) + \omega L_e}{1-\omega}\end{aligned}\quad (28)$$

The unloading stiffness is identified as

$$K_u = \frac{\Delta \sigma}{\Delta u} = \frac{(1-\omega)E}{(1-\omega)L + \omega L_e}\quad (29)$$

Therefore, the unloading stiffness depends on the element length. Furthermore, from Equation (29) it can be seen that if  $L_e$  approaches zero, the unloading stiffness approaches the initial stiffness

$$K_u = \frac{E}{L}\quad (30)$$

which concludes the problem.

## 5 CONCLUSIONS

A model for concrete subjected to cyclic loading in tension was presented. The model combines plasticity theory and damage mechanics and uses the concept of bounding surface to describe the hardening, making it possible to produce hysteresis loops representing loading and unloading. The model was tested with a direct tension test conducted by [12] and shows possibilities of simulating a series of unloadings and reloadings. The numerical result represents the experiment well; the important hysteresis loops are reproduced as well as the decrease in the softening branch, although the numerical result shows larger unloading-reloading stiffness than experimental results. A drawback in the used localization model is identified: the unloading stiffness is depending on the length of the element in which the deformations localize.

## ACKNOWLEDGEMENT

This work was supported by the Swedish Research Council for Environment, Agricultural Science and Spatial Planning. The simulations were made with the object-oriented finite element package OOFEM ([39], [40]) extended by the present authors.

## NOTATIONS

$\delta$	Euclidean distance
$\bar{\sigma}$	Stress on boundary surface
$\sigma$	Nominal stress
$\sigma_1$	Subscript: Maximum value of the principal directions
$\sigma_y$	Yield stress
$\sigma_0$	Subscript: unloading variables
$\sigma_{yini}$	Initial yield stress
$\Delta \sigma$	Stress increment

$\bar{\sigma}$	Effective stress
$M$	Mapping function
$F$	Bounding surface function
$\hat{L}$	Flow rule, bounding surface
$\hat{\lambda}$	Plastic multiplier, bounding surface
$K_p$	Plastic modulus
$K_{pf}$	Plastic modulus function
$\omega$	Damage parameter
$E_e$	Elastic stiffness tensor
$E$	Youngs modulus
$E_1$	Energy inside a hysteresis loop
$E_2$	Consumed energy by a hysteresis loop
$\varepsilon$	Strain
$\varepsilon_{0,p}$	Plastic strain at the initiation of damage
$\varepsilon_0$	Strain at initiation of damage
$\varepsilon_f$	Final strain at a fully opened crack
$\varepsilon_p$	Plastic strain
$\varepsilon_{p0}$	Plastic strain lower bound
$\Delta\varepsilon$	Strain increment
${}^{\text{unloc}}$	Subscript: Zone without localization of deformation
${}^{\text{loc}}$	Subscript: Zone with localization of deformation
$f$	Yield function
$f_D$	Damage function
$f_u$	Ultimate tensile stress
$H$	Hardening function
${}^N$	Superscript: Number of cycles
${}^n$	Superscript: Number of iterations
$\kappa_p$	Plastic hardening parameter
$\kappa_D$	Damage history variable
$G_f$	Fracture energy
$A$	Material parameter
$B$	Material parameter
$L$	Length of a bar
$L_e$	Element length
$\Delta u$	Decrease of deformation
$K_u$	Decrease of deformation
$\nu$	Poisson ratio
$w$	Deformation
$\dot{\phantom{x}}$	Superscript: Denoting the rate form of a variable
$\lambda$	Plastic multiplier

## REFERENCES

1. Papa, E., & Taliercio, A., "Anisotropic damage model for the multiaxial static and fatigue behaviour of plain concrete", *Engineering Fracture Mechanics*, Vol. 55, 1996, pp. 163–179.
2. Ragueneau, F., Norderie, C.L., & Mazars, J., "Damage model for concrete-like materials coupling cracking and friction, contribution towards structural damping: first uniaxial applications", *Mechanics of Cohesive-Frictional Materials*, Vol. 5, 2000, pp. 607–625.
3. Desmorat, R., Ragueneau, F., & Pham, H., "Continuum damage mechanics for hysteresis and fatigue of quasi-brittle materials and structures", *International Journal for Analytical and Numerical Methods in Geomechanics*, Vol. 31, 2007, pp. 307–329.
4. Dafalias, Y., "Bounding surface plasticity. i: Mathematical foundation and hypoplasticity", *Journal of Engineering Mechanics*, Vol. 112, No. 9, 1986, pp. 966–987.
5. Voyiadjis, G. Z., & Abulebdeh, T. M., "Damage model for concrete using bounding surface concept", *Journal of Engineering Mechanics-ASCE*, Vol. 119, No. 9, 1993, pp. 1865–1885.
6. Voyiadjis, G.Z., & Abulebdeh, T.M., "Plasticity model for concrete using the bounding surface concept", *International Journal of Plasticity*, Vol. 10, No. 1, 1994, pp. 1–21.
7. Yang, B.-L., Dafalias, Y. F., & Herrmann, L. R., "Bounding surface plasticity model for concrete", *Journal of Engineering Mechanics*, Vol. 111, No. 3, 1985, p. 359.
8. Winnicki, A., & Cichon, C., "Plastic model for concrete in plane stress state. i: Theory", *Journal of Engineering Mechanics*, Vol. 124, 1998, pp. 591–602.
9. Pandolfi, A., & Taliercio, A., "Bounding surface models applied to fatigue of plain concrete", *Journal of engineering Mechanics*, Vol. 124, 1998, pp. 556–564.
10. Abulebdeh, T. M., & Voyiadjis, G. Z., "Plasticity-damage model for concrete under cyclic multiaxial loading", *Journal of Engineering Mechanics-ASCE*, Vol. 119, 1993, pp. 1465–1484.
11. Reinhardt, H. W., Cornelissen, H. A. W., & Hordijk, D. A., "Tensile tests and failure analysis of concrete", *Journal of Structural Engineering*, Vol. 112, No. 11, 1986, pp. 2462–2477.
12. Gopalratnam, V., & Shah, S., "Softening response of plain concrete in indirect tension", *Journal of the American Concrete Institute*, Vol. 82, No. 3, 1985, pp. 310–323.
13. Plizzari, G., Cangiano, S., & Allieruzzo, S., "The fatigue behaviour of cracked concrete", *Fatigue and Fracture of Engineering Materials and Structures*, Vol. 20, No. 8, 1997, pp. 1195–1206.
14. Gylltoft, K., Fracture mechanics models for fatigue in concrete structures, Doctoral thesis, Luleå University of Technology, Luleå, Sweden, No. 1983:25D, 1983.
15. Karsan, I. D., & Jirsa, J. O., "Behaviour of concrete under compressive loadings", *Journal of Structural Division-ASCE*, Vol. 95, 1969, pp. 2543–2563.
16. Sinha, B. P., Gerstle, K. H., & Tulin, L. G., "Stress-strain relations for concrete under cyclic loading", *American Concrete Institute – Journal*, Vol. 61, No. 2, 1964, p. 195.
17. Holmen, J., Fatigue of concrete by constant and variable amplitude loading, Doctoral thesis, The Norwegian Institute of Technology, Trondheim, Norway, No. 79-1, 1979.
18. Petkovic, G., Properties of concrete related to fatigue damage with emphasis in high strength concrete, Doctoral thesis, Universitetet i Trondheim, Norgestekniskehogskole, 1991.
19. Tepfers, R., "En undersökning av betongens utmattningshållförmåga", Tech. Rep. R86:1978, Avdelningen för husbyggnadsteknik, Chalmers University of Technology, Sweden, 1978.
20. CEB, Fatigue of concrete structures, state of the art report, Technical Report 188, 1988, 300 pp.

21. van Mier, J., Strain-softening of concrete under multiaxial loading conditions., Doctoral thesis, Technische hogeschool Eindhoven, The Netherlands, 1984.
22. van Mier, J. G. M., "Fracture of concrete under complex stress", Tech. Rep. 31, *Heron*, 1986.
23. Hai-cheng, L., Wei, C., & Yu-pu, S., "Fatigue properties of plain concrete under triaxial compressive cyclic loading", *China Ocean Engineering*, Vol. 18, No. 3, 2004, pp. 457–468.
24. Spooner, D., & Dougill, J., "Quantitative assessment of damage sustained in concrete during compressive loading", *Magazine of Concrete Research*, Vol. 27, No. 92, 1975, pp. 151–160.
25. Cornelissen, H. A. W., Hordijk, D. A., & Reinhardt, H. W., "Experimental determination of crack softening characteristics of normal weight and lightweight concrete", *Heron*, Vol. 31, No. 2, 1986, pp. 45–56.
26. Baluch, M., Qureshy, A., & Azad, A., Fatigue crack propagation in plain concrete, *SEM-RILEM International Conference*, 1987, 112–119 pp.
27. Thun, H., Assessment of Fatigue Resistance and Strength in Existing Concrete Structures, Doctoral thesis, Luleå University of Technology, 2006.
28. Holmberg, G., Fatigue of Concrete Piles of High Strength Concrete Exposed to Impact Load, Licentiate thesis, Chalmers University of Technology, 2001.
29. Svahn, P.-O., Dynamic Behaviour of Reinforced Concrete Structures: Analyses with a strong discontinuity approach, Doctoral thesis, Chalmers University of Technology, 2005.
30. Johansson, U., Fatigue tests and analysis of reinforced concrete bridge deck models, Licentiate thesis, Royal Institute of Technology, 2004.
31. Simo, J., & Ju, J., "Strain-based and stress-based continuum damage models 1. formulation", *International Journal of Solids And Structures*, Vol. 23, No. 7, 1987, pp. 821–840.
32. Lee, J., & Fenves, G., "Plastic-damage model for cyclic loading of concrete structures", *Journal of Engineering Mechanics-Asce*, Vol. 124, No. 8, 1998, pp. 892–900.
33. Grassl, P., & Remping, R., "Influence of volumetric-deviatoric coupling on crack prediction in concrete fracture tests", *Engineering Fracture Mechanics*, Vol. 74, No. 10, 2007, pp. 1683–1693.
34. Jason, L., Pijaudier-Cabot, G., Huerta, A., Crouch, R., & Ghavamian, S., "An elastic plastic damage formulation for the behavior of concrete", in V. Li, C. Leung, K. Willam, & S. Billington, eds., *Fracture mechanics of concrete structures*, 2004, pp. 549–556.
35. Bazant, Z., & Oh, B., "Crack band theory for fracture of concrete", *Materiaux et Constructions*, Vol. 16, No. 93, 1983, pp. 155–177.
36. Dafalias, Y., & Popov, E., "Model of nonlinearly hardening materials for complex loading", *Acta Mechanica*, Vol. 21, No. 3, 1975, pp. 173–192.
37. Spooner, D., Pomeroy, C., & Dougill, J., "Damage and energy-dissipation in cement pastes in compression", *Magazine of Concrete Research*, Vol. 28, No. 94, 1976, pp. 21–29.
38. Bazant, Z., & Shieh, C., "Hysteretic fracturing endochronic theory for concrete", *Journal of the Engineering Mechanics Division-Asce*, Vol. 106, No. 5, 1980, pp. 929–950.
39. Patzák, B., "Object oriented finite element modeling", *Acta Polytechnica*, Vol. 39, No. 1, 1999, pp. 99–113.
40. Patzák, B., & Bittnar, Z., "Design of object oriented finite element code", *Advances in Engineering Software*, Vol. 32, No. 1, 2001, pp. 759–767.

## Moisture distribution in screeded concrete slabs



Magnus Åhs  
Licentiate in Engineering  
Div. of Building Materials, Lund University  
P.O. Box 118, 221 00 Lund  
E-mail: magnus.ahs@byggtek.lth.se

Ph.D. Anders Sjöberg  
Division of Building Materials, Lund University  
P.O. Box 118, 221 00 Lund  
E-mail: anders.sjoberg@byggtek.lth.se



### ABSTRACT

A qualitative model of moisture distribution in screeded concrete slabs is presented. From this model it is possible to identify humidity changes in each material and thus determine corresponding moisture properties. The distribution of relative humidity, RH, was determined in nine screeded concrete slabs before flooring and after a certain time of redistribution. Moisture redistribution is clearly demonstrated in the results section, where the increase in humidity beneath the flooring is exemplified. The initial moisture distribution and subsequent changes agreed with the presented qualitative model. This model may be used to develop current moisture distribution prediction tools further by introducing a more complex interrelation between moisture changes and corresponding changes in moisture related properties.

**Key words:** moisture redistribution, qualitative model, relative humidity, screeded concrete slab

### 1. INTRODUCTION

Drying of residual moisture in concrete floor slabs has been brought into focus during the last decade. Residual moisture in concrete is water that remains after the requirements associated with pouring and curing are fulfilled. Depending on the water/cement ratio and environmental conditions, different quantities of water will be released to the surroundings until moisture equilibrium is achieved. If a moisture barrier such as PVC flooring is installed on the top of the slab, residual moisture will be redistributed and increase the humidity at the surface. To reduce the humidity level attained beneath the flooring, drying of residual moisture in concrete slabs is crucial.

Insufficiently dried concrete slabs in the presence of high alkali levels have been accused of promoting and sustaining degradation of adhesives beneath PVC floorings [1]. Degrading adhesives are known to emit volatile organic compounds, VOC, to the indoor environment [2]. Exposure to such VOC in high concentration has a negative health impact on people living or working in such environments [3]. Emissions originating from the damaged floor constructions

are of rather low concentration. The impact on health due to long term exposure to such low concentrations is not yet established [4]. However, research has shown that there is a higher frequency of diffuse health related symptoms among people who live or work in buildings in which such damage has occurred. These symptoms are hard to correlate to moisture damaged floor constructions as they appear as *e.g.* runny nose and irritated respiratory passages.

Moisture distribution determination in concrete floor slabs, especially screeded concrete slabs, is difficult. Irrespective of the applied method, the outcome is affected by uncertainties originating from *e.g.* sampling methods, equipment or unforeseen moisture losses from samples prior to testing. One recently developed method to determine the relative humidity, RH, in a concrete slab is based on long term monitoring and logging of the RH. Temperature effects on in-situ measurements of RH are recognised by examining the results obtained through long term in-situ measurements [5].

Prediction of moisture distribution in screeded concrete slabs is even more difficult. It is strongly dependent not only on precise characterization of the constituent materials but also a detailed knowledge of moisture/material interactions, drying time, drying conditions and concrete/screed moisture interactions. One of the common drawbacks in current models [6-8], apart from simplification of the moisture related properties of materials used in floor constructions, is the often incomplete description of moisture interactions between flooring, screed, and concrete. Current models may therefore generate predictions subject to large uncertainties.

This study presents a model for qualitative analysis of the moisture distribution in a screeded concrete slab. The model is described in section 2, where the moisture distribution is shown for two cases through four phases. A brief description of vital moisture related aspects of each phase is included. In order to verify the model, moisture distribution was determined on a number of screeded slabs before flooring and after redistribution. The experimental set up is described in section 3 and the moisture distribution before and after flooring in each slab is presented in section 4. In section 5 the results obtained are discussed and compared with the qualitative model. Conclusions from the presented works are presented in the last section.

## **2. QUALITATIVE MODEL**

This section presents a qualitative model which describes moisture distribution in screeded concrete slabs during construction. The model covers the time from pouring of the structural slab, continues with screed casting and finishes after flooring installation.

Moisture is evenly distributed in a freshly poured concrete slab. During early hydration, the humidity level decreases uniformly as a result of chemical binding of moisture to the cement. Further drying occurs when the external humidity is lower than that in the slab. The surfaces dry first as this moisture must be released before that inside. This variation through the slab is presented as a moisture distribution profile that shows humidity at the centre of the slab in relation to the surfaces.

When a screed is laid on the slab, moisture from the screed will rewet the slab surface and initiate redistribution of interior moisture. Owing to the wet screed the humidity at the top surface of the slab will increase. However, drying at the slab base and screed top continues. The

humidity of the screed decreases as some moisture becomes chemically bound. Finally, impermeable flooring is laid on the screed and as a result residual moisture is redistributed.

Figure 1 show two cases of screeded concrete which represent important events related to moisture distribution.

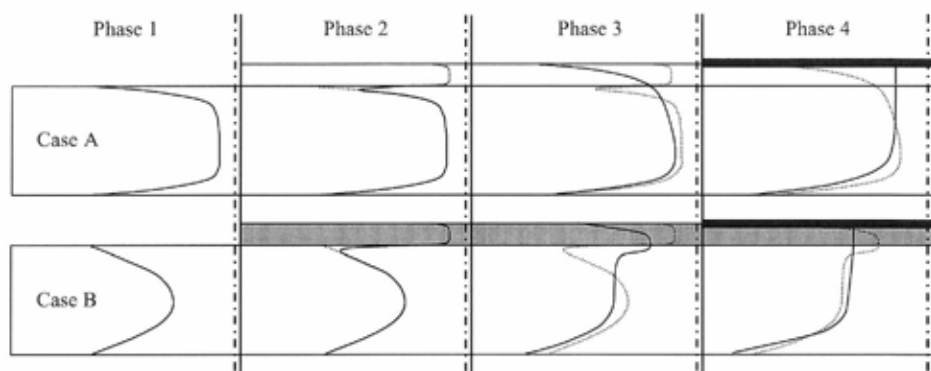


Figure 1. Phase 1 shows the distribution of residual moisture in a concrete slab. A wet screed is applied in phase 2. The applied screed dries in phase 3, and finally in phase 4 flooring is installed.

The top figure illustrates a screed applied on a newly poured concrete slab and the figure below when screed is applied on a slab subjected to years of drying. In each phase the dotted line represents initial moisture distribution and the solid line represents the moisture distribution prior to entering the next phase. The double dashed/solid line separates each phase; in addition it also indicates the highest attainable moisture level. It may be used for comparing the difference in absolute level between both cases and phases.

#### Phase 1. Drying of residual moisture in a concrete slab

- A. This profile illustrates the moisture distribution in a slab during initial drying. It occurs as a result of vertical moisture flow from the centre of the humid slab through the bottom and top surfaces. The slab surfaces have lost a lot of moisture in relation to the slab interior. A steep gradient on the moisture profile indicates a larger moisture flow in relation to a flat gradient.
- B. Like case A. However, this illustration shows a slab where drying has proceeded further. The moisture level in the central parts of the slab has significantly decreased.

#### Phase 2. Application of screed on top of the slab

- A. In this phase a screed is laid on the concrete slab. The top surface of the screed dries through moisture release to the less humid surroundings. Moisture flow at the top surface of the slab is reversed and as a consequence the screed base dries. However, this occurs at the expense of the slab top surface becoming increasingly humid. Just above the slab centre moisture transport is still directed towards the screed. However, the direction of moisture flow at the slab base remains unaffected. Additionally, drying in the screed occurs owing to chemical moisture binding of the cement.



- B. Like case A. However, the moisture level difference between slab and screed is significant, implying that the slab has a larger capacity to receive moisture from the screed than in case A.

#### Phase 3. Drying of the screed's residual water

- A. A significant amount of moisture has dried from the screed. Near the slab surface a considerable increase in humidity is evident. Humidity at the top surface of the screed is lower than at the base. This is a result of moisture redistribution from the interior parts of the slab.
- B. Like case A. However, the moisture level in the slab is substantially lower than in the screed. Moisture is still being transferred down from the screed into the slab.

#### Phase 4. Installation of an impermeable flooring and redistribution of moisture

- A. The surface is covered with moisture impermeable flooring, an efficient barrier which reduces moisture transport from the screed surface. The screed no longer dries but becomes increasingly humid as a result of redistribution of moisture from interior parts of the slab to the top surface. Drying will follow when the moisture flow from the screed becomes larger than the flow towards it. Future moisture profiles will never exceed this last phase, unless moisture is supplied from the outside.
- B. Like case A. Further drying of the central parts of the screed occurs as additional moisture is relocated down into the slab and up towards the flooring. Yet some moisture is transferred from the slab centre towards the screed.

### 3 EXPERIMENTAL SET UP

#### 3.1 Material

Nine screeded slabs, covering an area of  $800 \times 1200 \text{ mm}^2$ , with PVC flooring on top, were used in this study. Eight solid slabs were cast and preconditioned in the laboratory, the ninth, a hollow core slab, HCS, was cast in a factory. The solid slabs were made of concrete C, see table 1, and separated into two batches by their thickness, see table 2. Batch 1 consisted of slabs 1-4, 110 mm thick and batch 2 of slabs 5-8, 220 mm thick. Batch 3, the HCS, was manufactured with  $C_{HCS}$ , 265 mm thick with 5 longitudinal core holes.

Two different screeds were applied on the slab surfaces; cement mortar M, and a self levelling flooring compound SFC. The SFC labelled Floor 4310 Fibre Flow, manufactured by Maxit, was delivered as a dry powder mix in 25 kg bags. A detailed description of concrete, mortar and SFC mixes is given in table 1.

Table 1. Mixture description of the materials used. The quantities are in kg/m<sup>3</sup>.

Material w/c ratio	C	M	C <sub>HCS</sub> <sup>a</sup>	SFC <sup>a</sup>
CEM II/A-LL 42,5 R	250	400		
CEM I 52,5 R			390	
Portland Cement				1-5
Aluminous cement				5- 20
Gypsum				2 -10
Water	162	220	147	20
Dolomite 0.002-0.1 mm				31
Sand 0.1-1 mm				47
Sand 0-8 mm	976	1672	973	
Sand 6-13 mm			851	
Sand 8-12 mm	489			
Gravel 8-16 mm	489			
Polymer				1-5
P30			1.2	
Glenium 51	1.5	2.9		

<sup>a</sup> Mixture according to manufacturer, mass-% of dry powder, density=1900 kg/m<sup>3</sup>

All surfaces and material connections around the circumference were sealed with self adhesive bitumen alumina sheets; alumina tape without bitumen was also used. Cavities remaining after sampling for RH distribution were filled with a self expanding foam, DANA Joint - & insulation foam 591.

### 3.2 Methods

#### Formwork

Coated plywood, 13 mm, was used as formwork for the solid concrete slabs. Each form was put on a pallet, 800\*1200 mm<sup>2</sup>. Before pouring the forms were prepared with form oil, using an ordinary paint brush. No reinforcement bars were put inside the form. However, lifting tools were fixed on one vertical plywood sheet prior to pouring, to facilitate handling of the heavy concrete slabs in the laboratory. The web above the HCS mid core hole was cut off forming a 100\*800 mm slit. Coated plywood sheets prepared with form oil were used as formwork on each side of the mid core.

#### Pouring of slab

Concrete pouring was carried out in laboratory conditions, in formwork prepared for each of the three different batches. The HCS mid core hole was filled with material C through the slit. All castings were cured for 2 days covered by a plastic sheet, thereafter the formwork was stripped. Subsequently the vertical edges on each slab were sealed with self adhesive bitumen coated alumina sheets to obtain one dimensional moisture flow.

#### First drying

All slabs were drying in a climate room at 20 °C and 60 % RH. Batch 1 was dried laying flat on coated plywood and Batch 2 was vertically tilted.

In order to accelerate drying, slabs 7 and 8 were put in a climate box for 269 days at 32 °C, 39 days after pouring. The humidity in the climate box was obtained with a saturated solution of Sodium Bromide, NaBr, which generates an equilibrium humidity of 55 % RH at 32 °C, [9].

### *Pouring of screed*

Prior to screed application, a primer, Optiroc 6000, was evenly spread on the top surface of each slab by using an ordinary paint brush. Mixing was carried out in the laboratory by using a concrete mixer. On slabs 1, 2, 6, and 8 40 mm of material SFC was laid, and on slabs 3, 4, 5, and 7 40 mm of material M, see table 2. On the HCS 60 mm of material SFC was poured. All screeds were cured for 2 days, covered by a plastic sheet. The vertical screed edges were sealed subsequent to curing, by using self adhesive bitumen coated alumina sheets.

### *Second drying*

After curing the screed, all slabs were put in a 20 °C and 60 % RH climate for additional screed drying. Slabs in batch 2 were once again vertically tilted.

### *Installation of flooring*

On the day flooring was laid, adhesive was applied to the screed top surface. The quantity of applied adhesive is shown in table 2.

*Table 2. Description of drying and material application sequence*

Batch No.	1				2				3
Slab	1	2	3	4	5	6	7	8	9
Material	C	C	C	C	C	C	C	C	C <sub>HCS</sub>
1 <sup>st</sup> Drying [days]	105	105	110	110	9	11	408	408	28 <sup>1</sup>
Screed	SFC	SFC	M	M	M	SFC	M	SFC	SFC
2 <sup>nd</sup> Drying [days]	48	96	98	90	261	259	40	40	138
Adhesive [m <sup>2</sup> /l]	3.6	3.6	3.5	4.3	3.1	3.0	3.3	3.0	3.0
Flooring	PVC	PVC	PVC	PVC	PVC	PVC	PVC	PVC	PVC
Redistr.[days]	206	158	149	157	269	269	91	91	273

<sup>1</sup> Initial drying time of the C filling of the mid core. The HCS was cast approx. 60 days earlier.

Flooring installation was completed within 10 minutes after adhesive application. Immediately after flooring, additional aluminum tape without bitumen was used to seal the flooring rim to the previously installed aluminum sheets on the vertical slab edges.

### Determination of moisture distribution

The RH profile in all nine slabs was determined prior to flooring and after a certain time of moisture redistribution. All samples were obtained at least 100 mm from the vertical alumina sealing on the slab to avoid possible edge effects. To avoid possible drying disturbances, moisture profiles were always obtained not less than 260 mm from previous sampling.

Samples were obtained vertically through the slab using a 90 mm core drill which gradually penetrated the concrete in sections of 20 – 30 mm. Each section was chiselled off and crushed into gravel size pieces. Immediately after crushing, pieces of 5-15 mm size were put in glass test tubes, instantly sealed with elastic rubber plugs. Pieces considered to contain a high degree of cement paste were selected in order to maximize the quantity of moisture.

The RH was measured by using a carefully calibrated RH sensor, Vaisala HMP-44, inserted in the test tube. These sensors were connected to a computer logging system displaying the readings as curves in a diagram on a screen. When the curve in the diagram had levelled out the actual reading was performed, some 12-48 hours after inserting the sensor in the test tube. The RH sensors were preconditioned at 20 °C and 55 % RH prior to measurements.

One day after drilling, the cavities were filled with self expanding foam DANA 591. No water was used for cooling the core drill when sampling.

#### 4. RESULTS

Moisture distribution was determined in each slab prior to flooring, thin dashed lines, and after redistribution, thick solid lines, see fig 2. RH is shown on the x-axis in % RH and the y-axis represents the vertical distance in mm from the slab surface, positive figures for increasing depth. Each line marker represents the RH level obtained in each section. Flooring installation is defined as day 0 (zero) and each legend states when the profile was obtained in relation to flooring. The screed/concrete boundary is visualized at the top of each figure by a horizontal thick solid line. Dashed lines in the HCS figure represent edges of the longitudinal mid core hole.

The diagram representing slab 1 displays the RH distribution 1 day and 206 days after flooring. Each RH measurement has an uncertainty of 1 - 2 % RH, therefore changes within this range may not be significant. Drying of the screed base at the 30 mm level has decreased the RH from 93 to 87 % RH; a virtually uniform moisture profile in the screed is shown. Throughout the concrete slab, a considerable decrease exceeding 5 % RH is shown after moisture redistribution.

The moisture distribution in slab 2 was obtained 47 and 5 days prior to flooring and after 158 days of redistribution. Before flooring significant drying in excess of 10 % RH is shown in the top 60 mm of the slab. The increase in screed humidity after 158 days of redistribution is about 5 % RH. The humidity decrease of nearly 10 % RH in the concrete base indicates significant drying through the coated plywood.

In slab 3 the RH distribution is shown 56 and 14 days prior to and 158 days after flooring. Duplicate samples were obtained from different locations in the slab, 56 days before flooring. Screed humidity drops considerably by about 7 -10 % RH during the first 42 days of drying. After flooring the humidity level increases significantly, from 74 to 86 % RH in the top 20 mm of screed. Additionally, after 149 days of redistribution, slab humidity has decreased by about 4 % RH almost uniformly.

The moisture distribution in slab 4 is shown 48 and 6 days prior to flooring, and 157 days after redistribution. The screed humidity has decreased substantially during the initial 42 days of drying, by about 7 - 5 % RH. The moisture level 50 mm below flooring has decreased by about 2 - 4 % RH, showing larger decrease at the base, compared with the moisture profile obtained 6 days prior to flooring with 157 days of redistribution. The screed humidity has increased by about 2 - 7 % RH after redistribution, the larger increase was found at the 10 mm level close to the flooring.

After 269 days of redistribution shown in slab 5, humidity increases considerably by about 10 % RH in the screed compared with the profile obtained 3 days before flooring. A minor humidity increase in the slab top section is also indicated. The measurements also suggest a humidity decrease in the slab base after redistribution.

In slab 6, measurements made on day -3 and 269 clearly show an increase in humidity in the screed from 68 to 81 % RH. A humidity decrease of 5 % RH is shown at the slab base. Note that

the moisture level is nearly unchanged around the slab centre. There has been overall moisture redistribution and drying of the slab base has occurred.

Moisture distribution determined for the drier slab 7 shows a slight decrease of about 1 - 4 % RH at the screed top after 91 days of redistribution. Overall, the moisture profile obtained after redistribution is more or less equal to the moisture distribution obtained prior to flooring. However, the RH profile has flattened out in the screed layer and the slab bottom surface has dried further.

After 91 days of redistribution, the RH level in slab 8 increases 10 mm beneath the flooring. A moisture level decrease is shown both 30 mm and 50 mm below the screed top surface. The RH has increased between the 70 mm and 190 mm level.

The last three moisture profiles, HCS 1-3, show the moisture distribution in samples obtained from the HCS, 16 days prior to flooring and 273 days after. HCS 1 represents the humidity above the core hole next to the concrete filled mid core hole. A significant humidity increase, from 68 to 78 % RH, is shown in the screed surface and a minor decrease from 75 to 72 % RH in the HCS web at 90 mm level.

HCS 2 displays the results from RH determination performed on material from the wall separating the mid core hole from the neighbouring core hole. Top screed humidity has increased by some 3 - 5 % RH. The results from the slab mid section, at 175 mm depth, show a strange looking profile before flooring and after redistribution. This could be a result of the horizontal moisture distribution. However, a clear 5 % RH decrease in humidity is shown at the slab base.

HCS 3 diagram shows the moisture profiles on samples obtained from the concrete filled mid core hole. A minor increase by 1 - 2 % RH is shown in the top screed. Throughout the concrete filling, 60 mm and below, the moisture level has decreased from about 4 - 5 % RH, to slightly lower levels in the HCS base.

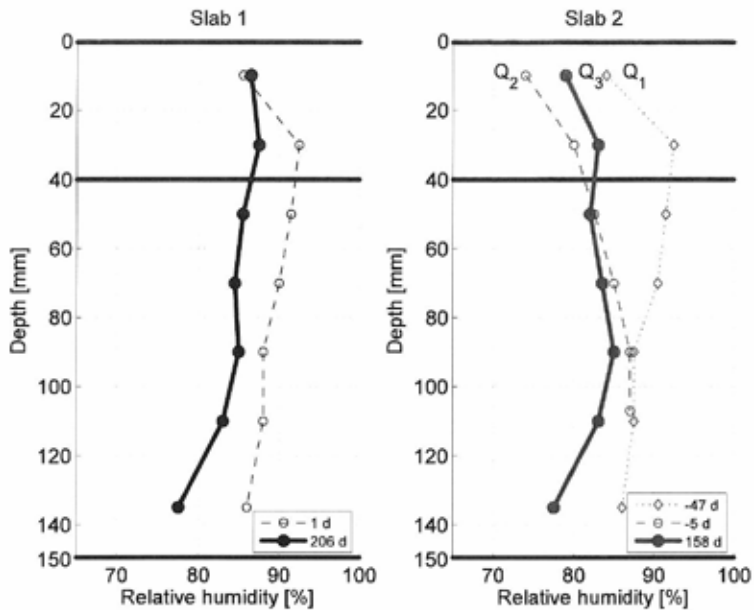


Figure 2. Moisture distribution determined for two SFC screeded concrete slabs on plywood before flooring (dashed lines) and after a certain time of redistribution (solid lines).

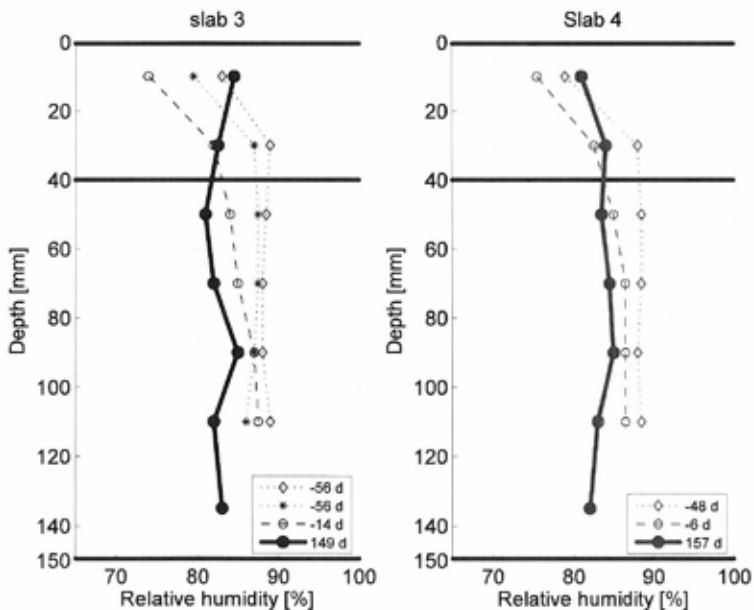


Figure 3. Moisture distribution determined for two M screeded concrete slabs on plywood before flooring (dashed lines) and after a certain time of redistribution (solid lines).

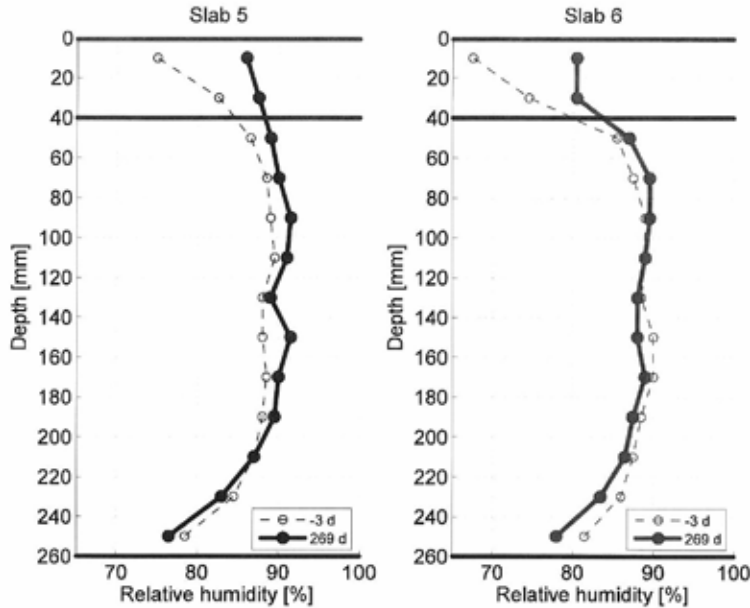


Figure 4. Moisture distribution determined for one M (left) and one SFC (right) screeded concrete slab before flooring (dashed lines) and after a certain time of redistribution (solid lines).

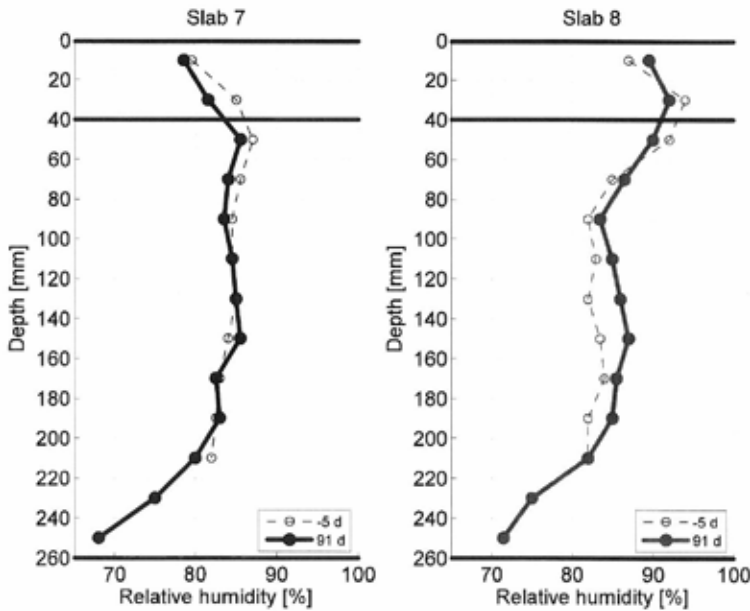


Figure 5. Moisture distribution determined for one M (left) and one SFC (right) screeded concrete slab before flooring (dashed lines) and after a certain time of redistribution (solid lines).

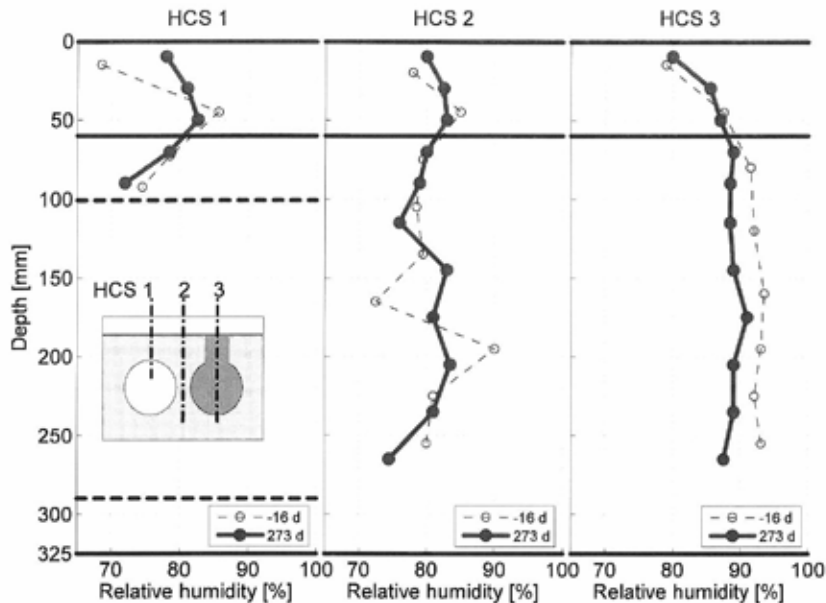


Figure 6. Moisture distribution determined in three sections of the SFC screeded hollow core slab, with one hollow core filled with material C, before flooring and after a certain time of redistribution.

## 5. DISCUSSION

### 5.1 Comparison of slabs 1 and 2, Case B

The influence of screed drying time on redistribution is discussed by comparing slabs 1 and 2. The screed on both slabs 1 and 2 had dried for 48 days, see table 2, when moisture profile 1 d and -47 d were obtained. Both these profiles are therefore almost identical and show an elevated RH level in the screed/concrete corresponding to Case B phase 3 in the qualitative model. Slab 2 dried for a further 42 days before a new RH profile -5 d was obtained. Judging from this moisture profile, drying has occurred mainly through the screed. The profiles 206 d and 158 d were obtained on the same day. Slab 1's shorter drying and longer moisture redistribution resulted in a more uniform screed moisture profile compared to slab 2. The moisture profile obtained in slab 1 after redistribution corresponds to phase 4 case B in the qualitative model. Further drying before flooring in slab 2 was accompanied by 158 days of moisture redistribution. This time was insufficient to achieve complete moisture redistribution in the screed. The moisture levels in slabs 1 and 2 are almost equal from slab centre and below, both before flooring and after redistribution, clearly demonstrating that equal drying conditions were achieved through the coated plywood at the base.



## 5.2 Comparison of slab 2 with 3 and 4, Case B

The influence of different screed materials with respect to moisture redistribution is discussed by comparing slab 2 with slabs 3 and 4. The screed dried for 48 days before the moisture profiles were determined on slab 3, -56 d, and slab 4, -48 d. Almost identical moisture profiles were obtained from slabs 3 and 4. The elevated screed humidity in slab 2 is not seen in slabs 3 and 4, this may be a result of further chemically bound moisture in the mortar. Additional moisture profiles -14 d and -6 d were obtained on the same day as profile -5 d for slab 2. These three moisture profiles are rather similar indicating that moisture has dried mainly through the screed as for slab 2 and that the moisture transfer rate is higher through hardened SFC than through hardened mortar. They also indicate that drying through further hydration diminishes with time as hydration mainly occurs early after pouring. The moisture distribution was finally determined after 149 and 157 days of redistribution in slabs 3 and 4, on the same day as slab 2. Moisture in the screed of slab 4 still needs additional time to achieve a uniform distribution. The lower parts of slabs 3 and 4 show equal moisture profiles, with allowance made for uncertainties. Finally, further drying of the slabs may occur mostly through the slab base as this is more open to moisture transport than PVC flooring. Therefore it is likely that the future profile will correspond to phase 4 in the proposed qualitative model.

## 5.3 Comparison of slab 7 with 8, Case B

The effect on residual moisture redistribution due to long drying before screeds are laid is discussed by comparing slabs 7 and 8. Screed drying on slabs 7 and 8 lasted for 35 days prior to determination of the moisture profiles, -5 d. The achieved RH profiles demonstrated the elevated moisture levels in the screed, corresponding to Case B phase 3 in the qualitative model. However, drying through cement hydration may have reduced the elevated screed moisture level in slab 7 compared to slab 8. In addition the benefits of the open SFC did not occur as a result of the short drying time. Both slabs were showing, within uncertainties, equally dry slab centres and bases. Flooring was applied on both slabs 40 days after screed application followed by 91 days of redistribution. A complete redistribution was not obtained. The moisture distribution after flooring of slab 7 shows drying of the screed and slab top. This may be a consequence of the unfavourable impact of uncertainties on the achieved results. The humidity determined after redistribution may be too low at the 10 mm level and too high before flooring, compared to a true humidity. In slab 8, moisture from the screed centre has redistributed to the bottom, but also upwards to the screed top. Both slabs, particularly slab 8, correspond to Case B's 4th phase in the qualitative model.

## 5.4 Comparison of slab 5 with 6, Case A

The influence that early flooring application on two different screed materials has on moisture redistribution is discussed by comparing slabs 5 and 6. Drying of the mortar in slab 5 and SFC in slab 6 lasted for 258 and 256 days respectively until the moisture profiles, -3 d, were obtained. The moisture profiles determined agree well with phase 3 Case A in the qualitative model as the moisture profile for slabs 5 and 6 both show pronounced drying of the screed and an equally pronounced drying of the slab base. The SCF has dried more than the mortar, possibly an effect of the hardened mortar that becomes less open to moisture transport compared to the SFC. The moisture profile after flooring was determined after 269 days of redistribution. The increase in humidity in the mortar is considerable and clearly shows the effect of moisture

redistribution from the slab centre and up. The moisture level increase seen in the upper 200 mm of slab 5 is within the uncertainties and may therefore not be significant. In slab 6, moisture from the slab centre has been redistributed to the top and increased the screed humidity, thus giving a uniform moisture profile. However, besides the continuing drying of the slab base, additional moisture will be redistributed to the screed top as the maximum level is not yet achieved after 269 days of redistribution. Moisture profiles determined for slabs 5 and 6 after the achieved redistribution correspond to phase 4 Case A in the qualitative model.

## 5.5 HCS1-3

Moisture profiles obtained from the HCS in section HCS1-3 are not compared with the qualitative model owing to significant horizontal moisture transfer that occurred as a consequence of the non solid slab. However, HCS3 obtained in the filled core hole could, judging from the results obtained without too much trouble, be compared with the qualitative model Case B.

Moisture profiles labelled -16 d in HCS1-3 were obtained 122 days after screed application. Flooring was applied 16 days after obtaining the first moisture profile. Redistribution continued for 273 days until the humidity profiles after flooring were obtained. The -16 d profile of HCS1 clearly shows significant drying from the screed base and down into the HCS top as well as drying upwards. The significant downward drying may be a consequence of the reduced cross section above the empty core hole. The HCS1 redistribution profile demonstrates a significant increase in humidity at the screed top originating from both vertical and horizontal moisture redistribution. Downward drying through the web top is also seen.

The moisture profile HCS2 determined for the web segment dividing the empty and the filled core hole showed some drying upwards, some moisture was also drying through the slab base. HCS2 profile shows disturbances in the slab centre presumably originating from horizontal moisture redistribution. The HCS2 screed top shows an increase as a consequence of 2-dimensional moisture redistribution. Top web centre profiles are less disturbed by the horizontal redistribution. Significant drying through the web base is seen in HCS2.

HCS3 moisture distribution 16 days before flooring shows drying through the screed top. The uniformly distributed moisture profile in HCS3 may be explained both by horizontal drying through the web to the neighbour core holes and vertical drying through the web base. HCS3 is showing a small increase at the top as a result of mainly vertical moisture redistribution from the filling. Further uniform drying is seen in the filling as a result of the horizontal drying through the web walls. The profile HCS3 shows lower humidity levels at the base than at the filling centre as a result of further downward drying.

## 6. CONCLUSIONS

Comparison of the qualitative model of moisture redistribution with the results obtained before application of flooring and after a certain time of redistribution indicates that moisture after flooring will be redistributed according to the proposed model. This is useful with regard to moisture redistribution simulations, as simulating tools should include the hysteresis concrete exhibits. If hysteresis is not included the simulations should be performed stepwise in order to incorporate the scanning phenomenon, thus reducing the uncertainty.

## REFERENCES

1. Wessén, B. and T. Hall. Directed Non-Destructive VOC-sampling: A method for source location of indoor air pollutants. In Proceedings of the 7:th International Conference on Indoor Air Quality and Climate. 1999. Edinburgh, Scotland: Construction Research Communications Ltd, pp. 420-425.
2. Sjöberg, A. and C. Engström, Measurements of stored decomposition products from flooring adhesives in a concrete floor, as a basis for choosing a new floor surface construction, in Building Physics 2002 - 6th Nordic Symposium. 2002.
3. Salthammer, T., Organic Indoor Air Pollutants. Occurrence, Measurement, Evaluation, ed. T. Salthammer. 1999, Weinheim, Germany: WILEY-VCH. 329.
4. Andersson, K., et al., TVOC and Health in Non-Industrial Indoor Environments. *Indoor Air*, 1996. 7(2): pp. 78-91.
5. Åhs, M. Remote monitoring and logging of relative humidity in concrete. In Proceedings of the 7th Symposium on Building Physics in the Nordic Countries 2005. Reykjavik, Iceland: The Icelandic Building Research Institute pp. 181-187.
6. West, R.P. and N. Holmes, Predicting moisture movement during the drying of concrete floors using finite elements. *Construction and Building Materials*, 2005. 19: pp. 674-681.
7. Obeid, W., G. Mounajed, and A. Alliche, Mathematical formulation of thermo-hygro-mechanical coupling problem in non-saturated porous media. *Computer Methods in Applied Mechanics and Engineering*, 2001. 190(39): pp. 5105-5122.
8. Leivo, V. and J. Rantala, Moisture behaviour of a massive concrete slab with a low temperature floor heating system during the initial drying period. *Construction and Building Materials*, 2005. 19: pp. 297-305.
9. Greenspan, L., Humidity fixed point of binary saturated aqueous Solutions. *Journal of Research of the National Bureau of Standards- A. Physics and Chemistry*, 1977. 81(1): pp. 89-96.